Fall 2010

Chitosan for biomedical applications

Aiman Omar Mahmoud Abbas
University of Iowa

CHITOSAN FOR BIOMEDICAL APPLICATIONS

by

Aiman Omar Mahmoud Abbas

An Abstract

Of a thesis submitted in partial fulfillment
of the requirements for the Doctor of
Philosophy degree in Pharmacy
in the Graduate College of
The University of Iowa

December 2010

Thesis Supervisors: Associate Professor Aliasger K. Salem
Professor Maureen D. Donovan

ABSTRACT

Chitosan, a copolymer of glucosamine and N-acetyl glucosamine, is a polycationic, biocompatible and biodegradable polymer. In addition, chitosan has different functional groups that can be modified with a wide array of ligands. Because of its unique physicochemical properties, chitosan has great potential in a range of biomedical applications, including tissue engineering, non-viral gene delivery and enzyme immobilization.

In our work, the primary amine groups of chitosan were utilized for chitosan modification through biotinylation using N-hydroxysuccinimide chemistry. This was followed by the addition of avidin which strongly binds to biotin. Biotinylated ligands such as polyethylene glycol (PEG) and RGD peptide sequence, or biotinylated enzymes such as trypsin, were then added to modify the surface properties of the chitosan for a variety of purposes. Modified chitosans were formulated into nano-sized particles or cast into films. Different factors affecting fabrication of chitosan particles, such as the pH of the preparation, the inclusion of polyanions, the charge ratios and the degree of deacetylation and the molecular weight of chitosan were studied. Similarly, parameters affecting the fabrication of chitosan films, such as cross-linking, were investigated for potential applications in tissue engineering and enzyme immobilization.

It was found that the inclusion of dextran sulfate resulted in optimum interaction between chitosan and DNA, as shown by the high stability of these nanoparticles and their high *in vitro* transfection efficiencies in HEK293 cells. When applying these formulations as DNA vaccines *in vivo*, chitosan nanoparticles loaded with the ovalbumin antigen and the plasmid DNA encoding the same antigen resulted in the highest antibody response in C57BL/6 mice.

Furthermore, engineering of the surface of chitosan nanoparticles was done by utilizing the avidin-biotin interaction for attaching PEG and RGD. The modified

formulations were tested for their *in vitro* gene delivery properties and it was found that these ligands improved gene transfection efficiencies significantly.

Chitosan nanoparticles were optimized further for enzyme immobilization purposes using sodium sulfate and glutaraldehyde as physical and chemical cross-linking agents, respectively. These particles and chitosan films were used for immobilizing trypsin utilizing several techniques. Enzyme immobilization via avidin-biotin interaction resulted in high immobilization efficiency and high enzymatic activity in different reaction conditions. Additionally, the immobilized trypsin systems were stable and amenable to be regenerated for multiple uses.

Finally, glutaraldehyde cross-linked chitosan films were modified with PEG and RGD for their cell repellant and cell adhesion properties, respectively, using avidin-biotin interaction. This method was again effective in engineering chitosan surfaces for modulating cell adhesion and proliferation.

In conclusion, using avidin-biotin technique to modify biotinylated chitosan surfaces is a facile method to attach a wide variety of ligands in mild reaction conditions, while preserving the functionality of these ligands.

Abstract Approved: _____
Thesis Supervisor

_____
Title and Department

_____
Date

_____
Thesis Supervisor

_____
Title and Department

_____
Date

CHITOSAN FOR BIOMEDICAL APPLICATIONS

by

Aiman Omar Mahmoud Abbas

A thesis submitted in partial fulfillment
of the requirements for the Doctor of
Philosophy degree in Pharmacy
in the Graduate College of
The University of Iowa

December 2010

Thesis Supervisors: Associate Professor Aliasger K. Salem
Professor Maureen D. Donovan

Graduate College
The University of Iowa
Iowa City, Iowa

CERTIFICATE OF APPROVAL

PH.D. THESIS

This is to certify that the Ph.D. thesis of

Aiman Omar Mahmoud Abbas

has been approved by the Examining Committee
for the thesis requirement for the Doctor of Philosophy
degree in Pharmacy at the December 2010 graduation.

Thesis Committee:
Aliasger K. Salem, Thesis Supervisor

Maureen D. Donovan, Thesis Supervisor

Daryl J. Murry

Jennifer Fiegel

Liu Hong

To my beloved parents, Omar Abbas and Shahira Khmous, for their continuous guidance and patience, to my wife, Khetam, for her love and to my brothers and sisters, Sadam, Suhel, Amal, Salah, Ahmad, Maram and Shatha for their support

ACKNOWLEDGMENTS

To start with, all the thanks and appreciations go to my advisors Dr. Aliasger Salem and Dr. Maureen Donovan, for their unconditional support and help, without which this work would have never been accomplished. I have gained tremendous knowledge and experience, academically and professionally, from interacting with them and being part of their research groups. I also thank the entire faculty members of Division of Pharmaceutics for their unhesitant aid whenever they are approached. I thank my other thesis defense committee members, Drs. Daryl Murry, Jennifer Fiegel and Liu Hong for sparing the time and effort to serve in the committee.

Special thanks and gratitude go to all members of Drs. Salem and Donovan laboratories for their help, quality and fun times and intellectually challenging discussions. Treniece Terry, Janjira Intra, Jessica Graham, Yogita Krishnamachari, Dahai Jiang, NaJung Kim, Caitlin Lemke, Sean Geary, Joanne Reiland, Hefei Zhang, Mow-Yee Foo, Chen-Ming Lee, Maya George, Manar Al-Ghabeish, Ahmad Abu Helwa and Varsha Dhamankar are just a few of my friends who have not spared any effort to help me.

I am also greatly thankful for the Pharm D and undergraduate students who worked with me; Michael Hirsch, Nicholas Dyson, Zsalanda Dixon, Tyler Gunn and David DeMik, for giving me a great opportunity to guide them and build their research skills and to learn from them at the same time. I am also very appreciative of the staff of the Central Microscopy Research Facility, especially Dr. Jonas Baltrusaitis, for providing me with their essential knowledge and expertise toward the completion of the research.

I wish to express my gratitude to my friends who have had a great influence in my life during the graduate program; Aktham Aburub, Shadi Gharaibeh, Fadi Alkhateeb, Thakir Almomani, Rania Hamed and Elizabeth Unni.

I also would like to thank Fulbright Program, The University of Iowa Pharmaceuticals, Center for Biocatalysis and Bioprocessing (CBB) Fellowship and Eli Lilly Foundation Applied Pharmaceutics Fellowship for their financial support.

Last but not least I would like to thank the special people who supported me throughout my educational endeavor, my family and my wife. I am deeply grateful to my parents who instilled in me the love of science and the ambition to do my best in every aspect of my life, to my siblings who did not spare any effort to inspire and help me through this process and to my wife, who her patience, unwavering love and belief in me provided me with a great strength along the way.

ABSTRACT

Chitosan, a copolymer of glucosamine and N-acetyl glucosamine, is a polycationic, biocompatible and biodegradable polymer. In addition, chitosan has different functional groups that can be modified with a wide array of ligands. Because of its unique physicochemical properties, chitosan has great potential in a range of biomedical applications, including tissue engineering, non-viral gene delivery and enzyme immobilization.

In our work, the primary amine groups of chitosan were utilized for chitosan modification through biotinylation using N-hydroxysuccinimide chemistry. This was followed by the addition of avidin which strongly binds to biotin. Biotinylated ligands such as polyethylene glycol (PEG) and RGD peptide sequence, or biotinylated enzymes such as trypsin, were then added to modify the surface properties of the chitosan for a variety of purposes. Modified chitosans were formulated into nano-sized particles or cast into films. Different factors affecting fabrication of chitosan particles, such as the pH of the preparation, the inclusion of polyanions, the charge ratios and the degree of deacetylation and the molecular weight of chitosan were studied. Similarly, parameters affecting the fabrication of chitosan films, such as cross-linking, were investigated for potential applications in tissue engineering and enzyme immobilization.

It was found that the inclusion of dextran sulfate resulted in optimum interaction between chitosan and DNA, as shown by the high stability of these nanoparticles and their high *in vitro* transfection efficiencies in HEK293 cells. When applying these formulations as DNA vaccines *in vivo*, chitosan nanoparticles loaded with the ovalbumin antigen and the plasmid DNA encoding the same antigen resulted in the highest antibody response in C57BL/6 mice.

Furthermore, engineering of the surface of chitosan nanoparticles was done by utilizing the avidin-biotin interaction for attaching PEG and RGD. The modified

formulations were tested for their *in vitro* gene delivery properties and it was found that these ligands improved gene transfection efficiencies significantly.

Chitosan nanoparticles were optimized further for enzyme immobilization purposes using sodium sulfate and glutaraldehyde as physical and chemical cross-linking agents, respectively. These particles and chitosan films were used for immobilizing trypsin utilizing several techniques. Enzyme immobilization via avidin-biotin interaction resulted in high immobilization efficiency and high enzymatic activity in different reaction conditions. Additionally, the immobilized trypsin systems were stable and amenable to be regenerated for multiple uses.

Finally, glutaraldehyde cross-linked chitosan films were modified with PEG and RGD for their cell repellant and cell adhesion properties, respectively, using avidin-biotin interaction. This method was again effective in engineering chitosan surfaces for modulating cell adhesion and proliferation.

In conclusion, using avidin-biotin technique to modify biotinylated chitosan surfaces is a facile method to attach a wide variety of ligands in mild reaction conditions, while preserving the functionality of these ligands.

TABLE OF CONTENTS

LIST OF TABLES

LIST OF FIGURES

CHAPTER 1

INTRODUCTION

1.1 Gene therapy

Gene therapy has caught the attention of therapeutic fields for more than two decades, with a series of successes and failures.[1] The main goal of gene therapy is introducing new genetic materials into targeted cells in the body for the treatment of genetic and infectious diseases. This can be done by introducing new genes to restore functions of defective genes causing certain diseases or by introducing genes that are designed to modify the way cells function.[2] For example, gene therapy has been investigated for targeting molecular causes of inherited single gene disorders, for inducing immune responses in viral diseases and for killing tumor cells by DNA cancer vaccines.[3] Gene transfer into targeted cells can be considered the most challenging barrier in gene therapy and simple treatments with naked DNA are not satisfactory (Figure 1-1). Consequently, gene delivery vectors or vehicles are necessary to aid the transference of exogenous genes to the tissues to be treated. Genes, carried by vectors, can be transferred via *ex vivo*, *in vivo* or *in situ* techniques. *Ex vivo* gene delivery is typically carried out by removing cells from the body, incubating them with the vector and then returning them to the diseased tissue, whereas *in vivo* gene delivery requires the ability of vectors to home in on their target cells once injected into blood stream. In comparison, *in situ* gene delivery protocols are designed to place vectors carrying the cloned genes directly into the tissues to be transduced.[4]

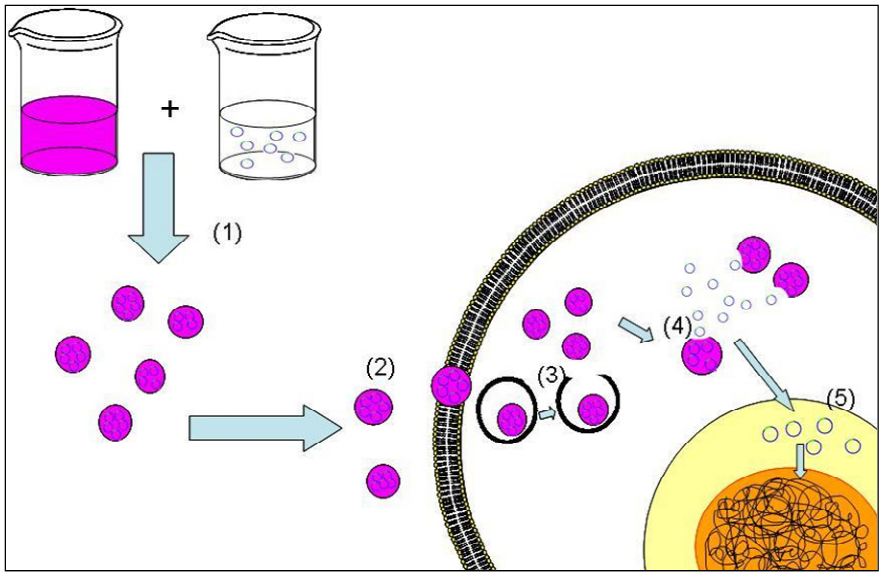

Figure 1-1. Schematic showing the hurdles facing non-viral gene delivery vectors from fabrication to gene expression. (1) Fabricating pDNA delivery system with high loading and minimum damage to pDNA, (2) delivering pDNA and its vehicles into the targeted sites and cellular uptake of the vectors, (3) releasing the pDNA with or without its vehicle from the endosomal compartments, (4) dissociation of the gene delivery vehicles and releasing pDNA to the cytosol and (5) transferring the pDNA to the nucleus and the transcription of genes into proteins in sufficient quantities.

There are two main broad approaches for gene delivery, viral and non-viral. In viral gene delivery, the inherent ability of viruses to infect cells, often with great specificity, is utilized. Viruses are modified to stop reproducing by removing genetic sequences needed for replication and retaining sequences that mediate viral binding, entry and gene delivery, which inhibits their ability to cause diseases but maintains their capability to deliver exogenous DNA.[5] Viral vectors used for gene therapy include retrovirus,[6] adenovirus,[7] adeno-associated virus,[8] herpes virus[9] and vaccinia virus.[10] Each viral system is suitable for distinctive applications. For instance, some of these viruses are capable of producing sustained gene expression but only in dividing cells, such as

retrovirus, whereas others can only infect non-dividing cells without integrating into the host cell chromosome, such as adenovirus and vaccinia virus.[11] Although viruses are naturally equipped for effective gene transfer, there are many drawbacks in using them. Among these are the possibility of undesired mutations through the integration of their DNA into the genome of the introduced cells and the inactivation of targeted genes when replacing the viral genes necessary for replication by recombination.[5]

Safety concerns about viral gene delivery, especially after the death of a patient following gene therapy of X chromosome-linked severe combined immune deficiency (SCID-X1), have raised interest in non-viral gene delivery systems.[12] Non-viral vectors are generally non-toxic with relatively low immunogenicity. In addition, non-viral vectors are capable of delivering larger fragments of DNA and are more amenable to formulation and control, especially in large scale production.[13] Although progress is being made in non-viral approaches for gene delivery, they are still significantly less efficient in transfecting mammalian cells compared to viral systems and they are unable to achieve sustained gene expression.[14] These reasons and others necessitate the development of novel delivery systems capable of protecting plasmid DNA, localizing its delivery, facilitating cellular uptake and sustaining gene expression for continual gene therapy.[15]

Non-viral gene delivery systems can be classified broadly into physical and chemical systems. Physical methods facilitate the transfer of genes into the cytoplasm of the targeted cells by creating transient defects in cellular membranes. These include using needle and jet injection, hydrodynamic gene transfer, gene gun, electroporation and sonoporation.[16] On the other hand, chemical-based non-viral vectors depend on the formation of condensed complexes between DNA and cationic polymers or lipids, or hybrids of both.[14] Cationic polymers can be natural, such as chitosan, or synthetic such as poly(L-lysine) (PLL),[17] polyethyleneimine (PEI)[18] and dendrimers.[19] Examples of cationic lipids include 3-β-[N-(N′,N′-dimethylaminoethanol) carbarmoyl]cholesterol

(DC-Chol), 1, 2-diolyoxy-3-(trimethylammonio) propane (DOTAP), and 1,2-dimyristyloxypropyl-3-dimethylhydroxyethyl ammonium bromide (DMRIE).[20]

1.2 Enzyme immobilization

Similar to non-viral gene delivery systems, polymers are essential elements for the success of other biotechnological applications, such as enzymatic processes. Enzyme technology focuses on improving the practical aspects of enzyme usage by forcing enzymatic reactions to proceed in a desired direction, which results in enhancing enzymatic selectivity and specificity, and stabilizing enzymes, as part of the effort towards finding the optimum cost-effective large-scale syntheses conditions.[21] Enzymes are naturally engineered for catalyzing the most complex chemical processes under mild experimental and environmental conditions.[22] This efficiency becomes more significant in the current ongoing quest of more green and sustainable methodologies for chemical processes.[23]

However, enzymes have evolved biologically to work in a framework of complex catalytic chains under highly regulated physiological conditions. In order to utilize the numerous advantages of enzymes for research, industrial and medical purposes, a multidisciplinary approach is required. Utilization of enzymes starts with screening the most efficient enzymes, followed by exploiting biotechnology in enhancing their enzymatic properties, finally improving the enzymatic activity and stability via immobilization techniques.[22]

Immobilization of enzymes offers many advantages, most prominently is enabling a facile and efficient separation of products from enzymes. This not only reduces the cost of production by enabling the recovery and reuse of enzymes, but also reduces the protein contamination of the final products. Moreover, it was shown that enzyme immobilization is a very powerful tool to augment the operational and storage enzymatic stability against denaturation caused by solvents, pH, autolysis or heat.[23,24]

Traditional enzyme immobilization techniques fall into five main categories; covalent attachment to solid supports, adsorption on solid surfaces, entrapment in polymeric gels, intermolecular cross-linking forming cross-linked enzyme crystals (CLECs) and cross-linked enzyme aggregates (CLEAs) and finally, encapsulation.[25] New technologies include microwave irradiation to increase enzyme loading into porous supports, single enzyme nanoparticles (SENs) which improve enzyme stability in harsh conditions,[26,27] photoimmobilization for covalent attachment of enzymes,[28] enzymatic immobilization of enzymes[29] and multi-step immobilization.[30]

However, current technologies for immobilization of enzymes have a number of shortcomings. Enzyme cross-linking may cause significant changes in the active sites of enzymes, whereas immobilizing on hard surfaces may lead to severe diffusional limitations and significant loss of activity. In addition, conformational changes in enzymes can occur as a result of the harsh conditions during chemical conjugation reactions.[31,32] Moreover, the lack of any site-directed positioning of the enzyme on a surface, which is a feature of most current immobilization methods, results in random orientation of enzymes and hindrance of accessibility of substrates and cofactors to the active site, restraining the enzymatic activity.[33] Therefore, controlled orientation of the immobilization via the introduction of defined binding sites would be much more appealing than an uncontrolled random approach.[34]

Several methods have been applied to control the orientation of immobilized enzymes, including modifications using specific tags by which enzymes are attached to surfaces, such as using His_6 tags for complex formation on Ni or Cu supports[35] or FLAG tags that are recognized selectively by antibodies.[36] Similarly, specific chemical activations at unique positions allow coupling of enzymes to functionalized surfaces. For example, introducing a single Cys residue by site-directed mutagenesis offers the potential for disulfide formation at support surfaces.[37] However, if the chosen coupling reaction lacks selectivity, multipoint attachments and cross reactions between enzyme

molecules can occur, which causes decreased activity. Under these circumstances, biotin labeling of proteins has the potential to be utilized by the introduction of short-biotin containing peptide linker through expressed protein ligation techniques, which ensures specific orientation of the enzyme on the (strept)avidin template, leading to increased stability and improved activity.[34,38]

1.3 Tissue engineering

A closely related science to gene delivery and enzyme immobilization, tissue engineering, can greatly benefit from the concepts of these fields and can be applied in conjunction with them. For example, gene delivery from polymer scaffolds represents a versatile approach to promote expression of tissue-inductive factors within the local environment of implants, promoting tissue regeneration. Also the inclusion of DNA and biomaterials into polymer scaffolds used as non-viral vectors represents a new approach in tissue engineering, which results in delaying the clearance of biomolecules from tissues, provides protection against denaturation and degradation, and maintains their effective concentrations for longer periods.[39-43] Also, enzyme immobilization can be critical for the success of tissue scaffolds. For instance, immobilizing trypsin onto scaffolds can help in replenishing skin tissues by removing dead tissue from wounds, burns, and ulcers to speed the growth of new tissue and skin grafts, as well as to inhibit the growth of some contaminant organisms.[44]

Tissue engineering has been a growing field that holds a great potential for replacing or restoring the function of lost and damaged tissue. Tissue engineering involves combining living healthy cells of patients into three dimensional temporary scaffolds, made of natural and synthetic materials, in order to produce functional organs to be replaced back into the body. The interest in this interdisciplinary science has evolved due to the lack of available effective alternative medical therapies and organ transplants, especially in the increasingly aging population of the Western world in a time

where high quality healthcare is expected. In addition to the shortage of donor organs, the high concern about transmissible diseases and the long term consequences of organ transplantation, such as using immunosuppressant drugs, have boosted the interest in tissue regeneration. Tissue engineering has been studied for applications in urology,[45] dentistry,[46,47] dermatology,[48] respiratory,[49] hepatic,[50] bone and cartilage replacement[51] and cardiac,[52] among other fields in medicine.

Compared to cellular therapy, the other branch of regenerative medicine, tissue engineering is utilized for cases where three-dimensional structures are needed, where cellular therapy becomes ineffective due to the scattering of injected cells. Tissue engineering depends on constructing guiding and scaffolding frameworks for cells to regulate and support cellular adhesion, spreading, differentiation and growth. Typically, targeted cells are firstly seeded in biodegradable polymer scaffolds and then are expanded in bioreactors, followed by implanting the artificial tissue into the recipient. In order to achieve the optimum performance, ideal scaffolds should have controllable characteristics regarding their biodegradability, bioresorbability and mechanical properties to fit the intended uses. In addition, scaffolds should encourage the growth, migration and functional organization of cells while allowing the replacement of the scaffold's polymer with new extracellular matrix secreted from the growing tissue. In order to achieve this, the scaffold should be suitable for carrying surface and imbedded bioactive agents, such as adhesion molecules and growth factors.[53]

Biodegradable polymers, the critical element in tissue engineering, can be from natural or synthetic sources and should ideally yield bioabsorbable degradation products. Natural polymers have the advantage of susceptibility to cell-triggered proteolytic activity and to remodeling, in addition to the intrinsic properties of cell recognition due to resemblance to extracellular matrix materials. However, natural polymers have a few shortcomings such as potential immunogenicity, complexity of purification and inconsistency. Moreover, most of natural polymers are hydrophilic and must be

converted into less water soluble forms to be useful as three dimensional scaffolds, except chitin and chitosan. Examples of natural polymers used in tissue engineering include proteins (collagens, gelatin, fibrin and silk fibroin) and polysaccharides (hyaluronic acid, alginate, chondroitin sulfate, chitosan and chitin).

1.4 Chitin and chitosan

Chitin and chitosan have been investigated thoroughly for different applications, including applications in the three fields mentioned above; gene delivery, tissue engineering and enzyme immobilization. Chitin is the most abundant nitrogen-bearing organic compound found in nature and is the second most available polysaccharide next to cellulose.[54] Chitin is a linear polymer composed of β(1,4)-linked N-acetyl glucosamine (NAG) units, which form a three dimensional α-helical configuration stabilized by intra-molecular hydrogen bonding.[55,56] The major sources of chitin production are the cuticles of crustaceans, especially shells of shrimp and crab and other byproducts of the food industry, and the exoskeletons of cephalopods.[57] Chitin is extracted by demineralization and deproteinization of crustacean shells using highly concentrated solutions of sodium hydroxide under high temperature.

Chitosan, the amino polysaccharide copolymer of 1,4 D-glucosamine and N-acetyl glucosamine (Figure 1-2),[58] is derived from chitin by alkaline[59,60] or enzymatic deacetylation.[61] Therefore, chitin and chitosan are essentially the same polymer but with arbitrarily defined degrees of deacetylation (DD). Generally, if the DD is more than 40%, the term chitosan is used. Although chitin and chitosan are absent in mammals, some mammalian enzymes, such as lysozymes, can hydrolyze them. Lysozymes are nonspecific proteolytic enzymes found in concentrations of 4–13 mg/l in serum and 450-1230 mg/ml in tears.[62] Chitosan's biodegradation process is dependent on two main factors; the DD and the distribution of NAG units. This was elucidated in the works of Lee et al. who showed that biodegradation declines sharply when the DD is more than

70%,[63] and Aiba et al. who found that chitosans with randomly distributed NAG units are less susceptible to lysozymic degradation than chitosans which have repeated blocks of three consecutive NAG units.[64] *In vitro* hydrolysis kinetics of chitosan by lysozymes follows the typical Michaelis-Menten kinetics, where k_m and V_{max} are 15 μg/ml and 0.083×10^{-3} g/L/min, respectively.[65] However, *in vivo* degradation of chitosan, which in theory parallels the rate of tissue regeneration, is variable. Tomihata et al. reported that only 10% of a chitosan film was degraded after 50 h of exposure to lysozymes and 80% of the dry film weight was retained after 12 week implantation in Wistar rats.[66]

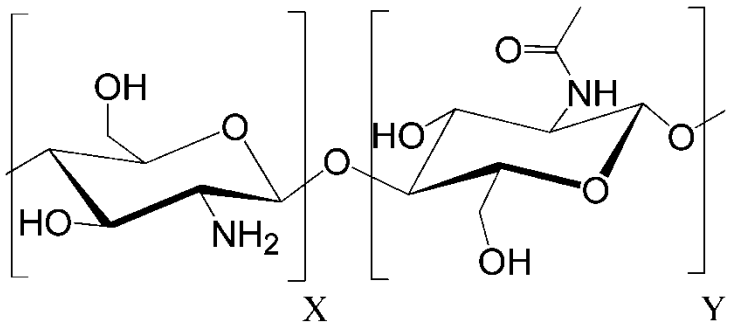

Figure 1-2. Molecular structure of chitosan.

In addition to being biodegradable, chitosan is a biocompatible polymer. This stems from chitosan's distinct structural similarities to the mammalian glycosaminoglycans (GAGs), which are a family of heteropolysaccharides in mammals that are located primarily on the surface of cells and in the extracellular matrix (ECM).[67] These molecules are long unbranched polysaccharides which contain repeating

disaccharide units. Each disaccharide unit contains either one of two modified sugars; N-acetyl galactosamine or N-acetyl glucosamine and uronic acid such as glucuronate or iduronate.[68] GAGs have extended conformation that imparts high viscosities and low compressibility properties to the ECM, which renders them suitable for joint lubrication. At the same time, their rigidity provides structural integrity to cells and provides passageways between cells, allowing for cell migration.

Chitosan has wide applications in medical fields, such as wound dressing, hypocholesterolemic agents, blood anticoagulant, antithrombogenic and drug delivery systems, in addition to other fields such as waste-water treatment, food and feed additives, wound-healing materials, cosmetic preparations and textile, paper and film technologies.[58,69,70]

Chitosan has many advantages for developing micro/nanoparticles, which can be used for preparing scaffolds and for gene and drug delivery. Chitosan's solubility in aqueous acidic solutions avoids the need for the use of organic solvents when fabricating particulate systems. In addition, the free amino groups become protonated at low pH values which allow the formation of ionic cross-linking with multivalent anions. Moreover, chitosan is mucoadhesive and also provides the ability to sustain the release of active agents such as transforming growth factor-β1.[71]

Chitosan has a significant potential for tissue regeneration purposes because of its biocompatibility, biodegradability and bioresorbability, in addition to its reactivity, having both reactive amino and hydroxyl groups that can be chemically modified. Also chitosan is amenable to molding into porous scaffolds with controllable characteristics. Moreover, chitosan surfaces support the attachment and the subsequent proliferation and growth of different types of cells, which have been attributed to the high cationic charge density of chitosan.[42,72] Also, chitosan promotes the production of transforming growth factor-beta 1 (TGF-β1) and platelet-derived growth factor (PDGF)[73] and maintains the chondrogenic phenotype.[74] For instance, Lahiji et al. and others showed that

chondrocytes seeded on chitosan film surfaces exhibited spherical morphology and expressed aggrecans and type II collagens.[75,76] Bone and cartilage regeneration therapy is an area where chitosan has been shown to be an attractive candidate. For example, chitosan has been investigated as a support matrix for bones[77] and as a biocompatible coating for orthopedic and craniofacial implant devices using palatal mesenchymal cells.[78] The large interest in chitosan for bone regeneration is due to the similarity of chitosan to GAGs and its ability to interact with common connective tissue components such as collagen to form insoluble complexes.

The two most important factors that determine the physicochemical properties, and consequently the specific applications of chitosan, are chitosan's degree of deacetylation (DD) and molecular weight (MW). DD, the percentage of the deacetylated units (glucosamine monomers) in chitosan's chains, affects the chemical, physical and biological properties of chitosan, such as the tensile strength of the films, the ability to chelate metal ions and the immunoadjuvant activity. DD also affects the intrinsic pKa (pK_o) of chitosan, leading to the alteration of chitosan's solubility in dilute acidic solutions. Generally, DDs ≥ 40% are soluble in dilute acidic solutions. Protonation of the amino groups of glucosamine units contribute to the disruption of hydrogen bonding, the solvation of cationic sites and then to the solubilization of chitosan when the balance between solvent/polymer and polymer/polymer interactions becomes favorable. When the DD becomes less than 40%, chitosan chains become completely insoluble in water, due to 1) the numerous H-bonds that occur between alcohol, amide and ether functionalities distributed on the repeating units all along the polymer chains and 2) the hydrophobic interactions due to the presence of the methyl groups of the acetamide functions and to the –CH and $–CH_2$ of the glucosidic rings.[57,79] When the DD is more than 40%, chitosan becomes soluble in acidic solution in a pH dependent manner. Decreasing the DD from 100% to 40% results in increasing the pH in which chitosan is soluble. This is due to 1) the increase in pK_o by decreasing the DD and 2) the increase in

stiffness of the polymer chain on decreasing DD, which results from the amplified steric hindrance from acetylated residues and the expanded excluded volumes.[57,79-81]

The effect of DD on chitosan use in biological systems appears clearly in its effect on gene delivery properties. Kiang et al. investigated the effect of DD of chitosan on the efficiency of gene transfection and found that DNA binding efficacy decreased with decreasing DD, therefore, requiring an increased positive to negative charge ratio for complete DNA complexation.However, the *in vivo* and *in vitro* behaviors were different. Decreasing DD resulted in decreased overall luciferase expression levels *in vitro* but increased luciferase expression levels *in vivo* up to two fold. The decreased *in vitro* transfection efficiency can be due to destabilization of the nanoparticles by the bulky acetyl groups in the polymer chains, but this same destabilization, along with higher degradation, were hypothesized to improve the transgene expression in muscles. Therefore, it can be concluded that cellular uptake and gene transfection of chitosan/DNA complexes can be mediated by the DD by controlling electrostatic interactions with the cell membrane to proceed to efficient transfection.[83]

In addition, the effect of the DD on cell adhesion has been studied for different cell lines. [84] It was shown that even as little as 10% difference in the extent of acetylation caused significant modification of chitosan's cell attachment properties. The higher %DD of chitosan, the higher amount of free amino groups ($-NH_2$), which in turn, can become protonated to form cationic amine groups ($-NH_3^+$) producing positively charged surfaces. This polycationic nature of chitosan is expected to enhance the interactions between the chitosan surface and the negatively charged cells, and therefore, chitosans with higher extent of deacetylation facilitate cell adhesion.[84] However, high adhesion of some cell lines, such as fibroblasts, to the highly deacetylated chitosan films was also shown to affect cell proliferation.[85] These results show that DD should be carefully selected in order to obtain optimum cellular adhesion and proliferation as well as film biodegradation *in vitro* and *in vivo*.

The molecular weight (MW) of chitosan has significant impact on its effectiveness for a variety of applications. This appears in the efficacy of chitosan to accelerate burn healing, coagulate pollutants, lower blood cholesterol levels, enhance drug dissolution, control viscosity or improve crop yields, which were found to be molecular weight dependent.[86] The size of chitosan polymers necessary to achieve this wide range of application varies by 3 to 4 orders of magnitude. For example, it was reported that 9.3 kDa chitosan prevented the growth of E coli, but 2.2 kDa chitosan promoted its growth.[87] Therefore, it is essential to precisely control the molecular weight of chitosan to suit the different applications and outcomes. This can be done using low concentrations of sodium nitrite ($NaNO_2$) to depolymerize chitosan chains in a controlled manner, offering a possible solution to problems regarding consistency of commercially available chitosans.[86,88]

The effect of chitosan's molecular weight on gene delivery systems interplays in the complex formation with DNA. Once the electrostatic interactions between polyelectrolytes occur, high MW chitosans result in more entanglement that leads to stronger complexes.[82] With decreasing MW of the chitosan, chain entanglement contribution to complex formations decreases, yielding weaker complexes. Therefore, low MW chitosans are less efficient in retaining condensed DNA upon dilution and are less capable of protecting the DNA from degradation by DNase and other serum components. Huang et al. found that these factors resulted in lower transfection efficiencies when using low MW chitosans.[83] However, by increasing the charge ratio (N/P) of chitosan to DNA, the transfection efficiencies of low MW chitosans complexed with DNA supersede that of high MW.[89] Hence, it appears that a fine balance must be achieved between extracellular DNA protection (better with high MW) versus efficient intracellular unpacking (better with low MW) to obtain high transgene expression of chitosan.

In tissue regeneration, the effect of chitosan's molecular weight is most important on the physicochemical properties of chitosan scaffolds.[90] Using higher molecular weight chitosans lead to higher tensile strength due to stronger inter-chain associations via H-bonding, which also results in a lower solubility. On the other hand, molecular weight has a minimal direct effect on cell attachment; the lower molecular weight chitosans show only slight enhancement in cell attachment.[91]

1.5 Modifications of chitosan

Chitosan is the only cationic polysaccharide in nature derived from biomass. Its unique physicochemical and biological properties make it worthy in regard to pharmaceutical and biomedical applications. However, chitosan properties, such as aqueous solubility in neutral to basic media and mechanical characteristics, can be enhanced via chemical modifications, physical interactions (inorganic composites and polyelectrolyte complexes) and other miscellaneous methods (such as using avidin-biotin interaction). Some of the trials reported in literature to exploit the unique properties and to realize full potential of this versatile polysaccharide, especially in the gene delivery and tissue engineering fields, are discussed below.

1.5.1 Chemical modifications

Chemical modifications of chitosan have been investigated extensively in literature for improving the physicochemical properties of chitosan. The main goals of modifying chitosan chemically are to provide derivatives that are soluble at neutral and basic pH values, to control hydrophobic, cationic, and anionic properties as well as to attach various functional groups and ligands. Fortunately, chitosan is amenable to chemical modifications due to having of hydroxyl, acetamido and amine functional groups.[92] For that reason, generally speaking, chemical modifications would not change the fundamental skeleton of chitosan and would keep the original physicochemical and biochemical properties while bringing new or improved properties.

PEG-grafted chitosan (chitosan-g-PEG) was synthesized by Jiang et al. using the reaction between methoxy PEG-nitrophenol carbonate and chitosan.[93] The average size of nanoparticles prepared from chitosan/DNA was slightly smaller than that of

chitosan-*g*-PEG/DNA complexes in the preparation media, however, chitosan/DNA complexes were highly susceptible to aggregation in the presence of serum and bile. PEG-grafted chitosans effectively shielded the positively charged chitosan surface when compared to unmodified chitosans and were able to maintain complex sizes in the presence of bile and serum, in addition to affording protection to the complexed DNA against enzymatic degradation. Ultimately, this improved the transfection efficiency *in vivo*.[93]

Chitosan-graft-polyethylenimine (CHI-g-PEI) copolymer was synthesized by imine reaction in two steps. In the first step, periodate-oxidized chitosan was prepared by a modified method described by Vold and Christensen,[94] followed by reacting PEI with periodate-oxidized chitosan for two days.[95] It was found that the addition of chitosan to PEI resulted in significant reduction in cytotoxicity compared to PEI (25 kDa), in three different cell lines as measured by the Cell Titer96® assay. In addition, this polymer resulted in enhanced gene transfer efficiency, even in the presence of serum.[95]

Trimethylated chitosans (TMCs) were prepared by Kean et al. in order to produce more permanent cationic charges on chitosan's chains.[96] TMCs were evaluated for the effect of the quaternization on cytotoxicity and transfection efficiency. Trimethylation increased the toxicity of chitosans; however, the toxicity remained far below that of PEI up to the 24 h incubation with cells. On the other hand, both trimethyl oligomers (TMOs) and TMCs complexed with pGL3 luciferase reporter gene yielded appreciable transfection in COS7 and MCF7 cell lines. TMOs showed the highest transfection efficiency at 44% degree of methylation (TMO44), whereas, TMCs showed high transfection efficiency only at two methylation degrees, 57 and 93%. TMO44 yielded 40% of PEI transfection in COS-7 and a 16-fold increase over PEI in MCF-7 cells, while

TMCs with degrees of trimethylation of 57% and 93% gave 23 and 50-fold increase, respectively, over PEI transfection efficiency in MCF-7 cells.[96] The toxicities and transfection efficiencies of trimethylated chitosan derivatives were dependent on size and degree of methylation.

Galactose molecules were coupled to chitosan chains using lactobionic acid bearing the galactose groups via active ester intermediates using 1-ethyl-3-(3-dimethylaminopropyl)-carbodiimide hydrochloride (EDC). In addition, the prepared polymers were grafted with hydrophilic dextrans, and their structure was confirmed using IR.[97] This polymer has the potential to be used as a hepatocyte-targeting gene delivery system since galactose functions as a specific ligand to asialoglycoprotein receptors (ASGRs) and dextran sulfate serves as the hydrophilic ligand.[97] Similarly, galactosylated chitosans (GCs) were tested for hepatocyte's adhesion in comparison to galactose-carrying polystyrene (PS), poly(*N*-*p*-vinylbenzyl-4-*o*-*β*-D-galactopyranosyl-D-gluconamide) (PVLA), that mediates hepatocyte's adhesion through the galactose-specific interactions between ASGRs of the hepatocytes and galactose residues of the PVLA.[98] The results showed that hepatocyte's adhesion to the GC-coated PS dish was as high as 94.7% after 120 min incubation, which was similar to PVLA-coated PS dish. In contrast, hepatocytes adhesion to unmodified chitosan-coated PS dishes was about 69.1%.[97]. Finally, the morphology of hepatocytes was studied in the presence and absence of epidermal growth factor (EGF). It was shown that at low concentrations of GC (0.05 μg/ml), cells adhered to the surface showing extended spreading shapes after 24 h in the absence of EGF whereas this happened after 10 h in the presence of EGF, indicating enhanced spreading in the presence of EGF. Therefore, GC showed potential as a synthetic ECM for liver tissue engineering.[98] Galactose-modified chitosans were also coupled with hydrophilic PEG forming galactosylated chitosan-graft-poly(ethylene glycol) (GCP).[99] The incorporation of a flexible hydrophilic polymer into the gene delivery systems produces steric barriers to interaction with proteins and phagocytes and

prolonged plasma circulation time. Turbidity measurements were performed to study the dispersive stability of GCP/DNA complexes. GCP/DNA complexes expressed constant or slightly decreasing turbidity without precipitation, which is an indication of enhanced stability. The grafted PEG chains were suggested to be responsible for protecting the GCP/DNA complexes from self-aggregation and precipitation.[99]

Similarly, polyvinylpyrrolidone (PVP) was conjugated as another hydrophilic group onto GC chains.[97] PVP is a nontoxic, water soluble neutral hydrophilic polymer that is used as an additive in pharmaceuticals. GC was chemically conjugated with PVP via the formation of an amide bond between the amino group of GC and the activated terminal carboxyl group of the PVP by N-hydroxysuccinimide (NHS)/EDC dissolved in buffer solution.[97] The purpose of adding hydrophilic ligands such as PVP was mainly to reduce clearance by the reticuloendothelial systems (RES), and to minimize mononuclear phagocyte system uptake, extending circulation time of these particles *in vivo*.[100] Moreover, it was found that hydrophilic groups, introduced onto the surface of DNA complexes, prevent them from aggregating and being adsorbed onto plasma proteins, especially albumin, which can stimulate the clearance of DNA vectors from the plasma by RES. The effect of albumin on the surface charge of GC-PVP 10K/DNA complexes were examined and compared to PEI, a commonly used polycationic gene carrier. The zeta potential values of PEI/DNA complexes at charge ratios of 1 and 3 were significantly decreased to negative values even at low concentrations of albumin. On the other hand, GC-PVP 10K/DNA had a constant surface charge regardless of the amount of albumin added.

Mannose receptors have an important role in endocytosis and are expressed in high levels in antigen presenting cells, such as dendritic cells (DCs) which are essential for activating immune response. Gene modification of DCs is of particular interest for immunotherapy of diseases where the immune system has failed or is abnormally regulated, such as in cancer or autoimmune diseases. In these cases increasing the

synthesis of immunomodulatory cytokines such as IL-12 in tumor tissues can allow better T-cell activation.[101] Mannosylated chitosans (MCs) were prepared by reacting water soluble chitosans with mannopyranosyl phenylisothiocyanate in dimethyl sulfoxide (DMSO).[101] MC/DNA complexes were induced to self-assemble by mixing the plasmid DNA with MC in phosphate buffer at pH 7.4. The transfection results of these complexes clearly show that MC-mediated pGL3 DNA transfection was mannose receptor–dependent, as confirmed by the ability of mannose to block the binding of complexes onto Raw 264.7 macrophage cells expressing moderate mannose receptors in a concentration-dependent manner.[102] In addition, the levels of plasmid encoding murine IL-12 (pmIL-12), as well as murine IFN-γ, were significantly increased by both MC/pmIL-12 and chitosan/pmIL-12 complexes compared with naked mIL-12, but MC-mediated cytokine production was distinctively higher than that of chitosan's.[101] Similarly, MC showed promising results in transferring genes to the mouse peritoneal macrophages.[103]

The water soluble carbodiimide (EDC) was reacted with the carboxyl groups of deoxycholic acid to form active ester intermediates. These intermediates were reacted with the primary amine of chitosan to form an amide bond, releasing isourea as a by-product, and the formation of the amide bonds was confirmed by FTIR.[104] Hydrophobically modified chitosans by deoxycholic acid (DAMCs) provide colloidally stable self-aggregates in aqueous media. The prepared self-aggregates had small sizes (mean diameter of ca. 160 nm) with a unimodal size distribution, and were able to form charge complexes when mixed with plasmid DNA.[104] In addition, it was found that the optimum condition for cell transfection could be controlled using DAMC self-aggregates with different physicochemical properties, including size and structure.[105,106]

In a similar fashion, highly purified chitosan oligosaccharides (COSs), prepared by ultrafiltration methods, were chemically modified with hydrophobic moieties of deoxycholic acid.[107] The hydrophobized COSs (COSDs) formed core-shell type

nanoparticles in aqueous media due to their amphiphilic character. Compared to unmodified COSs, the COSDs nanoparticles showed greater potential as gene carriers by having more efficient DNA condensation and protection. The COSDs, especially COS3D25 (M_n = 3 kDa, degree of substitution = 5.4%), mediated high levels of gene transfection in HEK293 cells compared to that of poly(L-lysine) (PLL), in the absence and presence of FBS.

Chitosan oligosaccharides were also modified chemically with hydrophobic cholesterol groups. Cholesterol-modified chitosan oligosaccharides (COSs) were fractionized according to molecular weight using ultrafiltration technique.[108] COSs were dissolved in DMSO/H_2O mixture and reacted with cholesteryl chloroformate to form hydrophobized COS. Due to their amphiphilic characteristics, modified COSs formed core shell nanoparticles with low critical aggregation concentration in aqueous milieu. COS6C5 (M_n= 6 kDa, containing 5% of cholesteryl chloroformate) showed the best DNA condensation and the highest transfection efficiency compared to the unmodified chitosans.[108]

Alkylated chitosans (ACSs) were prepared by modifying chitosan with alkyl bromide.[109] It was found that ACSs self-aggregate in acetic acid solution, whereas 99% deacetylated chitosans do not, due to strong electrostatic repulsion. The transfection efficiency of plasmid-encoding chloramphenicol acetyltransferase (CAT) mediated by chitosan and ACS into C2C12 cells, a mouse skeletal muscle cell line, was dependent on the hydrophobicity of chitosan. Increasing the length of the added alkyl side chain, up to 8 carbons, caused the transfection efficiency to increase, after which it leveled off. It was suggested that higher transfection efficiencies of ACS was due to easier unpacking of DNA from ACS carriers inside cells in addition to enhancing entry into cells facilitated by hydrophobic interactions.[109]

Primary amines of glycol chitosans were modified with 5β-cholanic acid to prepare hydrophobically modified glycol chitosan (HGC).[110] DNA was complexed with

cetyltrimethylammonium bromide (CTAB) at a charge ratio of 1, which resulted in the highest DNA stability. This was followed by encapsulating the DNA in the HGC nanoparticles by hydrophobic interactions between 5β-cholanic acid moieties and the hydrophobized DNA. Increasing the HGC/GC ratio caused the encapsulation efficiency of DNA to increase slowly and the particle sizes to decrease. This was attributed to the hydrophobic interactions between 5β-cholanic acids of HGC and CTAB/DNA complexes. HGC with high degrees of 5β-cholanic acids substitution were found to have lower critical micelle concentrations (CMC) and to have the ability to be formulated in smaller particles.[110,111]

Amphiphilic grafted copolymers based on CSO were prepared by conjugating stearic acid (SA) molecules to chitosan chains to form hydrophobic segments using EDC chemistry.[112]. CSO-SA micelles formed spontaneously upon dispersion in distilled water with the help of ultrasonication and were found to have CMC value of 0.035 mg/ml as determined by fluorometry with pyrene. The CSO–SA micelles were used to condense plasmid DNA and the CSO–SA/DNA complex nanoparticles with N/P ratios from 0.25 to 58 were tested for DNA stability, cytotoxicity and *in vitro* transfection efficiency.[112] *In vitro* transfection testing showed higher transfection efficiencies of CSO–SA micelles in A549 cells compared to that of CSO. Moreover, the transfection efficiencies of these micelles were comparable to Lipofectamine™ 2000 in serum free media, but greater than this known transfection agent in the presence of 10% fetal bovine serum. On the other hand, the cytotoxicity of CSO–SA was significantly lower than that of Lipofectamine™ 2000 (The IC_{50} of CSO–SA and Lipofectamine™ 2000 were found to be 543 μg/ml and 6 μg/ml, respectively). The low cytotoxicity of the studied CSO–SA micellar vectors in conjunction with superior DNA condensation capacity are critical improvements for non-viral gene transfer.

Poly (chitosan-g-DL-lactic acid) (PCLA) was investigated for tissue engineering applications. PCLA was synthesized by dissolving chitosan in an aqueous solution of

DL-lactic acid, and then the polymer was left on a Teflon dish at 85°C to shape into a membrane during the ongoing polymerization for 5 h.[113] During the synthesis of the PCLA copolymer, chitosan amino lactate salts were formed first through the protonation of chitosan. This was followed by establishing the real linkages between chitosan and lactic acid by dehydrating the resultant lactate salts while the polycondensation of lactic acid was happening simultaneously.[113] Fibrous mesh scaffolds were successfully fabricated by using PCLA with an improved wet-spinning technique.

Several key processing conditions, such as the concentration of PCLA dopes, the nitrogen pressure applied to the dopes, and the concentration of coagulant were used to modulate the morphologies of the fabricated filaments and the structure of the scaffolds. PCLA mesh scaffolds showed well-defined tensile and compressive mechanical properties similar to chitosan scaffolds in their dry states. After being hydrated, greatly improved tensile and compressive characteristics as well as enhanced dimensional stability in PCLA mesh scaffolds were obtained, in comparison to wet chitosan mesh scaffolds. [113]

1.5.2 Chitosan composites

Chitin, the precursor of chitosan, exists as a natural composite with minerals and proteins in invertebrates and functions as essential component for preserving the structural integrity of the shells of arthropods.[114] Also, blends or composites of chitosan with other materials have been widely investigated in literature. Such blends have resulted in a range of modifications of chitosan properties and applications.[115] Chitosan composites can be classified into two main categories; chitosan–inorganic material composites and chitosan polyanion complex composites.

Various inorganic materials, including metals, have been incorporated into chitosan composites which resulted in unusual and interesting biochemical properties.[116] The collective characteristics of these admixtures of inorganic compounds with chitosan

have been applied in several appealing biotechnological applications.[117] Hydroxyapatite, for example, was extensively studied in combination with chitosan as a bioactive inorganic material to further enhance bone regenerative efficacy and osteoconductivity. These materials have been applied in bone tissue recovery, such as bone-filling materials, and in drug delivery systems intended to accelerate reconstitution of damaged bones.[118,119]

The focus of this study is on the second type of chitosan composites, polyelectrolyte complexes (PECs). Complexes between macromolecules can be formed by several types of intermolecular interactions. Some of these forces include van der Waals interactions, hydrogen bonding, coordination forces, covalent bonding and polyelectrolyte interactions to form PECs. Generally, combined interpolymer forces contributes to the stability of the macromolecular complexes.[120] PECs formation is a simple but very attractive principle of particle formation with high practical potential.

PECs are formed as a result of condensation between oppositely charged polyions that are stabilized by intermolecular ionic bonds,[120] and their main driving force for the reaction is the concomitant release of corresponding counterions, increasing the entropy of the system.[121] PECs can be generally categorized into two types; water-soluble and aggregated PECs. Water-soluble PECs are formed as a result of non-stoichiometric mixing of weakly charged polyelectrolytes that varies in molecular dimensions, whereas water insoluble and highly aggregated PECs are formed from highly charged and/or high molecular weight polyelectrolytes.[122]

One of the more widely used polycations for the fabrication of PECs is chitosan. Chitosan is considered the only available cation from biomass. This cationic property of chitosan allows it to form non-covalent complexes with other negatively charged polyelectrolytes. Examples of polyanions used to form PECs with chitosan are DNA,[123] carboxymethyl cellulose,[124] gum kondagogu,[125] sodium alginate,[126,127], acrylamido

glycolic acid,[128] poly(acrylic acid),[129] pectin,[130] hyaluronic acid[131] and sodium dextran sulfate.[132]

The complexation process of chitosan with polyanions depends on many factors, including the degree of deacetylation of chitosan, and consequently the dissociation constant (pKa), the molecular weight of chitosan, the degree of polydispersity, chitosan's chain conformation, polymer's concentrations and ratios, charge density and the distribution of amine to acetylated groups along the polymer chains. In addition, the complexation environment, such as solution pH, temperature and ionic strength plays an important role.[120,133] For example, changing the ionic strength by adding salt to the chitosan solution will partially inhibit the repulsion forces between charged groups throughout chitosan chains, which decreases the rigidity of the chains. The substantial role of chitosan's degree of deacetylation on the complexation process appears in the effect on chain conformation. For instance, at a degree of deacetylation of more than 80%, chain extension happens due to the predomination of electrostatic repulsion between protonated amino groups. At degrees of deacetylation between 50% and 80%, the effect of acetyl groups becomes dominant, causing stronger intermolecular hydrogen bonds and increased steric hindrance of acetamide groups compared to amino groups. This limits the flexibility of chitosan chains and increases their rigidity. Decreasing the degrees of deacetylation to values less than 50% causes the polymer to start aggregating, which increases the local concentrations of polymeric segments.[133]

In addition to forming films, PECs between chitosans and other negatively charged molecules have been utilized to form nanoparticles in a process called ionic gelation. Other methods commonly used for the preparation of chitosan nanoparticles include spray drying, emulsion cross-linking and complex coacervation. However, ionic gelation technique gained the most interest because of its dependence on the electrostatic interaction mechanism, which 1) obviates the use of the commonly harsh conditions associated with chemical cross-linking and residual effects of organic solvents and 2)

provides a reversible process that can be optimized and controlled.[71,134] Polyanions such as sodium tripolyphosphate, sodium polyphosphate and sodium sulfate have been investigated for cross-linking chitosan chains. However, chitosan nanoparticles fabricated using ionic gelation have stability issues. For examples, chitosan gel nanoparticles formed by ionic interactions of chitosan chains with tripolyphosphate were found to be extremely labile to environmental conditions such as pH and salt content.[135] Changes in pH values affect the swelling of particles; the more acidic the solution, the larger the diameter of chitosan particles due to the intra-molecular electrostatic repulsions. Also, particle aggregation has been observed in basic pH solutions. Salt content, on the other hand, caused particle disintegration due to swelling of the particle as a result of the difference in osmotic pressure.[135]

Gelatin, an example of a polyanion used for the fabrication of chitosan composites, was incorporated with chitosan to fabricate tissue regeneration scaffolds.[136] In the presence of gelatin, mechanical properties of chitosan membranes were significantly affected. Gelatin caused the stiffness of chitosan membranes to decrease in dry conditions but to increase significantly in wet conditions, despite the fact that gelatin possesses very low stiffness relative to chitosan in wet conditions.[136] In addition, the presence of gelatin enhanced the degradation rate and maintained the dimensions of the membranes in the presence of lysozymes.[136] *In vivo* study was performed by isolating autologous chondrocytes from pig's auricular cartilage and seeding them onto chitosan-gelatin scaffolds. This scaffold was successfully engineered into elastic cartilages that have acquired not only normal histological and biochemical, but also mechanical properties after 16 weeks of implantation.[137]

γ-Poly (glutamic acid) (γ-PGA), a hydrophilic and biodegradable polymer, was used to produce γ-PGA/chitosan composite biomaterials in order to enhance the hydrophilicity and cytocompatibility of chitosan-based matrices.[138] To prepare this composite, chitosan powder was uniformly dispersed in γ-PGA solution in water,

followed by the addition of acetic acid which caused the chitosan powder to immediately dissolve, thus avoiding aggregation caused by γ-PGA/chitosan polyion complexes and forming a homogeneous solution. Dense films were prepared by drying in the oven, whereas porous films were prepared by freeze-gelation. It was found that the porous matrices have an interconnected pore structure with a pore size of 30 to 100 μm. The addition of γ-PGA increased the maximum load (strength) of the composite matrices. Also hydrophilicity and serum protein adsorption properties of the composite matrices were significantly enhanced. Cytocompatibility of γ-PGA/chitosan composites was enhanced as shown by increased ROS cell attachment and proliferation when compared to chitosan matrices. This makes γ-PGA/chitosan composite matrix a very promising biomaterial for tissue engineering applications.[138]

Collagen/chitosan scaffolds were prepared in order to overcome the fast biodegradation rate and the low mechanical strength of untreated collagen scaffolds for skin regeneration purposes. The scaffolds were fabricated by mixing the two polymers followed by lyophilization in cold ethanol. Finally, the two polymers were cross-linked with glutaraldehyde. Confocal laser scanning microscopy (CLSM) images of FITC-chitosan and rhodamine-collagen confirmed that the scaffold was composed of chitosan and collagen filaments which were evenly dispersed throughout the scaffold. Cross-linking with glutaraldehyde resulted in larger pore sizes and in less biodegradability compared to collagen alone, in addition to higher tensile strength compared to uncross-linked chitosans. However, the wettability also decreased significantly, as shown by the swelling test of the different scaffolds.[139] It appears that chitosan/collagen composites are promising scaffold materials for periodontal tissue engineering, as well as for dermal equivalents.[139]

Chitosan-alginate composites were studied for potential uses as scaffolding materials, especially for cartilage repair and regeneration.[140] Chitosan and alginate solutions were prepared separately by dissolving chitosan and sodium alginate in

1N acetic acid and NaOH, respectively, and then mixing the two solutions together. The lyophilized discs were then cross-linked by immersion in 1% w/v $CaCl_2$ solution. The cells increased consistently on both chitosan and chitosan-alginate scaffolds over cell culture time, and proliferated faster on the chitosan-alginate scaffold than on the chitosan scaffold. Furthermore, the cell viability assay revealed more live cells on chitosan-alginate than on pure chitosan. These results are due to the known property of alginate to promote cell expansion; which augmented chitosan's excellent cell adhesive property due to its cationic nature. Thus, chitosan-alginate hybrid materials may have combined favorable properties of chitosan and alginate in terms of cellular attachment and proliferation.[140] In addition, chitosan-alginate composites in the form of nanoparticles were prepared in mild aqueous conditions through ionic gelation, driven by the electrostatic interactions between the two species.[141] The prepared nanoparticles had small size and narrow distribution. Particles had a mean *Z*-average diameter of ca. 157 nm and a zeta potential of 32 mV. Chitosan-alginate nanoparticle-mediated transfection of HEK293T cells resulted in transfection levels as high as achieved with Lipofectamine™ after 48 h. Transfection efficiency of complexes prepared at a 5:1 N/P ratio was higher than with chitosan nanoparticles or naked plasmid. The improvement in transfection efficiency was explained by the presence of alginate which reduces the interaction strength between chitosan and DNA but does not prevent it, helping the dissociation of the complexes inside the cells.

One of the macromolecules that shows a great practical potential for complexing with chitosan for forming composites is dextran sulfate (Figure 1-3).[132,142] Dextran sulfate, a biodegradable polymer similar to heparin, contains approximately 17% sulfur, which is equivalent to approximately 2.3 sulfate groups per glucosyl residue. Dextran sulfate is derived by esterification of dextrans using sulfuric acid. Dextran is a polymer of anhydroglucose and is composed mainly of alpha-D-(1-6) linkages and a small percentage of (1-3) linkages that account for the branching of dextran. Most

commercially available dextrans are obtained from *Leuconostoc mesenteroides*. Some of the dextran sulfate applications include lipoprotein separation, accelerating hybridization, releasing DNA from DNA-histone complexes and inhibiting ribonucleases. Dextran sulfate showed potential to be used as antiviral agent and for enzyme and protein stabilization, as well as in cosmetic preparations.

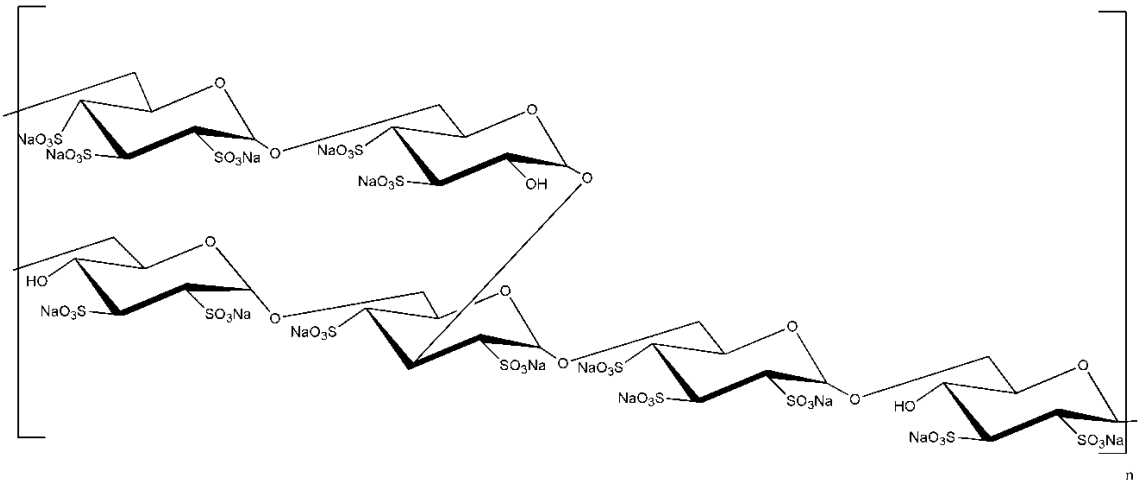

Figure 1-3. Molecular structure of dextran sulfate.

The mechanism of formation of colloidal PECs from chitosan and dextran sulfate depends on which species is in excess. When dextran sulfate is in excess, Drogoz et al. proposed that the two polymers interact to form primary complexes, which rearrange to form colloidal species.[121] In this case, the mechanism of polymer interaction depends on chitosan molecular weight. For low molecular weight chitosans, a residue-to-residue mechanism was proposed, which results from the guest-host model introduced by

Kabanov.[121,143] This requires large difference of molecular weights between the two polymers and a stiff guest polymer. On the other hand, using high molecular weight chitosans and when chitosan is in excess, charge-to-charge neutralization predominates.[143]

Chitosan-dextran sulfate PECs have been studied for a wide range of applications, mainly for peptide delivery, such as anti-angiogenesis,[144] hexapeptide dalargin[145], repifermin (R)[146], HIV-1 p24 antigen [147] and insulin.[148] In addition, chitosan-dextran sulfate PECs have been studied for delivery of small molecules such as amphotericin B.[149]

1.5.3 Modifications via avidin-biotin

Biotin, hexahydro-2-oxo-1*H*-thieno[3,4-d]imidazole-4-pentanoic acid or vitamin H, is a naturally occurring vitamin found in all living cells. The tissues with the highest amounts of biotin are the liver, kidney and pancreas. Cancerous tumors have more biotin than normal tissue.[150] Biotin is involved as an enzyme cofactor in a variety of carboxylase, decarboxylase and transcarboxylaze reactions,[151-153] and is known to have a strong affinity to a number of proteins, such as avidin and streptavidin.

Avidin is a tetrameric glycoprotein which was originally isolated from chicken egg white and is found in the tissues of birds. Avidin has four identical subunits, which consist of 128 amino acids each. The reported molecular weight of avidin ranges from 66-69 kDa depending on the method of analysis. Avidin is soluble in aqueous solutions and stable over a wide pH and temperature range. Early work involving avidin-biotin chemistry centered on biotin's function as a vitamin, yet in 1927, rats fed large quantities of egg white developed dermatitis, indicating malnutrition. Vitamin H, structurally identified as biotin in 1940, prevented this dermatitis. The malnutrition induced by avidin was eventually attributed to the depletion of biotin.[154]

The avidin-biotin interaction is the strongest known non-covalent, biological interaction between a protein and a ligand (K_d for avidin-biotin complex $=10^{-15}M^{-1}$). The binding capacity of avidin is 4 moles biotin to 1 mole avidin. Bond formation is very rapid and once formed is unaffected by wide extremes of pH, temperature, organic solvents and other denaturing agents. The avidin-biotin complex is also resistant to enzymatic proteolysis.

Avidin-biotin chemistry is popular for a broad range of technologies, such as diagnostic applications,[154] biosensoring[155] and affinity based separation.[156] Also, avidin-biotin technology has proved to be a versatile tool for a variety of pharmaceutical applications such as targeted drug delivery.[157]

As an example of applications of avidin-biotin technology, novel biotinylated nanotemplated degradable hydrogels that integrate cell interactivity into their surface were prepared.[158] These kinds of modifications are critical in the development of biomaterials for drug delivery and tissue engineering applications.

Biotin modification has been applied to several polymers, including poly(styrene-co-N-acryloxysuccinimide),[159] poly(ethylene glycol) (PEG)-ylated polyethyleneimine,[160] PEG-poly[lactic-co-(glycolic acid)] (PLGA)[161] and poly(lactic acid)-PEG.[162] This method has been studied only in a limited way for natural polymers such as chitosan. For instance, avidin-biotin interaction has been applied to prepare chitosan supports for protein electrodeposition by Shi et al.[163] Chitosans modified using this technique have potential for a vast range of applications in different biomedical fields. Nonetheless, utilizing the numerous advantages of this polymer using this technique necessitates studying chitosan biotinylation reaction, ligand attachment conditions and fabrication methods.

1.6 Objectives

As discussed above, chitosan has been investigated for gene delivery, tissue engineering and enzyme immobilization, among other biomedical applications. Despite the well known advantages of exploiting chitosan in these fields, additional work needs to be done to optimize chitosan's formulations and to enhance its physicochemical properties for different uses. An example of a vital approach to improve chitosan's properties is modifying chitosan chains with different ligands. This research investigates the formulation of chitosan particles and films for different applications and presents a novel method for modifying chitosan via avidin-biotin interaction, as explained in the following objectives and specific aims:

Objective 1: Optimization of formulation parameters of chitosan nanoparticles and films for different applications.

Specific Aim 1.1: Prepare chitosan samples with different degrees of deacetylation and molecular weights and characterize the prepared chitosans.

Specific Aim 1.2: Optimize the formulation of chitosan nanoparticles intended for gene delivery purposes using ionic gelation method by testing the effect of the inclusion of different polyanions, especially dextran sulfate on the efficiency of gene delivery. The target particle sizes were to be less than 0.2 μm in order to ensure longer circulation time and better cellular uptake. The target zeta potential values were to be more than 20 mV to ensure the stability of particles. Chitosan particles were designed to be able to completely condense DNA, protect it from the surrounding environment and be able to release it inside cells.

Specific Aim 1.3: Optimize the formulation of chitosan nanoparticles intended for enzyme immobilization purposes using precipitation/coacervation method. The target particle sizes were to be less than 1 μm and the target zeta potential values were to be more than 20 mV. Chitosan particles were designed to be stable and easily separable from the reaction media.

Specific Aim 1.4: Optimize the fabrication of chitosan films intended for enzyme immobilization and tissue engineering purposes using dry-casting. Chitosan films were designed to be stable, resistant to disintegration and have controllable degradation behavior.

Objective 2: Biotinylation of chitosan to provide a rapid and facile method for the addition of biomolecules for different purposes in mild aqueous environments by utilizing avidin linking.

Specific aim 2.1: Test the feasibility of biotinylating chitosan films and nanoparticles as well as chitosan solutions using N-hydroxysuccinimide chemistry and assess the extent of the biotinylation of chitosan using HABA/avidin assay.

Specific aim 2.2: Control the degree of biotinylation via controlling the degree of deacetylation of chitosan, type and concentration of biotinylation agent, concentration of chitosan and pH of the reaction buffer.

Objective 3: Engineering chitosan nanoparticles with cell recognition peptides (RGD sequence) and dispersion stabilization molecules (PEG) using avidin-biotin interaction to improve the gene delivery capabilities of chitosan.

Specific aim 3.1: Demonstrate the feasibility of ligand attachment on chitosan nanoparticles by surface and bulk modifications.

Specific aim 3.2: Assess the effect of RGD and PEG on the transfection efficiency of chitosan's nanoparticles *in vitro* using HEK293 cells.

Objective 4: Engineering chitosan surfaces with enzymes, such as trypsin, using the avidin-biotin interaction to serve as mild and effective immobilization technique.

Specific aim 4.1: Biotinylate trypsin using N-hydroxysuccinimide chemistry.

Specific aim 4.2: Immobilize trypsin on biotinylated chitosan films and nanoparticles using avidin linker and compare this technique to other immobilization methods.

Specific aim 4.5: Demonstrate the effect of trypsin immobilization on its activity and stability in different buffers and at high temperatures using casein as a substrate.

Objective 5: Engineering chitosan with cell adhesive molecules (RGD sequence) and cell repellant molecules (PEG) using avidin-biotin interaction to increase or decrease cell attachment and proliferation, respectively.

Specific aim 5.1: Assess the effect of batch-to-batch variations of chitosan and the purification methods on cell attachment onto non-treated chitosan films.

Specific aim 5.2: Assess the effect of glutaraldehyde cross-linking and using different neutralizing agents on cytotoxicity of chitosan films.

Specific aim 5.3: Assess adherence and viability of HEPM and HEK293 cell using MTT assay.

Specific aim 5.4: Assess cellular attachment on PEGylated chitosan and RGD treated chitosan films.

CHAPTER 2
EFFECTS OF POLYANION INCLUSION ON THE VECTOR PROPERTIES OF CHITOSAN BASED NANOPARTICLES

2.1 Introduction

Gene therapy is a modern technology that has been expected to offer solutions to a number of diseases, hereditary and acquired, due to its potential to treat the causes of abnormalities rather than symptoms.[164,165] However, gene therapy approaches have been hampered by the limitations of the current gene delivery methods, viral and non-viral. Hydrophilic and biodegradable polymers have been suggested as effective carriers to overcome the hurdles of gene therapy. These polymers have the potential to protect DNA from the extra- and intra-cellular environment, to transport large plasmids, to be ligand-modified for targeting and to facilitate the engulfment of the DNA by cells. Moreover, these polymers offer important manufacturing advantages such as the simplicity of fabrication in mild aqueous conditions and the ability to control the sizes and charges of particles.[166,167] Chitosan, atelocollagen and poly-L-lysine (PLL) are examples of hydrophilic biodegradable polymers that have been investigated for gene and drug delivery.[168-170]

Chitosan, a natural linear polysaccharide that is composed of D-glucosamine and N-acetyl-D-glucosamine units, has the advantage of being biocompatible and biodegradable with low immunogenicity and toxicity compared to some synthetic polymers.[171] Since chitosan is a polycationic polymer in acidic and neutral pH solutions, it is able to form complexes with the negatively charged plasmid DNA. These nanoparticulate complexes are capable of transfecting cells more efficiently than naked plasmid DNA but have inferior transfection efficiency compared to synthetics polymers, such as polyethyleneimine (PEI), and to some liposomal formulations, such as lipofectamine™.

Hence, in order to improve chitosan's ability to deliver DNA, several modifications of chitosan have been reported in literature, such as conjugating PEG,[93] PEI[95] and galactose.[97] Although most modifications showed improvements in certain aspects of the gene delivery capabilities of chitosan nanoparticles, some modifications negatively affected other desirable properties of chitosan, such as the safety profile of this polymer. In addition, most of these modification methods require lengthy and difficult to control processes, which add complexity to the formulation of chitosan nanoparticles and lead to mixed conclusions regarding their applicability.

The aim of this research was to improve the gene transfection properties of chitosan nanoparticles while keeping their low toxicity and their formulation simplicity at the same time. This was achieved by targeting optimal interaction between DNA and chitosan via incorporating polyanions, such as tripolyphosphate and sulfate, modifying chitosan's strength of interaction with plasmid DNA and its ability to deliver DNA efficiently into cells.

Although the inclusion of different polyanions for gene delivery purposes within chitosan nanostructures has been reported in literature, using dextran sulfate has only been studied in a limited way for the delivery of proteins and drugs.[144,149] In this study, polyelectrolyte complexes between chitosan, dextran sulfate and DNA were thoroughly studied and the role of dextran sulfate in the efficiency of gene delivery was illustrated.

2.2 Materials and Methods

2.2.1 Purification of chitosans

Low molecular weight chitosans were obtained from Aldrich® (batches 06513AE, 61496MJ, 06714DJ, and 13604PC). Various grades of chitosan were purified by either one of three methods: 1) cleaning the samples by the removal of insoluble particles only, 2) more through washing by dialysis, or 3) extensive purification. In all the three cases, insoluble particles were removed first by dispersing chitosan in distilled water and then

solubilizing it by the addition of acetic acid (final concentration was 1% (w/v) chitosan in 1% (v/v) acetic acid), followed by filtering the solution through Whatman® filter paper grade 541 (particle retention in liquids equals 22 µm with over 98% efficiency). In the first method, this solution was used directly assuming the concentration remained constant (1% (w/v) or 10 mg/ml). In the second method, chitosan was precipitated from filtered chitosan solution by titration with 1 N NaOH until pH value of 8.5. This was followed by centrifugation and resuspending of chitosan in distilled water. Chitosan suspensions were then dialyzed against distilled water for 2 days using Pierce SnakeSkin® pleated dialysis tubing (molecular weight cut-off (MWCO) = 10,000), changing the water three times. Finally, chitosan suspensions retrieved from the dialysis tubes were frozen at -80^{o}C and lyophilized in a Labconco FreeZone 4.5 Liter freeze dry system (chamber pressure of less than 0.02 mbar and collector temperature of less than -50°C).

In the third method, chitosan was extensively purified by deproteinization, decolorization and demetallization in the presence of reducing agent, in order to provide more consistency and reproducibility between chitosan batches for biomedical applications. Filtered chitosan solutions (equivalent to 1 g in 1000 ml of 1 % (v/v) acetic acid solution) were heated to 40°C while stirring for 15 min and then centrifuged for 1 h at 8,500 rpm using Fisher accuSpin 400 provided with 45° fixed-angle rotor, and then decanted to remove insoluble particulates. Washing of chitosan was then done by first precipitating chitosan through dropwise titration with 1 N NaOH with stirring, until the pH of the suspension reached 8.5, then centrifugation and resuspending with fresh distilled water several times. This was followed by the addition of 1 ml of 10% w/v aqueous solution of sodium dodecyl sulfate (SDS, RPI, IL) and stirring for 30 min. Dithiothreitol (DTT, EMD) was added directly to chitosan solution and the mixture was heated at 90-95^{o}C with stirring for 5 min in the hood. After leaving the solution stirring at room temperature overnight, 3.3 ml of 5% w/v ethylenediaminetetraacetic acid (EDTA,

Sigma®, MO) was added and stirred at room temperature for 2 additional hours. The water insoluble chitosan precipitate was collected by centrifugation at 4,300 rpm for 30 min using Fisher accuSpin 400 and washed several times with distilled water by resuspending and re-centrifugation for 30 min. Chitosan was resuspended in distilled water and dialyzed for 2 days using Pierce SnakeSkin® pleated dialysis tubing 10,000 MWCO, changing the water three times. Finally, chitosan suspensions retrieved from the dialysis tubes were frozen at -80^{o}C and lyophilized in a Labconco FreeZone 4.5 Liter freeze dry system(chamber pressure of less than 0.02 mbar and collector temperature of less than -50°C).[172]

2.2.2 Chitosan reacetylation and depolymerization

Chitosans with various combinations of characteristics regarding molecular weight and degree of deacetylation were prepared and tested to see the effect of these parameters on the efficiency of the gene delivery.

Reacetylation of the commercially available chitosans (reported degree of deacetylation = 90.8%) was carried out by a heterogeneous acetylation reaction using acetic anhydride.[82] Chitosan (0.4 g) was dissolved in 8 ml 2% aqueous acetic acid, followed by dilution with 10 ml water. Twenty milliliters of methanol was then mixed with chitosan solution. Based on the calculations discussed in the Appendix (section A.1), acetic anhydride was added and the mixtures were stirred at room temperature overnight. Chitosans were then precipitated with 1N NaOH, washed extensively with aqueous methanol and finally freeze-dried.

Degree of acetylation was determined using first derivative UV spectrophotometry (1DUVS) and the analyses was performed using Hewlett Packard (HP 8453A) diode array spectrophotometer. Calibration curves were plotted using N-acetyl glucosamine (NAG, Sigma®, MO) dissolved in 0.01 M acetic acid solutions. 1DUVS method and theory is described in details in the Appendix, section A.1.

Depolymerization of the commercially available low molecular weight chitosans was done using sodium nitrite ($NaNO_2$) (Sigma®, MO). Aqueous solutions that contain the desired amounts of sodium nitrite (1, 1.5, 2 and 4% w/w relative to chitosan's weight) were added drop wise to solutions of chitosan dissolved in 2% aqueous acetic acid at 4°C with stirring. The solutions were stirred for 5 h at room temperature and then neutralized with 1N NaOH. Chitosan precipitates were collected by centrifugation at 10,000 rpm for 20 min and the precipitates were washed with distilled water until the pH of the supernatant is similar to that of the water.[109,173] The intrinsic viscosities of the resulting chitosans were determined using an Ostwald 100 viscometer (Fisher Scientific, PA) and the viscosity average molecular weights were calculated from intrinsic viscosities using Mark–Houwink–Sakurada equation ($K = 1.4 \times 10^{-4}$ and $a = 0.83$).[174] The importance of chitosan's molecular weight and the calculation of viscosity average molecular weights are discussed in the Appendix, section A.2.

2.2.3 Competition binding and polyanionic displacement assays

The complexation of DNA (UltraPure™ salmon sperm DNA solution (10 mg/ml), Invitrogen™, CA) with chitosan was studied by recording the fluorescence obtained with the fluorescent probe ethidium bromide (EtBr, Sigma®, MO). Fluorescence of EtBr was measured in polypropylene 96 well plates (Corning® Costar® 96 well flat bottom cell culture plates) using a SpectraMax® M5 multi-mode microplate reader (Molecular Devices, CA). EtBr was added to each well and mixed with DNA solution (final concentrations were 2.5 μg/ml and 10 μg/ml, respectively). Solutions of different grades of chitosan (HM-HD, MM-HD and LM-HD) were added at increasing chitosan's cationic to DNA's anionic charge ratios (N/P ratios) and mixed well. Also, dextran sulfate (5 kDa) was mixed with the DNA solution followed by adding LM-HD chitosan at different N/P ratios. Fluorescence intensities were measured at an excitation wavelength of 519 nm and

emission spectra from 580 to 630 nm were recorded. The maximum fluorescence intensities within the recorded emission spectra were obtained and normalized relative to the average fluorescence signal of DNA-EtBr without the added polycation. Prior to fluorescence measurement of all samples, a 3 min incubation time was applied following each addition. In order to obtain an exact N/P ratio, the molecular weights of the protonable repeating units in chitosan (glucosamine) was calculated from the measured molecular degree of deacetylation as shown in the Appendix, section A.1. The molecular weight of the repeating unit in PEI is 43.07 Da, calculated from the empirical formula of these units (C_2H_5N), whereas the average molecular weight of the phosphate groups of DNA used for calculations is 330 Da.

To investigate the compaction of DNA by chitosan and the effect of exposing the polyplexes to other polyanions, fluorescence signals were recorded after each stepwise addition of three polyanion species, dextran sulfate, tripolyphosphate or sodium alginate, at 3 min time intervals. Polyanions compete with DNA for the polycation and cause a decomplexation and release of DNA from the polyplexes, increasing EtBr fluorescence signal upon intercalation with the exposed DNA. The effect of dextran sulfate grade (molecular weights of 5, 20 and 500 kDa) on the complexation of chitosan with DNA was investigated in a similar way. Results from 3 independent experiments were averaged. Optimization of the EtBr assay is discussed in the Appendix, section A.5.

2.2.4 Preparation of chitosan/pDNA nanoparticles

Chitosan/pDNA nanoparticles were prepared through the complex formation between the two oppositely charged polyelectrolytes, chitosan and DNA. Phase separation occurred under defined conditions as a result of the macromolecular interaction to yield coacervates that represented the aggregated colloidal complexes. Different polyanions were included as desolvating agents to facilitate the phase separation through the removal of the associated water layer from around the dissolved

colloidal chains. This method for fabricating chitosan nanoparticles is called the ionic gelation method.[175] Chitosan nanoparticles were formulated at various ratios of chitosan's nitrogen to pDNA's phosphate groups (N/P ratios). As a positive control, branched polyethyleneimine (PEI)/pDNA nanoparticles were formulated at an N/P ratio of 10. Stock solutions of DNA and polyanions were prepared in distilled water, and chitosan solutions were prepared in 1% (v/v) aqueous acetic acid. In order to prepare nanoparticles, cationic solutions containing chitosan or PEI and anionic solutions containing DNA and/or polyanion were prepared separately by pipetting the calculated volumes from stock solutions and then diluting them with the different studied buffers. Concentrations of chitosan, DNA and polyanions were calculated based on the final concentrations in the preparation solution. In a typical formulation procedure, cationic solutions were transferred into the anionic solutions containing pDNA using a micropipette and mixed by pipetting up and down several times. Solutions were then mixed by vortex for 10 seconds and left at room temperature for 15 min to equilibrate before using. Different formulation parameters were studied, including buffer type, pH of the preparation solution, volume ratios of the cationic and anionic solutions, the order of addition of the two solutions, cryoprotectant use and the concentration of different components. Dextran sulfate (DS, reported molecular weights of 5, 6.5-10, 9-20 and 500 kDa, Sigma®, MO), sodium tripolyphosphate (TPP, Sigma®, MO), sodium alginate (SA, alginic acid sodium salt from brown algae, reported molecular weight of 240 kDa, Sigma®, MO), sodium sulfate (SS) and sodium hyaluronate (SH, hyaluronic acid sodium salt from *Streptococcus equi*, reported molecular weight of 1.63×10^3 kDa, Fluka®, Switzerland) were used for ionically cross-linking chitosan chains. Salmon sperm DNA (UltraPure™ salmon sperm DNA solution (10 mg/ml), Invitrogen™, CA) was used as the polynucleotide of choice for the stability studies of nanoparticles, whereas plasmid DNA encoding luciferase (VR1255) was used as the model polynucleotide for the *in vitro* gene delivery studies. Chitosan formulations were lyophilized by mixing equal volumes of

these formulations with cryoprotectant solutions. Sucrose, mannitol and sorbitol were used as cryoprotectants at final concentration of 1, 5, 7.5 and 10% (w/v).

2.2.5 Determination of particle sizes and zeta potential values

Size measurements of nanoparticles were conducted using a Zetasizer Nano ZS particle analyzer (Malvern, UK). This instrument performs size measurements using dynamic light scattering (DLS). Briefly, nanoparticles were suspended in the studied buffers at a concentration of 1 mg/ml using vortexing for 5 seconds. Size measurements were performed at 25°C at a 173º scattering angle and the mean hydrodynamic diameters were determined by cumulative analysis. Zeta potential determinations were based on electrophoretic mobility of the nanoparticles in aqueous medium after applying Henry's equation. Electrophoretic mobility was obtained by subjecting samples to electrophoresis and measuring the velocity of particles using laser Doppler velocimetry (LDV). Zeta potential measurements were performed using folded capillary cells (Malvern, UK) in automatic mode.[176] The theory of zeta potential and particle size analysis is discussed in the Appendix, sections A.3 and A.4, respectively.

2.2.6 Stability of chitosan formulations

Chitosan nanoparticles were prepared by ionic gelation method as mentioned above at DNA concentration of 10 μg/ml using either dextran sulfate or TPP as polyanions, in a range of pH values. Different chitosan to pDNA N/P ratios, chitosan/polyanion weight ratios and various molecular weight grades of dextran sulfate were investigated in order to find their effect on the stability of chitosan particles. Anionic buffers used to prepare and store chitosan formulations were sodium acetate (pKa = 4.46, Sigma®, MO) and sodium phosphate (pKa_2 = 7.2, Sigma®, MO), whereas the cationic buffers used were Tris (2-amino-2-hydroxymethyl-propane-1,3-diol, pKa = 8.06 at 25°C, RPI, IL) and Bis-Tris (2-[bis(2-hydroxyethyl)amino]-2-

(hydroxymethyl)-1,3-propanediol, pKa = 6.45-6.65 at 25°C, RPI, IL). All buffers were prepared at 500 mM concentration and 154 mM ionic strength adjusted by NaCl. Electrical states of the ionizable groups on chitosan nanoparticles were studied by measuring the electrophoretic mobility of particles, represented by zeta potential, as a function of time, buffer type and pH, and polyanion inclusion.

2.2.7 Microscopic imaging

The morphologies of chitosan nanoparticles were studied using transmission electron microscopy (TEM), atomic force microscopy (AFM) and scanning electron microscopy (SEM).

TEM images were taken by JEOL 1230 transmission electron microscope provided with Gatan UltraScan 1000 2k x 2k CCD camera. TEM beam current was used at accelerating voltage of 120 kV. Suspensions of chitosan nanoparticle were prepared by the ionic gelation method mentioned above. A drop of each suspension was left on a carbon coated Formvar film on 400-mesh TEM copper grid for 10 min. Then, filter paper was used to withdraw any excess liquid. Uranyl acetate was used for negatively staining the chitosan nanoparticles by adding 1 drop of 1% (w/v) uranyl acetate dissolved in water to each grid for 30 seconds followed by the removal of the excess dye.

MFP-3D Asylum atomic force microscope (AFM, Asylum Research, CA) was used to further investigate the morphological properties of the chitosan nanoparticles. DNA stock solution (100 µg/ml) was prepared by diluting salmon sperm DNA or pDNA (VR1255) in 10 mM Tris/HCl and 1 mM EDTA buffer, pH 6.6. This solution was kept in a refrigerator for a maximum of 2 weeks until use. Just before imaging, the DNA solution was diluted further to 0.5 µg/ml using 5 mM $NiCl_2$/40 mM HEPES buffer (4-(2-Hydroxyethyl)piperazine-1-ethanesulfonic acid sodium salt, pH 6.6). Naked pDNA was fixed on a freshly cleaved mica film glued on a glass slide by leaving 5 µl droplet of the DNA solution to air dry. The mica film was then washed with distilled water and

dried under a stream of nitrogen gas. Suspensions of chitosan nanoparticles were left on a freshly cleaved mica film slide for 10 min. The excess liquid was taken off using filter paper and the sample was left to dry. The samples were scanned using AFM cantilevers (MikroMasch, CA) which have spring constants of 46 N/m and resonant frequencies of 325 Hz by tapping mode.

Surface morphologies of chitosan nanoparticles were assessed further by scanning electron microscopy (SEM, Hitachi S-4000). Suspensions of chitosan nanoparticles were left to air-dry on silica wafers mounted on SEM specimen stubs. The specimen stubs were sputter coated with approximately 5 nm of 60% gold 40% palladium ion by beam evaporation using E550 Emitech sputter coater set at 10 mA for 10 seconds and then the samples were examined under SEM operated at 2 kV accelerating voltage.

2.2.8 Determination of complex formation and integrity using gel electrophoresis

The formation of chitosan and PEI polyplexes was determined by their electrophoretic mobility using agarose gel electrophoresis. This test is based on the same principal as the competition binding assay using EtBr for intercalation with DNA. Sample solutions or suspensions, mixed with 10% 10X BlueJuice™ gel loading buffer (Invitrogen™, CA), were analyzed on a 0.8% (w/v) agarose gel stained with 0.5 µg/ml of EtBr and immersed in Tris-acetate-EDTA buffer (TAE) (0.04 M Tris, 0.02 M acetate and 1 mM EDTA pH 8.3). The gel electrophoresis was performed at a constant 80 V for 60 min. Gels were then visualized on a UV illuminator (Spectroline®, NY) in order to monitor the mobility of the DNA. Pictures were taken using a digital camera. Nanoparticles were fabricated using 3 grades of chitosan (LM-HD, MM-HD and MM-LD) to study the effect of molecular weight and degree of deacetylation (chitosan/DS w/w ratio of 10) on DNA complexation. LM-HD chitosan-DS/DNA nanoparticles were studied further at different N/P ratios (0.5, 1, 2, 3, 5 and 10) and at

different chitosan/DS w/w ratios (5, 10, 15 and 20). Also LM-HD chitosan/DNA nanoparticles prepared with sodium hyaluronate, sodium tripolyphosphate, sodium sulfate and sodium alginate were studied using gel electrophoresis.

Gel electrophoresis was also used to study the DNA loading efficiency of chitosan polyplexes. Chitosan-DS/DNA nanoparticle solution (chitosan/DS w/w ratio of 10, N/P ratio of 15) was centrifuged using a Sorvall Discovery Hitachi 90SE ultracentrifuge provided with a T1270 rotor at 30,000 rpm for 60 min. Free DNA contents in the supernatant and in the resuspended nanoparticle pellet were determined by gel electrophoresis as mentioned above.

2.2.9 DNase protection assay

In order to evaluate the ability of chitosan formulations to protect DNA from nuclease degradation, deoxyribonuclease (DNase) I assays were performed. Briefly, 100 µl of chitosan nanoparticles (N/P ratio = 15) containing 1 µg of plasmid DNA were suspended in DNase and RNase free water and incubated with 3 µl DNase I amplification grade solution at a concentrations of 1 U/µl (Sigma®, MO) at 37°C for 60 min. The reactions were terminated by the addition of quenching solution containing 100 mM EDTA and 400 mM NaOH (pH 8). Finally, 5 µl of 20% (w/v) sodium lauryl sulfate (SDS) solution was added and the mixture was further incubated at 65°C overnight. After incubation, the mixture was analyzed on 0.8% (w/v) agarose gel stained with 0.5 µg/ml of EtBr at 80 V for 60 min as previously mentioned.

2.2.10 Cell culture

Human Embryonic Kidney cells (HEK293) and Monkey African Green Kidney cells (COS7) were purchased from American Type Culture Collection (ATCC®, MD). The cells were maintained in 75 cm^2 tissue culture flasks (Corning® Costar®, MA) and supported with Modified Eagle's Minimum Essential Media (EMEM modified to contain Earle's balanced salt solution, non-essential amino acids, 2 mM L-glutamine,

1 mM sodium pyruvate, and 1500 mg/L sodium bicarbonate) supplemented with 10% (w/v) fetal bovine calf serum (FBS) (Gibco™ Invitrogen™, NY), antibiotic-antimycotic (ABAM) that consists of 0.5% penicillin and 0.5% streptomycin (Sigma®, MO) and 1% (w/v) L-glutamine. The cells were kept in a humidified incubator at 37°C and 5% CO_2.

Subcultivation was done in a ratio of about 1:6 every 5 days or when confluence was 90% reached, whichever comes first. Old culture media was first removed and discarded, followed by rinsing with phosphate buffered saline (PBS) to remove all traces of serum that contained trypsin inhibitors. Then, cell culture flasks were incubated with 3 ml of 0.25% (w/v) trypsin-0.53 mM EDTA solution (Gibco™ Invitrogen™, NY) and placed at 37°C to facilitate cell dispersal. Flasks were consistently observed under an inverted microscope (Nikon TMS) until even cell dispersion was achieved (usually within 5 to 15 min). Agitation of cells by hitting or shaking the flask while waiting for cells to detach was avoided in order to prevent cellular clumping. EMEM (10 ml) was added to the flask and the cells were aspirated by gentle pipetting. Appropriate aliquots of the cellular suspension were added to new culture vessels and the cultures were incubated at 37°C in 5% CO_2 incubator.

2.2.11 Cytotoxicity evaluation using the MTT assay

Cytotoxicity of different polymers and nanoparticles was evaluated using the MTT assay (3-[4,5-dimethylthiazol-2-yl]-2, 5-diphenyl tetrazolium bromide, Sigma®, MO) as described in the Appendix, section A.6. Chitosan/pDNA nanoparticles were prepared as mentioned above using dextran sulfate, 5 and 500 kDa, or TPP, at chitosan to polyanion w/w ratio of 10 and N/P ratio of 25. Similarly, the cytotoxicity of solutions of chitosan, high and low molecular weight dextran sulfate and TPP was evaluated. PEI/pDNA polyplexes were also tested for comparison. COS7 and HEK293 cells were seeded in 96-well plates (Corning® Costar®, MA) at a density of 1×10^4 cells per well. Twenty-four hours later, cells were incubated with 200 µl of complete DMEM containing

chitosan/pDNA nanoparticles, PEI/pDNA nanoparticles or polymer solutions at various concentrations. After 4 h of incubation, the medium in each well was replaced with 100 µl of fresh, phenol-free complete medium containing MTT at a concentration of 1 mg/ml. The MTT solutions were incubated with cells for an additional 2 h at 37°C. In order to reduce uneven evaporation of the wells, Parafilm M plastic wraps were used to cover the edges of microplates during incubation with MTT solution. Cells were then lysed with 100 µl of MTT solubilization solution (extraction buffer containing 10% Triton X-100 plus, 0.1 N HCl in anhydrous isopropanol) for 15 min. Gentle mixing and trituration by pipetting up and down were done to help dissolve MTT formazan crystals. The optical densities of the lysate were measured at 570 nm using a SpectraMax® Plus^{384} microplate reader (Molecular Devices, CA). The background absorbance of multi-well plates was measured at 690 nm and subtracted from the absorbance at 570 nm. Values were expressed as a percentage of the control wells in which only media without formulations were added.

2.2.12 Amplification and purification of plasmid DNA

The firefly luciferase gene was used as a reporter gene to monitor gene expression. The plasmid DNA (pDNA) encoding firefly luciferase is a 6.4-kb complementary DNA driven by the cytomegalovirus (CMV) promoter/enhancer and is called VR1255.

In order to transform pDNA in *Escherichia coli* Subcloning Efficiency™ DH5α™ Competent cells (Invitrogen™, CA), an aliquot of DH5α (100 µl) was mixed with stock plasmid DNA and incubated on ice for 15-30 min. This was followed by heat shocking the bacteria at 42°C for 60 seconds and additional incubation on ice for 30 min. Then DH5α cells were mixed with SOC medium (super optimal broth with catabolite repression by glucose) and then spread on a pre-warmed kanamycin containing lysogeny

broth (LB) agar plates using glass beads. Agar plates were placed in the incubator at 37°C upside down overnight.

pDNA was amplified and purified by an endotoxin-free QIAGEN Mega plasmid purification kit according to the manufacturer protocol (QIAGEN, Valencia, CA).[177] A single colony was picked from a freshly streaked selective plate and used to inoculate a starter culture of 5 ml LB medium containing kanamycin and incubated for approximately 8 h at 37°C with vigorous shaking (300 rpm). The starter culture was diluted 500 times in LB medium and kept to grow at 37°C for 16 h with vigorous shaking (300 rpm). The target final cell density was approximately 3-4×10^9 cells per milliliter (corresponding to ~ 3 g pellet/liter medium).The bacterial cells were harvested by centrifugation at 6000 × *g* for 15 min at 4°C (Beckman Instruments, CA). Bacterial pellets were resuspended completely by vortexing or pipetting up and down in 10 ml resuspension buffer containing 50 mM Tris•Cl, pH 8.0, 10 mM EDTA and 100 μg/ml RNase A until no cell clumps remained. Bacterial pellets were then lysed using 10 ml lysis buffer containing 200 mM NaOH, 1% (w/v) SDS over ice for 5 min. Precipitation of cell debris, genomic DNA and proteins was done by vigorously mixing the lysate with 10 ml of chilled 3.0 M potassium acetate, pH 5.5, buffer followed by incubation on ice. The supernatants were separated from the fluffy white materials by centrifuge at 20,000 × *g* for 30 min at 4°C. Supernatants were then applied to the QIAGEN-tip 500 and allowed to enter the resin by gravity flow. QIAGEN-tips were washed twice with 30 ml washing buffer containing1.0 M NaCl, 50 mM MOPS, pH 7.0, and 15% (v/v) isopropanol. The DNA was then eluted with elution buffer containing 1.25 M NaCl, 50 mM Tris HCl, pH 8.5 and 15% (v/v) isopropanol. Finally, the DNA was precipitated by adding 10.5 ml (0.7 volumes) room-temperature isopropanol to the eluted DNA and centrifuged immediately at 15,000 × *g* for 30 min and at 4°C, followed by washing with 70% (v/v) ethanol. Purified pDNA was dissolved in Tris-EDTA solution and its purity

and concentration were determined by UV absorbance at 280 and 260 nm, respectively. The plasmid DNA structure was confirmed by gel electrophoresis.

2.2.13 *In vitro* transfection efficiency testing

Evaluation of luciferase expression was done in HEK293 and COS7 cell lines. Cells were seeded into 24-well plates at a density of 1×10^6 cells/well 24 h before transfection. Different formulations were prepared to contain 1 µg of pDNA/well in the corresponding buffers. Serum-free transfection was done by first changing the cell media with pre-warmed fresh media which did not contain FBS. Then 50 µl of the pDNA-containing formulations suspended in serum-free transfection medium was added and incubated for 4 h at 37ºC. This was followed by changing the media into a serum-containing medium and incubating the plate further for 44 h. After the incubation period, cells were treated with 200 µl of lysis buffer (Promega®, WI). The lysate was then subjected to two cycles of freezing and thawing, then transferred into 1.5 ml tubes (Eppendorf) and centrifuged at 13,200 rpm for 5 min using Eppendorf 5810R centrifuge. Twenty microliters of supernatant were mixed with 100 µl of luciferase assay reagent (Promega®, WI) and samples were measured on a luminometer for 10 seconds (Lumat LB 9507, EG&G Berthold, Germany). Luciferase activities were expressed as the normalized relative light units (RLU) relative to protein contents in the cell extracts measured by a micro bicinchoninic acid (BCA) using Pierce® protein assay kit (Thermo Scientific®, IL) (RLU/mg protein). The data were reported as mean ± standard deviation for triplicate samples. Every transfection experiment was repeated at least twice.

2.2.14 DNA vaccination

Chitosan nanoparticles were prepared as mentioned above with some modifications. Briefly, 2% depolymerized LM-HD chitosans (viscosity average molecular weight = 42.4 kDa) were used for preparing nanoparticles. Either plasmid DNA encoding ovalbumin (pOva), ovalbumin from chicken egg white (Ova) (Sigma®,

MO) or both were dissolved in Dulbecco's Phosphate Buffered Saline (DPBS) buffer and mixed with dextran sulfate or TPP to form the anionic solutions. Chitosan solutions were added to the anionic solutions and vortexed for 10 seconds using Vortex-Genie Mixers (VWR, IL) to form chitosan nanoparticles. Formulations were fabricated and suspended in acetate buffer (10 mM, pH of 5.75 and ionic strength of 154 mM adjusted using NaCl). Chitosan nanoparticles were prepared at chitosan/polyanion ratio of 10 and N/P ratio of 25. Suspensions of nanoparticles were left undisturbed for 15 min, followed by the addition of CpG-oligodeoxynucleotides (CpG-ODN) at a final concentration of 0.1 mg/ml to be adsorbed onto the nanoparticles. All solutions were sterile filtered before using and the preparations were performed under sterile environment in the laminar flow hood.

Animal experiments were conducted in accordance with the principles and procedures described in the University of Iowa's Guidelines for Care and Use of Experimental Animals. Female C57BL/6 6-8 week-old mice were obtained from Charles-River Laboratories and maintained in a pathogen-free environment. Mice were anesthetized using 100 µl of ketamine/xylazine mixture (17.5 mg/ml ketamine and 2.5 mg/ml xylazine) per mouse intraperitoneally (IP) using 1 ml BD™ U-100 insulin syringe with 28-gauge (28 G) x 1/2 inch insulin needles and were left until complete anesthesia was confirmed by the loss of the leg retraction response upon compression. This was followed by obtaining blood samples from mice submandibularly using 5 mm Goldenrod Animal Lancet (Medipoint) for the initial time point ELISA study. Mice were injected with different formulations subcutaneously (SQ) using insulin needles. *In vivo* tested formulations were chitosan-DS/pDNA encoding Ova, chitosan-DS/Ova, chitosan-DS/(pOva + Ova) and chitosan-TPP/(pOva + Ova) nanoparticles, and four mice per group were used. Solutions of Ova-encoding pDNA and ovalbumin protein dissolved in acetate buffer were used as negative controls throughout the study period in addition to pretreatment naïve mice. After initial vaccination, mice were given booster vaccinations

on days 14 and 28, and blood samples were withdrawn at these time points in addition to the last time point (day 35) when animals were euthanized using cervical dislocation after being anesthetized.

2.2.15 Quantification of antigen-specific antibody response by ELISA

To obtain serum, the coagulated blood samples obtained from mice at different time points were left to clot at room temperature for approximately 30 min. The completely clotted blood samples were centrifuged for 20 min at 10,000 rpm using Eppendorf 5810R centrifuge at 4°C and then the supernatant fluid (serum) was separated. Serum ovalbumin-specific IgG_1 and IgG_{2a} from mouse bleeds were determined using enzyme-linked immunosorbent assay (ELISA). Immulon 2HB microtiter plates (Thermo Scientific®, IL) which have high binding irradiated surface to provide increased binding affinity for hydrophilic proteins and complexes were coated with 100 µl/well of 5 µg/ml ovalbumin dissolved in PBS. The plates were sealed with a plastic tray-sealer and incubated for a minimum of 24 h and up to1 week at 4°C. After the incubation, the plates were washed 3 times with 150 µl of pH 7.4 phosphate buffered saline containing 0.05% Tween-20 (PBS-Tween). Anti-Ova IgG_1 and IgG_{2a} standards (eBioscience, CA) were diluted 1/160,000 in PBS-Tween and transferred into the Immulon plates (columns 6 and 7), where they were serially diluted with mixing using Eppendorf Research® multichannel pipette. Serum samples were serially diluted by transferring 100 µl from the original wells to the rows beneath, which contained 100 µl of PBS-Tween, with mixing 3-4 times. The Immulon trays were sealed and incubated overnight at room temperature then washed 3 times with PBS-Tween. Goat anti-mouse IgG_1 antibodies (100 µl) linked to alkaline phosphatase (AP) (Southern Biotech, diluted 1/3000 in PBS-Tween) were added into each well and the plates were then incubated, sealed, for 3 to 4 h at room temperature and washed again with PBS-Tween.

Alkaline phosphatase substrate, p-nitrophenyl phosphate (pNPP, SIGMA*FAST*™, Sigma®, MO), was dissolved in water in the dark to yield a solution containing1.0 mg/ml pNPP, 0.2 M Tris buffer, and 5 mM magnesium chloride substrate. One hundred microliters of the substrate was added to each well and left in the dark until the highest concentrated standard (~12 ng/ml) reached an absorbance of approximately 1.2 to 1.8 at 405 nm.

2.2.16 Enumeration of antigen-specific $CD8^+$ T-cells by tetramer staining

Enumeration of $CD8^+$ cytotoxic T lymphocyte (CTL), which are specific for ovalbumin antigen, was done using a tetramer staining technique.[178,179] Briefly, mice were euthanized and spleens were harvested at different time points. After that, spleens were ground using 2 frosted microscope slides in 10 ml mouse R10 media (RPMI 1640 containing 10% heat inactivated FBS (Sigma®, MO)). Cell suspensions were spun at 1000 rpm for 10 min at 4°C. Supernatants were then resuspended in ACK lysing buffer (Gibco™ Invitrogen™, NY), a neutral-pH buffer used to lyse red blood cells, for 5 min at room temperature. Cells were washed in R10 media and resuspended in CTL media (RPMI 1640, 25 mM HEPES, 2 mM L-glutamine and 10% FBS) to a dilution of 3×10^7 splenocytes/ml. One hundred microliters of splenocyte solution was seeded in Corning® Costar® 96 well round bottom cell culture plates and spun down. Cell membranes were blocked with purified monoclonal rat anti-mouse CD16/CD32 antibodies (2.4G2, Mouse BD Fc Block™). This was followed by adding phycoerythrin (PE) conjugated anti-mouse MHC class I molecule (H-2Kb) bound to SIINFEKL peptide, an Ova agonist peptide (eBioscience, CA) and was incubated on ice for 30 min. Then anti-CD8 FITC and phycoerythrin-Cy5 (PE-Cy5) hamster anti-mouse CD3e (epsilon subunit) and fluorescein isothiocyanate (FITC) anti-mouse CD8a (alpha subunit, Ly-2)

(eBioscience) were added and left to incubate in the dark for 20 min. The cell pellets were washed twice with FACS buffer then fixed with BD Cytofix/Cytoperm™ solution.

2.2.17 Statistical analysis

Group data are reported as mean+/-SD. Differences between groups were analyzed by one way analysis of variance with a Tukey's post-test analysis. Levels of significance were accepted at the $\rho < 0.05$ level. Statistical analyses were performed using Prism 5.02 software (GraphPad Software, Inc., CA).

2.3 Results and Discussions

2.3.1 Preparation of different chitosan grades

Chitosan and its precursor, chitin, are typically prepared from waste shells of crustaceans, particularly crab, shrimp and lobster.[180] The conventional process for producing chitin from crustacean shells involves grinding the shells and treating them with a dilute base such as sodium hydroxide under heat to remove proteins and lipids (deproteinization). After that, chitosan is treated with a dilute acid, mostly hydrochloric acid, at room temperature in order to extract calcium carbonate (demineralization). An optional decolorization step is commonly done by extraction with ethanol and ether or bleaching with sodium hypochlorite. Following deproteinization and demineralization, the resulting product is predominantly chitin, from which removal of acetyl groups (deacetylation) produces chitosan. Deacetylation is usually performed by reacting chitin with concentrated sodium hydroxide or potassium hydroxide under heat.[56] The deacetylation process does not remove any contaminants existing in the chitin starting materials; therefore, impurity removal from chitosan only occurs during production of the chitin precursor.

The biocompatibility and biodegradability of chitosan render it as suitable candidate material for medical applications. However, extra purification steps are critical

for generating chitosan polymers which are more suitable for biological applications. By substantially removing impurities from chitosan, the polymer produces fewer variations in biological systems and medical devices and becomes more biocompatible by minimizing immunological and other undesired interactions.

In this research, chitosan was purified exhaustively by doing extra steps of deproteinization, decoloration and demetallization. The purification procedure included removing insoluble contaminations and adding deproteinization and demetallization agents, SDS and EDTA, respectively, in the presence of the reducing agent, DTT. This resulted in the formation of water insoluble chitosan precipitates or flocculants, and water soluble supernatants that included the deproteinization agent and any proteins that have complexed with it and the demetallization agent with the extracted metals. Adding the reducing agent enhanced the water solubilization of protein impurities by dissociating any disulfide bonds present in the proteins. The demetallization agent was mixed with the chitosan solutions under basic pH conditions to avoid the formation of chitosan-metal chelate conjugates.

It was found that deproteinization of chitosan reduced chitosan's protein content to 0.09 % ± 0.04% (w/w) as measured by micro BCA assay, in comparison to 1.9 % ± 0.13% (w/w) for the untreated chitosans. In addition, chitosan purification was found to reduce batch-to-batch variations in transfecting HEK293 cells.

The degree of deacetylation (DD) of chitosan plays a significant role for determining the specific applications of chitosan. Degree of deacetylation affects the chemical, physical and biological properties of chitosan, such as DNA condensation and release, immunoadjuvant activity and cellular uptake.[181]

Chitosan samples with various degrees of deacetylation were prepared using heterogeneous acetylation with acetic anhydride and the degree of deacetylation was measured using first derivative UV spectrophotometry (1DUVS). 1DUVS provides simple, convenient, rapid, precise and non-destructive determination of the acetyl content

of chitin/chitosan with minimal interference from protein contamination.[182,183] Table 2-1 shows the actual degrees of deacetylation derived from the 1DUV spectra and the theoretical degrees of deacetylation of chitosans based on the molar calculations of acetic anhydride used in the reacetylation reaction of chitosan. The expected values of DD showed good correlation with the measured values for MM-HD, MM-MD, MM-LD and MM-VLD chitosans. However, when reacetylation was carried out further (theoretical DD of 55% and less), the reacetylation was less efficient (the 55% calculated DD resulted in 60.23% actual DD). Chitosan w 55.54% DD was prepared by adding acetic anhydride equals the calculated volume needed for the 45% theoretical DD. This is hypothesized to be due to the increased viscosity of the solution with lower DD and to the bulkiness of acetyl moieties which hinders further acetylation.

Similar to the degree of deacetylation, the molecular weight of the chitosan has a significant influence on its different applications, such as the formulation of successful drug and gene delivery systems.[90] The effect of molecular weight of chitosan on the complex formation with DNA has been attributed to the chain entanglement effect, which means that high molecular weight chitosans have more entanglement once the electrostatic interaction has occurred.[184]

Chitosans with a variety of reported molecular weights were obtained from a commercial source and purified exhaustively as mentioned above. Table 2-2 shows the reported and measured degrees of deacetylation, in addition to intrinsic viscosities and average viscosity molecular weights of chitosans obtained commercially. Table 2-3 shows the characterization of chitosans fragmented oxidatively in order to reduce molecular weight. This shows that using sodium nitrite was an effective method in depolymerizing chitosan while minimally affecting the degree of deacetylation. The decrease in molecular weight of chitosan upon depolymerization using sodium nitrite exhibited a linear relation with sodium nitrite concentration ($r^2 = 0.9930$).

2.3.2 Competition binding and polyanion displacement assays

Ethidium bromide exclusion assay (competition binding assay) was performed to better understand chitosan's ability to complex with DNA and to identify the role dextran sulfate plays in the interaction between chitosan and DNA. Ethidium bromide (EtBr) assay for DNA is a sensitive test with a limit of detection that can reach as low as 2 ng of DNA per well.[185] Gradual addition of different grades of chitosan to DNA mixed with ethidium bromide in solution resulted in a sharp reduction in fluorescence intensities up to N/P ratio of 2.5, after which the relative fluorescence intensities leveled off at less than 20% of the control (Figure 2-1). DNA mixed with ethidium bromide without chitosan was used as the positive control in this experiment. The point at which the relative fluorescence curve reached a plateau represents the maximum exclusion of ethidium bromide from DNA molecules, after which, any further addition of the polycationic polymers did not affect this reading. Adding high concentrations of PEI, a strong binder of DNA, into DNA-EtBr solutions resulted in similar behavior to chitosan, as the curve reached relative fluorescence intensity of 15.7% at N/P of 0.75 and remained constant upon addition of more PEI. Figure 2-2 shows the initial slope values of HM-HD, MM-HD and MM-MD RFU vs. N/P ratio curves (-0.8509, -0.5993 and -0.4858, respectively). The more negative initial slope of HM-HD chitosan resulted from the strongest complexation efficiency with DNA, compared to MM-HD and MM-MD chitosans. Moreover, HM-HD chitosan showed the earliest slope change at N/P of 1.0, whereas curves of MM-HD and MM-MD chitosans started to plateau at 1.5 and 2, respectively (Figure 2.1). This demonstrates the requirement for greater amounts of the latter two polymers in order to complex with DNA efficiently compared to the higher degree of deacetylation and higher molecular weight chitosans.

When dextran sulfate was added to the DNA-EtBr solution, the interaction between chitosan and DNA was reduced, as shown by the less negative RFU vs. N/P

ratio slope (-0.2392). In addition, the curve of chitosan and DNA complexation in the presence of dextran sulfate was slightly curving upward and had an abrupt change in slope at N/P ratio of 2. The higher relative fluorescence in the presence of dextran sulfate indicates weaker interactions between chitosan and DNA at lower chitosan to DNA ratios due to competition between DNA and dextran sulfate but the change in slope shows strong interactions at higher chitosan concentrations, hence, comparable protection of DNA to other formulations.

In order to detect the ability of different polyanions to compete with DNA for complexing with chitosan, the effect of incremental additions of dextran sulfate, tripolyphosphate and sodium alginate to solutions containing chitosan-DNA complexes was investigated (Figure 2-3). It was found that none of the three polyanions were able to completely displace DNA from chitosan nanoparticles. Also, it was found that dextran sulfate relative fluorescence curves differed significantly than the other two polyanions. The sodium alginate curve has abrupt increase in fluorescence due to the release of DNA from the nanoparticles, whereas the dextran sulfate curve shows a more gradual increase in fluorescence, indicating weaker competition with DNA. TPP curve shows behavior similar to sodium alginate but with milder effect on chitosan/DNA complexation. The competition between polyanions and DNA lead to decreased binding strength between DNA and chitosan in the presence of these polyanions, which facilitated the dissociation of these complexes to release DNA. Ideally, this interaction between chitosan and DNA should be strong enough to protect DNA and not release it before being delivered into targeted cells. Dextran sulfate appears to be able to perform well at these two levels. Interestingly, the change of chitosan/DNA ethidium bromide slope occurred at dextran sulfate/chitosan w/w ratio of 0.1, which coincides with the ratio that yields the smallest particle sizes (as shown in Figure 2-5 for the w/w ratio of chitosan to dextran sulfate of 10).

When comparing the three molecular weight grades of dextran sulfate (Figure 2-4), it was observed that the higher the molecular weight of dextran sulfate the stronger the interaction with chitosan, which weakened the chitosan complexation efficiency with DNA considerably. Therefore, dextran sulfate which is 5 kDa in molecular weight appears to be the best candidate for inclusion in the chitosan nanoparticles.

2.3.3 Fabrication and stability of chitosan nanoparticles

Cross-linking of chitosan is an essential step in the formation of chitosan micro- and nano-particles.[71,134] In addition, cross linking affects biodegradability and chitosan's mechanical properties, such as tensile strength.[186] Ionic gelation, one of the physical cross-linking approaches, is an interesting fabrication technique of chitosan nano- and microparticles for its simplicity and reversibility. This method depends on the reversible physical complexation mechanism between oppositely charged molecules through electrostatic interaction. Ionic gelation leads to the formation of polyelectrolyte complexes (PECs) of chitosan with other polyanionic compounds. Sodium dextran sulfate (DS), sodium tripolyphosphate (TPP), sodium alginate (SA), sodium sulfate (SS) and sodium hyaluronate (SH) have been tested for ionically cross-linking chitosan chains to form nanoparticles.

The effect of different polyanions on the sizes of chitosan nanoparticles was screened, as shown in Figure 2-5. Zetasizer size measurements of MM-HD chitosan nanoparticles showed fairly unimodal distributions. Z-average sizes of chitosan particles formed using different polyanion were found to be weight ratio dependent. Surprisingly, a chitosan to polyanion ratio of 10 showed the smallest particles in all studied formulations, ranging from 94.4 to 175.8 nm. The smallest average nanoparticle sizes and the least variations were observed for chitosan-TPP nanoparticles (100.8 ± 5.2 nm). Generally, macromolecular polyanions (SA, SH and DS) showed smaller and more

consistent sizes compared to low molecular weight polyanions (TPP and SS) only at extremely low or high concentrations of these polyanions. On the other hand, the inclusion of low molecular weight polyanions resulted in more consistent and smaller particle sizes at medium chitosan/polyanion w/w ratios. Among macromolecular polyanions, SH showed the most uniform particle formation even at high concentration of SH (chitosan/SH w/w ratio of 1 resulted in 244.1 ± 17.4 nm particles), whereas particles formed using DS resulted in the smallest sizes at low concentrations of the polyanion (134.5 ± 37.7 nm at chitosan/DS w/w ratio of 100). Larger particles were obtained from using higher concentrations of dextran sulfate due to the abrupt decrease in zeta potential (from 23.3 ± 2.0 mV at 2:1 chitosan to DS w/w ratio to -9.8 ± 4.9 mV at 1:1 ratio). Chitosan nanoparticles fabricated using DNA as the only incorporated polyanion showed similar behavior to other macromolecules with Z-average sizes of 156.0 ± 8.4 nm at 10:1 chitosan to DNA ratio. This study was done using salmon sperm DNA; however, comparable results were obtained when using luciferase encoding plasmid DNA, VR1255 (chitosan/DNA w/w ratio of 10 resulted in 137.2 ± 10.4 nm particles).

In addition to the type of polyanion, other parameters affecting the fabrication of chitosan nanoparticles were investigated in order to reach the most stable and consistent formulations. The effect of volume ratio was studied by preparing two separate solutions for cationic and anionic species. As shown in Table 2-4, when the volume of anionic solution was double that of cationic solution, it resulted in significantly smaller particle sizes and fewer variations compared to when the volume of cationic solution was less than the anionic solution. The Z-average size of particles at 1:2 cationic to anionic solutions volume ratio was 133.7 ± 1.4 nm and the zeta potential was 34.8 ± 0.4 mV (compared to 183.0 ± 10.0 nm and 33.8 ± 1.3 mV, respectively, at 2:1 ratio). The order of addition of the two solutions did not result in significant variations; however, adding cationic solution to the anionic solution resulted in slightly smaller sizes and more consistency (Z-average sizes of 130.3 ± 3.5 nm, Table 2-5).

Freeze-drying of chitosan-dextran sulfate formulations was performed in order to find the long term storage capabilities of these formulations. Sucrose, mannitol and sorbitol were used as cryoprotectants to preserve the nanoparticles during the freeze-dry cycle. Lyophilization caused some aggregation in chitosan-dextran sulfate nanoparticles as shown by the change in size from 136.9 ± 4.2 nm to 313.7 ± 23.2 nm, a 129.2% increase. Similar to chitosan-DS nanoparticles, chitosan-TPP and chitosan-SS nanoparticles increased significantly in size upon lyophilization (139.5% and 142.8% change in size, respectively). Aggregation of particles caused by lyophilization affects the transfection properties of these formulations and their practical applications at larger scales. It was found that using cryoprotectants, especially sucrose, helped in maintaining the sizes and zeta potentials of chitosan nanoparticles formulations. As shown in Figure 2-6, chitosan-DS nanoparticles which were coated with sucrose before freezing (7.5% (w/v) final concentration) showed the least change in particle sizes with only 6.6% increase from the original particle size. Adding mannitol and sorbitol up to 10% (w/v) final concentration were not able to fully protect chitosan nanoparticles. Mannitol-added formulations showed 36.9% ± 8.2% deviation in particle size, whereas sorbitol-added formulations had 20.1% ± 3.7% deviation. A similar trend was obtained for zeta potential for chitosan nanoparticles after lyophilization (Figure 2-7). Sucrose protected formulations showed the least decrease in zeta potential (4.1 ± 2% decrease in zeta potential compared to 42.7 ± 6.8% for formulations lyophilized without cryoprotectant). Therefore, it was concluded that sucrose has superior properties in protecting chitosan nanoparticles and preserving the sizes and charges of these particles, in comparison to sorbitol and mannitol.

Polyelectrolyte complexes between macromolecules have shown a great potential for applications in drug and gene delivery, however, the stability of these complexes is questionable. In this study, the physical stability of chitosan-DNA PECs in the presence of dextran sulfate was investigated under several formulation and stability conditions.

Blank chitosan nanoparticles made with TPP or DS without incorporating DNA were tested for their stability as shown in Table 2-6. Initially, the Z-average sizes of CS-DS nanoparticles were larger than CS-TPP nanoparticles (127.9 compared to 96.2 nm), but the zeta potential values were comparable (29.2 and 28.8 mV, respectively). The sizes of CS-TPP and CS-DS nanoparticles remained relatively constant over 22 days with only slight increase in the Z-average sizes.

Next, the effect of dextran sulfate grade on the size and zeta potential stability of chitosan nanoparticles was studied over 37 days. As shown in Table 2-7, dextran sulfate that has a molecular weight of more than 500 kDa resulted in the smallest and most reproducible chitosan nanoparticles. Particle sizes were between 132.2 to 148.5 nm during the whole length of the study (37days). Slightly larger particles resulted from using DS with reported molecular weights of 9-20 and 6-10 kDa, and more variations between preparations were noticed. When the smallest molecular weight DS (5 kDa) was used, particles increased in size with time up to 199.4 nm at day 37 from 166.0 nm initially. In addition, variation between replicates appears to increase when 5 kDa dextran sulfate was used. For the different grades of dextran sulfate that were used, zeta potential values remained relatively constant during storage (Table 2-8).

Figure 2-8 shows the effect of CS/DS w/w ratio for the different grades of chitosan, HM-HD, MM-HD, LM-HD, MM-MD and MM-LD. As observed earlier, it was found that CS/DS w/w ratio of 10 resulted in the smallest particle sizes for all of the molecular weight and degree of deacetylation chitosans. The more acetylated the chitosan chains, the larger the particle sizes formed with dextran sulfate (125.0, 185.8 and 240.3 nm for MM-HD, MM-MD and MM-LD chitosans, respectively). This is due to the increased stiffness of chitosan chains with decreasing the degree of deacetylation as a result of the repulsion of the acetyl groups, in addition to the less efficient ionic interactions with polyanions. The effect of the molecular weight of chitosan was less significant, but more condensed particles were observed for higher molecular weight

chitosans (average particle size for the HM-HD chitosan/DS nanoparticles with w/w ratio of 10 was 116.3 nm, whereas for the LM-HD chitosan nanoparticles was 136.9 nm). Chitosan/DS ratios of less than 10 resulted in aggregated particles due to the interparticle complexation with the excess dextran sulfate. Large and visible aggregations were observed for nanoparticles formed at chitosan/DS ratio of 1. This can be explained by the negative and small zeta potentials for these particles as shown in Figure 2-9. The zeta potential values for all other ratios were higher than 24 mV and positive.

Further studies were carried out on LM-HD chitosan nanoparticles at different chitosan/DS ratios in order to investigate the stability of these particles upon storage at room temperature. All formulations that contained dextran sulfate at different ratios showed stability in sizes and zeta potential values up to 29 days. Similar results were obtained for other grades of chitosan, showing that chitosan-DS nanoparticles are stable and good candidate vehicle for gene and drug delivery.

In order to study the effect of pH and buffer type on the size and size stability of chitosan nanoparticles, different anionic and cationic buffers were used as suspending media. All buffers were prepared at 50 mM concentrations and 154 mM ionic strength. Anionic buffers used were acetate (pKa 4.66) and phosphate (pKa_2 7.21) (Table 2-9), whereas cationic buffers were tris(hydroxymethyl)aminomethane (Tris, pKa 8.06) and bis(2-hydroxyethyl)imino-tris(hydroxymethyl)methane (Bis-Tris, pKa 6.46) (Table 2-10). Chitosan-DS/DNA nanoparticles suspended in acetate buffer pH 3.46 showed the smallest particle sizes initially, which was due the highest percentage of protonated glucosamine units on chitosan chains which result in stronger complexes with dextran sulfate and DNA. However, using acetate buffer at pH 3.46 and pH 4.46, particle sizes increased with time during room temperature storage (131.0 and 35.4% increase in size, respectively) as a result of the higher solubility of chitosan in these pH ranges, leading to decomplexation of CS-DS nanoparticles and forming new particles with larger diameters. In comparison, particles suspended in acetate buffer at pH 5.46 showed constant particle

sizes throughout the study period of 29 days (initial particle size was 145.7 ± 12.2 nm and the size at the end of the experiment was 144.5 ± 7.6 nm). Anionic buffers species which have multiple anionic groups were found to exert noticeable effects on the stability of chitosan nanoparticles as shown by using citrate buffers (pH 5.46 and 6.46). Citrate buffers caused instant destabilization of chitosan particles forming larger aggregates with high polydispersity index (PDI).

Higher pH values affected the formulation of the nanoparticles considerably. Although initial particles suspended in phosphate buffer at pH 6.46 were 159.0 ± 10.7 nm in Z-average, the particles aggregated quickly forming visible particles within 30 min, but these particles could be redispersed quickly upon vortexing. The zeta potential values were significantly lower than that of nanoparticles dispersed in acetate buffers at pH 5.46 (12.7 ± 2.3 mV compared to 27.9 ± 0.9 mV). On day 8, chitosan particles had formed irreversible aggregates at pH 6.46. Chitosan nanoparticles suspended in phosphate buffer (pH 7.46) had an average zeta potential of 2.2 ± 0.4 mV and formed immediate aggregates. These polymeric clumps were not redispersable after less than 30 min of preparation, even with high shear vortexing. The polydispersity indices of these particles were high and out of the range of reliable measurement using the dynamic light scattering.

Using the cationic buffers Tris and Bis-Tris for redispersing chitosan-dextran sulfate nanoparticles incorporating DNA resulted in particle sizes in the same range as the anionic buffers at the same pH values. Also, similar initial behavior of particles at higher pH values was noticed. However, chitosan nanoparticles suspended in Bis-Tris at pH 6.46 showed superior stability over using phosphate buffer at the same pH value. This can be explained by the different mechanism of interactions between different buffer species and the components of nanoparticles. Cationic buffers have less deteriorating effect on the chitosan/polyanion interactions, whereas anionic species can cause decomplexation of these structures by replacing the polyanionic species. This effect

becomes stronger at higher pH values because the percentage of protonation of chitosan was considerably lower and was scarcely enough for successful initial complexation with the polyanion and DNA.

In order to compare the stability of chitosan-DS/DNA and chitosan-TPP/DNA nanoparticles (N/P = 25, CS/polyanion = 10), these formulations were suspended in Bis-Tris buffers at pH 5.46 and 6.46 and particle sizes were measured up to 29 days (Figure 2-10). Chitosan-TPP/DNA nanoparticles were initially larger than chitosan-DS/DNA suspended in Bis-Tris pH 5.46 buffer (298.4 ± 3.1 nm compared to 143.5 ± 1.2), but were insignificantly different at pH 6.46. However, within 29 days, the Z-average sizes for chitosan-TPP/DNA nanoparticles increased dramatically to 487.6 ± 16 nm and 336.3 ± 19.9 nm in Bis-Tris buffer at pH 5.46 and 6.46, respectively. On the other hand, CS-DS/DNA nanoparticles suspended in Bis-Tris at pH 6.46 buffers did not significantly change in size, whereas CS-DS nanoparticles suspended at pH 5.46 increased slightly in size. This shows the favorable effect dextran sulfate has on the stability of particles compared to TPP, a commonly used polyanion in the preparation of chitosan nanoparticles for therapeutic agent delivery. The stabilization of the complexes between chitosan and DNA or other macromolecules during storage in the presence of dextran sulfate is hypothesized to be due to the optimization of the strength of interaction between the two species by strengthening the polymer chain entanglement. Zeta potential values of particles made with TPP and dextran sulfate were comparable, which indicates that the charges on the chitosan particles were not the contributing factor to aggregation of particles made with TPP upon storage.

The effect of storage temperatures on the size stability of chitosan-DS/DNA and chitosan-TPP/DNA nanoparticles (N/P = 25, CS/polyanion = 10) was also studied (Table 2-11). It was found that chitosan-TPP/DNA nanoparticles are affected by the storage temperature differently compared to chitosan-DS/DNA. Chitosan-TPP/DNA nanoparticles were larger in size initially (299.0 ± 3.4 nm), as shown before, and have

enlarged with time at all storage conditions in a temperature-dependent manner. On the other hand, chitosan-DS/DNA nanoparticle sizes remained constant over the 29 day study period when stored at room temperature. Surprisingly, a slight increase in size of DS formulations stored at 4^{o}C has occurred (from 134.4 ± 12.5 nm to 161.6 ± 6.5 nm). Higher temperatures played a key role in the destabilization of chitosan nanoparticles by increasing the polymer chain mobility, but the effect on particles formed using dextran sulfate was less significant compared to TPP. After 29 days of storage at 37^{o}C, the chitosan-DS/DNA nanoparticle sizes reached 246.9 ± 22.9 nm compared to 575.6 ± 24.5 nm for chitosan-TPP/DNA.

The effect of DNA concentration on the sizes of chitosan-DS/DNA nanoparticles was studied by preparing particles with increasing concentration of pDNA but fixed N/P and CS/DS ratios (N/P = 25, CS/polyanion = 10) (Table 2-12). It was found that at lower DNA concentrations (less than 0.05 mg/ml), particle sizes were in the range of 130.2 to 143.7 nm. At concentrations of 0.06 mg/ml and higher, DNA concentration started to considerably affect chitosan nanoparticles. For example, at 0.1 mg/ml, the nanoparticles were 235.5 ± 14.1 nm in size, a 173% increase in size compared to 0.01 mg/ml DNA concentration. Interestingly, zeta potential values for chitosan-DS nanoparticles showed a proportional increase with increasing final concentrations of DNA.

One of the other important formulation parameters in the fabrication of nanoparticles using ionic gelation method is the total volume of solution. This factor determines the large scale applicability of this method. Several final solution volumes were tested (0.5, 1, 2, 5 and 10 ml). It was found that increasing the preparation volume up to 10 ml did not significantly affect the sizes of nanoparticles, and all the formulations stayed within the expected range of sizes (128.5 nm to 151.3 nm), with only a slight increase in particle sizes as the volume increases.

In conclusion, it was found that that dextran sulfate inclusion plays a major role in the stability of chitosan/DNA nanoparticle. PECs that included dextran sulfate were most

stable at pH 5.46 with no significant difference in sizes using cationic or anionic buffers. Using buffers at pH values of more than 6 resulted in particle aggregation due to the lack of sufficient number of protonated amine groups on the chitosan chains which are needed for an efficient complexation process. The inclusion of dextran sulfate in the chitosan-DNA nanoparticles increased their stability compared to other polyanions, especially when stored at room temperature, and improved resistance to decomplexation and aggregation at higher temperatures.

2.3.4 Imaging of chitosan nanoparticles

The morphologies of chitosan nanoparticles were studied by transmission electron microscopy (TEM) using JEOL 1230 TEM instrument. Figure 2-11 shows the morphology of chitosan-dextran sulfate nanoparticles (chitosan/dextran sulfate w/w ratio = 10, N/P ratio =15) negatively stained with 1% uranyl acetate. The average diameter of chitosan nanoparticles from the TEM images was 140.3 ± 26.3 nm which was obtained by masking the areas of chitosan nanoparticles and using ImageJ 1.42q (average of 5 images). This result correlates well with the data obtained from the light diffraction measurements using the Malvern Zetasizer Nano ZS.

AFM was used to study the condensation of DNA by chitosan. Figure 2-12 shows naked plasmid DNA dissolved in $NiCl_2$/HEPES buffer and fixed on Mica film. The AFM image clearly shows the circular nature of the plasmid DNA strands in the range of 200 to 500 nm. When chitosan-dextran sulfate/pDNA complexes were fabricated at N/P ratio of 2, a network of DNA formed around the chitosan particles as a result of incomplete condensation (Figure 2-13). This confirms the results obtained from the DNA loading study and ethidium bromide quenching assay which showed that at N/P ratios less than 2, the condensation was not complete. This incomplete condensation phenomenon was absent from formulations containing chitosan at N/P ratios of 5 and more.

AFM imaging was carried out further to compare particle sizes and morphologies of chitosan nanoparticles which incorporated different polyanions. Special focus was made on chitosan-DS/pDNA nanoparticles at different N/P ratios and chitosan/DS w/w ratios. Comparing the AFM images of chitosan nanoparticles made by incorporating sodium sulfate, sodium tripolyphosphate and dextran sulfate without DNA (Figures 2-14A, 2-14B and 2-14C, respectively), it was found that chitosan-SS nanoparticles were larger in size, followed by chitosan-TPP and then chitosan-DS nanoparticles. Chitosan-SS nanoparticles also showed a wider size distribution and more irregularities in shape, whereas chitosan-TPP nanoparticles were the most uniformly spherical and showed the least size variations. This was confirmed by the quantitative analysis done on these images using Igor Pro 6.1.1.0 (Table 2-13), which shows that the order of chitosan nanoparticles in terms of larger surface areas was CS-SS > CS-TPP > CS-DS.

Chitosan nanoparticles were prepared by the inclusion of dextran sulfate and pDNA (VR1255) at different DNA and dextran sulfate ratio. Figures 2-15A, 2-15B, 2-15C, 2-15D and 2-15E show examples of chitosan-DS/pDNA nanoparticles at N/P ratios of 5, 10, 15, 25 and 35, respectively, and their quantitative analysis is shown in Table 2-13. At N/P ratio of 5, chitosan nanoparticles were significantly larger and more irregular, indicating poor condensation of DNA by chitosan due to the saturation of complexation sites on chitosan chains. At N/P ratio of 10, the particles appeared more uniform and smaller, indicating a better complexation. Increasing the ratio of chitosan to DNA (10 and higher) caused the average area of particles to increase proportionally. This increase in size with increasing N/P ratio is due to the change in the delicate balance of anionic and cationic species inside chitosan nanoparticles. However, the inclusion of dextran sulfate inside the particles helped in keeping the particles intact even at low DNA content and minimized particle enlargement. At N/P ratio of 35 it was noticed that nano-sized aggregations of particles became more visible and that particles exhibited a wider

range of sizes. However, even at N/P ratio of 35, the particles were significantly smaller than that at N/P of 5.

Similar to the effect of high DNA content, the presence of high dextran sulfate content in the particles lead to a significant size enlargement (130% increase in size when chitosan/DS w/w ratio was 5 compared to 10 (Figure 2-16A and 16B, respectively)). This indicates weakening of the entanglement between chitosan chains and polyanionic species due to the saturation of charged sites. Decreasing the incorporated dextran sulfate further lead to slightly more compaction of the DNA inside the nanoparticles but the shrinking of the particles was insignificant (Figure 2-16C).

The morphology of chitosan-DS/pDNA (N/P ratio = 15, CS/DS w/w ratio of 10) was studied further using scanning electron microscopy (SEM) under 2.0 kV accelerating voltage. Figure 2-17 shows that the general morphological features of chitosan particles confirm the results obtained by AFM. Within chitosan nanoparticles, patches of dense and light areas were observed, showing the complex interaction process between the incorporated polyelectrolytes. In addition, external edges of particles appeared rough, which is an expected feature of PECs. The rough exterior of particles can play an important role in cell targeting and adhesion by exposing cells to larger surface area of the polymeric particulates.

2.3.5 Gel electrophoresis

The DNA condensation ability of chitosan was determined by the electrophoretic mobility of chitosan/DNA complexes in agarose gel. The relative amounts of free or incorporated DNA were assessed qualitatively as a function of the type of chitosan, N/P ratio, the type of polyanion used and the ratio of chitosan to dextran sulfate. As shown in Figure 2-18, the amount of uncomplexed or free VR1255 pDNA decreased as the N/P ratio increased, as shown by stronger bands at origin with less migration. At N/P ratios of 5 and more, there was no visible DNA migration in the gel, suggesting strong and

complete DNA binding capacities of chitosans at these ratios. In addition, it was noticed that the molecular weight and degree of deacetylation of chitosan had no significant impact on their ability to condense DNA at N/P ratio of 10. However, subtle differences in the complexation efficiencies using different grades were detected using ethidium bromide competition assay as shown above.

Figure 2-19 shows the effect of the inclusion of different polyanions on the condensation of DNA by chitosan. Again, there were no visible migrations for all used polyanions at chitosan/polyanion w/w ratio of 10, and it was comparable to PEI-DNA polyplexes band at origin. Doubling the content of polyanions (chitosan/polyanion w/w ratio of 5) still resulted in strong bands at the wells. This indicates that these ratios are safe ratios to be used for formulating chitosan nanoparticles, providing the necessary condensation and protection of DNA.

Furthermore, gel electrophoresis, along with UV readings, was used to confirm 1) chitosan's ability to complex completely with all DNA in the solution and 2) ultracentrifugation can be used to collect chitosan nanoparticles without affecting DNA condensation. Ultracentrifugation was done using a Sorvall Discovery centrifuge at 30,000 rpm for 60 min and the supernatant was collected. The precipitated pellets of particles were resuspended in 50 mM acetate buffer, pH 5.5. At this ultracentrifugation speed and time, only condensed particles are expected to precipitate, but not the dissolved molecules or subnano-sized particles. Figure 2-20 shows the electrophoresis bands of naked pDNA and the resuspended particles at the origin. Also it shows the absence of any bands for the supernatant solution, which indicates a virtually complete condensation of DNA. UV absorbance at 260 nm for the supernatant, compared to the original nanoparticle solution, verified the results by showing that only 12.48% of the original absorbance was obtained. This absorbance falls within the error margins of the spectrophotometer at this low detected DNA concentration in the supernatant, and can be

increased by the presence of any remaining small nanoparticles that were not settled down during centrifugation or disturbed and resuspended as a result of handling.

To determine the stability of DNA in chitosan/DNA complexes, an endonuclease degradation study was carried out as described in the experimental design and methods. The results showed that free DNA was rapidly degraded by DNase I within a short period of time (less than 30 min), whilst DNA in PEI-DNA complexes was partially resistant to DNase I. Figure 2-21 shows the differences between naked pDNA which migrated through the gel (lane 5) and pDNA complexed with LM-HD chitosan-dextran sulfate which remained at the origin (lane 4). pDNA encapsulated in chitosan nanoparticles was comparable to untreated naked pDNA (100 units/ml) even after 60 min treatment with DNase I, with only slight decrease in band intensities. On the other hand, no district bands were observed for DNase I treated naked pDNA.

2.3.6 Cytotoxicity assay

The cytotoxicity of the polymers used to fabricate gene delivery particles was tested using the MTT assay. MTT (3-[4,5- dimethylthiazol-2-yl]-2,5-diphenyltetrazolium bromide) is a monotetrazolium salt that is widely used to detect cell proliferation and cytotoxicity of materials.[187,188] TheMTT assay measures the activity of living cells mainly via mitochondrial dehydrogenases, which is supported by NADH-linked mitochondrial substrates, such as malate, glutamate or pyruvate.[187]

As shown in Figure 2-22, chitosans which were purified exhaustively were significantly less toxic to HEK293 cells compared to raw chitosans and to the chitosans from which the insoluble particles were filtered without further purification. Filtration followed by dialysis resulted in improved safety profile of chitosan but to a lesser degree compared to the fully purified chitosans. Figures 2-23 and 2-24 show the effect of chitosan's molecular weight and degree of deacetylation on the cytotoxicity of chitosan solutions compared to branched PEI, studied on HEK293 and COS7 cell lines,

respectively. It was found that branched PEI exhibited significantly higher cytotoxicity compared to all chitosan grades. It was also found that lower degree of deacetylated chitosans (MM-MD) expressed slightly lower cytotoxicity compared to higher degree of deacetylated chitosans (MM-HD), which have the same molecular weight. Chitosans with higher degrees of deacetylation have more surface charges at acidic to neutral pH values and consequently cause more repulsion between chitosan monomers. This results extended conformation of chitosans in solution, which is a contributing factor in the binding of chitosan chains to cell membranes, compared to less binding for the coiled structures. Ultimately, the higher interactions with cellular membranes leads to higher cytotoxicity.[83] When comparing the small and medium molecular weight chitosans, LM-HD and MM-HD, it was found that decreasing the molecular weight of chitosans resulted in less harmful effect on cells due to significantly weaker interactions with cell membranes when decreasing the size of the polymer chains. These conclusions were noticed on both HEK293 and COS7 cell lines, but with higher sample-to-sample variations observed in COS7 due to the susceptibility of COS7 to detachment during the assay. In order to find out the 50% inhibitory concentration (IC_{50}), the MTT cytotoxicity assay was performed on solutions of chitosan at concentration ranges where IC_{50} were expected. As shown in Figure 2-25, PEI showed more than 60 times more cytotoxicity compared to chitosans (IC_{50} was 0.019 ± 0.002). Among the different grades of chitosan, the differences were not significant between MM-MD and LM-HD chitosans (IC_{50} results were 1.293 ± 0.064 mg/ml and 1.253 ± 0.058 mg/ml, respectively), whereas MM-HD chitosans showed slightly higher toxicities (IC_{50} was 1.110 ± 0.010 mg/ml).

In addition to the cytotoxicity of chitosans, the cytotoxicities of dextran sulfate and TPP were studied in HEK293 and COS7, as shown in Figures 2-26 and 2-27, respectively. It was found that dextran sulfate with high molecular weights (~500 kDa) has significantly higher toxicity compared to TPP and dextran sulfate with lower molecular weights using both cell lines. IC_{50} of dextran sulfate (500 kDa) was

0.843 mg/ml compared to 1.945 and 2.012 mg/ml for dextran sulfate (5 kDa) and TPP, respectively.

Formulations of chitosan and PEI nanoparticle were tested for their toxicity to investigate the effect of fabrication on the biocompatibilities of these polymers. LM-HD chitosans were used to fabricate chitosan-TPP/pDNA and chitosan-DS/pDNA nanoparticles (DS molecular weight = 5 kDa and 500 kDa) and branched PEI (25 kDa) were used to fabricate PEI/DNA nanoparticles. Compared to using solutions of polymers, condensing chitosan into nanoparticles decreased the toxicity of individual polymers (Figure 2-28). Using dextran sulfate with molecular weight of 500 kDa to fabricate the particles still resulted in higher toxicity than TPP or dextran sulfate with molecular weight of 5 kDa, but the difference was less significant than using their solutions. PEI/pDNA nanoparticles were still extremely toxic compared to chitosan nanoparticles, as shown by having an IC_{50} less than 25 μg/ml.

2.3.7 *In vitro* transfection efficiency testing

As mentioned in the Methods section, crude chitosans obtained commercially were purified and washed in three different ways, either by filtration of the insoluble particles, dialysis or extensive purification process. It was expected that the degree of purity of chitosan affects the transfection efficiencies of chitosan nanoparticles since it also affected the biocompatibility of different chitosan grades. Indeed, it was found that dialyzed and fully purified chitosans have significantly higher transfection efficiencies compared to untreated chitosans that were only filtered (Figure 2-29). This was due to two main reasons; 1) the enhanced biocompatibility of chitosans upon purification and 2) maximizing the efficiency of complexation with desired polyanions by removing protein impurities.

Initial screening of the inclusion of different polyanions to fabricate chitosan nanoparticles was done using 5, 10 and 20 chitosan/polyanion w/w ratio (Figure 2-30).

These results showed the ability of dextran sulfate to positively influence the gene transfection of chitosan nanoparticles over the use of other polyanions. Naked pDNA, the negative control, generated 8.4 x 10^4 RLU/mg protein mean luciferase activity, whereas branched PEI/pDNA nanoparticles prepared at an N/P ratio of 10 generated 1.09 x 10^9 RLU/mg protein mean luciferase activity in HEK293 cells. PEI/pDNA nanoparticles were used as a positive control for the known properties of PEI to condense pDNA and deliver it efficiently into cells. However, PEI is a toxic material and its use for therapeutic purposes is questionable. Chitosan/pDNA nanoparticles which were formulated without the use of other polyanions showed significantly lower transfection efficiencies compared to other formulations, but higher than naked DNA, which is due to the lack of the strengthening effect of polyanions inside the nanoparticles. Generally, the incorporation of any of the studied polyanions in the formulation of chitosan nanoparticles showed significant improvement in gene transfection, especially at chitosan/polyanion w/w ratio of 10.

In order to have a better understanding of the factors that affect transfection, chitosan nanoparticles formulated with the different polyanion or with only pDNA were used for transfecting HEK293 in the presence of serum in comparison to using serum-free media. Figure 2-31 shows the results of transfection when carried out in the presence of 10% fetal bovine serum, which is a more realistic model for the *in vivo* applications, in comparison to using serum-free media. It was found that all the formulations showed higher transfection in serum containing media, which was due to the prolongation of the incubation time of these vehicles with the cells. This indicates that chitosan nanoparticles can effectively deliver genes inside cells but require sufficient incubation time. Again, dextran sulfate-strengthened nanoparticles showed significantly higher transfection efficiency in comparison to all other chitosan formulations in both transfection media types (serum-containing and serum-free media).

The age of cell line is considered another important factor in assessing the transfection efficiencies. HEK293 cells, subcultivated either 6 or 25 times (approximately 100-day difference in age), were used for this purpose and the experiments were performed simultaneously to minimize experimental variabilities. As shown in Figure 2-32, the effect of the age of the cell lines was significant. The reduction in transfection efficiencies for all formulations as a factor of increasing the age of the cells is hypothesized to occur as the result of morphological and biological changes that happen to cells during the stress conditions of each passage. However, the relative transgene activities of the studied formulations were similar. This also applied to the positive control (PEI/pDNA nanoparticles).

When COS7 (an African Green Monkey kidney fibroblast-like cell line) was compared to HEK293 as the *in vitro* transfection model, a significant reduction in transfection was noticed (Figure 2-33). The COS7 cell line appeared to be more resistant to gene introduction compared to HEK293 as a result of a weaker adhesion to the tissue culture plates and the subsequent loss of viable cells. Branched PEI/pDNA nanoparticles prepared at an N/P ratio of 10 generated 6.81×10^8 RLU/mg protein mean luciferase activity in HEK293 cells, but generated only 6.79×10^7 RLU/mg protein mean luciferase activity in COS7 cells. Chitosan nanoparticles which incorporated dextran sulfate still showed transfection efficiency in COS7 (9.5×10^6 RLU/mg protein), which was significantly higher than the formulations with other polyanions.

Using HEK293 cells, the effect of changing chitosan/dextran sulfate w/w ratio on transfection was studied. As shown in Figure 2-34, the presence of dextran sulfate at w/w ratio of 10 achieved optimal complexation between chitosan and pDNA in this nanoparticulate system. This fine balance in charges is required for protecting DNA before the cellular uptake, and then is needed for allowing the release of DNA at the right time into the cytoplasm. This was shown by the significantly higher transfection efficiencies of this ratio compared to using chitosan/dextran sulfate w/w of 1, 5, 7.5 and

12.5, in addition to the nanoparticles in which dextran sulfate was not added. For all chitosan/dextran sulfate ratios, transgene expression in serum-free media was reduced as discussed before (Figure 2-31), but the transfection order remained the same.

The pH of the preparation and suspending buffer also showed significant effect on transfection efficiencies of chitosan nanoparticles (Figure 2-35). It was found that chitosan-DS/pDNA nanoparticles prepared in 10 mM acetate buffer, pH 4.46, generated the highest gene expression. This is due to maximizing the availability of charged sites on chitosan chains during the complexation process. Preparations fabricated at lower pH values (3.46) showed a decline in gene expression, which can be the result of the adverse effects of low pH on DNA and the transfected cells.

The effects of various grades of chitosan on the transgene expression were studied on HEK293 cells using medium molecular weight and low degree of deacetylation (MM-LD), medium molecular weight and medium degree of deacetylation (MM-MD), low molecular weight and high degree of deacetylation (LM-HD), medium molecular weight and high degree of deacetylation (MM-HD) and high molecular weight and high degree of deacetylation (HM-HD) chitosans (Figure 2-36). The results show that low and medium degree of acetylation chitosans (74.36% and 83.94%, respectively) have weak abilities to delivery DNA into the cells as shown by the low transfection efficiencies. Between higher degrees of deacetylated chitosans (> 90% DD), the order of the transfection efficiency from the highest to lowest was MM-HD > LM-HD > HM-HD chitosans, at N/P ratio of 15. This phenomenon was studied further by preparing LM-HD and MM-HD chitosan-DS/pDNA nanoparticles at different N/P ratios (Figure 2-37). Decreasing the molecular weight of chitosan was found to have a profound improvement on transfection, provided that the N/P ratios are increased. An abrupt increase in transfection efficiencies after N/P ratio of 15 were noticed for LM-HD chitosan, followed by a gradual decrease. When MM-HD chitosan was used to formulate the nanoparticles, it showed similar behavior, except of higher transfection at lower N/P ratios (15)

compared to LM-HD chitosan. This indicates that decreasing chitosan's molecular weight necessitates more of the polymer to be able to condense and deliver pDNA effectively, and when this is done, this results in enhanced transgene expression over higher molecular weight chitosans. These results were in accordance with some other reports in literature.[189]

Further reduction of molecular weight was carried by depolymerization in the presence of sodium nitrite. Using 1, 1.5 and 2% $NaNO_2$ depolymerized LM-HD chitosans (molecular weight range of 42.4 to 65.9 kDa), transfection efficiencies in HEK293 cells increased significantly with decreasing molecular weights (Figure 2-38). However, the transfection efficiencies of chitosan nanoparticles reached a plateau after that point and started to decrease. Using chitosan with molecular weight of 8.6 kDa (at 4% $NaNO_2$ depolymerization), the transfection efficiency was significantly less than using chitosan molecular weight 42.4 kDa (at 2% $NaNO_2$ depolymerization). Depolymerized MM-HD and HM-HD showed similar behavior to depolymerized LM-HD in term of increasing transfection efficiencies with decreasing chitosan molecular weight. Figure 2-39 shows the effect of depolymerization when increasing the percentage of acetylated chitosan units (DD 83.94% and 74.36%). Unlike higher degree of deacetylated chitosans, decreasing the molecular weights of medium and low acetylated chitosans caused only initial rise in transfection efficiencies, followed by a gradual decrease. Generally, the transfection efficiencies of MM-MD and MM-LD chitosans and their depolymerized fragments were very low due to the low percentage of protonated amine groups and therefore they are not suitable for the preparation of non-viral gene delivery vehicles.

2.3.8 *In vivo* applications: chitosan nanoparticles for DNA vaccination

Gene-based vaccination has shown a great potential to replace traditional vaccination strategies. In delivering antigen encoding DNA into the cells, the body's own

cells start affecting the immune response in similar ways as live infection. This is expected to have a greater impact on body's defense systems compared to traditional non-replicating vaccines.[190] DNA vaccine systems can be easily altered to target other pathogens by changing the sequence of DNA. Chitosan and its different derivatives have been studied in various dosage forms as adjuvants and delivery systems for vaccines.[191]

Chitosan nanoparticles were prepared using the optimized formulation conditions mentioned above with some modifications. In addition to mixing plasmid DNA (pOva) with the polyanion (dextran sulfate), ova albumin (Ova) was also added. Also, CpG oligodeoxynucleotides (ODN) were adsorbed on the surface of nanoparticles by mixing the diluted CpG-ODN with the fabricated nanoparticles. Table 2-14 shows the characterization of chitosan nanoparticles used for animal studies. Inclusion of pOva in the chitosan nanoparticles resulted in particle sizes in the same range of plasmid DNA encoding luciferase nanoparticles but slightly decreased zeta potential values as a result of CpG-ODN adsorption. Inclusion of the protein alone (Ova), resulted in larger particles (199.0 ± 24.1 nm). Incorporating both the plasmid DNA and protein inside chitosan nanoparticles yielded even larger particles (231.7 ± 12.9 nm and 286.2 ± 18.4 nm for chitosan-DS nanoparticles and chitosan-TPP nanoparticles, respectively). The zeta potential values decreased significantly compared to particles prepared with either one of the species (pOva or Ova).

Cytosine–phosphorothioate–guanine oligodeoxynucleotides (CpG-ODN) which have sequence patterns similar to those found in bacterial DNA activates potent cell-mediated immune responses. This response starts after the unmethylated CpG-ODNs are uptaken by cells via adsorptive endocytosis and bind to the toll-like receptor 9 (TLR9) in the intracellular compartment of B cells and plasmacytoid dendritic cells. This binding triggers an immunostimulatory cascade that leads to inducing the maturation, differentiation and proliferation of multiple immune cells including B and T lymphocytes, in addition to natural killer cells, monocytes and macrophages that produce

interleukin 1, 6,12 and 18, interferon-γ and tumor necrosis factor-α. This will induce the production of antigen-specific cytotoxic T lymphocytes (CTL) and positively influence antibody production by B cells.[192,193] CpG ODN was used in this study to boost the immune response for the antigen presenting microparticles.

Type 1 and Type 2 helper T cells (Th1 and Th2 cells, respectively) can promote humoral immune responses to protein antigens, but they stimulate production of different immunoglobulin subtypes. Production of IgG_1 antibodies depends on Th2-type $CD4^+$ T cells, whereas induction of IgG_{2a} requires Th1 cells.[194-196]

ELISA was performed to quantify anti-Ova IgG_1 and IgG_{2a} antibody production in mice injected with chitosan-nanoparticles intraperitoneally compared to naïve mice. Blood samples were collected initially and before each injection and ELISA was done according to Materials and Methods section. A calibration curve was plotted using mouse IgG_1 and IgG_{2a} standards. Figure 2-40 and 41 show the 35 day study of the plasma concentration of anti-Ova IgG_1 and IgG_{2a} for chitosan formulations, respectively. Naïve mice and mice that which received solution mixtures of Ova-encoding pDNA and Ova did not show any Ova specific antibody production and this is why they were not shown on the graph. In a preliminary small scale study, it was found that antibody production using chitosan nanoparticles without using CpG-ODN as an immunoadjuvant was not satisfactory; therefore it was included in all formulations. As shown in Figure 2-40, formulations that contain chitosan-DS/(pOva + Ova) showed the highest antibody production initially. The difference between this formulation and other preparations increased significantly up to day 35. Incorporating both the Ova protein and the plasmid DNA induced more humoral immune response due to the immediate availability of Ova antigen and the long term protein production by the expression of Ova plasmid DNA. Formulations which delivered pDNA encoding Ova yielded humoral immune response represented by both IgG_1 and IgG_{2a}, but resulted in less antibody production than that from protein delivery. pDNA induced antibody production slowly increased over time

and became greater than protein induced production. This shows that using DNA vaccines enabled presenting the antigen to the immune system in a sustained manner compared to using vaccines that contained the antigen itself. Although antibody production induced by the administration of chitosan-TPP/(pOva + Ova) was higher than introducing either of the antigens alone, it was significantly less than that obtained with using dextran sulfate nanoparticles. The superiority of chitosan-DS in delivering the protein antigen and the plasmid DNA is a result of the optimized complexation between these anionic species and the polycationic polymer, chitosan.

Enumeration of antigen-specific $CD8^+$ T-cells was done by tetramer staining. MHC (major histocompatibility complex) peptide tetramers allow visualizing of antigen-specific T-cell immunity in humans and in animal model systems. MHC tetramers are complexes of four MHC molecules, which are associated with a specific peptide and bound to a fluorochrome. There are two types of Tetramers, Class I and Class II, class I Tetramers bind to a distinct set of T cell receptors (TCRs) on a subset of $CD8^+$ T cells, and class II Tetramers bind to a distinct population of $CD4^+$ T cells. Thus, by mixing Tetramers with serum or spleen extract and using flow cytometry as a detection system, a count of all $CD4^+$ or $CD8^+$ T cells that are specific for one peptide and its matched MHC allele is provided, regardless of functionality, allowing the measurement of the cellular response directed toward single peptide specificity.[197,198]

For the duration of the study, MHC peptide tetramer staining of spleen cells obtained from mice vaccinated with chitosan nanoparticle formulations showed that cellular response against Ova has not increased significantly. This could be as a result of the relatively short study period which were not sufficient for the sustained release particles to introduce the antigen and invoke the cellular immune response (Figure 2-42).

2.4 Conclusions

Chitosan/pDNA nanoparticles were prepared using an ionic gelation (complex coacervation) method which was optimized under defined conditions for gene delivery purposes. The most prominent force for the ionic gelation process in the formation of particles is the electrostatic interactions between chitosan, a polycationic polymer, and polyanionic species such as DNA, dextran sulfate, alginate, tripolyphosphate and sulfate. Sizes of chitosan nanoparticles were optimized using chitosan/polyanion w/w ratio. Generally, chitosan/polyanion w/w ratio of 10 yielded the smallest particles, a property targeted for better gene and drug delivery properties. Incorporation of dextran sulfate into chitosan nanoparticles enhanced their stability and resulted in narrowly distributed small particles. In addition, chitosan-DS nanoparticles were able to complex tightly with pDNA and protect the plasmid from degradation by DNase I. Ethidium bromide polyanionic displacement assay showed that dextran sulfate has a distinctive effect on chitosan/pDNA complexation compared to TPP and SA. It was found that the presence of dextran sulfate inside chitosan nanoparticles strengthened these structures and caused milder weakening of the interaction between chitosan and DNA, significantly less than SA and TPP. This means that dextran sulfate is more capable of protecting DNA inside chitosan nanoparticles, whilst it is capable to facilitate the release of DNA at certain conditions, such as inside the lysosomes. Using dextran sulfate, different formulation parameters were investigated and the fabrication of chitosan nanoparticles was optimized.

Images of chitosan/DNA nanoparticles showed relatively spherical particles which completely condensed DNA into submicron ranges. The efficiency of complexation by chitosan in the presence of dextran was confirmed by gel electrophoresis.

In vitro studies showed that chitosan and dextran sulfate exhibit significantly reduced toxicity compared to polyethyleneimine (PEI), a standard transfecting agent. Moreover, when optimizing the percentages of dextran sulfate and plasmid DNA as well

as chitosan grade, chitosan nanoparticles showed significant improvement in their ability to transfect HEK293. The best formulations were tested *in vivo* using C57BL/6 mice for their potential to be used as DNA vaccines. It was found that these particles delivered pDNA encoding Ova effectively into mammalian cells and caused expression of Ova protein which was able to induce humoral immune response. In addition, these formulations were capable of delivering both the plasmid DNA and the antigen (Ova) concurrently, causing enhanced immune response by providing immediate and sustained antigen exposure.

Therefore, it was shown in this study that the formulation conditions of chitosan nanoparticles can be optimized to result in efficient gene and protein delivery systems. These systems can be applied in numerous applications. Cancer therapy, DNA vaccines and treating single gene abnormities are examples of potential applications of chitosan nanoparticle.

2.5 Figures and Tables

Table 2-1. Theoretical and measured degrees of deacetylation of the prepared chitosans using heterogeneous reacetylation.

Chitosan grade	Theoretical degree of deacetylation	Measured degree of deacetylation
MM-HD	90.8%	90.92%
MM-MD	85.0%	83.94%
MM-LD	75.0%	74.36%
MM-VLD	65.0%	66.27%

Table 2-2. Degrees of deacetylation and molecular weights of the commercially available chitosans used for preparing chitosan nanoparticles.

Chitosan grade	Reported degree of deacetylation	Measured degree of deacetylation	Intrinsic viscosity (dL/g)	Viscosity molecular weight (Mv)
HM-HD	91.1%	91.28%	2.35	181686
MM-HD	90.8%	90.92%	1.97	144760
LM-HD	92.0%	92.10%	1.49	102017
MM-MD	84.3%	84.02%	1.83	132578

Table 2-3. Viscosity molecular weights of the prepared chitosans using oxidative fragmentation (OF) at different ratios of sodium nitrite.

Chitosan grade	Intrinsic viscosity (dL/g)	Viscosity molecular weight (M_v)	Measured degree of deacetylation
LM-HD	1.49	102017	92.10%
LM-HD OF1%	1.05	65940	91.30%
LM-HD OF1.5%	0.90	54222	91.42%
LM-HD OF2%	0.74	42460	90.89%
LM-HD OF4%	0.21	8642	90.19%

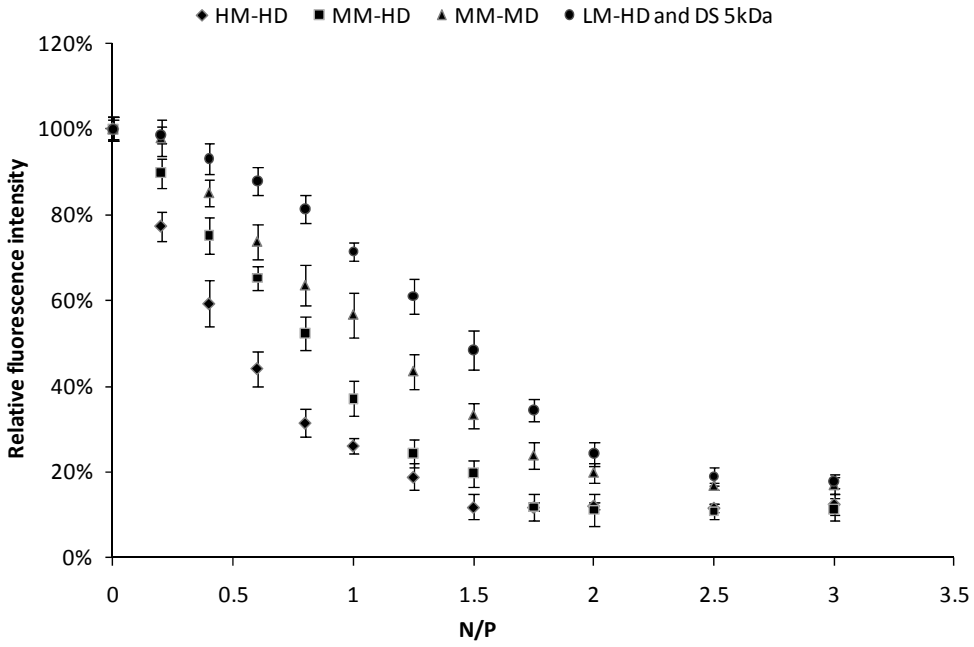

Figure 2-1. Quenching of ethidium bromide-DNA fluorescence after the incremental addition of three grades of chitosan; MM-HD, HM-HD and MM-MD, into solutions containing DNA-ethidium bromide complexes. Also the curve of LM-HD addition onto solution containing DNA, ethidium bromide and dextran sulfate 5 kDa is shown. Data are represented as the mean ± SD (n = 6).

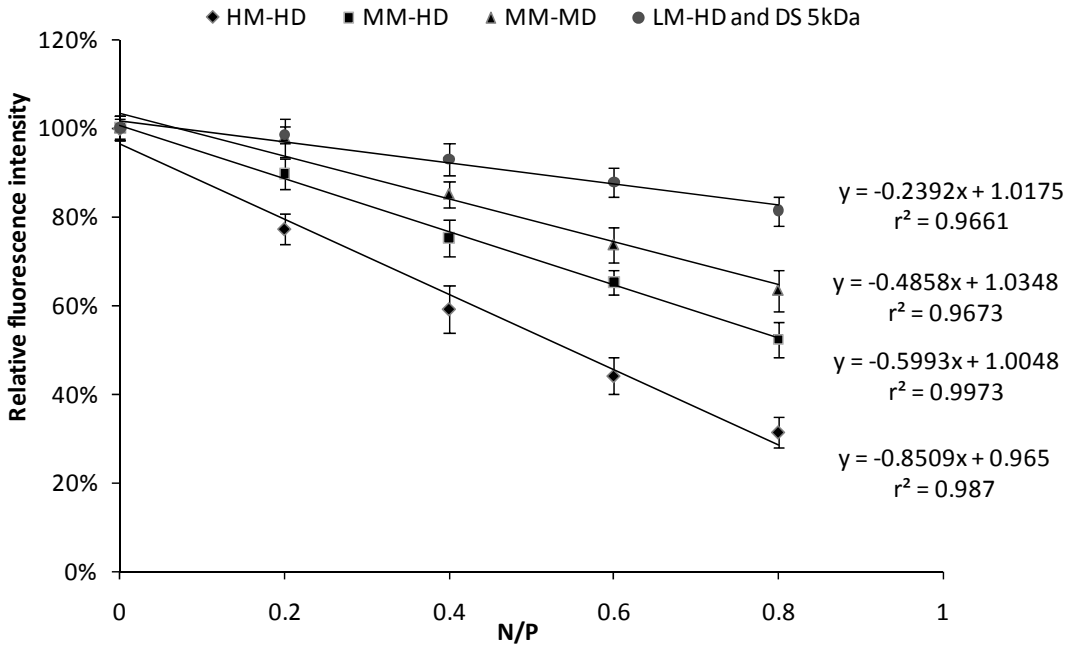

Figure 2-2. Initial curves and their linear regression for the addition of the three grades of chitosan; MM-HD, HM-HD and MM-MD, into solutions containing DNA-ethidium bromide complexes. Also the initial curve of LM-HD addition onto solution containing DNA, ethidium bromide and dextran sulfate 5 kDa is shown. Data are represented as the mean ± SD (n = 6).

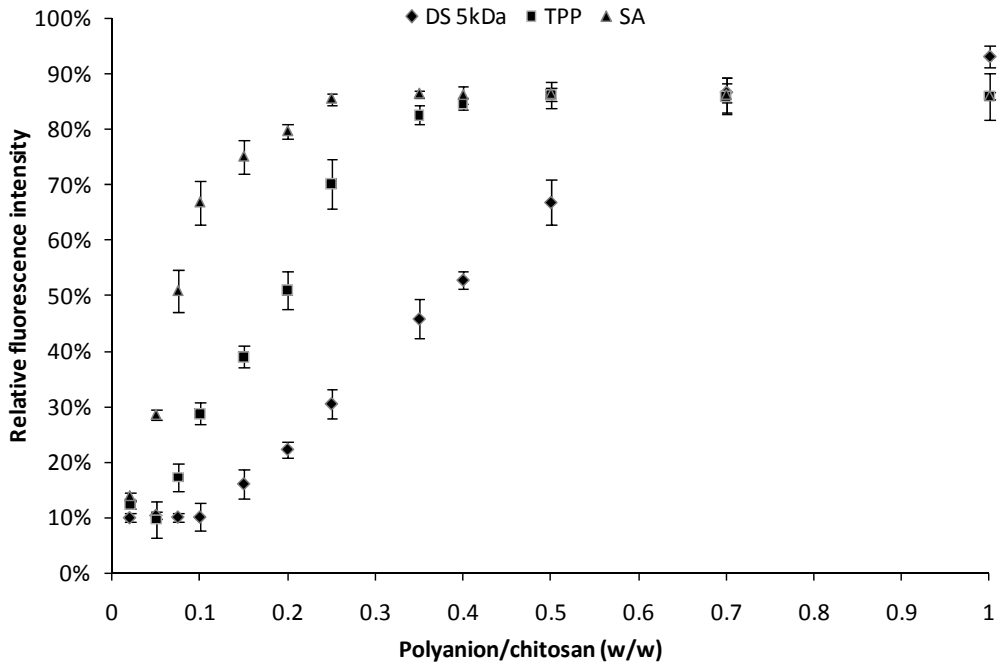

Figure 2-3. The effects of the incremental addition of different polyanions; sodium dextran sulfate 5 kDa, sodium tripolyphosphate and sodium alginate, on the fluorescence intensities of ethidium bromide in the presence of LM-HD chitosan-DNA complexes. Data are represented as the mean ± SD (n = 6).

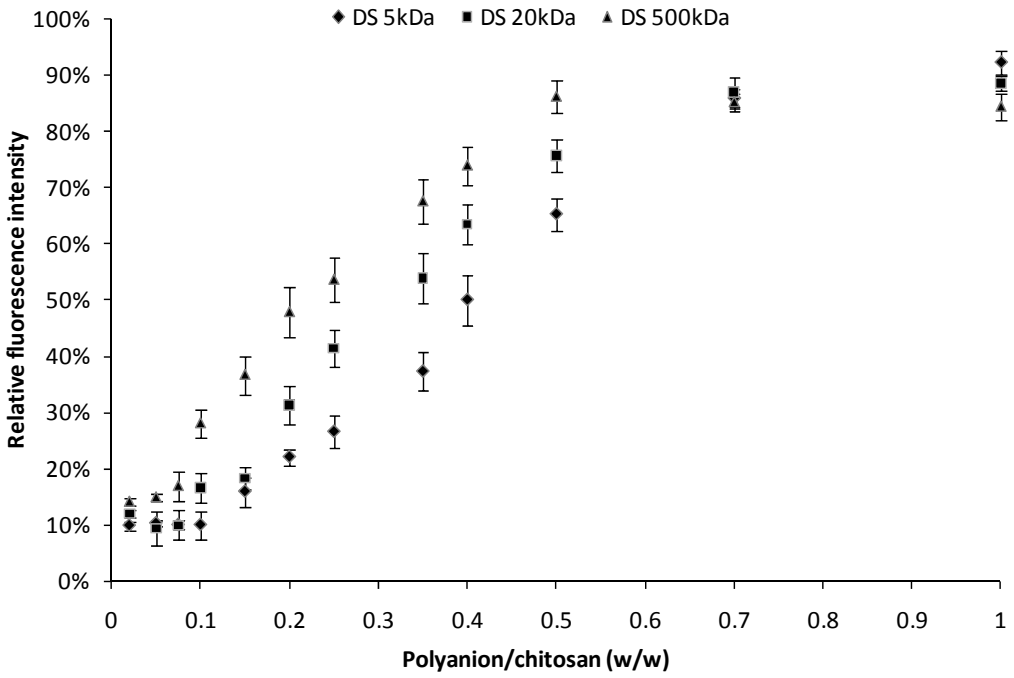

Figure 2-4. The effects of the incremental addition of different molecular weight dextran sulfate polymers (molecular weights 5, 20 and 500 kDa) on the fluorescence intensities of ethidium bromide in the presence of chitosan-DNA complexes. Data are represented as the mean ± SD (n = 6).

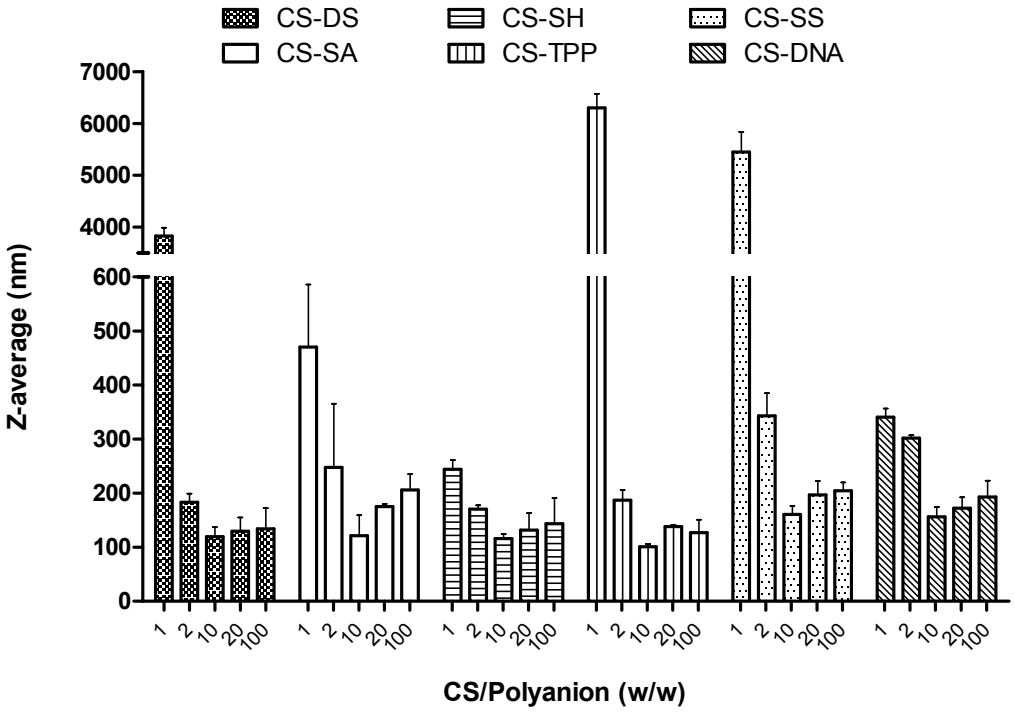

Figure 2-5. Z-average sizes of MM-HD chitosan nanoparticles prepared using various polyanions; dextran sulfate (DS), sodium alginate (SA), sodium hyaluronate (SH), tripolyphosphate (TPP), sodium sulfate (SS) and DNA by ionic gelation method. Data are represented as the mean ± SD (n = 3).

Table 2-4. The effects of cationic to anionic solution volume ratios on Z-average sizes and zeta potential values of chitosan-DS nanoparticles.

Volume ratio of cationic to anionic solutions	Z-average (nm) ± SD	Average zeta potential (mV) ± SD
2:1	183.0 ± 10.0	33.8 ± 1.3
1:1	169.9 ± 9.2	34.1 ± 0.8
1:2	133.7 ± 1.4	34.8 ± 0.4
1:3	135.6 ± 9.7	34.9 ± 1.1
1:5	138.3 ± 8.0	32.6 ± 3.3
1:7	140.2 ± 17.6	32.4 ± 1.4

Note: Final concentrations of dextran sulfate, chitosan and DNA in all formulations were the same.

Table 2-5. The effect of order of addition of cationic and anionic solutions on Z-average sizes and zeta potential values of chitosan-DS nanoparticles.

Order of addition	Z-average (nm) ± SD	Average zeta potential (mV) ± SD
Anionic solution added to cationic solution	150.9 ± 9.3	34.4 ± 1.3
Cationic solution added to anionic solution	130.3 ± 3.5	33.7 ± 1.0
Both mixed together at the same time	133.2 ± 8.2	34.7 ± 1.8

Note: Volume ratio of anionic to cationic solution for all formulations was 2 to 1.

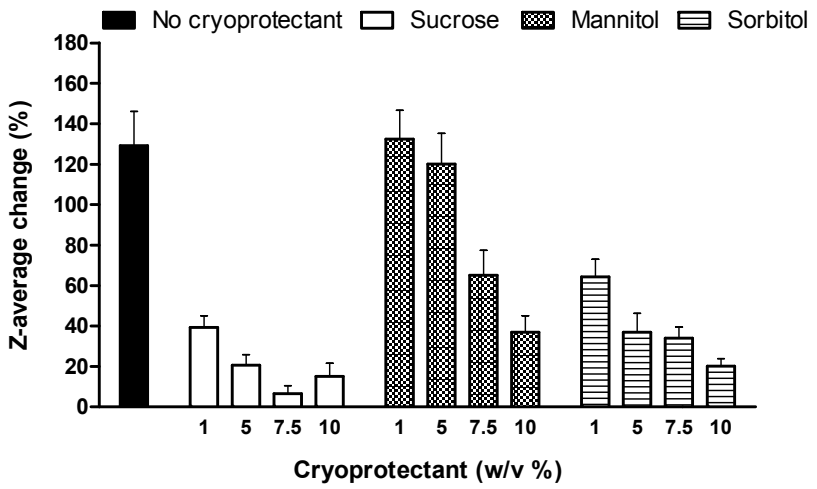

Figure 2-6. The percentage change in particle sizes of MM-HD chitosan-dextran sulfate/pDNA nanoparticles (w/w ratio of 10) after lyophilization as a function of the type and concentration of the cryoprotectants.

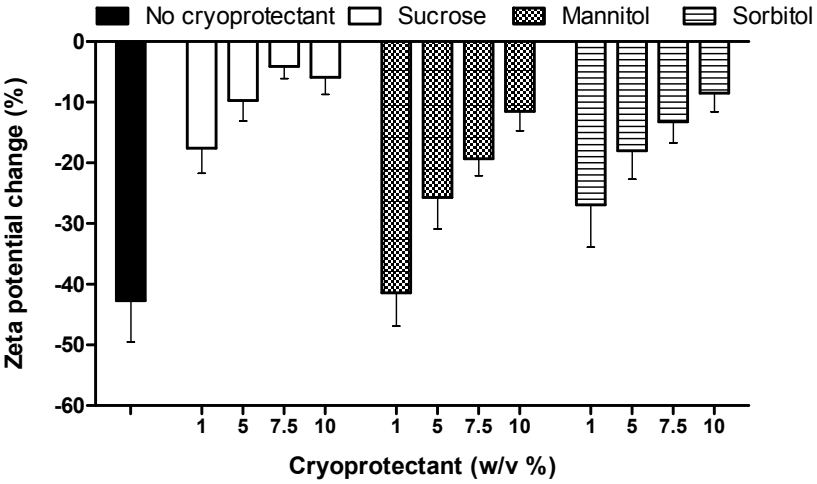

Figure 2-7. The relationship between the percentage change in zeta potential values of MM-HD chitosan-DS/pDNA nanoparticles (w/w ratio of 10) after lyophilization as a function of the type and concentration of the cryoprotectants.

Table 2-6. Z-average and zeta potential values of blank chitosan-TPP and chitosan-DS nanoparticles (without pDNA) up to 22 days at room temperature.

	Day 0			Day 13			Day 22		
Formulation	**Z-average (nm) ± SD**	**PDI**	**Zeta potential (mV) ± SD**	**Z-average (nm) ± SD**	**PDI**	**Zeta potential (mV)± SD**	**Z-average (nm) ± SD**	**PDI**	**Zeta potential (mV) ± SD**
CS-DS	127.9 ± 6.9	0.151	29.2 ± 0.5	131.8 ± 2.1	0.208	32.2 ± 1.8	136.9 ± 8.3	0.229	32.5 ± 2.1
CS-TPP	96.2 ± 5.2	0.229	28.8 ± 1.1	111.6 ± 7.9	0.206	29.2 ± 0.4	115.2 ± 5.1	0.180	29.1 ± 1.5

Table 2-7. The effect of the reported molecular weights of dextran sulfate on the sizes of chitosan-DS nanoparticles upon storage at room temperature.

	Day 0		Day 8		Day 15		Day 22		Day 30		Day 37	
Dextran sulfate type	**Z-average (nm) ± SD**	**PDI**	**Z-average (nm) ± SD**	**PDI**	**Z-average (nm) ± SD**	**PDI**	**Z-average (nm) ± SD**	**PDI**	**Z-average (nm) ± SD**	**PDI**	**Z-average (nm) ± SD**	**PDI**
DS 500kDa	138.8±7.1	0.211	143.7±7.1	0.191	148.5±2.5	0.236	135.5±11.0	0.225	138.8±12.9	0.208	132.2±12.3	0.195
DS 9-20kDa	165.4±15.5	0.269	172.1±12.8	0.214	166.3±22.0	0.270	156.3±16.6	0.227	163.0±31.5	0.185	162.7±17.3	0.173
DS 6-10kDa	167.1±11.6	0.222	166.1±19.9	0.217	173.5±32.7	0.266	162.2±24.1	0.246	161.0±24.3	0.214	160.6±24.2	0.169
DS 5K	166.0±25.9	0.235	170.0±32.2	0.208	189.8±14.8	0.245	179.4±16.8	0.217	193.5±37.1	0.233	199.4±48.4	0.237

Table 2-8. The effect of the reported molecular weights of dextran sulfate on the zeta potential values of chitosan-DS nanoparticles.

	Zeta potential (mV)± SD					
Dextran sulfate type	**Day 0**	**Day 8**	**Day 15**	**Day 22**	**Day 30**	**Day 37**
DS 500K	29.5 ± 1.5	30.7 ± 1.8	29.4 ± 0.5	28.6 ± 0.4	31.2 ± 3.0	29.4 ± 0.5
DS 9-20K	29.4 ± 2.6	30.5 ± 2.7	30.3 ± 1.7	30.4 ± 1.1	28.5 ± 1.5	29.0 ± 2.9
DS 6-10K	29.8 ± 1.4	32.3 ± 1.5	30.5 ± 0.4	27.6 ± 0.8	32.4 ± 2.2	30.9 ± 2.4
DS 5K	27.8 ± 1.1	30.5 ± 1.8	29.7 ± 1.4	32.1 ± 2.5	31.4 ± 1.0	32.0 ± 2.6

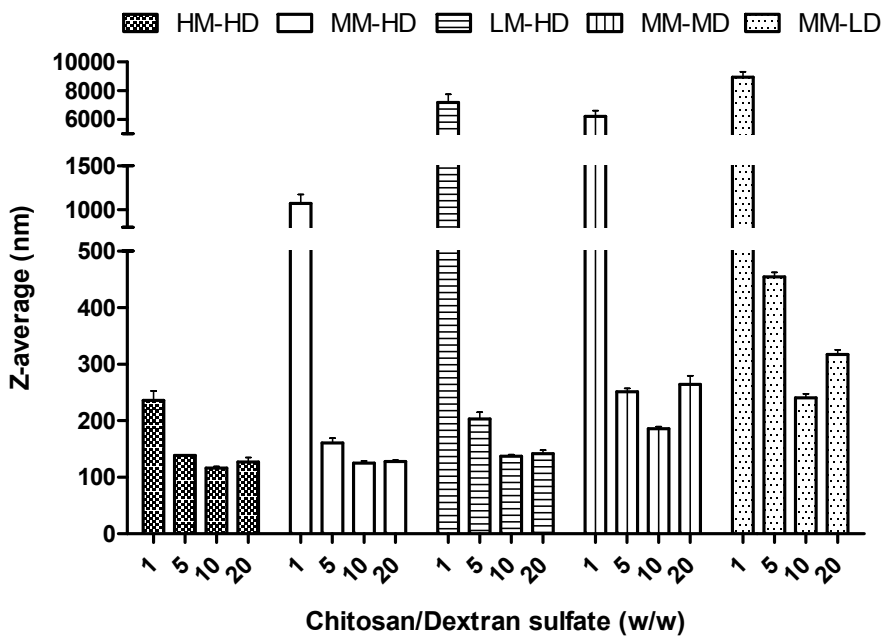

Figure 2-8. Z-average sizes of chitosan-DS/pDNA nanoparticles at different chitosan to DS w/w ratios for the five grades of chitosan; HM-HD, MM-HD, LM-HD, MM-MD and MM-LD. Data are represented as the mean ± SD (n = 3).

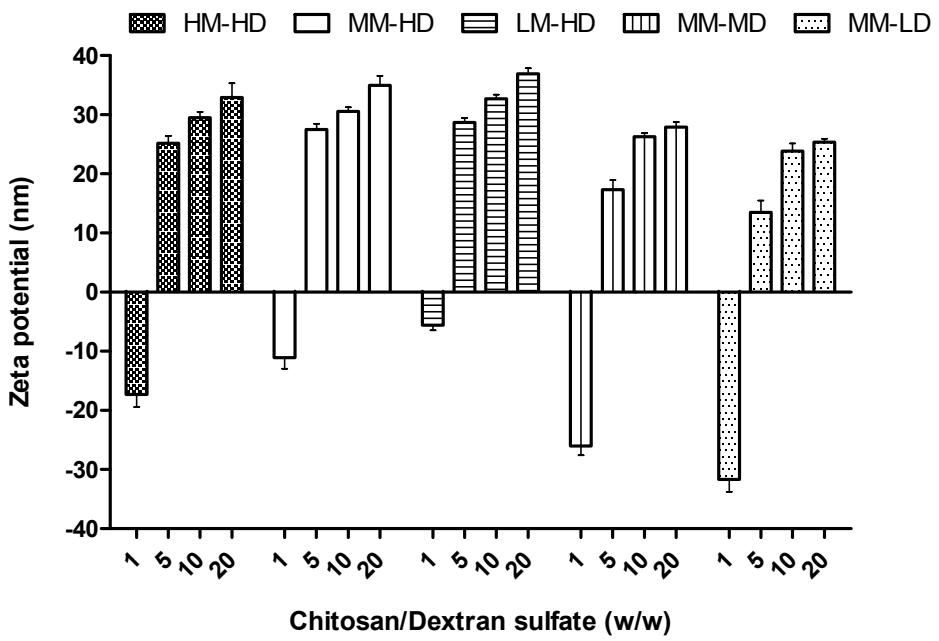

Figure 2-9. Zeta potential values of chitosan-DS/pDNA nanoparticles at different chitosan to DS w/w ratios for the five grades of chitosan; HM-HD, MM-HD, LM-HD, MM-MD and MM-LD. Data are represented as the mean ± SD (n = 3).

Table 2-9. Particle sizes and zeta potential values of CS-DS/DNA nanoparticles (N/P ratio = 25, CS/polyanion w/w ratio= 10) stored in 0.5 M anionic buffers having a range of pH values at room temperature.

		Day 0		Day 8		Day 23		Day 29	
Buffer and pH	**Zeta potential (mV) ± SD**	**Z-average (nm) ± SD**	**PDI**	**Z-average (nm) ± SD**	**PDI**	**Z-average (nm) ± SD**	**PDI**	**Z-average (nm) ± SD**	**PDI**
Acetate 3.46	30.7 ± 1.3	134.3 ± 0.8	0.186	175.3 ± 26.3	0.191	305.0 ± 29.7	0.245	310.1 ± 19.3	0.221
Acetate 4.46	30.3 ± 0.9	140.9 ± 13.2	0.238	161.0 ± 3.2	0.237	176.3 ± 10.5	0.159	181.2 ± 15.7	0.275
Acetate 5.46	27.9 ± 0.9	145.7 ± 12.2	0.263	133.3 ± 3.5	0.240	141.2 ± 5.4	0.245	144.5 ± 7.6	0.324
Phosphate 6.46	12.7 ± 2.3	159.0 ± 10.7	0.132	aggregated	NA	aggregated	NA	aggregated	NA
Phosphate 7.46	2.2 ± 0.4	1191.5 ± 84.1	0.864	aggregated	NA	aggregated	NA	aggregated	NA

Table 2-10. Particle sizes and zeta potential values of CS-DS/DNA nanoparticles prepared in 0.5 M cationic buffers having a range of pH values at room temperature.

Buffer and pH	Zeta potential (mV) ± SD	Z-average (nm) ± SD	PDI
Bis-Tris 5.46	28.3 ± 1.3	136.2 ± 4.8	0.200
Bis-Tris 6.46	13.3 ± 1.7	152.0 ± 1.6	0.127
Bis-Tris 7.46	2.7 ± 1.2	915.3 ± 217.4	0.769
Tris 7.46	2.6 ± 3.3	1135.5 ± 91.2	0.647
Tris 8.46	-18.7 ± 1.6	2648.5 ± 1601.6	0.508

Note: N/P ratio = 25 and CS/DS w/w ratio= 10.

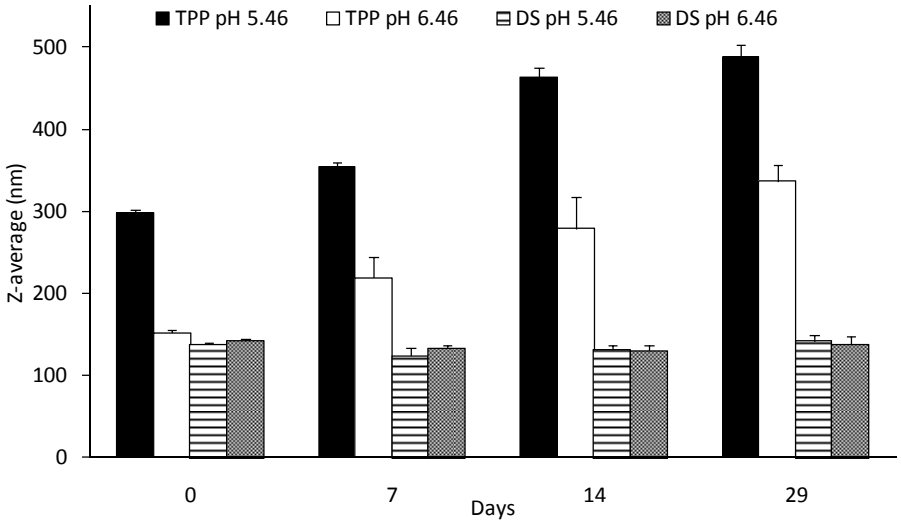

Figure 2-10. Comparison of the sizes of CS-TPP/DNA and CS-DS/DNA nanoparticles (N/P ratio = 25, CS/polyanion w/w ratio= 10) suspended in 0.5 M Bis-Tris buffer (pH 5.46 and 6.46). Data are represented as the mean ± SD (n = 3).

Table 2-11. Stability profiles of CS-TPP/DNA and CS-DS/DNA nanoparticles stored in 0.5 M Bis-Tris buffer pH 5.46 at 4, 25 and 37°C.

Day 0						
Sample ID	**Z-average (nm) ± SD**	**PDI**				
CS-TPP	299.0 ± 3.4	0.298				
CS-DS	134.4 ± 12.5	0.233				
Day 7						
	4°C		**25°C**		**37°C**	
Sample ID	**Z-average (nm) ± SD**	**PDI**	**Z-average (nm) ± SD**	**PDI**	**Z-average (nm) ± SD**	**PDI**
CS-TPP	334.1 ± 16.7	0.254	345.7 ± 15.6	0.229	362.8 ± 21.6	0.283
CS-DS	154.8 ± 18.5	0.260	135.7 ± 5.6	0.236	193.6 ± 4.2	0.264
Day 24						
	4°C		**25°C**		**37°C**	
Sample ID	**Z-average (nm) ± SD**	**PDI**	**Z-average (nm) ± SD**	**PDI**	**Z-average (nm) ± SD**	**PDI**
CS-TPP	369.1 ± 28.4	0.343	403.6 ± 29.9	0.257	453.8 ± 30.9	0.329
CS-DS	153.7 ± 10.3	0.266	138.2 ± 7.3	0.240	207.8 ± 16.2	0.306
Day 29						
	4°C		**25°C**		**37°C**	
Sample ID	**Z-average (nm) ± SD**	**PDI**	**Z-average (nm) ± SD**	**PDI**	**Z-average (nm) ± SD**	**PDI**
CS-TPP	395.6 ± 18.9	0.369	528.6 ± 37.0	0.329	575.6 ± 24.5	0.403
CS-DS	161.6 ± 6.5	0.373	141.6 ± 10.0	0.282	246.9 ± 22.9	0.358

Note: N/P ratio = 25 and CS/polyanion w/w ratio= 10.

Table 2-12. The effect of DNA concentration on the sizes and zeta potential values of CS-DS/DNA nanoparticles.

DNA concentration (mg/ml)	Z-average (nm) ± SD	PDI	Average zeta potential (mV) ± SD
0.01	135.7 ± 10.8	0.191	28.7 ± 0.5
0.02	130.2 ± 7.6	0.220	29.6 ± 1.5
0.04	137.0 ± 11.1	0.193	31.4 ± 0.7
0.05	143.7 ± 6.7	0.225	31.8 ± 1.3
0.06	174.9 ± 16.4	0.219	34.2 ± 1.9
0.08	204.6 ± 9.9	0.252	37.8 ± 1.4
0.10	235.5 ± 14.1	0.232	41.1 ± 2.6

Note: N/P ratio = 25 and CS/DS w/w ratio= 10.

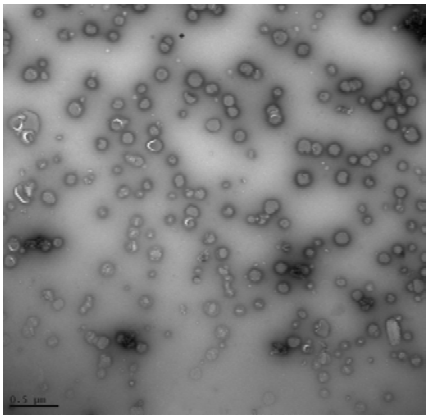

Figure 2-11. Transmission electron micrographs (TEM) of chitosan-DS/pDNA nanoparticles. Nanoparticles were prepared at CS/DS w/w ratio = 10 and N/P ratio = 15 and were negatively stained by 1% uranyl acetate on Formvar coated grids (JEOL 1230 TEM).

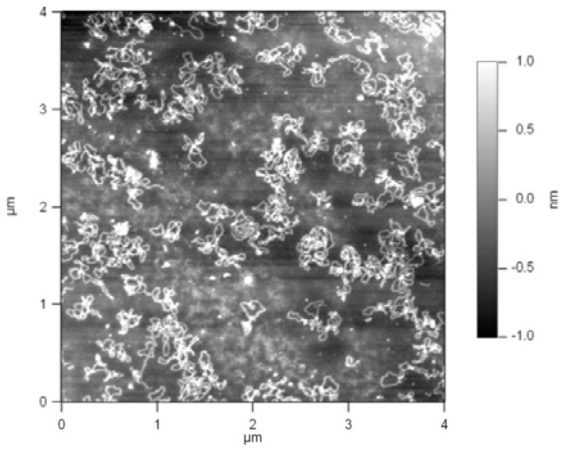

Figure 2-12. Tapping mode atomic force microscopy (AFM) images of naked 0.5 µg/ml plasmid DNA (VR1255) fixed on Mica film (Asylum AFM).

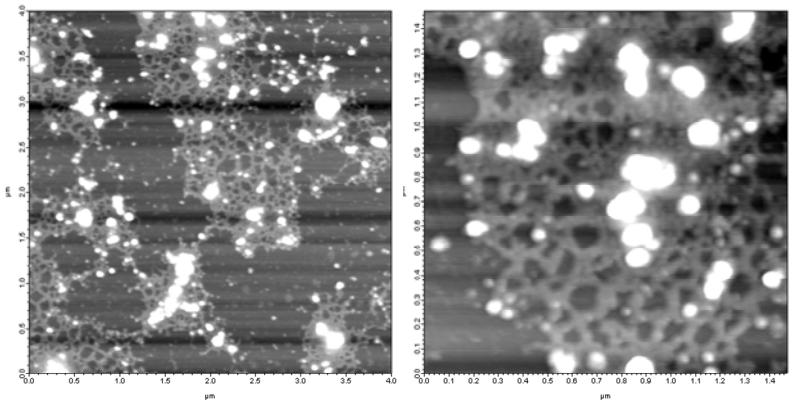

Figure 2-13. Tapping mode atomic force microscopy (AFM) images of chitosan-dextran sulfate/DNA nanoparticles at N/P ratio of 2 fixed on Mica film. White spots represent chitosan nanoparticles.

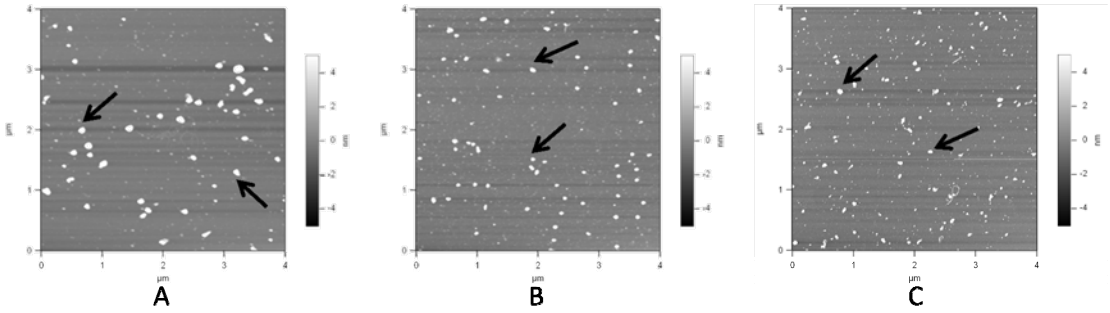

Figure 2-14. Tapping mode atomic force microscopy (AFM) images of chitosan nanoparticles prepared using SS, TPP or DS. Chitosan nanoparticles were prepared at A) CS/SS w/w ratio = 10, B) CS/TPP w/w ratio = 10 or C) CS/DS w/w ratio = 10. Black arrows point to some of the imaged chitosan nanoparticles (white spots).

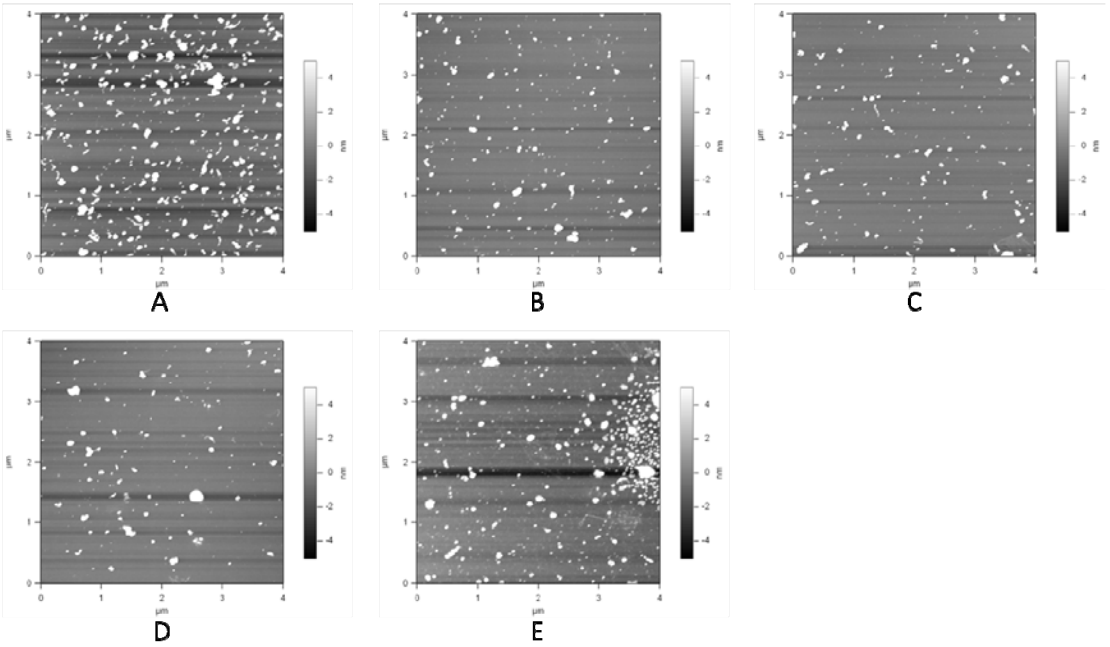

Figure 2-15. Tapping mode atomic force microscopy (AFM) images of chitosan-DS/pDNA nanoparticles at different N/P ratios. Chitosan nanoparticles were prepared at CS/DS w/w ratio = 10 and N/P ratio of A) 5, B) 10, C) 15, D) 25 and E) 35.

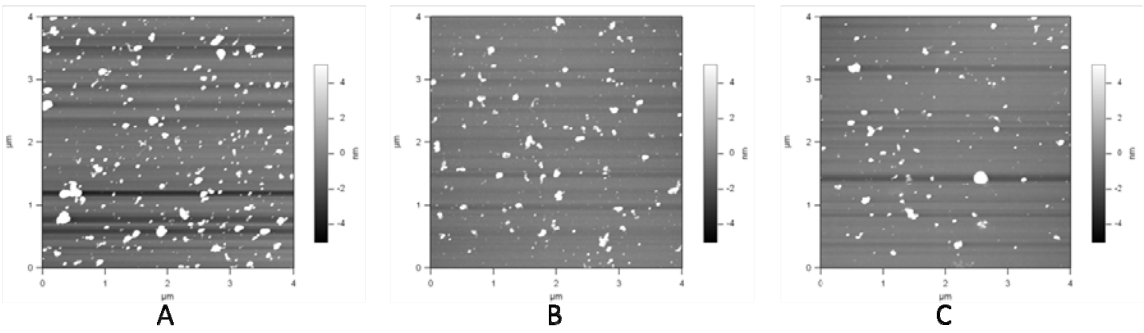

Figure 2-16. Tapping mode atomic force microscopy (AFM) images of chitosan-DS/pDNA nanoparticles prepared at different w/w ratios. Chitosan nanoparticles were prepared at N/P ratio = 25 and CS/DS w/w ratio of A) 5, B) 10 or C) 20.

Table 2-13. Quantitative analysis of AFM images (Figures 2-14 to 2-16) using Igor Pro 6.1.1.0.

		Average Area (nm^2)	Average perimeter (nm)	Average Volume (nm^3)
Polyanions	DS	731.13	79.37	4061.22
	TPP	1068.58	90.98	5181.63
	SS	2999.43	168.61	15497.89
CS/pDNA (N/P)	5	4158.39	234.53	29481.48
	10	1849.01	130.34	10733.02
	15	2255.26	151.69	13662.78
	25	2572.19	157.75	17248.96
	35	2948.39	180.42	12965.19
CS/DS (w/w)	5	3360.38	188.50	26649.37
	10	2572.19	157.75	17248.96
	20	2301.17	144.63	11050.45

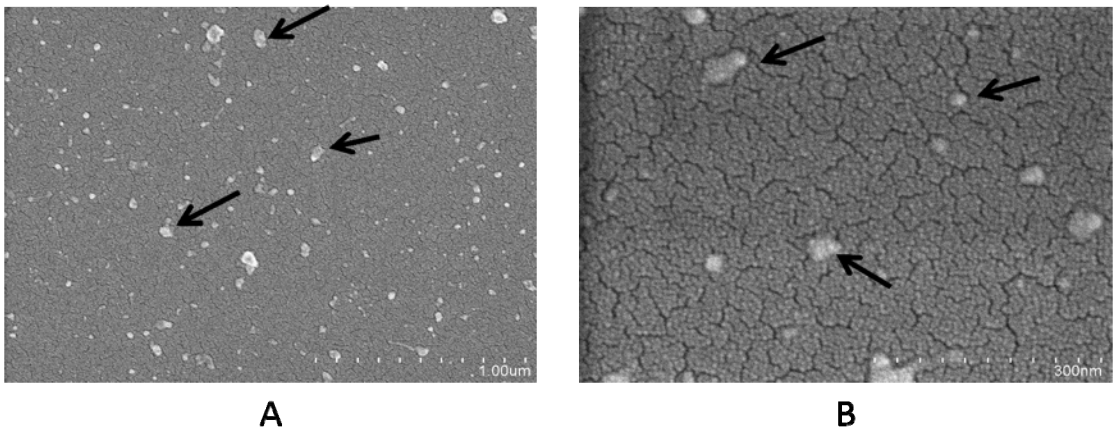

Figure 2-17. Morphology of chitosan-DS/pDNA nanoparticles by scanning electron microscopy (SEM). Chitosan/DS w/w ratio = 10 and N/P ratio = 15. Accelerating voltage = 2.0 kV, magnification of A) 50,000 and B) 180,000. Black arrows point to some of the imaged chitosan nanoparticles.

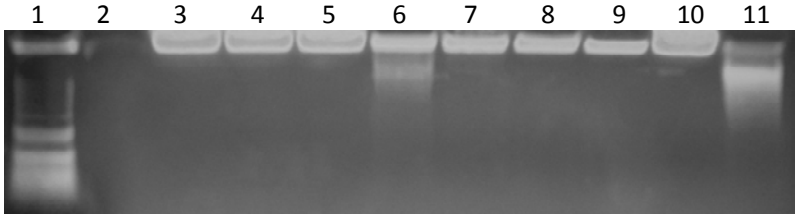

Figure 2-18. Agarose gel electrophoresis of chitosan-DS/DNA nanoparticles at different N/P ratios. (1) TrackIt™ 1 Kb DNA Ladder (Invitrogen™), (2) LM-HD CS-DS without DNA (3) LM-HD CS-DS/DNA, N/P = 10 (4) MM-HD CS-DS/DNA N/P = 10 (5) MM-LD CS-DS/DNA N/P = 10 (6) LM-HD CS-DS/DNA N/P = 0.5 (7) LM-HD CS-DS/DNA N/P = 1 (8) LM-HD CS-DS/DNA N/P = 2 (9) LM-HD CS-DS/DNA N/P = 3 (10) LM-HD CS-DS/DNA N/P = 5 (11) Naked DNA.

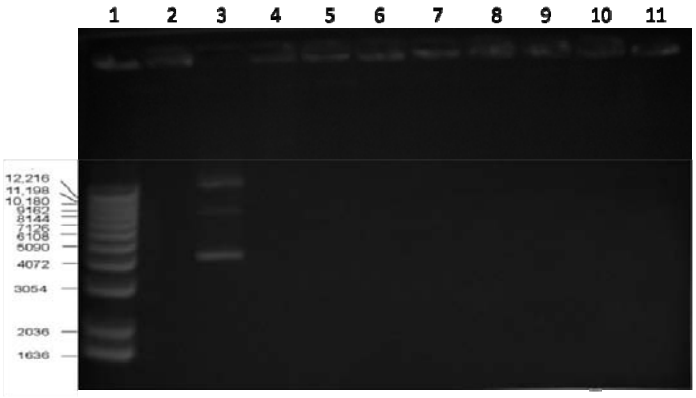

Figure 2-19. Agarose gel electrophoresis of chitosan/DNA nanoparticles fabricated using different polyanions and at different w/w ratios. (1) TrackIt™ 1 Kb DNA Ladder (Invitrogen™), (2) PEI/pDNA, N/P = 10 (3) VR1255 naked pDNA (4) LM-HD CS-SH/DNA, N/P = 10 (5) LM-HD CS- TPP/DNA, N/P = 10 (6) LM-HD CS-SS/DNA, N/P = 10 (7) LM-HD CS-SA/DNA, N/P = 10 (8) LM-HD CS-DS/DNA, N/P = 10, CS/DS w/w ratio = 5 (9) LM-HD CS-DS/DNA, N/P = 10, CS/DS w/w ratio = 10 (10) LM-HD CS-DS/DNA, N/P = 10, CS/DS w/w ratio = 15 (11) LM-HD CS-DS/DNA, N/P = 10, CS/DS w/w ratio = 20.

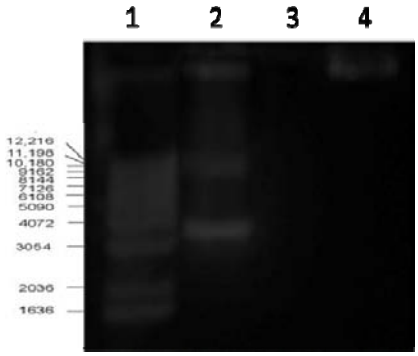

Figure 2-20. Agarose gel electrophoresis of chitosan-DS/DNA nanoparticles and their supernatant after centrifugation. (1) TrackIt™ 1 Kb DNA Ladder (Invitrogen™) (2) VR1255 naked pDNA (3) Supernatant after centrifugation of LM-HD chitosan- DS/DNA, N/P = 10, nanoparticles at 30,000 rpm using Sorvall Discovery 90 SE ultracentrifuge and T-1270 rotor (4) LM-HD CS-DS/DNA, N/P = 10, nanoparticles.

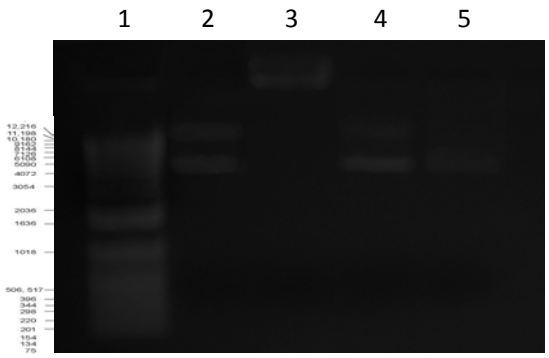

Figure 2-21. Agarose gel electrophoresis of chitosan-DS/DNA nanoparticles after exposure to DNase I enzyme. (1) TrackIt™ 1 Kb DNA Ladder (Invitrogen™), (2) VR1255 naked pDNA without treatment (3) LM-HD chitosan- DS/DNA without treatment, N/P = 10 (4) LM-HD chitosan-DS/DNA treated with 100 unit/ml of DNase I for 60 min (5) VR1255 naked pDNA treated with 100 unit/ml of DNase I for 60 min.

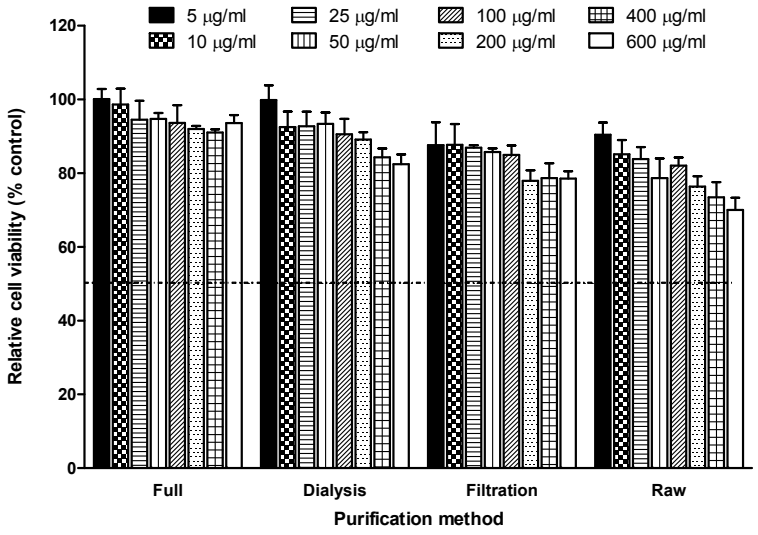

Figure 2-22. Cytotoxicity of untreated chitosan (raw) and purified chitosan samples by filtration, dialysis and full purification in HEK293 cells. Cell viability was measured using MTT assay as described in the experimental section. Data are represented as the mean ± SD (n = 6).

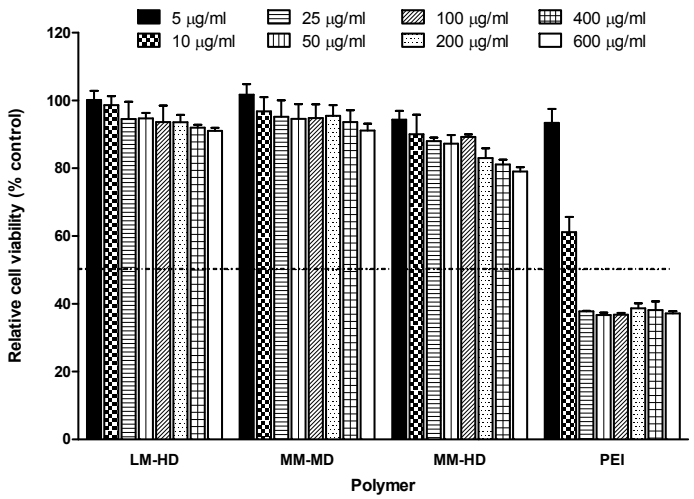

Figure 2-23. Cytotoxicity of LM-HD, MM-HD and MM-MD chitosans in HEK293 cells, in comparison to branched PEI. Cell viability was measured using MTT assay. Data are represented as the mean ± SD (n = 6).

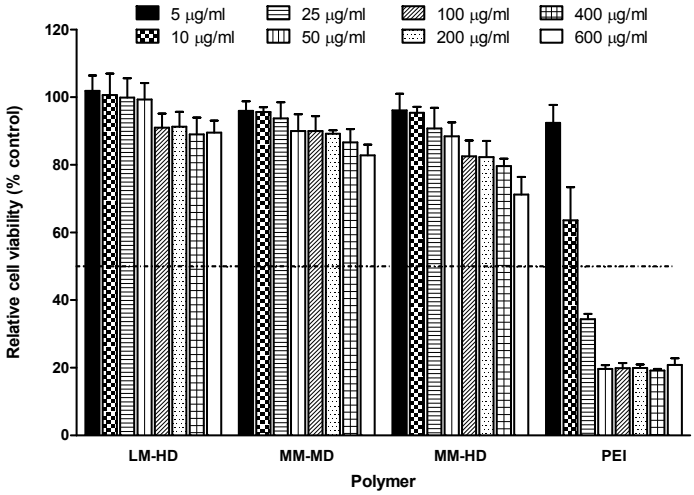

Figure 2-24. Cytotoxicity of LM-HD, MM-HD and MM-MD chitosans in COS7 cells in comparison to branched PEI. Cell viability was measured using MTT assay. Data are represented as the mean ± SD (n = 6).

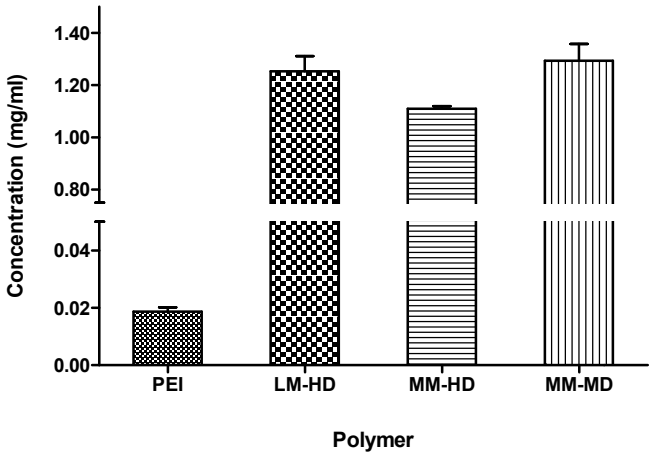

Figure 2-25. IC_{50} of LM-HD, MM-HD and MM-MD chitosans in HEK293 cells, in comparison to branched PEI. Cell viability was measured using MTT assay. Data are represented as the mean ± SD (n = 6).

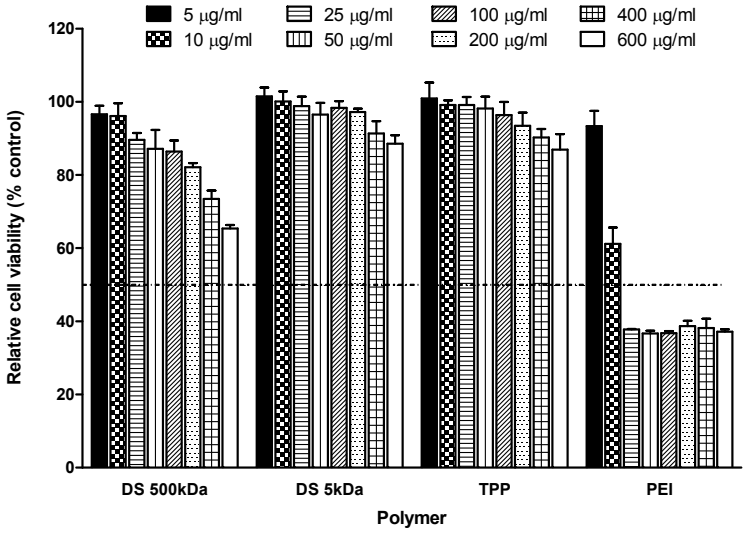

Figure 2-26. Cytotoxicity of TPP and dextran sulfate (5 and 500 kDa) in HEK293 cells in comparison to branched PEI. Cell viability was measured using MTT assay. Data are represented as the mean ± SD (n = 6).

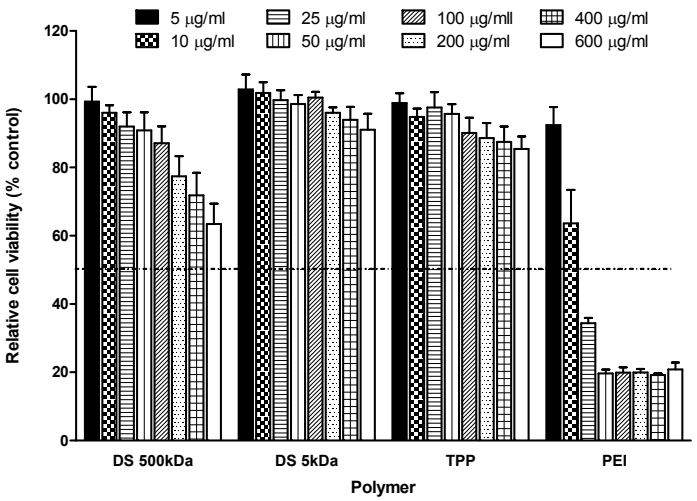

Figure 2-27. Cytotoxicity of TPP and dextran sulfate (5 and 500 kDa) in COS7 cells in comparison to branched PEI. Cell viability was measured using MTT assay. Data are represented as the mean ± SD (n = 6).

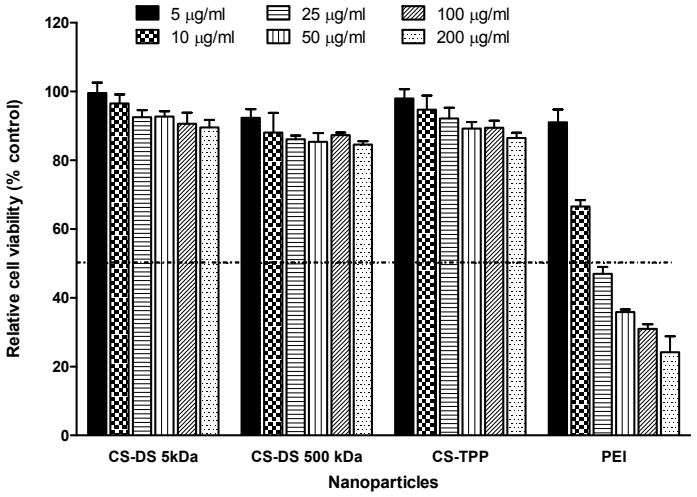

Figure 2-28. Cytotoxicity of chitosan nanoparticles containing pDNA encoding luciferase prepared with TPP and DS (5 and 500 kDa) in HEK293 cells in comparison to branched PEI nanoparticles. Cell viability was measured using MTT assay. Data are represented as the mean ± SD (n = 6).

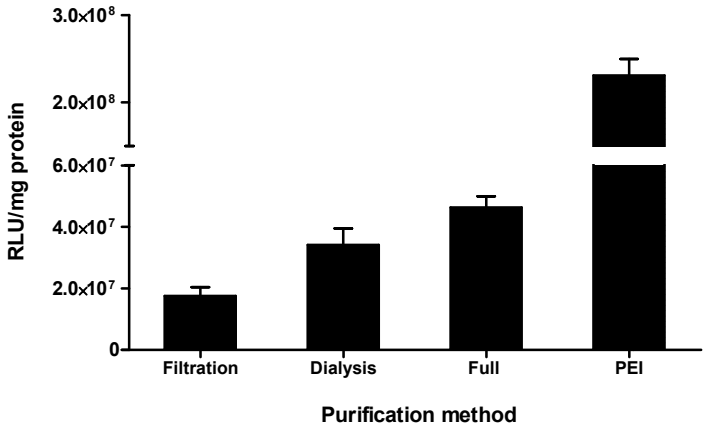

Figure 2-29. The effect of chitosan purification method (described in section 2.2.1) on the transfection efficiencies of chitosan-DS nanoparticles in HEK293 cells. Data are represented as the mean ± SD (n = 3).

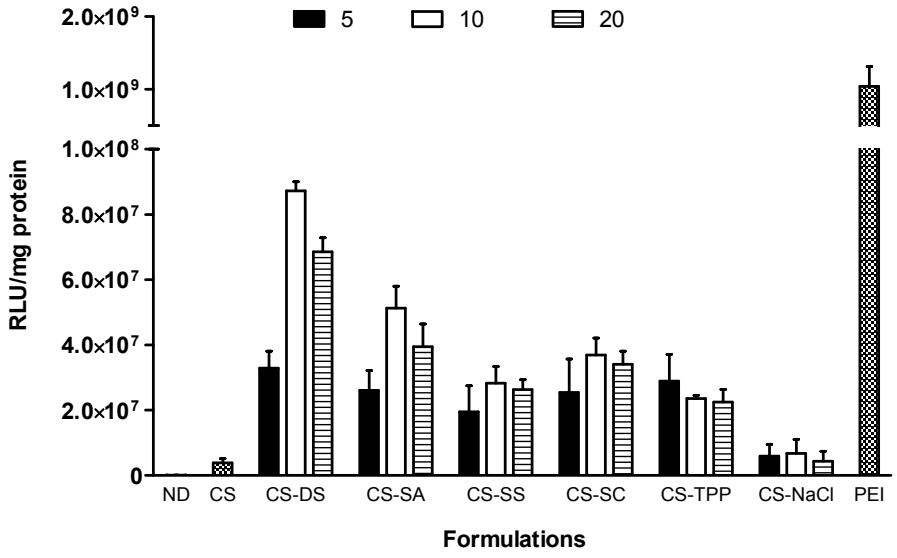

Figure 2-30. Results of screening various polyanions for their transfection efficiencies in HEK293 cells. Numbers on the legend represent the CS/polyanion w/w ratio. Data are represented as the mean ± SD (n = 3).

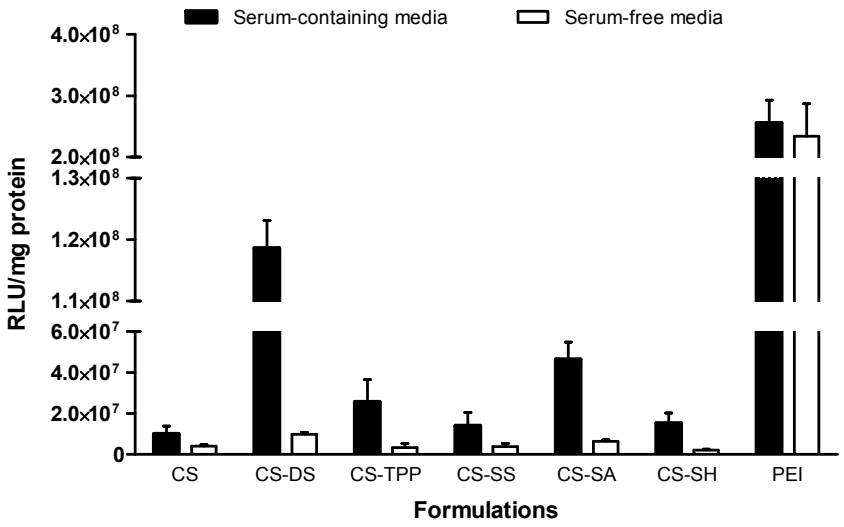

Figure 2-31. Transfection efficiencies of LM-HD chitosan nanoparticles (N/P ratio = 25) prepared using different polyanions in serum-containing and serum free media. Data are represented as the mean ± SD (n = 3).

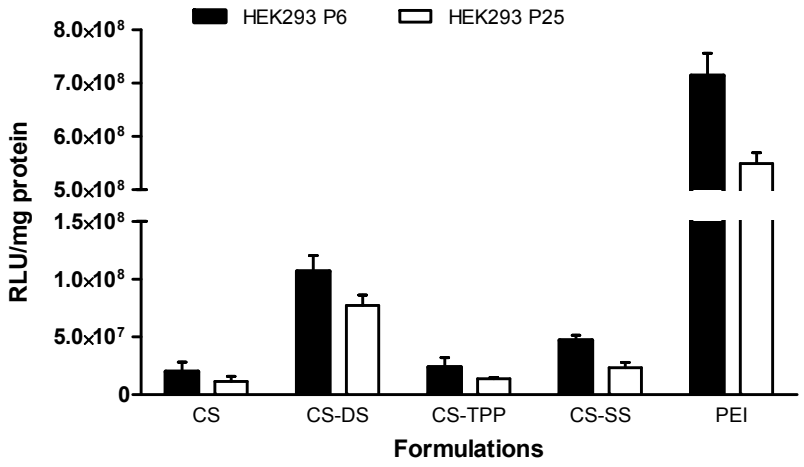

Figure 2-32. Transfection efficiencies of LM-HD chitosan nanoparticles (N/P ratio = 25) using different polyanions in HEK293 cell lines (passage numbers 6 and 25). Data are represented as the mean ± SD (n = 3).

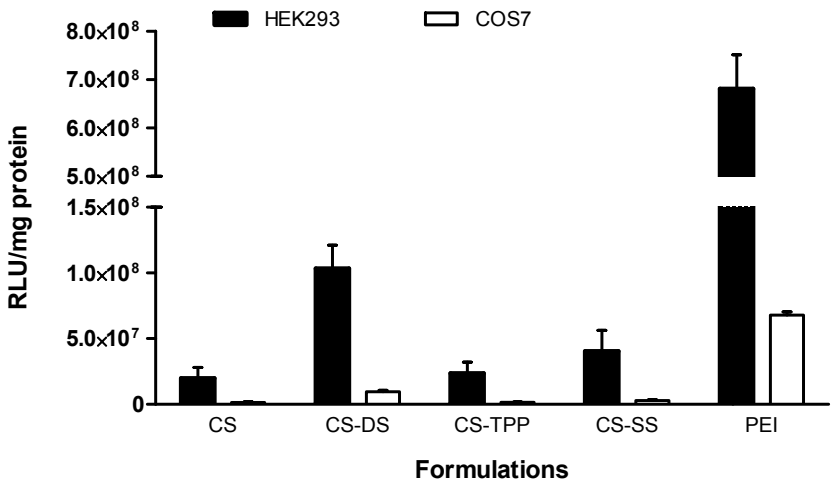

Figure 2-33. Transfection efficiencies of LM-HD chitosan nanoparticles (N/P ratio = 25) using different polyanions in HEK293 and COS7 cell lines. Data are represented as the mean ± SD (n = 3).

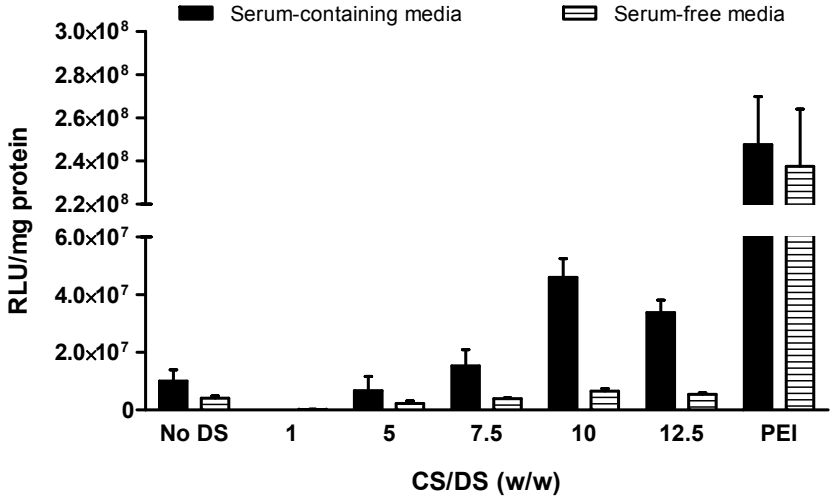

Figure 2-34. Transfection efficiencies of MM-HD chitosan nanoparticles (N/P ratio = 15) prepared at different chitosan to DS w/w ratios in serum-containing and serum-free media. Data are represented as the mean ± SD (n = 3).

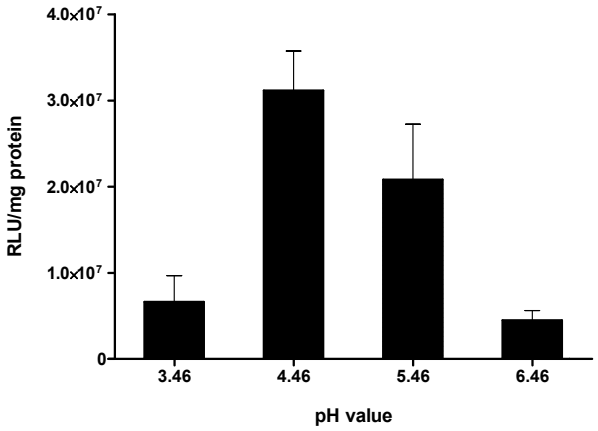

Figure 2-35. Transfection efficiencies of MM-HD chitosan nanoparticles (N/P ratio = 15) prepared in 50 mM acetate buffer at pH values of 3.46, 4.46 and 5.46, and 6.46. Data are represented as the mean ± SD (*n* = 3).

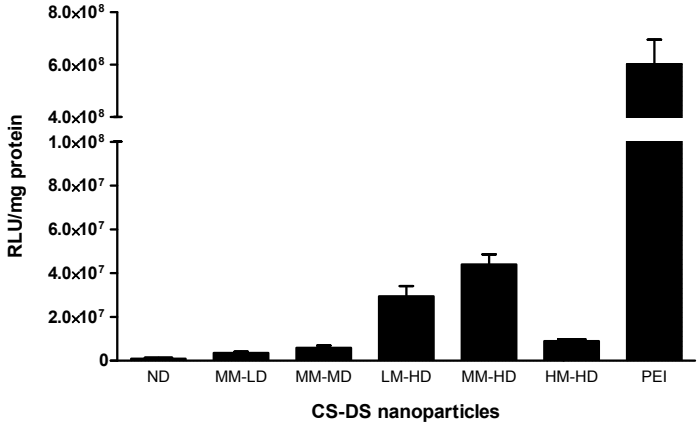

Figure 2-36. Transfection efficiencies of chitosan-DS/pDNA nanoparticles made using various chitosan grades; MM-LD, MM-MD, LM-HD, MM-HD and HM-HD. Chitosan/DS w/w ratio = 10 and N/P ratio = 15. Data are represented as the mean ± SD (*n* = 3).

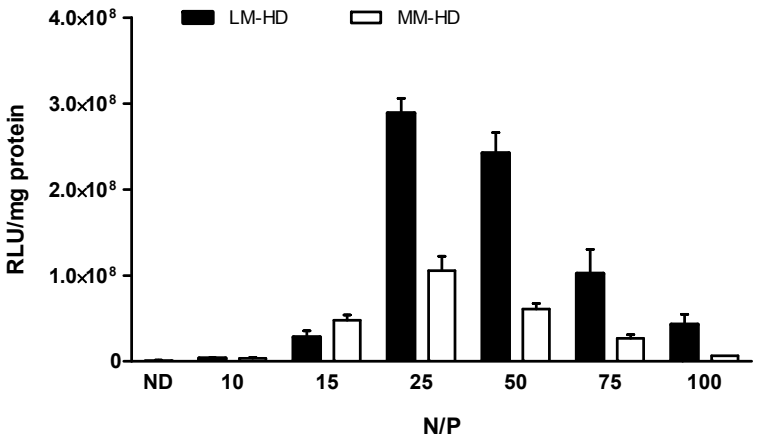

Figure 2-37. Transfection efficiencies of LM-HD and MM-HD chitosan nanoparticles at different N/P ratios in HEK293. Chitosan/DS w/w ratio = 10. Data are represented as the mean ± SD (n = 3).

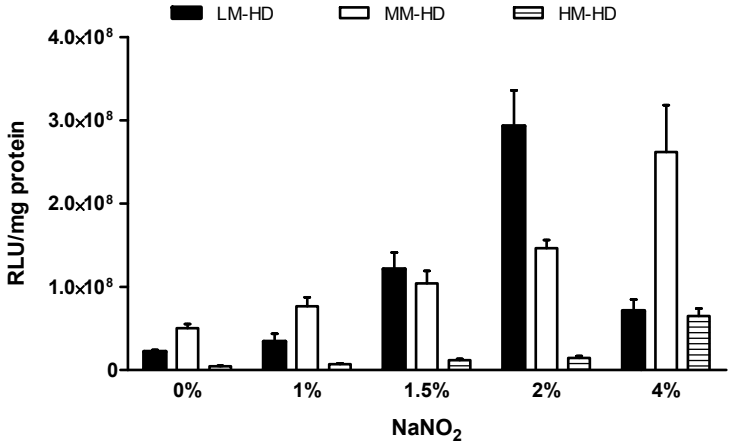

Figure 2-38. Transfection efficiencies of nanoparticles made of LM-HD, MM-HD and HM-HD chitosans and their oxidative fragmentation products at various chitosan to sodium nitrite weight ratios. Chitosan/DS w/w ratio = 10 and N/P ratio = 15. Data are represented as the mean ± SD (n = 3).

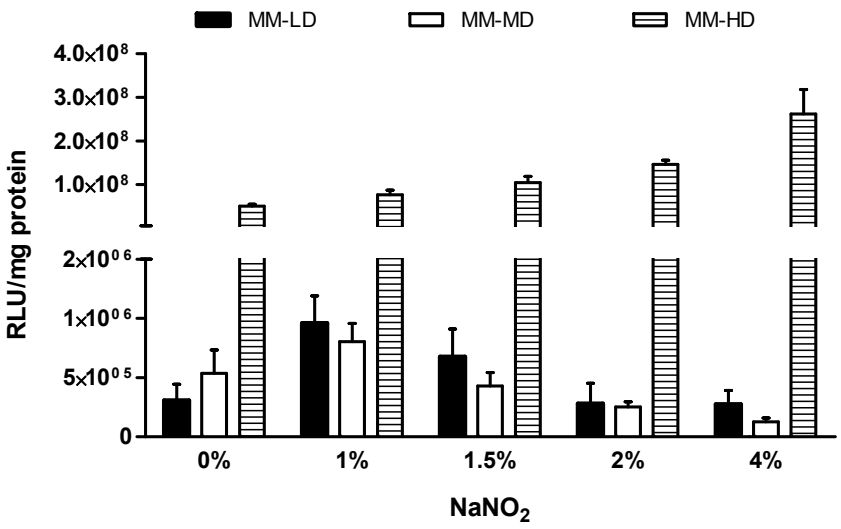

Figure 2-39. Transfection efficiencies of nanoparticles made of MM-MD, MM-MD and MM-HD chitosans and their oxidative fragmentation products at various chitosan to sodium nitrite weight ratios. Chitosan/DS w/w ratio = 10 and N/P ratio = 15. Data are represented as the mean ± SD (n = 3).

Table 2-14. Formulations of chitosan nanoparticles used for mouse vaccination.

Formulations	CS/mouse (μg)	pDNA/mouse (μg)	Ova/mouse (μg)	CpG-ODN/mouse (μg)	Z-average (nm) ± SD	PDI	Average zeta potential (mV) ± SD
CS-DS/pOva	700	50	0	50	162.6 ± 11.9	0.322	27.6 ± 1.6
CS-DS/Ova	700	0	100	50	199.0 ± 24.1	0.236	26.6 ± 1.1
CS-DS/(Ova + pOva)	700	25	50	50	231.7 ± 12.9	0.269	23.4 ± 1.8
CS-TPP/(Ova + pOva)	700	25	50	50	286.2 ± 18.4	0.255	23.5 ± 1.0

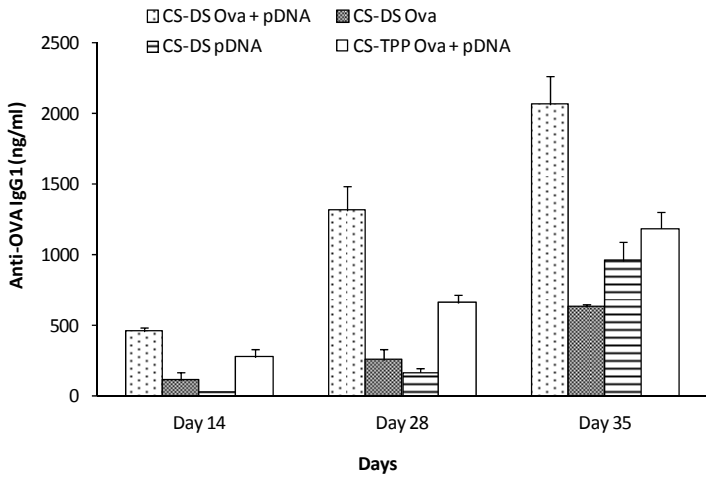

Figure 2-40. Detection of anti-Ova IgG_1 in C57BL/6 mice using ELISA for different formulations of chitosan nanoparticles.

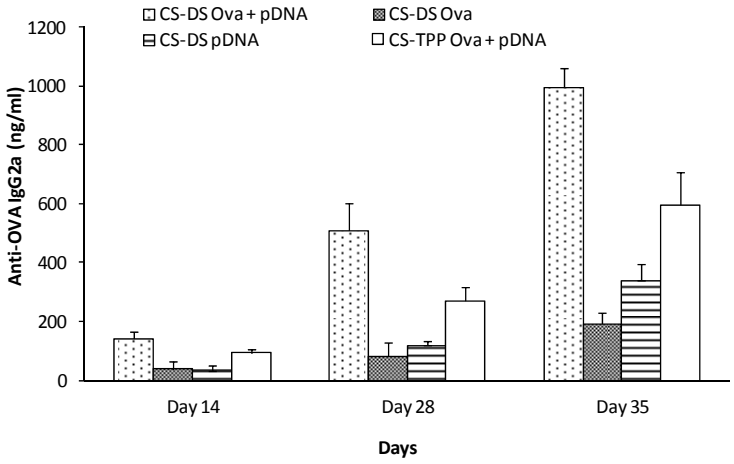

Figure 2-41. Detection of anti-Ova IgG_{2a} in C57BL/6 mice using ELISA for different formulations of chitosan nanoparticles.

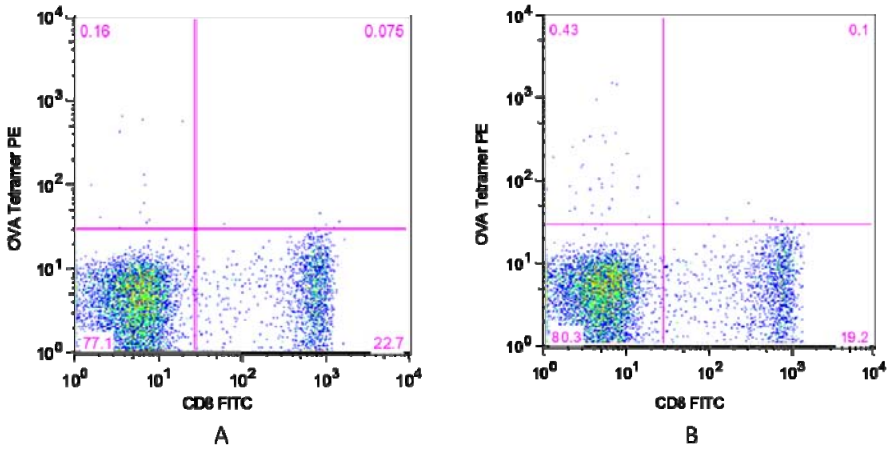

Figure 2-42. Tetramer staining results by flow cytometry for one of the mice that was injected with chitosan nanoparticles encapsulating pDNA encoding Ova. A) Initial time point and B) at 35 days.

CHAPTER 3
CHITOSAN MODIFICATION USING AVIDIN-BIOTIN INTERACTION. PART I: APPLICATIONS IN GENE DELIVERY

3.1 Introduction

Gene delivery is a promising field with great potential to enable the management and correction of human diseases, especially inherited single gene disorders. It also holds significant potential for use in the immunotherapy of cancer and viral diseases. Non-viral gene delivery systems have considerable advantages over their viral counterparts for numerous reasons. They offer greater control of molecular composition, simplified manufacturing and analysis, greater ability to control the size of the transgene to be delivered, as well as a relatively lower, although still existent, immunogenicity.[199-202] Unfortunately, the efficacy of non-viral gene delivery methods is still far below that of viral methods, as shown by the need of approximately 10^6 plasmid copies to transfect a single cell in order to produce considerable gene expression.[201] This low efficiency is explained by the barriers encountered following the delivery of naked plasmid DNA (pDNA), where the pDNA should reach the target cells without degradation and then be transferred across cellular membranes to enter the nucleus.[201] Furthermore, the transient expression of the delivered gene, which is attributed to the inability of pDNA to integrate in the nucleus, leads to the need for re-administration.[15] These reasons and others necessitate the development of novel delivery systems capable of protecting pDNA, localizing its delivery and offering a sustained delivery for continual gene uptake.[15]

Chitosan, a natural polycationic polymer, have been extensively investigated as non-viral gene delivery vectors, mainly because they offer lower immunogenicity and sustained gene delivery. Additionally, they are cheaper and potentially have more flexibility for controlling plasmid delivery. There have been many published attempts in literature involving the improvement of gene delivery capabilities of chitosan, mainly

through the modification of chitosan chains with different ligands via covalent attachment, adsorption or physical entrapment. Generally, peptide and polymer ligands need to be firmly anchored onto the polymeric surface without adversely affecting their activity. Covalent binding, although it guarantees strong ligand attachment, often involves harsh reaction conditions and the use of organic solvents which can result in denaturation of biomolecules and reduction of their activity.[203] Adsorption, on the other hand, is usually reversible and can result in protein denaturation due to interactions with surfaces, especially when the proteins or biomolecules are bound directly to the substrate without a spacer. Finally, physical entrapment inside the polymer vehicle is usually an inefficient way for ligand addition due to masking the active components of biomolecules.

This study focuses on a new technique for modification of chitosan surfaces with various types of ligands, which overcomes the above mentioned drawbacks of other modification methods. The utilized method is based on the modification of chitosan via avidin-biotin interactions. Cell recognition peptide containing RGD sequence and the hydrophilic flexible polymer, polyethylene glycol, were used as model ligands.

3.2 Materials and Methods

3.2.1 Purification and preparation of chitosans

Chitosan was fully purified and prepared as discussed in the Materials and Methods section in Chapter 2. Briefly, high molecular weight and high degree of deacetylation (HM-HD), medium molecular weight and high degree of deacetylation (MM-HD) and low molecular weight and high degree of deacetylation (LM-HD) chitosans were obtained from Sigma®, MO. These chitosans were fully purified by first dissolving them in 1% acetic acid solution and filtering the solutions to remove the insoluble particles. This was followed by decolorization and deproteinization in the presence of dithiothreitol and demineralization using ethylenediaminetetraacetic acid

(EDTA). Very low molecular weight and high degree of deacetylation (VLM-HD) was prepared by oxidative depolymerization using sodium nitrite (Sigma®, MO). Sodium nitrite ($NaNO_2$) aqueous solutions was added drop wise to chitosan solutions (1% (w/v) in 2% (v/v) aqueous acetic acid solution), at a final $NaNO_2$ to chitosan ratio of 2% (w/w) and the reaction solution was stirred for 5 h at room temperature. Viscosity average molecular weights were calculated from intrinsic viscosities using Mark–Houwink–Sakurada equation.

Medium molecular weight and medium degree of deacetylation (MM-MD) and medium molecular weight and low degree of deacetylation (MM-LD) chitosans were prepared by heterogeneous reacetylation using acetic anhydride. Degrees of deacetylation were measured by first derivative UV spectrophotometry (1DUV).

3.2.2 Chitosan biotinylation and avidin conjugation

Biotinylation of chitosan was performed using EZ-Link® NHS-Biotin (N-hydroxysuccinimidobiotin, molecular weight: 341.38 Da, spacer arm length: 13.5 Å), EZ-Link® NHS-LC-Biotin (succinimidyl-6-(biotinamido) hexanoate, molecular weight: 454.54 Da, spacer arm length: 22.4 Å) and EZ-Link® NHS-LC-LC-Biotin (succinimidyl-6-(biotinamido)-6-hexanamido hexanoate, molecular weight: 567.70 Da, spacer arm length: 30.5 Å) (Figure 3-1), all obtained from Thermo Scientific®, IL. Biotinylation reactions were carried out at different pH values by mixing the biotinylating agent with chitosan, as explained below. Figure 3-2 shows the schematic of NHS-biotin reaction with chitosan.

3.2.3 Chitosan solution, 1% (w/v) dissolved in 1% (v/v) acetic acid solution, was diluted in a range of buffer systems. Buffers were prepared to have final concentrations of 0.5 M and ionic strength of 1.5 M, adjusted using sodium chloride. The following buffers were used: acetate buffer (pH 3.2, 4.2 and 5.2), phosphate buffer (pH 6.2, 7.2 and 8.2) and carbonate buffer (pH 9.25, 10.25 and 11.25). Biotinylation efficiencies of

chitosan using the three mentioned biotinylation agents were studied using 5 mg/ml of chitosan suspended in phosphate buffer, pH 8.2, at different theoretical biotinylation degrees. Biotinylation reagents were dissolved in N,N-dimethylformamide (DMF, 100 mM) and added directly. Theoretical biotinylation was based on the approximate calculations of the molarity of glucosamine units in the chitosan polymer as described in the Appendix, section A.1. In order to see the effect of chitosan concentration on the biotinylation efficiency, three different chitosan concentrations were reacted with NHS-biotin; 1.25, 2.5 and 5 mg/ml in phosphate buffer pH 8.2. Chitosan and the biotinylation reagent were left to react for 45, 60 or 120 min. In order to study the effect of chitosan's molecular weight and degree of deacetylation on the biotinylation reaction, 5 mg/ml solutions of different grades of chitosan (HM-HD, MM-HD, LM-HD, VLM-HD, MM-MD and MM-LD chitosans) were reacted with NHS-biotin at pH 8.2. The reactions were allowed to proceed for 15, 30, 45, 60, 120, 300 and 720 min. Studying chitosan biotinylation using NHS-biotin was carried out further by using different buffers. NHS-Biotin dissolved in DMF, yielding a 20% theoretical chitosan biotinylation degree, was added to 5 mg/ml chitosan dissolved in each of the above mentioned buffers. Biotinylation reactions were quenched by adding equal volumes of 1 M Tris-HCl buffer and stirring for 1 h, followed by precipitating chitosan and dialysis against distilled water for 2 days using Pierce SnakeSkin® Pleated Dialysis Tubing 10,000 MWCO, changing the water three times. Finally, chitosan suspensions retrieved from the dialysis tubes were frozen at -80°C and lyophilized in a Labconco FreeZone 4.5 Liter freeze dry system (chamber pressure of less than 0.02 mbar and collector temperature of less than -50°C).

As another variation of the avidin-biotin ligand attachment technique using biotinylated chitosans, avidin molecules were directly attached to chitosan through covalent linkage formed by reductive amination. AminoLink Reductant (sodium cyanoborohydride, $NaCNBH_3$, Thermo Scientific®, IL) was used to promote the formation of stable bonds between aldehyde- and amine-containing molecules according

the manufacturer protocol. Briefly, avidin, which is a glycoprotein, was oxidized to produce reactive aldehyde groups using sodium meta-periodate (10 mM) which is known to be sufficient for general carbohydrate oxidization without undue risk of oxidizing amino acids. The reaction was quenched by glycerin and the oxidizing agent was removed using a PD-10 desalting column (GE Healthcare Bio-Sciences, NJ), pre-equilibrated with 25 ml PBS. The eluted oxidized avidin was added to chitosan solution and mixed with 50 mM sodium cyanoborohydride ($NaCNBH_3$) as a reductant solution. Non-reacted aldehyde sites were blocked by adding 50 mM ethanolamine, pH 9.6. The conjugates were purified from excess reactants using dialysis against distilled water followed by lyophilization.

3.2.3 Quantification of the biotinylation degree and avidin content

The biotinylation degree was quantitatively assessed using the HABA/avidin assay. D-biotin standard calibration curves were plotted to find the degree of biotinylation. Spectroscopy studies were completed on a SpectraMax Plus^{384} plate reader (Molecular Devices, CA). HABA/avidin reagent (Sigma®, MO) was reconstituted in water to yield 0.3 mM HABA (4´-hydroxyazobenzene-2-carboxylic acid), 0.45 mg/ml avidin, 0.3 M NaCl, 0.01 M HEPES (N-2-Hydroxyethylpiperazine-N'-2-ethanesulfonic acid, pKa = 7.5), 0.01 M $MgCl_2$ and 0.02% sodium azide. For plotting the calibration curve, D-biotin (Sigma®, MO) was dissolved in distilled water (at concentrations of 5, 10, 25, 35 and 40 nmol/ml). 96 well quartz SpectraPlate® microtiter plate (Molecular Devices, CA) was used for HABA/avidin analysis by adding the assay solution (180 µl) to each of the wells that were used for analyzing chitosan and control samples, and the absorbance was measured at 500 nm. This was followed by adding and mixing 120 µl of biotin solution (in case of standard wells), chitosan solution (0.1 mg/ml) or blank buffer for 10 min before measuring again at 500 nm. The differences between the absorbance

before and after the addition of biotin or biotinylated chitosans (ΔA_{500nm}) were plotted against biotin concentration in order to obtain the standard calibration curves. Biotinylation degrees (nmol biotin/mg chitosan) and the biotinylation efficiencies (%) were calculated as following:

$$Biotinylation\ degree\ = (\Delta A_{500nm} - intercept)/(slope \times sample\ weight\ (mg))$$

$$Biotinylation\ efficiency\ (\%) = \frac{measured\ biotinylation\ degree}{theoretical\ biotinylation\ degree} \times 100\%$$

The percentage of avidin attachment on chitosan nanoparticles was measured using HABA dye. Standard avidin solutions and avidin-modified samples were prepared in acetate buffer pH 5.5 and were diluted in a flat-bottomed 96 well plate (Corning® Costar®, MA). HABA dye, dissolved in the same buffer, was added to each well for a final concentration of 0.34 mM and mixed well. The assay solutions were left covered for 15 min and then the initial readings were taken at 500 nm using a SpectraMax Plus^{384} spectrophotometer (Molecular Devices, CA) provided with SoftMax PRO 1.3.4. LS software. This was followed by adding biotin (0.04 mM) to saturate the avidin binding sites and release HABA dye. Readings were taken at 500 nm and subtracted from the initial readings.

3.2.4 PEG and RGD-biotin

PEG-biotin was synthesized as follows.[162] About 0.5 g of α-methoxy-ω-amine PEG (mPEG-NH2) (Nektar, Huntsville, AL), which has molecular weight of approximately 5,809 Da, was dissolved in acetonitrile (1 ml). Dichloromethane (0.5 ml) and triethylamine (40 µl) were added to the solution and the mixture was stirred for 2 min. NHS-biotin (0.125 g) was added and the reaction was stirred overnight under dry air. Diethyl ether (20ml) was added to precipitate the polymer, which was filtered on Whatman® number 1 filter paper using a Buchner funnel. The polymer was washed with diethylether (about 10ml) and dissolved in hot isopropanol (70°C) to give an opaque-

cloudy solution. The polymer was re-precipitated on cooling and separated on a filter paper. Finally, the polymer was dried under vacuum.

In order to confirm the conjugation of biotin to PEG, ^{1}H-NMR spectra were recorded using Bruker AVANCE-300 spectrometers operating at 300 MHz. ^{1}H-NMR chemical shifts were measured in parts per million (ppm) relative to $CHCl_3$. Deuterochloroform ($CDCl_3$, Sigma®, MO) was used to dissolve the synthesized sample as well as mPEG-NH_2.

RGD with a spacer arm, G_{11}GRGDS, was used to improve chitosan's cell adhesion properties. Custom synthesis of biotin conjugated G_{11}GRGDS was done by Sigma-Genosys®, Texas.

3.2.5 Preparation of Chitosan-pDNA nanoparticles

Chitosan/plasmid DNA (pDNA) nanoparticles were prepared through complex coacervation between the two oppositely charged polyelectrolytes, chitosan and pDNA. Dextran sulfate was the polyanion used for optimizing the interaction between chitosan and pDNA and for enhancing the stability of chitosan nanoparticles. Chitosan nanoparticles were formulated at various ratios of chitosan's nitrogen to pDNA's phosphate groups (N/P ratio). As a positive control, branched polyethyleneimine (PEI)/pDNA nanoparticles were formulated at N/P ratio of 10. Stock solutions of PEI, DNA and polyanions were prepared in water, and chitosan in 1% (v/v) acetic acid solution. In order to prepare the nanoparticles, cationic solutions containing chitosan (biotinylated, ligand modified or avidin conjugated chitosans) or PEI and anionic solutions containing DNA and/or dextran sulfate were prepared separately by pipetting the calculated volume from stock solutions and then diluting with 50 mM acetate buffer at pH 5.46. In a typical formulation procedure, cationic solutions were transferred into the anionic solution containing the plasmid DNA (pDNA) encoding luciferase (VR1255) using a micropipette and mixed through pipetting up and down several times. The volume

ratios of anionic to cationic solutions were 2:1. The solutions were mixed by vortex for 10 seconds and left at room temperature for 15 min to equilibrate. Formation of ligand modified nanoparticles incorporating pDNA using biotinylated chitosan was done by one of two methods, A or B. In method A, biotinylated chitosan nanoparticles were fabricated first as mentioned above, then ligands were attached to the nanoparticles through avidin linker. Ligand addition was done by suspending biotinylated chitosan nanoparticles in 50 mM acetate buffer, pH 6.46, followed by addition of avidin. Then biotinylated ligands (either RGD or PEG) were added. In method B, ligand attachment through avidin linker was done before the formation of chitosan/pDNA nanoparticles and the ratio of surface avidin on chitosan nanoparticles was adjusted to be equivalent to that of method A. For comparison purposes, avidin-conjugated chitosans were used to prepared chitosan/pDNA nanoparticles, followed by addition of biotinylated ligands.

3.2.6 Particle size and zeta potential analysis

Nanoparticle size measurements were conducted using the Zetasizer Nano ZS (Malvern, UK). This instrument performs size measurements using dynamic light scattering (DLS). Briefly, the nanoparticles were suspended in deionized water at a concentration of 1 mg/ml by using vortexing for 5 min. The size measurements were performed at 25°C at a 173º scattering angle. The mean hydrodynamic diameter was determined by cumulative analysis. The zeta potential determinations were based on electrophoretic mobility of the nanoparticles in aqueous medium after applying Henry's equation. Electrophoretic mobility was obtained by performing an electrophoresis experiment on samples and measuring the velocity of particles using laser Doppler velocimetry (LDV). Zeta potential measurements were performed using folded capillary cells in automatic mode.[176]

3.2.7 Microscopic imaging

The morphology of chitosan nanoparticles was studied using an Asylum atomic force microscopy (AFM) MFP-3D. Nanoparticles were fixed on a freshly cleaved mica film glued on a glass slide by leaving 5 µl droplet of the DNA solution to air dry. The nanoparticle suspensions were left on freshly cleaved mica film slides for 10 min. The excess liquids were removed using filter paper and the mica films then were washed with distilled water and dried under streams of nitrogen. Samples were scanned using AFM cantilevers (MikroMasch, CA) which have spring constant of 46 N/m, and resonant frequency of 325 Hz. by tapping mode.

3.2.8 Determination of complex formation and integrity using gel electrophoresis

The formation of chitosan polyplexes was determined by their electrophoretic mobility using agarose gel electrophoresis. This test is based on intercalation of ethidium bromide (EtBr) with DNA which increases the fluorescence quantum yield of the dye. Nanoparticle formulations were fabricated using method A at different N/P ratios (10, 15, 25, 35 and 50). Formulations were mixed with 10% 10X BlueJuice™ gel loading buffer (Invitrogen™, CA) and analyzed for their migration on a 0.8% (w/v) agarose gel stained with 0.5 µg/ml of ethidium bromide (EtBr) in Tris-acetate-EDTA buffer (TAE) (0.04 M Tris, 0.02 M acetate and 1 mM EDTA pH 8.3). The gel electrophoresis was performed at a constant 80 V for 60 min. The gel was visualized on a UV illuminator (Spectroline®, NY) in a dark box and pictures were taken using a digital camera.

3.2.9 Cell culture

Human Embryonic Kidney cell line (HEK293) was purchased from American Type Culture Collection (ATCC®, MD). The cells were maintained in 75 cm^2 tissue culture flasks (Corning® Costar®, MA) and supported with Modified Eagle's Minimum Essential Media (EMEM) (MEM modified to contain Earle’s balanced salt solution,

non-essential amino acids, 2 mM L-glutamine, 1 mM sodium pyruvate, and 1500 mg/L sodium bicarbonate) supplemented with 10% fetal bovine calf serum (FBS) (Gibco™ Invitrogen™, NY), antibiotic-antimycotic (ABAM) that consists of 0.5% penicillin and 0.5% streptomycin (Sigma®, MO) and 1% L-glutamine in a humidified incubator at 37°C at 5% CO_2. Subcultivation was done in a ratio of about 1:6 every 5 days when 90% confluence was reached.

3.2.10 Cytotoxicity evaluation using MTT assay

MTT assay (3-[4,5-dimethylthiazol-2-yl]-2, 5-diphenyl tetrazolium bromide, Sigma®, MO) was used to evaluate the cytotoxicity of the different prepared chitosans. Cytotoxicity of PEI, chitosan, biotinylated chitosans at 8.3% and 25.8% biotinylation degrees, avidin-modified biotinylated chitosan, avidin conjugated chitosan, RGD-modified chitosan and PEG-modified chitosan. HEK293 cells were seeded in 96-well plates (Corning® Costar®, MA) at a density of 1 x 10^4 cells per well. Twenty-four hours later, cells were incubated with 200 µl of complete DMEM containing a range of concentrations of polymer solutions. After 4 h of incubation, the medium in each well was replaced with 100 µl of fresh phenol free complete medium containing MTT at concentration of 1 mg/ml. MTT solution was incubated with cells for an additional 2 h at 37°C. In order to reduce uneven evaporation of the wells, Parafilm M plastic wrap was used to cover the edges of the well plate during incubation with MTT solution. Cells were then lysed for 15 min with 100 µl of the MTT solubilization solution (10% Triton X-100 plus, 0.1 N HCl and anhydrous isopropanol extraction buffer). Gentle mixing and trituration by pipetting up and down were done to help dissolving the MTT formazan crystals. The optical density of the lysate was measured at 570 nm using a SpectraMax plus^{384} Microplate Reader (Molecular Devices, CA). The background absorbance of multi-well plates was measured at 690 nm and subtracted from the absorbance at 570 nm. The half maximal inhibitory concentration (IC_{50}) was calculated by averaging the

concentrations at which approximately 50% of the cells died after 4 h incubation with the polymer.

3.2.11 *In vitro* transfection efficiency testing

Evaluation of luciferase expression was done in Human Embryonic Kidney cells (HEK293). Cells were seeded into 24-well plates at a density of 1×10^5 cells/well, 24 h before transfection. Different formulations were prepared to contain 1 μg of pDNA encoding luciferase (VR1255) per well. Transfection was done by first changing the cell media with pre-warmed FBS-containing fresh media. Then 50μl of the pDNA-containing formulations suspended in medium was added and incubated for either 4 or 12 h at 37ºC. This was followed by gently washing cells with pre-warmed phosphate buffered saline (PBS) and adding fresh media. The cells were incubated for additional 44 or 36 h, respectively. After the incubation period, cells were treated with 200 μl of lysis buffer (Promega®, WI) and the plates were subjected to two cycles of freezing and thawing. The lysates were then transferred to 1.5 ml Eppendorf tubes and centrifuged at 13,200 rpm for 5 min using Eppendorf 5810R centrifuge. Twenty μl of supernatant from each well was added to 100 μl of luciferase assay reagent (Promega®, WI) and samples were vortexed for 10 seconds exactly and measured on a luminometer (Lumat LB 9507, EG&G Berthold, Germany). Protein contents in the cell extracts were measured by micro bicinchoninic acid (BCA) Pierce® protein assay kit (Thermo Scientific®, IL). Luciferase activity was expressed as relative light units per protein content (RLU/mg protein in the cell lysate). The data were reported as mean ± standard deviation for triplicate samples.

3.2.12 Statistical analysis

Group data are reported as mean+/-SD. Differences between groups were analyzed by one way analysis of variance with a Tukey's post-test analysis. Levels of significance were accepted at the $\rho < 0.05$ level. Statistical analyses were performed using Prism 5.02 software (GraphPad Software, Inc., CA).

3.3 Results and Discussions

3.3.1 Preparation of different chitosan grades

Chitosan, the amino polysaccharide, is derived from chitin by alkaline deacetylation [59,60] or enzymatic deacetylation,[61] which results in a copolymer of glucosamine and N-acetyl glucosamine.[58] Chitosan has many advantages for developing micro and nano-sized particles, which can be used for preparing drug and gene delivery. Chitosan has a low toxicity profile and is biocompatible and biodegradable. In addition, chitosan's solubility in aqueous acidic solutions circumvents the need for the use of organic solvents when fabricating particulate systems. At acidic pH values, the free amino groups become protonated which allows for cross-linking with multivalent anions, such as DNA and proteins. Moreover, chitosan is mucoadhesive and also provides the ability to sustain the release of active agents.[71]

It has been shown that complexes composed of chitosan and DNA are capable of protecting DNA from degradation by nucleases and delivering it into different cell types. These observations are raising much interest in the development of DNA-vaccines and other gene therapy agents using chitosan.[204,205] Although chitosan has intrinsic properties which facilitate cellular uptake through chitosan-induced destabilization of lipid bilayers,[206] modification of the chitosan surface can be advantageous in achieving higher cellular uptake and subsequently higher transfection rates *in vivo*. Adding cell targeting ligands to the surface of chitosan particles is an example of the techniques that can be used to overcome low efficiency of the non-viral gene delivery vector by improving cellular uptake. In addition, other ligands can have other positive effects on the overall characteristics of chitosan formulations, such as stability and stealth shielding.

Chitosan samples with various degrees of deacetylation were prepared using heterogeneous acetylation with acetic anhydride and the degree of deacetylation was measured using first derivative UV spectrophotometry (1DUVS). Lower molecular

weight chitosans were prepared by oxidative fragmentation using sodium nitrite (2% w/w) and the average viscosity molecular weights for chitosans dissolved in 0.25 mM acetate buffer were determined using Ostwald viscometer at 25°C.

Table 3-1 shows the different grades of chitosan used in performing the biotinylation and transfection experiments and their characteristics. Namely, high molecular weight and high degree of deacetylation (HM-HD), medium molecular weight and high degree of deacetylation (MM-HD), low molecular weight and high degree of deacetylation (LM-HD), very low molecular weight and high degree of deacetylation (VLM-HD), medium molecular weight and medium degree of deacetylation (MM-MD) and medium molecular weight and low degree of deacetylation (MM-LD) chitosans. These chitosans were used to study the biotinylation reaction and the parameters that affect it.

3.3.2 Chitosan biotinylation and avidin addition

Biotin, hexahydro-2-oxo-1*H*-thieno[3,4-d]imidazole-4-pentanoic acid or vitamin H, is a naturally occurring vitamin found in all living cells. The tissues with the highest amounts of biotin are the liver, kidney and pancreas, in addition to high presence in cancerous tumors.[150] Biotin is involved as an enzyme cofactor in a variety of carboxylase, decarboxylase and transcarboxylaze reactions,[151-153] and is known to have a strong affinity to a number of proteins, such as avidin and streptavidin. Avidin is a tetrameric glycoprotein which was originally isolated from chicken egg white. Avidin has four identical subunits, which consist of 128 amino acids each, having a combined molecular weight of 66-69 kDa. Avidin is soluble in aqueous solutions and stable over a wide pH and temperature range.[154]

The avidin-biotin interaction is the strongest known non-covalent, biological interaction between a protein and a ligand (K_d for avidin-biotin complex $=10^{-15}M^{-1}$). The binding capacity of avidin is 4 moles biotin to 1 mole avidin. Bond formation is very

rapid and, once formed, is unaffected by wide extremes of pH, temperature, organic solvents and other denaturing agents. The avidin-biotin complex is also resistant to enzymatic proteolysis.[154] This strong biological interaction was utilized in this research to modify chitosan with targeting ligands of choice, providing feasible method for improving gene and drug delivery.

Biotinylation of chitosan was performed utilizing N-hydroxysulfosuccinimide (NHS) chemistry. Ester groups on NHS-biotin, NHS-LC-biotin and NHS-LC-LC-biotin reagents react with the primary amines of glucosamine residues of chitosan to produce stable biotinylated products. NHS esters react with primary amines in the deprotonated form and, therefore, the reaction typically requires neutral to basic solutions to proceed. Primary amines react with NHS esters by nucleophilic attack and N-hydroxysuccinimide groups are released as a byproduct. However, hydrolysis of the NHS-ester competes with the reaction in aqueous solution. The rate of NHS-biotin hydrolysis increases with increasing pH values and is expected to occur more readily in dilute protein and polymer solutions.

Conditions used for conjugating NHS-biotin to proteins or peptides are considerably flexible regarding temperature (NHS ester reactions proceed at 4-37°C), reaction mixture pH values (6-9), and incubation times (few minutes to hours).
A particular set of conditions will result in different degrees of label incorporation and may affect the specificity of the biotinylation reaction in cases where there are multiple potential sites of biotinylation, therefore an optimal set of conjugation conditions is needed for the successful biotinylation. The effect of biotinylating agent type, chitosan concentration, reaction time and pH value on chitosan biotinylation reaction was studied.

Figure 3-3 shows the biotinylation efficiency (theoretical calculated biotinylation percentage vs. actual biotinylation percentage) of NHS-biotin measured by HABA/avidin assay (optimization of HABA/avidin assay is discussed in the Appendix, section A.7). Chitosan-conjugated biotin content was quantified as nmol biotin/mg chitosan and the

biotinylation percentage was calculated relative to the number of moles of glucosamine units of chitosan. At theoretical percentages of 35% or less, a linear correlation existed between the theoretical biotinylation percentage and the actual percentage as measured by HABA/avidin as shown in Figure 3-6 ($r^2 = 0.9917$). The biotinylation efficiency at the addition of more biotinylating agent declined significantly and the biotin content leveled off. This happens as a result of the reduced availability of biotinylation sites on chitosan chains and the change in polymer solubility and conformation. However, generally speaking, chitosan biotinylation efficiency was significantly higher compared to protein biotinylation, for which most protocols recommend a 20 molar excess of the biotinylation agent in order to achieve acceptable biotinylation.

Compared to NHS-biotin, NHS-LC-biotin and NHS-LC-LC-biotin showed a slightly less efficient biotinylation of chitosan (Figures 3-4 and 3-5, respectively). Also, the plateau of NHS-biotin curve was reached at higher conjugated biotin content compared to the other two reagents. However, the biotinylation patterns were similar, as shown by the theoretical versus actual biotinylation degree plots. It was noted that the initial reaction slope using NHS-LC-LC-biotin was significantly less steep than the other two biotinylating reagents, indicating a slower initial reaction (Figure 3-6).

Chitosan concentration was found to have a significant effect on the biotinylation reaction. The effect of chitosan concentration is a complex interaction between many factors, including the viscosity of solution, polymer chain interaction and the exposure time of the primary amine groups of chitosan to the NHS biotinylation agent before degradation occurs. Figure 3-7 shows the effect of chitosan concentrations (1.25, 2.5 and 5 mg/ml) on the biotinylation efficiency for reactions that were carried out for 45, 60 and 120 min before quenching. Increasing the time of biotinylation reaction resulted in increasing the biotinylation degree at each concentration. Also, it was found that higher concentrations of chitosan solution resulted in more effective biotinylation at the same reaction time. For example, at 120 min reaction time, 5 mg/ml chitosan concentration

reaction mixture resulted in 662.7 ± 15.5 nmol biotin/mg chitosan, compared to 616.0 ± 5.3 and 566.0 ± 15.1 nmol/mg for 2.5 and 1.25 mg/ml solutions, respectively.

The effect of reaction time on biotinylation of different grades of chitosans was studied further as shown in Figure 3-8. Generally, it was found that a plateau concentration of attached biotin onto chitosan chains was reached after 120 min of reaction for all grades of chitosan. Also, it was noted that decreasing chitosan's molecular weight caused faster biotinylation reactions and higher conjugated biotin contents. Chitosans which have molecular weights of 102 kDa or less (LM-HD and VLM-HD) showed similar behavior. The slope of the initial biotinylation curve of medium molecular weight chitosan (MM-HD) was not significantly different than the lower molecular weight chitosans (Figure 3-9), but the plateau was reached at lower biotin content. On other hand, higher molecular weight chitosans (HM-HD) showed slower reaction and the maximum biotinylation was significantly less than medium and low molecular weight chitosans. This can be caused by the increased viscosity of the reaction solution which hindered accessing the biotinylation sites on chitosan chains, slowing the reaction and allowing more time for the degradation of NHS-biotin.

Figure 3-10 shows the effect of chitosan's degree of deacetylation on the biotinylation reaction. Three grades of chitosan which have the same molecular weight but different degrees of deacetylation were tested. As expected, the lower the degree of deacetylation, the lower the degree of biotinylation, as a result of steric hindrance of the acetyl groups on chitosan chains and the lower availability of biotinylation sites. The highest degree of deacetylation chitosan (MM-HD, 90.92%) showed higher initial reaction slope compared to medium and low degree of deacetylation chitosans (MM-MD (84.02%) and MM-LD (74.36%), respectively) (Figure 3-11), which indicates a faster reaction time. In addition, higher plateau concentrations of biotin were found conjugated to MM-HD chitosan compared to the lower degree of deacetylation chitosans

(at 120 min, biotin concentration was 756.9 ± 10.1 nmol/mg chitosan compared to 646.6 ± 11.4 and 375.9 ± 43.0 nmol/mg for MM-MD and MM-LD, respectively).

Another important factor affecting biotinylation is the influence of deprotonation degree of the primary amine group. Protonation depends on the pKa of the polymer and the pH of the solution. According to literature and biotinylation agent manufacturer protocols, the recommended pH value for biotinylation reaction is between 7 and 9, and the applicability of this pH range for chitosan biotinylation was tested. Figure 3-12 shows the effect of pH values of non-amine buffers on biotinylation of chitosan using NHS-biotin. In this study, the solubility of chitosan played a key role in the biotin conjugation reaction since chitosan started to precipitate at pH values greater than 7, forming hazy suspensions. However, the suspension turbidity appears to be homogenous and was maintained via continuous stirring. The combination of two factors, chitosan's solubility and ionization status, determines the availability of amine sites for biotinylation at neutral and low pH values. It was found that at pH 6.2 the biotinylation reaction yielded the highest biotin conjugation (752.0 ± 11.1 nmol biotin/mg chitosan). On the other hand, the biotinylation at pH 11.25 was the lowest (408.7 ± 19.6 nmol biotin/mg chitosan). At higher pH values, the hydrolysis of the N-hydroxysuccinimide biotinylation agents is significantly higher, which is expected to lower the biotinylation efficiency, adding another contributing factor to the reduced efficiency of chitosan biotinylation by NHS reagents.

The above results indicate that chitosan can be successfully biotinylated in a simple one step method and that the biotinylation degree can be optimized based on chitosan's grade and concentration, pH of the reaction media, reaction time and type of biotinylation agent, among other factors.

3.3.3 Ligand selection and biotinylation

RGD (arginine-glycine-aspartic acid) was discovered in 1984 to be an essential recognition peptide sequence for cells. The sequence is contained in a large number of proteins, including fibronectin, an extracellular matrix (ECM) protein that surrounds fibroblasts in the body and is responsible for adhesion of cells to the ECM. Cell surface receptors, such as integrins, recognize the RGD sequence of various proteins. The small sizes of these minimal binding sequences enable them to be incorporated at much higher concentrations than may be possible with entire protein structures, compensating for the loss of activity for not using the entire proteins. Moreover, their nature renders them more straightforward to chemical derivatization.[207] To overcome the topological issues of different surfaces, it was found that using peptide adhesive moieties that contain spacer arms, such as G_{11}GRGDS, instead of using the short peptide, enhanced cell recognition properties compared to directly grafting the short peptide sequence into the biomaterial surface.[207,208] Therefore G_{11}GRGDS (RGD) was used in this study for enhancing gene delivery capability of chitosan polymer by promoting cellular uptake of chitosan nanoparticles.

RGD modified chitosans have been covalently prepared and studied mainly for tissue regeneration purposes. RGD immobilization on chitosan has been accomplished by imide bond formation between the amino groups of the chitosan and the carboxyl groups on the peptides, utilizing carbodiimide and NHS,[209]and by photochemical immobilization based on phenyl azido chemistry.[58]

PEGylation is a term referred to PEG-modification to the drug delivery vehicle, which implies the covalent binding, non-covalent entrapment or adsorption of PEG onto an object. PEGylation imparts a stealth shielding on the surface of drug delivery systems and prevents the plasma proteins, opsonins, from recognizing these particles, inhibiting the subsequent phagocytosis by cells of the reticulo-endothelial system (RES). This leads to prolongation of the systemic circulation time from minutes to hours or even days.[210,211]

In addition, PEGylation of nanoparticles improves the stability of colloidal suspensions through inter-particle steric repulsion. PEG is a hydrophilic polymer with flexible linear chains, which allow free rotation of polymer chains and creates shields around the drug delivery vehicles.[212-214]

PEG modified chitosan nanoparticles has been investigated for their ability to deliver proteins[215,216] and to encapsulate DNA.[134,217] PEG conjugation to chitosan was achieved by several methods, including using (NHS)-mPEG,[218] using PEG-aldehyde formed by reacting PEG with acetic anhydride,[219]and using methoxy PEG (mPEG)-aldehyde formed by reacting mPEG with 2,2,6,6-tetramethylpiperidine-1-oxyl and trichloroisocyanuric acid followed by reaction with chitosan.[217] Generally, PEGylation enhanced the stability of chitosan nanoparticles, reduced aggregation and improved cellular uptake.

Biotinylated RGD and PEG were utilized as model ligands to modify chitosan particles via avidin linkers. Biotin conjugation to methoxy PEG-NH_2 (mPEG-NH_2) was achieved using NHS-biotin as shown in Figure 3-13. The success of conjugation was confirmed by taking the ^{1}H-NMR spectrum of the final compound (mPEG-biotin) and analyzing it in relation to ^{1}H-NMR spectra of mPEG and NHS-biotin (Figure 3-14). The peaks of the ^{1}H-NMR spectrum of mPEG-biotin (Figure 3-15) were labeled with the corresponding proton numbers from the mPEG conjugated with biotin molecular structure (Figure 3-13). mPEG-biotin ^{1}H-NMR spectrum showed triplet signals at 1.20, 1.42, 1.70 and 2.22 ppm that can be assigned to the first four methylene groups from the carbon chain of the biotin moiety attached to mPEG by the amide linkage. In addition, the conjugated biotin group was identified by the two methine protons (H-3, H-4) from the cyclic biotin structure at 4.21 and 4.28 ppm and two urea protons (H-1′, H-2′) from the cyclic biotin structure at 5.50, 5.60 ppm. Also the spectrum revealed the appearance of a broad singlet belonging to the free amido proton at 5.93 ppm which was not present in the ^{1}H-NMR spectra of NHS-biotin and mPEG.[162,220,221]

3.3.4 Fabrication and characterization of chitosan nanoparticles

Chitosan nanoparticles were fabricated using ionic gelation under defined conditions. Formulation parameters of chitosan nanoparticles were optimized previously. Briefly, it was found that using low molecular weight chitosan (M_v = 42.5 kDa) and incorporating dextran sulfate (chitosan/dextran sulfate w/w ratio = 10) into chitosan nanoparticles enhanced their transfection efficiency. In addition, other formulation parameters were adjusted to result in the most stable and reproducible formulations which yield the smallest particle sizes.

Ligand attachment on chitosan nanoparticles were done by one of two methods, namely method A and B. These methods are represented in Figures 3-16 and 3-17, respectively. Chitosan modification method type, charge ratio (N/P ratio) and the type of ligand were studied for their effect on particle sizes and zeta potential values. In addition, avidin was covalently conjugated to chitosan using reductive amination and the avidinylated chitosans were used to fabricate nanoparticles, followed by adding biotinylated ligands. Table 3-2 shows the percentage of attached avidin onto the surface of chitosan nanoparticles prepared by method A, B or avidin conjugation, before the addition of the biotinylated ligands. It was found that adding avidin to chitosan nanoparticles made of biotinylated chitosan (method A) showed high avidin surface immobilization efficiency (82.6% to 94.5%). Adding avidin to biotinylated chitosan before the fabrication of nanoparticles (method B) caused a decline in the efficiency of surface immobilizing of avidin (57.6%) as a result of avidin being concealed inside the nanoparticles. Therefore, in order to obtain comparable content of surface avidin between method A and B, approximately two times the quantity of avidin was need for method B, resulting in 53.7 ± 6.4 and 55.5 ± 8.2 μg avidin/ml, respectively (for 60 μg/ml added avidin). The efficiency of avidin immobilization was the lowest for avidin covalently conjugated to chitosan chains prior to nanoparticles formulations (27.9%), which is due

to the loss of avidin structure during activation and due to the direct conjugation of avidin on chitosan.

Table 3-3 shows the effect of chitosan's amine to pDNA's phosphate (N/P) ratio on the size and zeta potential values of chitosan nanoparticles modified with RGD (CS-RGD) and PEG (CS-PEG) via method A, compared to unmodified VLM-HD chitosan nanoparticles. As shown previously, at N/P ratio of 10, unmodified chitosan nanoparticles exhibited the smallest sizes, and the particles increased in size and zeta potential values with increasing the N/P ratio. This occurred as the result of the availability of more binding sites on chitosan with increasing the N/P ratio, exceeding the amount needed for DNA condensation and leading to larger complexes. In comparison, CS-RGD nanoparticles decreased in size with increasing N/P ratios from 10 to 25 (the average particle size decreased from 194.5 ± 9.0 nm to 142.4 ± 11.9 nm). This is speculated to be the result of weakened condensation with DNA in the presence of conjugated biotin and ligands, occupying some of the chitosan cationic binding sites. Particle sizes did not change significantly between N/P ratios of 25 and 35, but started to increase again at N/P ratio of 50 as a result of less efficient complex formation in the presence from low DNA concentration. As expected, zeta potential values at low N/P ratios were significantly less than that of the control formulations because free ionizable surface amine groups were masked by the attached ligands. However, it was noticed that with increasing the N/P ratio to 25, zeta potential values reached 27 mV, which was shown in the previously discussed stability study to be sufficient for the stability of chitosan particles and resulted in minimal aggregation. CS-PEG showed similar behavior to CS-RGD regarding the change in particle size and zeta potential values with increasing N/P ratio. Generally, CS-PEG nanoparticles were larger than CS-RGD nanoparticles at the corresponding N/P ratios and the minimum particle size (163.1 nm) was reached at N/P ratio of 35, compared to N/P ratio of 25 for CS-RGD. In addition, the zeta potential

values were slightly larger compared to CS-RGD nanoparticles, which can be due to the presence of glutamic acid in the RGD sequence.

Method B, on the other hand, yielded significantly larger particles compared to method A (Table 3-4). In addition, the N/P ratio at which the minimum particle sizes were reached has changed from 25 for CS-RGD particles in method A to N/P ratio of 35 in method B, and from 35 for CS-PEG particles in method A to 25 in method B. This switch in the minimum N/P ratios was the result of the effect of the RGD peptide inside the particles. RGD has glutamic acid which was ionized at the pH of the preparation. The presence of other anionic charges modified the interaction between chitosan and pDNA by competing with DNA, therefore requiring more chitosan to condense DNA molecules. On the other hand, PEG is a nonionic polymer and its effect is confined to exhibiting a sterical strain on the chitosan/pDNA interaction. Therefore, PEG had slightly less effect on chitosan nanoparticles than RGD and the minimal particle sizes were reached at lower N/P ratio.

From these results, it was concluded that using method A in formulating ligand-modified chitosan nanoparticles appears to have mild effect on particle sizes and zeta potential values, as long as the ratio of chitosan is increased to compensate for the lost binding sites on chitosan chains. Method B, on the other hand, affected chitosan nanoparticles significantly by modifying the interactions between the system components.

The effect of the percentage of ligand attachment on sizes and zeta potential values of chitosan nanoparticles is shown in Table 3-5. Added avidin was used as a measure of percentage ligand attachment. Chitosan nanoparticles were fabricated using method A at N/P ratio of 35 and chitosan to dextran sulfate w/w ratio of 10. It was found that increasing the attached ligands on CS-RGD and CS-PEG nanoparticles caused enlargement in particles and decrease in zeta potential values. At each ligand modification degree, CS-RGD samples yielded smaller particles compared to the

corresponding CS-PEG samples. One of the reason of this phenomena is the large molecular weight of the used PEG (~5.8 kDa) compared to RGD (~1.18 kDa).

The morphology of CS-RGD and CS-PEG nanoparticles was investigated using Asylum AFM with tapping mode. Figure 3-18 shows the AFM images of the control unmodified CS nanoparticles, whereas Figures 3-19 and 3-20 show the AFM images of CS-RGD and CS-PEG nanoparticles, respectively. Modified nanoparticles were prepared according to method A described above. It was noted that CS-RGD nanoparticles, although smaller in size compared to CS-PEG nanoparticles but showed more tendency for aggregation. This is due to the hydrophilic linear nature of PEG chains which repel other nanoparticles from approaching the particle surface and reduce clustering of particles. Both RGD and PEG modified chitosan particles appeared to have more surface roughness compared to unmodified chitosan particles, as a result of having the conjugated molecules. Interestingly, at higher magnification, AFM images showed that CS-PEG nanoparticles have external cilia-shaped protrusions indicating the success of ligand attachment (Figure 3-20B).

Ethidium bromide gel electrophoresis on chitosan nanoparticles was performed in order to investigate the effect of chitosan's biotinylation and ligand attachment on the ability of chitosan to complex with pDNA. It was found that both RGD and PEG modified chitosans were able to completely condense with DNA at all studied N/P ratios (10, 15, 25, 35 and 50).This was shown by the ethidium bromide bands at the wells of origin, where no visible migration of the DNA was noticed, indicating that these formulations are capable of protecting DNA for gene delivery purposes (Figure 3-21).

3.3.5 Cytotoxicity of ligand modified chitosans

Cytotoxicity assay was performed using MTT assay (3-[4,5- dimethylthiazol-2-yl]-2,5-diphenyltetrazolium bromide), which measures the activity of living cells mainly via mitochondrial dehydrogenases. Mitochondrial

dehydrogenases of viable cells cleave the tetrazolium ring of MTT, yielding purple formazan crystals which can be solubilized and measured colorimetrically.[187] In order to find the 50% inhibitory concentration (IC_{50}), MTT cytotoxicity assay on HEK293 cells was done using a range of polymer concentrations at which IC_{50} is expected from the preliminary data. As shown in Figure 3-22, branched PEI showed significantly higher cytotoxicity (more than 60 times higher) compared to unmodified chitosans (IC_{50} values were 0.019 ± 0.002 and 1.253 ± 0.058 mg/ml, respectively). Among the different modified chitosans, CS-RGD showed the least toxicity (1.693 ± 0.042 mg/ml) followed by CS-PEG (1.653 ± 0.031 mg/ml). Adding avidin to chitosan did not show any improved safety when the avidin was conjugated directly to chitosan, but showed slightly lower toxicity when linked through biotin (IC_{50} values were 1.287 ± 0.031 and 1.347 ± 0.012 mg/ml, respectively). Biotinylated chitosans showed biotinylation degree-depended decline in toxicity compared to unmodified chitosans. This stems from masking the positive charges on chitosan chains by biotin, causing reduction in polymer/cell membrane interaction. This study shows that biotinylation and ligand attachment of chitosan not only retained the safety profile of chitosan, but in fact improved on it.

3.3.6 *In vitro* transgene expression

Using non-viral delivery systems for gene therapy has been increasingly proposed as safer alternatives to viral vectors. They are targetable, easily produced in large quantities, stable in storage and have the potential for repeated administration with minimal host immune response. Compared with other non-viral gene delivery systems, especially liposomal or cationic lipid systems, polymeric polycation/pDNA complexes generally are more stable and have greater loading capacity. One of the cationic polymers that has been proposed as a promising vector among the non-viral gene delivery systems is chitosan. Chitosan is a biocompatible and biodegradable polysaccharide and has been

shown to be non-toxic using a range of toxicity tests, both in experimental animals and in humans.

Based on our earlier findings with chitosan-dextran sulfate/pDNA nanoparticles, we have prepared ligand modified chitosan/pDNA nanoparticles using a similar complex coacervation approach to study the applicability of modifying chitosan for targeting and stabilization of particles. Distinct particles with defined physicochemical properties were obtained, comparable with other polycation-DNA colloidal complexes.

Transfection efficiencies of these particles were assessed using pDNA encoding firefly luciferase (VR1255) on HEK293 cells. This system provides suitable comparison base with other gene delivery studies in literature and for comparison with the work done in optimizing chitosan-dextran sulfate formulations.

Firstly, the effects of the individual components on the transgene expression were studied and compared to the transfection efficiency of polyethyleneimine (PEI), a known polycationic polymer with strong transfection capabilities. Figure 3-23 shows the normalized emitted luminescence intensities per mg of the total protein of lysed HEK293 cells transfected with VR1255 using nanoparticles made of chitosan conjugated with biotin, LC-biotin, LC-LC-biotin and avidin. Also it shows the transfection efficiencies of nanoparticles made of chitosan physically mixed with biotin, avidin, RGD and PEG. It was found that all conjugated and mixed chitosan groups were significantly less efficient compared to PEI. Among the various chitosan groups, only chitosan mixed with RGD showed slight improvement in transgene expression (only significant relative to CS-LC-biotin, CS-Av and CS/PEG groups). This shows that physical mixing of targeting/ stabilizing ligands does not have a noteworthy enhancement of transgene expression.

Figures 3-24 and 3-25 show the effect of methods A and B for linking RGD to chitosan through avidin linker on transfection efficiency, respectively. Conjugating RGD ligand on the already formed nanoparticles through avidin linker (method A) resulted in

significantly improved transfection efficiency compared to unmodified chitosans, and yielded comparable results to the positive control, PEI. When N/P ratios of 10, 15, 25, 35 and 50 were studied, it was found that the N/P ratio has a significant effect on the ability of RGD modified chitosan to transfect HEK293 cells. Transfection efficiencies increased with increasing N/P ratios up to 35. At this N/P ratio, the complexation between conjugated chitosan and pDNA is expected to be optimal; providing sufficient chitosan cationic charges to complex with pDNA and compensating for the effect of biotinylated amine groups. The intrinsic properties of RGD as cell recognizing peptide sequence played an important role in the improvement of transgene expression by aiding in the endocytosis of chitosan nanoparticles carrying the pDNA.

On the other hand, the process of conjugation of RGD on chitosan chains prior to the fabrication of the nanoparticles (method B), resulted in significantly less transfection compared to method A, although higher than unmodified chitosans. Similar to method A, the transfection efficiency increased with increasing N/P ratios of modified chitosans but up to N/P ratio of 25, which was not significantly different than N/P ratio of 35. Transfection efficiency declined sharply after that (N/P ratio = 50), as a result of the less efficient formation of particles and complexation with DNA.

Figures 3-26 and 3-27 show the effect of PEG addition on chitosan nanoparticles via method A and B, respectively. Linking PEG to nano and micro-sized particles helps in particle stabilization and prevents serum proteins from adhesion on particles. By fabricating the particles using method A, the transfection efficiency of PEG modified chitosan nanoparticle increased significantly compared to unmodified chitosans. However, the improvement in transfection efficiency was less significant compared to RGD modified chitosans. The maximum transgene expression was obtained by using N/P ratio of 35 (6.12×10^{8} RLU/mg), after which an abrupt diminishing of CS-PEG nanoparticle transfection capabilities was noticed. Contrary to method A, using method B in fabricating CS-PEG nanoparticles resulted in significantly lower transfection

efficiency compared to unmodified chitosans. This was caused by the effect of inclusion of PEG inside the nanoparticles, which modified the interaction between chitosan cationic groups and phosphate groups of DNA, and possibly caused premature release of DNA at the surface of cell membrane or inside the lysosomes exposing it to lysosomal enzymes. Additionally, the increase in particle size as a result of PEG inclusion inside the particles contributed to the decline in the transgene expression. It was noteworthy that the transfection efficiency of CS-PEG nanoparticles fabricated through method B followed the same pattern of increasing the transfection efficiency with increasing the N/P ratio noticed for method A, confirming the previous results of the importance of increasing the N/P ratio to make up for the lost binding capacity of chitosan.

CS-RGD nanoparticle formulations prepared by method A at N/P of 35, which showed the best gene delivery capability, were used for studying the effect of percentage of ligand attachment, as measured by added avidin. There are two major factors that played key roles in determining the efficiency of ligand modified chitosan nanoparticles in gene delivery; the effect of biotinylation on weakening the interaction between chitosan and pDNA and the effect of ligand properties on enhancing the uptake of nanoparticles. Chitosan formulations were left to incubate with cells for either 4 or 12 h. It was found that the cell attachment ligand (RGD) helped in improving the immediate uptake of particles, as well as the long term exposure to the gene delivery vehicle. As shown in Figure 3-28, the highest gene transfection occurred at 80 μg/ml added avidin (7.783×10^{8} RLU/mg). The differences between transgene expression between 80 μg/ml avidin addition and other ratios were more prominent when the formulations were incubated for only 4 h. Higher percentages of ligand caused the transfection efficiency to start to decline as a result of the interference of the attached ligand on DNA condensation.

CS-PEG nanoparticle formulations (N/P ratio of 35) were also tested for their transfection efficiencies (Figure 3-29). As observed before, PEG modified chitosans

showed significantly higher transfection efficiency than unmodified chitosans, but lower than PEI nanoparticles. It was noticed that at the lowest percentage of PEG (represented by the added avidin), there was no significant difference between the luciferase transgene expressions for 4 and 12 h incubation, and that the transfection efficiencies of the 4 h incubation samples were at maximum. This indicates that at lower degrees of PEGylation, chitosan nanoparticles were more capable to have quicker gene delivery by protecting the nanoparticles from aggregation in media and minimizing interaction with proteins, while preserving their intrinsic transfecting abilities. However, at higher degree of PEGylation, chitosan nanoparticles incubated for only 4 h with HEK293 cells started to lose their intrinsic transfection capabilities in the expense of higher PEG content. On the other hand, samples incubated with cells for 12 h yielded the maximum transfection efficiency at higher percentage of PEGylation. The effect of PEGylation becomes more important than the lost cationic sites on chitosan chains with increasing the incubation time, mainly due to the extra protection provided against the potential detrimental effects from exposure to the transfection media.

Finally, the effect of the method used for RGD ligand attachment onto the surface of chitosan nanoparticles on their transfection efficiencies was studied. Chitosan was biotinylated with NHS-biotin, NHS-LC-biotin or NHS-LC-LC-biotin, providing a control over the distance the ligand existed away from the surface of chitosan. In addition, avidin was conjugated with chitosan using reductive amination to compare the effect of more direct conjugation of the protein linker to the chitosan surface. It was found that increasing the arm length of the biotin moiety from 13.5 Å to 22.4 Å (using NHS-biotin and NHS-LC-biotin, respectively) caused significant enhancement in the transfection efficiency, whereas increasing the arm length further to 30.5 Å by using NHS-LC-LC-biotin resulted in inhibiting the transgenic effect to a slightly lower levels than when using NHS-biotin. This indicates the importance of optimizing the distance of attached ligands from the surface of polymer for the best interaction with cells and the

subsequent uptake of nanoparticles. Conjugating avidin directly into chitosan caused drastic decline in transgene expression compared to biotinylated chitosans, which resulted from the effect of the conjugation conditions on avidin properties and the stronger interaction of avidin with chitosan in the absence of linker arm, affecting both chitosan surface properties and ligand effect.

3.4 Conclusions

This study is a continuation of our previous work and others that shows that chitosan is a promising polymer for biomacromolecule delivery, especially for gene therapy purposes. Optimized fabrication techniques of chitosan nanoparticles were utilized for fabricating ligand modified chitosan nanoparticles through a facile and relatively rapid method that obviates the use of harsh conjugation environments. This method is based on the strong avidin-biotin interaction and the ability to biotinylate chitosan and control the biotinylation reaction. It was found that immobilizing the adhesion peptide, RGD, onto the surface of chitosan nanoparticles resulted in significant improvement in transgene expression due to enhancing cell interaction and uptake of nanoparticles. Similarly, immobilizing PEG onto the surface of chitosan nanoparticles resulted in higher transfection efficiency due to stabilization of the nanoparticles, although to a lesser degree compared to RGD. These findings show that this ligand modification method can be used to modify chitosan nanoparticles with any ligand of choice or with multiple ligands at the same time. Although the present study was targeted for injectable routes of administration, the nanoparticles developed may also have an application in other modes of delivery, such as nasal. Moreover, this method of ligand modification are potentially suited for a wide range of *in vivo* biomedical applications, since all the involved component in preparing these delivery systems have been proven to be tissue-compatible.

3.5 Figures and Tables

Table 3-1. Degrees of deacetylation, measured by first derivative UV spectrophotometry, and viscosity average molecular weights of different grades of chitosan.

Chitosan grade	Measured degree of deacetylation	Viscosity average molecular weight (M_v)
HM-HD	91.28%	181686
MM-HD	90.92%	144760
MM-MD	84.02%	132578
LM-HD	92.10%	102017
VLM-HD	90.89%	42460
MM-LD	74.36%	140708

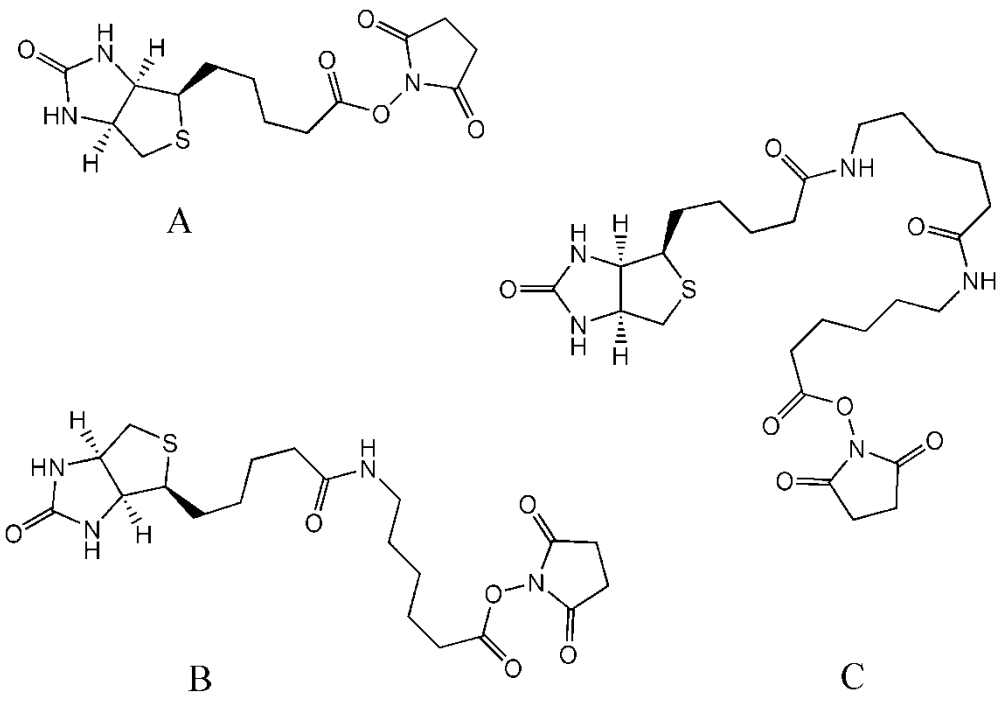

Figure 3-1. Molecular structures of EZ-Link® reagents. A) N-hydroxysuccinimide (NHS)-biotin, B) NHS-LC-biotin (succinimidyl-6-(biotinamido)hexanoate) and C) NHS-LC-LC-biotin (succinimidyl-6-(biotinamido)-6-hexanamido hexanoate).

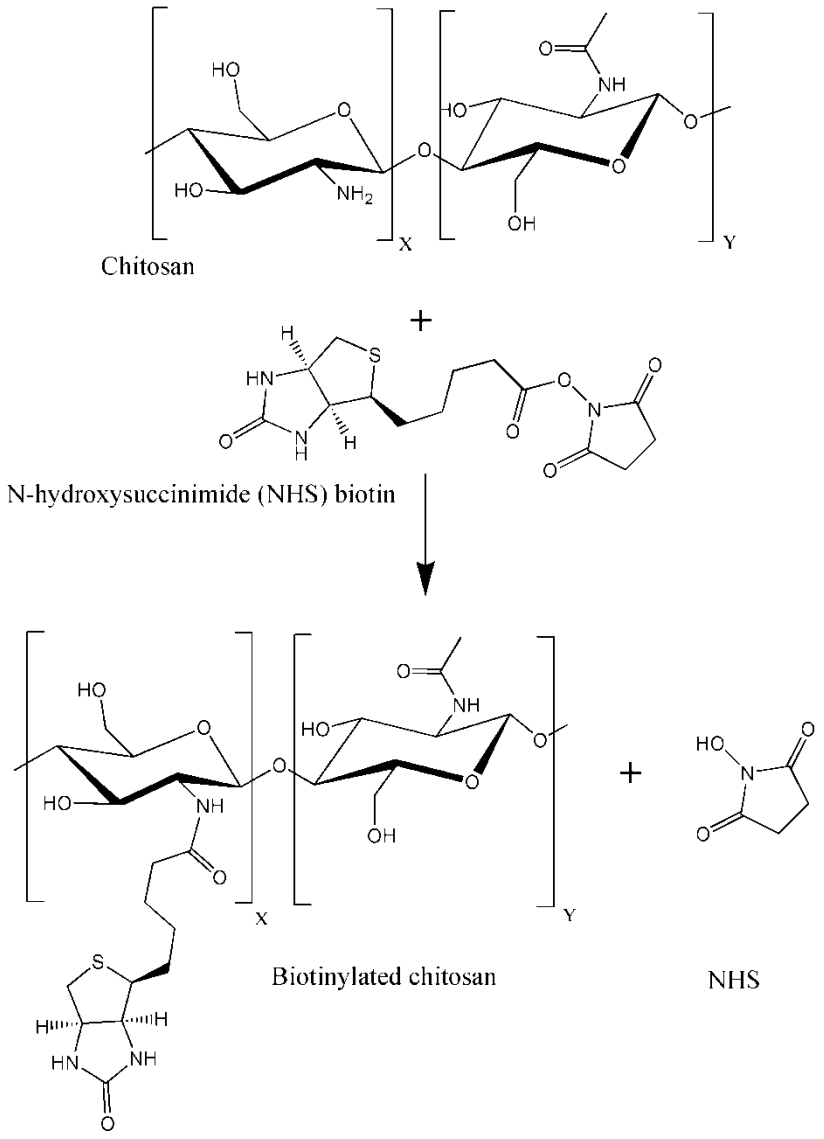

Figure 3-2. Schematic of chitosan biotinylation reaction using NHS-biotin.

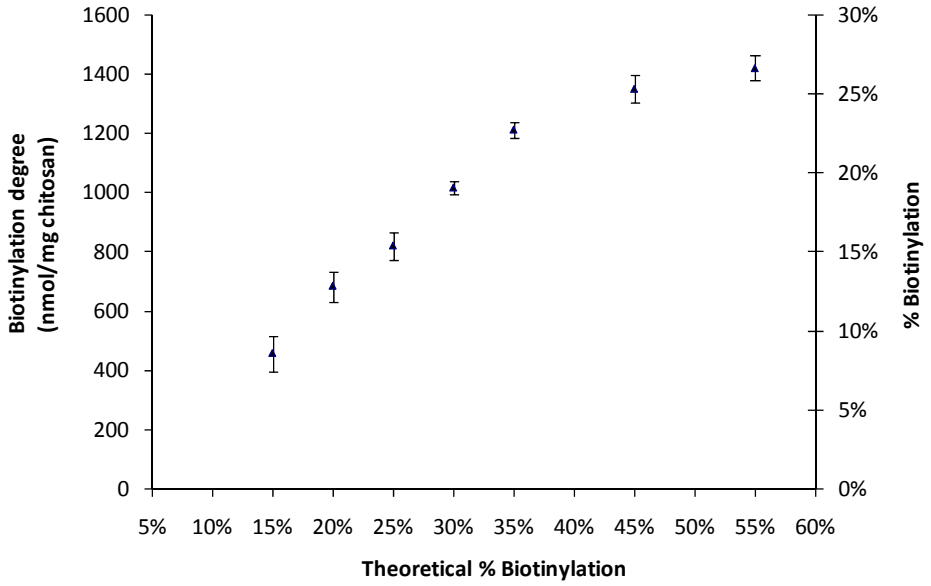

Figure 3-3. Biotinylation efficiencies of EZ-Link® NHS-biotin on low molecular weight and high degree of deacetylation (LM-HD) chitosan. Chitosan concentration was 5 mg/ml suspended in phosphate buffer pH 8.2 and at different theoretical biotinylation degrees. Biotinylation degree as nmol biotin/mg chitosan was measured using HABA/avidin assay. Data are represented as the mean ± SD (n = 3).

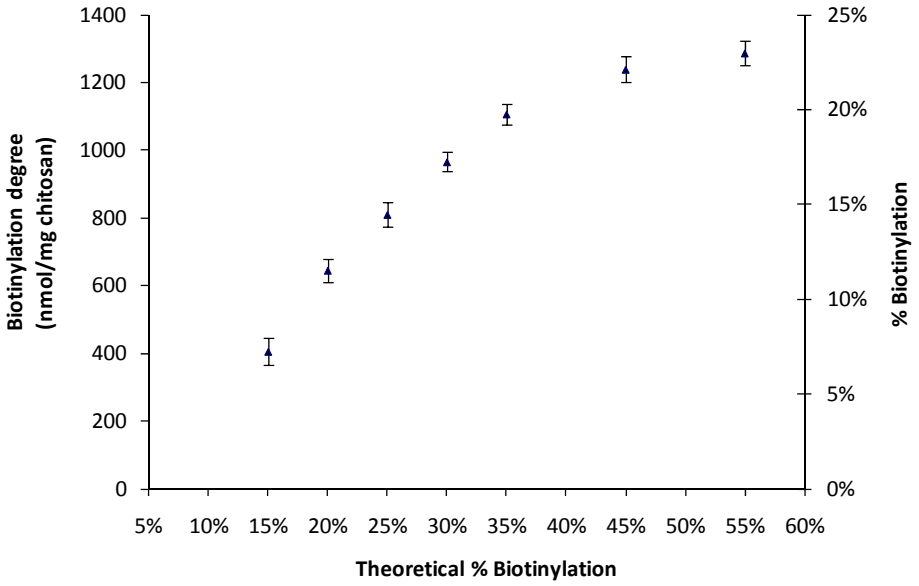

Figure 3-4. Biotinylation efficiencies of EZ-Link® NHS-LC-biotin on low molecular weight and high degree of deacetylation (LM-HD) chitosan. Chitosan concentration was 5 mg/ml suspended in phosphate buffer pH 8.2 and at different theoretical biotinylation degrees. Biotinylation degree as nmol biotin/mg chitosan was measured using HABA/avidin assay. Data are represented as the mean ± SD (n = 3).

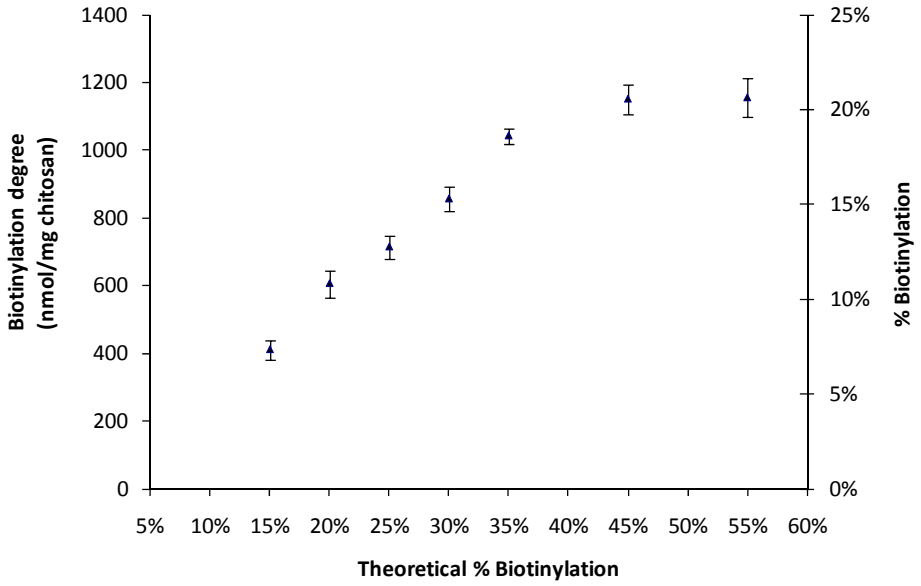

Figure 3-5. Biotinylation efficiencies of EZ-Link® NHS-LC-LC-biotin on low molecular weight and high degree of deacetylation (LM-HD) chitosan. Chitosan concentration was 5 mg/ml suspended in phosphate buffer pH 8.2 and at different theoretical biotinylation degrees. Biotinylation degree as nmol biotin/mg chitosan was measured using HABA/avidin assay. Data are represented as the mean ± SD (n = 3).

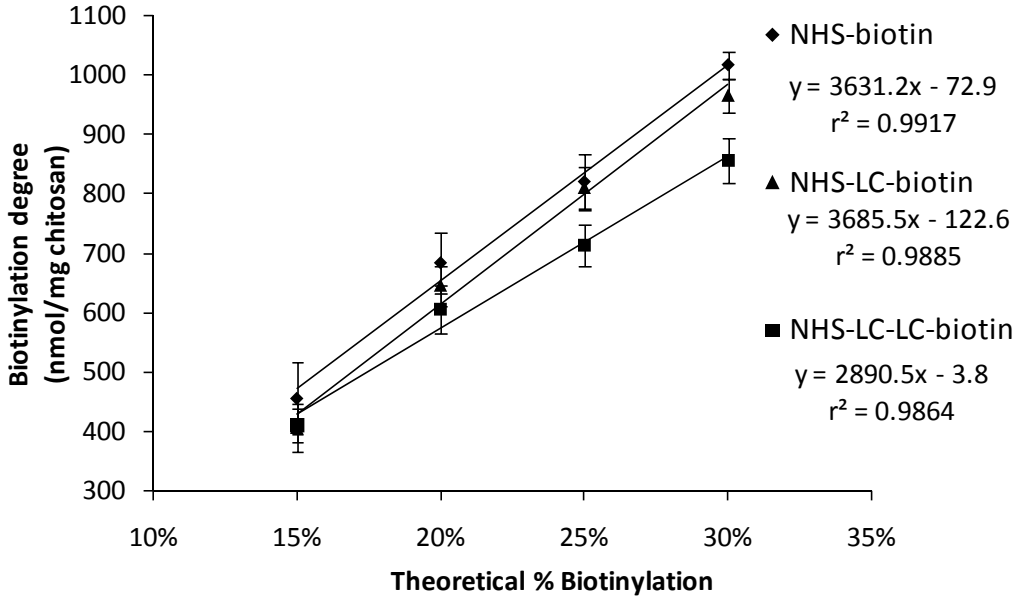

Figure 3-6. Linear regression of the initial biotinylation reactions of chitosans using EZ-Link® NHS-biotin, NHS-LC-biotin and NHS-LC-LC-biotin. Biotinylation degree as nmol biotin/mg chitosan was measured using HABA/avidin assay. Data are represented as the mean ± SD (n = 3).

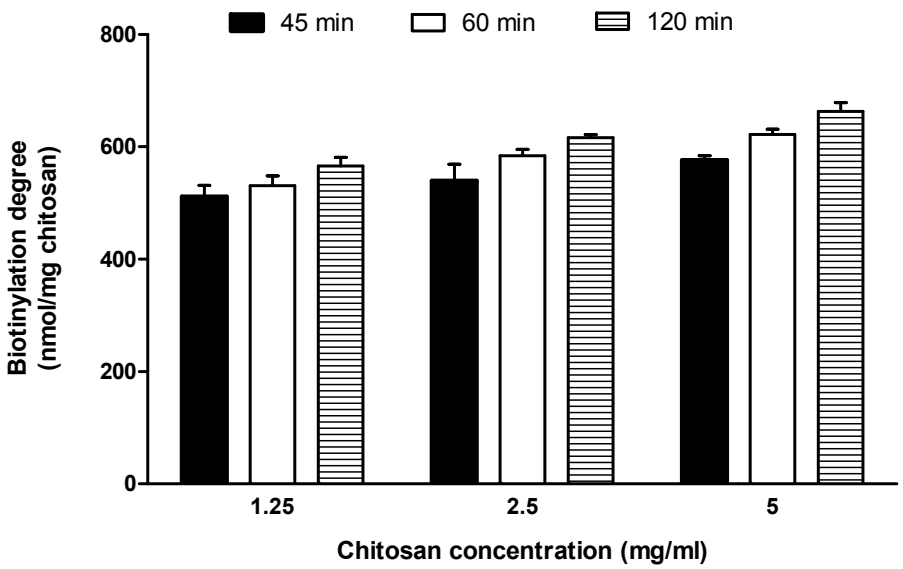

Figure 3-7. Biotinylation efficiencies of EZ-Link® NHS-biotin on low molecular weight and high degree of deacetylation (LM-HD) chitosan as a function of chitosan's concentration. Chitosan was suspended in phosphate buffer pH 8.2 at 1.25, 2.5 and 5 mg/ml concentration and at 20% theoretical biotinylation degree. The reactions were allowed to proceed for 45, 60 or 120 min. Data are represented as the mean ± SD (n = 3).

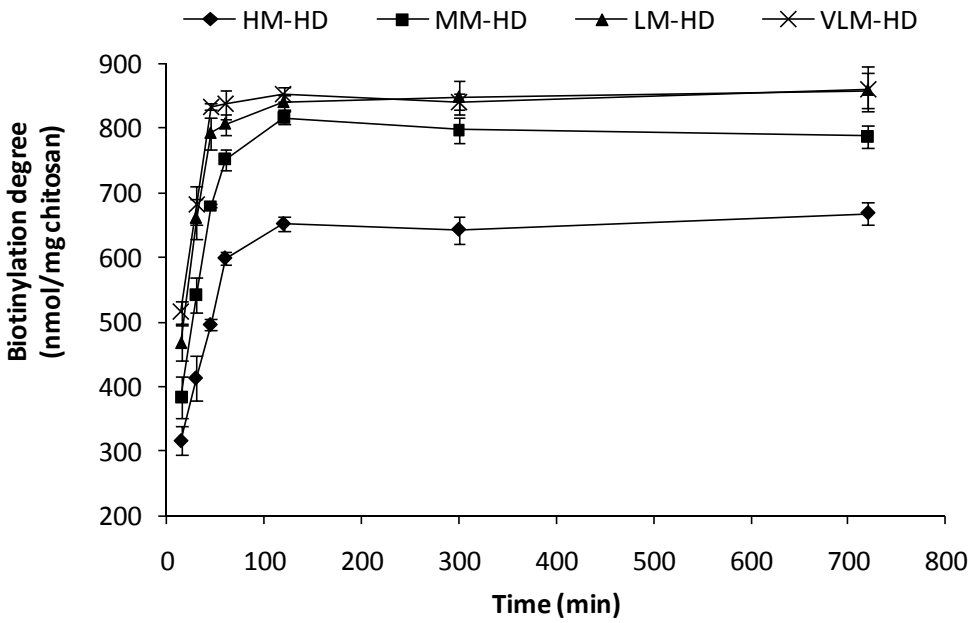

Figure 3-8. Biotinylation efficiencies of EZ-Link® NHS-biotin on chitosan as a function of chitosan's molecular weight. HM-HD, MM-HD, LM-HD and VLM-HD chitosans were used at 25% theoretical biotinylation degrees. The reactions were allowed to proceed for 15, 45, 60, 120, 300 or 720 min in phosphate buffer pH 8.2. Biotinylation degree as nmol biotin/mg chitosan was measured using HABA/avidin assay. Data are represented as the mean ± SD (n = 3).

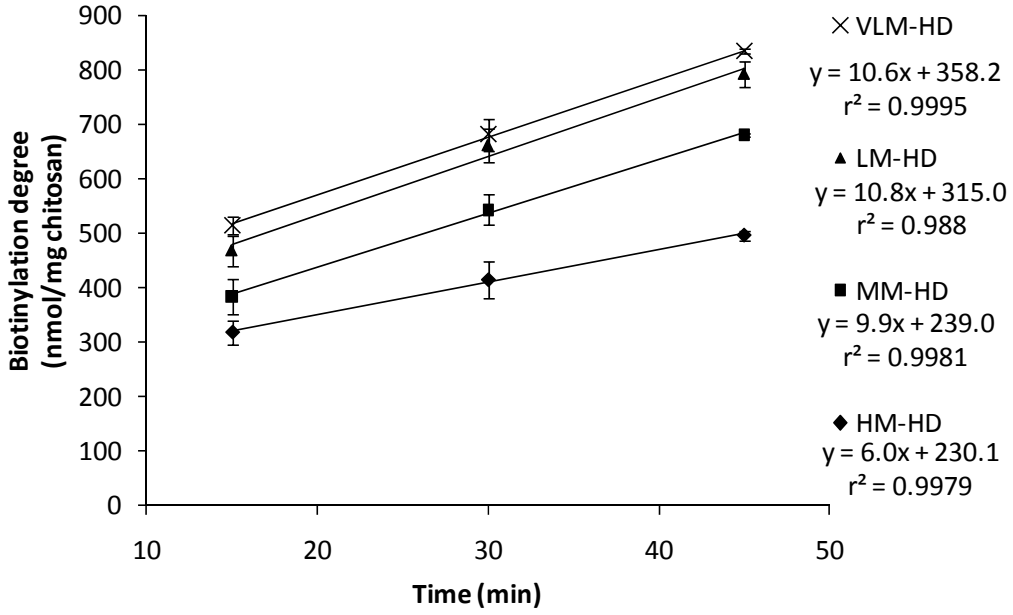

Figure 3-9. Linear regression of the initial biotinylation reactions between EZ-Link® NHS-biotin and chitosan as a function of chitosan's molecular weight. HM-HD, MM-HD, LM-HD and VLM-HD chitosans were suspended in phosphate buffer pH 8.2 at 25% theoretical biotinylation degrees. Biotinylation degree as nmol biotin/mg chitosan was measured using HABA/avidin assay. Data are represented as the mean ± SD (n = 3).

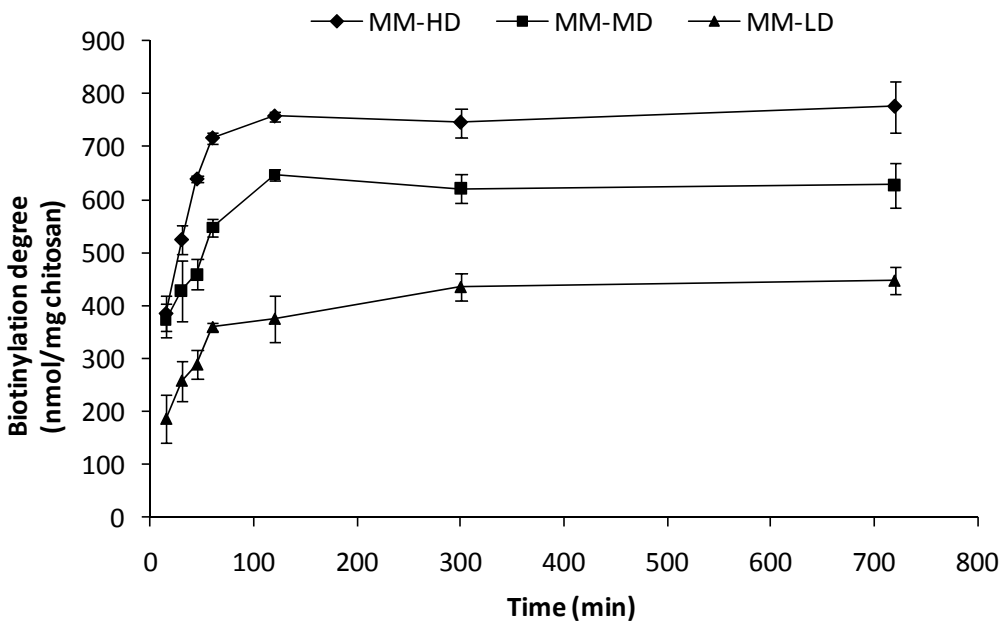

Figure 3-10. Biotinylation efficiencies of EZ-Link® NHS-biotin on chitosan as a function of chitosan's degree of deacetylation. MM-HD, MM-MD and MM-LD chitosans were used at 25% theoretical biotinylation degrees. The reactions were allowed to proceed for 15, 45, 60, 120, 300 or 720 min in phosphate buffer pH 8.2. Biotinylation degree as nmol biotin/mg chitosan was measured using HABA/avidin assay. Data are represented as the mean ± SD (n = 3).

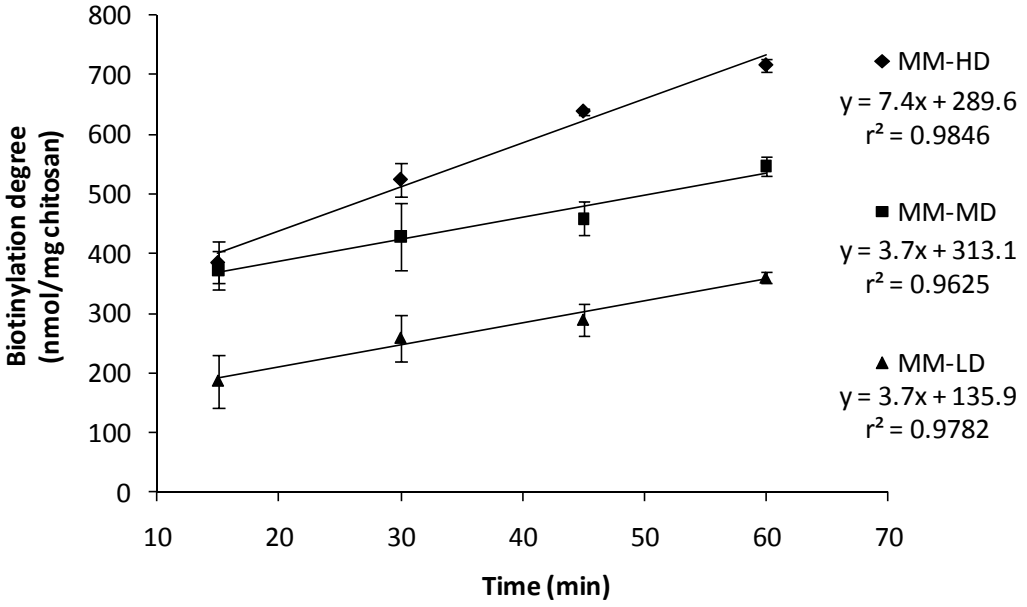

Figure 3-11. Linear regression of the initial biotinylation reactions between EZ-Link® NHS-biotin and chitosan as a function of chitosan's degree of deacetylation. MM-HD, MM-MD and MM-LD chitosans were suspended in phosphate buffer pH 8.2 at 25% theoretical biotinylation degrees. Biotinylation degree as nmol biotin/mg chitosan was measured using HABA/avidin assay. Data are represented as the mean ± SD (n = 3).

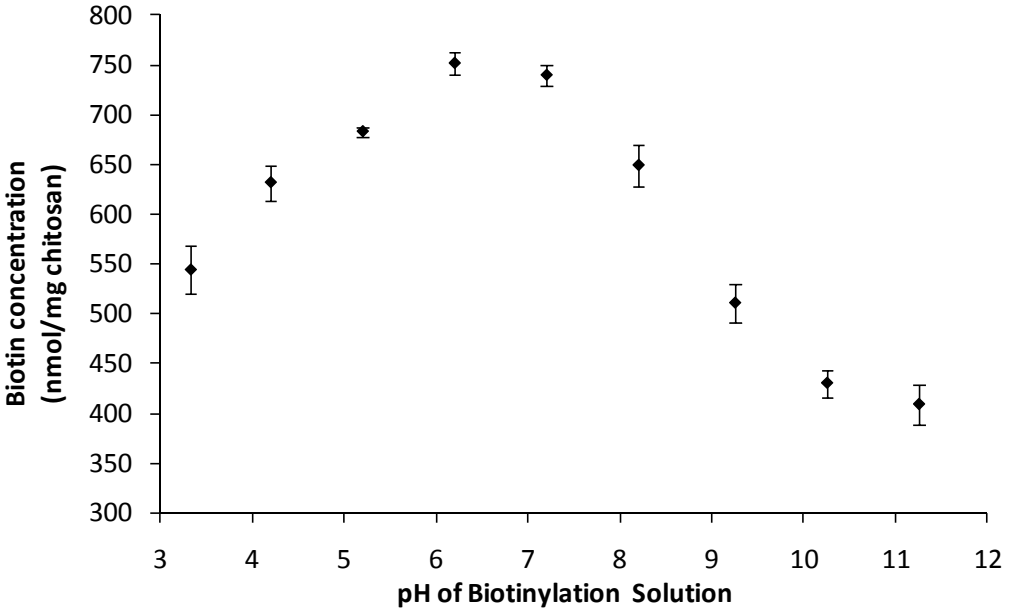

Figure 3-12. Biotinylation efficiencies of EZ-Link® NHS-biotin on low molecular weight and high degree of deacetylation (LM-HD) chitosan at different pH values. Chitosan (5 mg/ml) was dissolved or suspended in acetate buffer (pH 3.2, 4.2 and 5.2), phosphate buffer (pH 6.2, 7.2 and 8.2) or carbonate buffer (pH 9.25, 10.25 and 11.25) at 20% theoretical biotinylation degrees. Ionic strengths were adjusted to 1.5 M using NaCl. Biotinylation degrees as nmol biotin/mg chitosan were measured using HABA/avidin assay. Data are represented as the mean ± SD (n = 3).

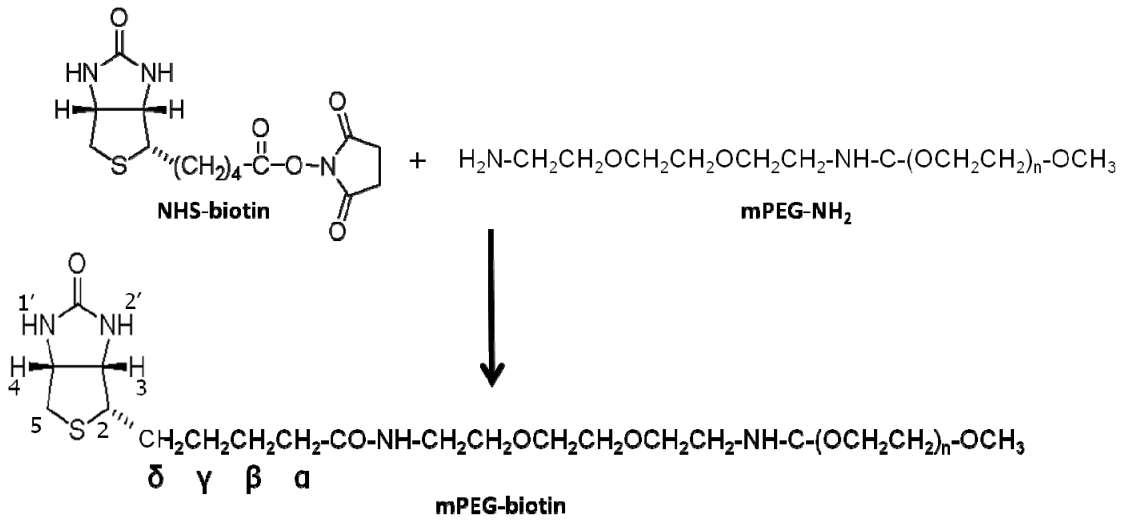

Figure 3-13. Schematic showing NHS-biotin reaction with mPEG-NH_2.

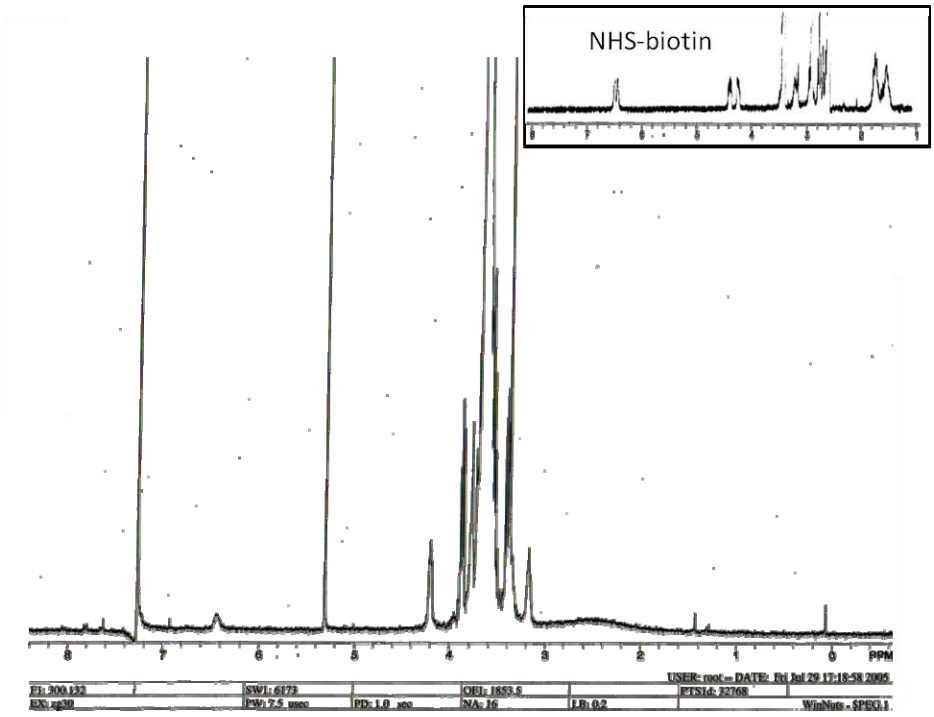

Figure 3-14. ^{1}H-NMR spectrum of mPEG-NH_2 using Bruker AVANCE-300 spectrometer operating at 300 MHz in comparison to NHS-biotin (in box).

NHS-biotin spectrum was reproduced from Salem AK, Cannizzaro SM, Davies MC, et al. Synthesis and characterization of a degradable poly(lactic acid)-poly(ethylene glycol) copolymer with biotinylated end groups. *Biomacromolecules* 2001; 2(2):575-80.[162]

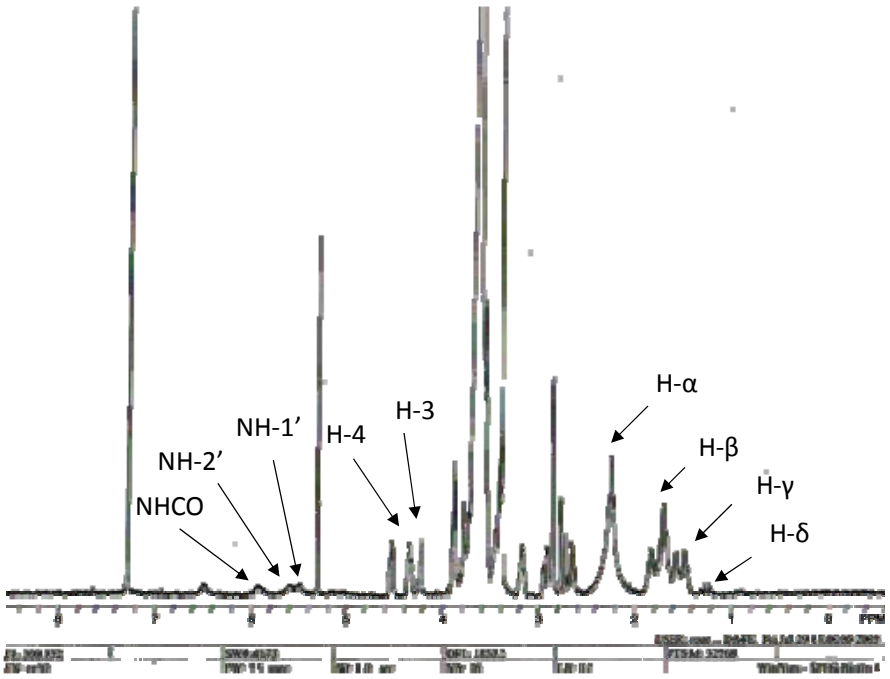

Figure 3-15. ^{1}H-NMR spectrum of mPEG-biotin. The hydrogen numbers correspond to Figure 3-13.

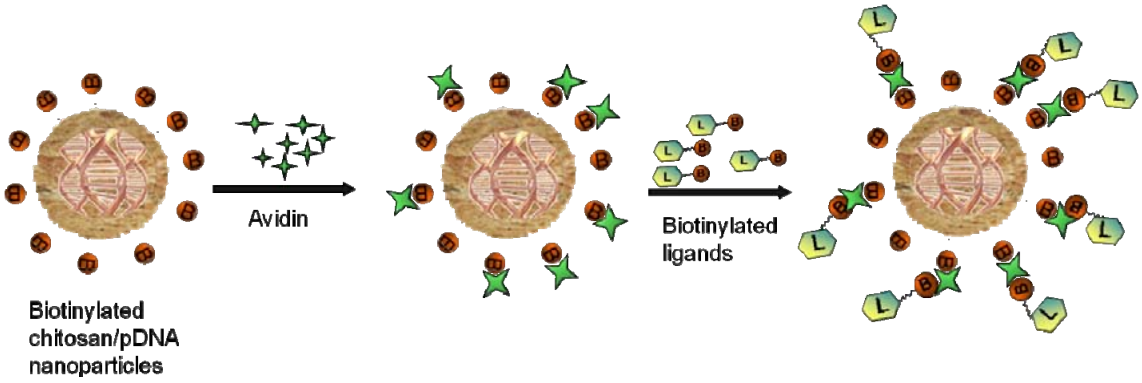

Figure 3-16. Schematic of the ligand attachment on chitosan nanoparticles via method A.

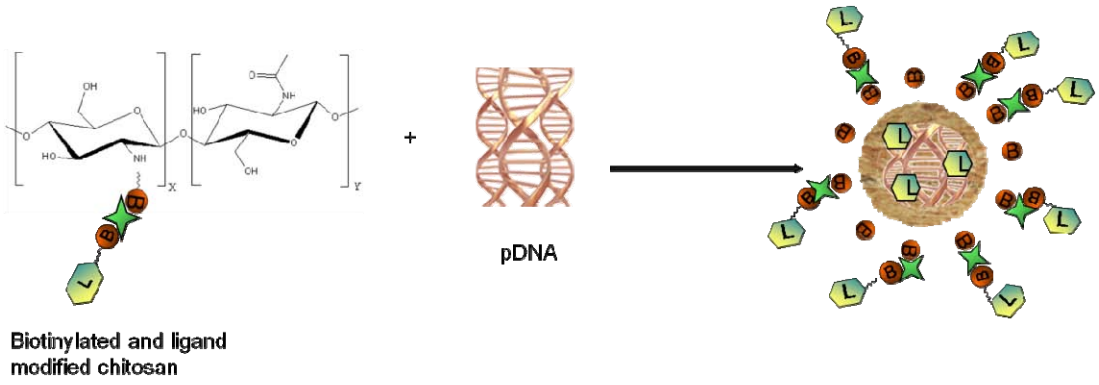

Figure 3-17. Schematic of the ligand attachment on chitosan nanoparticles via method B.

Table 3-2. Surface avidin content on chitosan nanoparticles as measured by the HABA assay.

Avidinylation method	Added avidin (μg/ml)	Surface avidin (μg/ml)	Avidinylation efficiency
Method A	0	0	NA
	40	37.8 ± 7.8	94.5%
	60	53.7 ± 6.4	89.6%
	80	70.4 ± 7.6	88.0%
	100	82.6 ± 11.4	82.6%
Method B	60	55.5 ± 8.2	57.6%
Avidin conjugation	NA	53.8 ± 4.1	27.9%

Note: Nanoparticles were prepared using biotinylated chitosans followed by the addition of avidin (method A), adding avidin to biotinylated chitosans followed by formation of nanoparticles (method B) or by avidin conjugation on chitosan followed by preparation of nanoparticles (avidin conjugation method).

Table 3-3. Particle sizes and zeta potential values of unmodified chitosan nanoparticles (CS) and chitosan nanoparticles modified with RGD and PEG by method A (CS-RGD and CS-PEG, respectively).

	N/P ratio	Z-average (nm) ± SD	Average zeta potential (mV) ± SD
CS	10	126.8 ± 4.5	28.0 ± 0.6
	15	132.5 ± 10.6	28.8 ± 0.7
	25	143.6 ± 8.8	30.3 ± 0.4
	35	151.5 ± 5.2	31.4 ± 0.5
	50	171.7 ± 14.0	32.4 ± 1.1
CS-RGD	10	194.5 ± 9.0	22.6 ± 1.2
	15	175.3 ± 6.2	24.4 ± 0.7
	25	142.4 ± 11.9	27.2 ± 0.8
	35	141.2 ± 12.2	27.3 ± 0.8
	50	164.2 ± 13.3	28.3 ± 0.9
CS-PEG	10	201.7 ± 10.4	23.2 ± 0.6
	15	192.3 ± 6.1	24.4 ± 0.7
	25	173.6 ± 10.2	27.9 ± 0.5
	35	163.1 ± 7.2	28.0 ± 0.9
	50	165.9 ± 11.3	28.7 ± 1.1

Note: Avidin was added at a concentration of 60 μg/ml for all formulations.

Table 3-4. Particle sizes and zeta potential values of chitosan nanoparticles modified with RGD and PEG by method B (CS-RGD and CS-PEG, respectively).

	N/P ratio	Z-average (nm) ± SD	Average zeta potential (mV) ± SD
CS-RGD	10	210.7 ± 18.6	22.2 ± 0.8
	15	213.7 ± 6.7	23.8 ± 0.7
	25	192.8 ± 11.2	26.3 ± 1.0
	35	181.1 ± 8.0	26.7 ± 0.7
	50	201.3 ± 24.8	26.8 ± 0.9
CS-PEG	10	220.7 ± 25.3	23.0 ± 0.9
	15	199.8 ± 14.6	23.9 ± 0.9
	25	188.0 ± 16.6	26.9 ± 0.7
	35	222.6 ± 32.7	27.3 ± 0.8
	50	277.8 ± 23.5	27.0 ± 0.7

Note: Avidin was added at a concentration of 60 μg/ml for all formulations.

Table 3-5. Particle sizes and zeta potential values of chitosan nanoparticles modified with RGD and PEG by method A at different ligand modification degrees.

	Added avidin (μg/ml)	Z-average (nm) ± SD	Average zeta potential (mV) ± SD
CS-RGD	0	149.3 ± 6.5	30.2 ± 0.7
	40	133.5 ± 6.8	29.0 ± 1.2
	60	144.6 ± 12.9	27.4 ± 1.0
	80	164.7 ± 4.8	23.6 ± 1.3
	100	204.1 ± 12.0	18.6 ± 1.5
CS-PEG	0	149.3 ± 6.5	30.2 ± 0.7
	40	155.6 ± 14.9	29.0 ± 0.6
	60	165.3 ± 12.1	28.5 ± 0.7
	80	200.5 ± 16.1	25.4 ± 1.2
	100	232.3 ± 20.2	19.6 ± 1.3

Note: Chitosan/dextran sulfate w/w ratio = 10 and N/P ratio = 35.

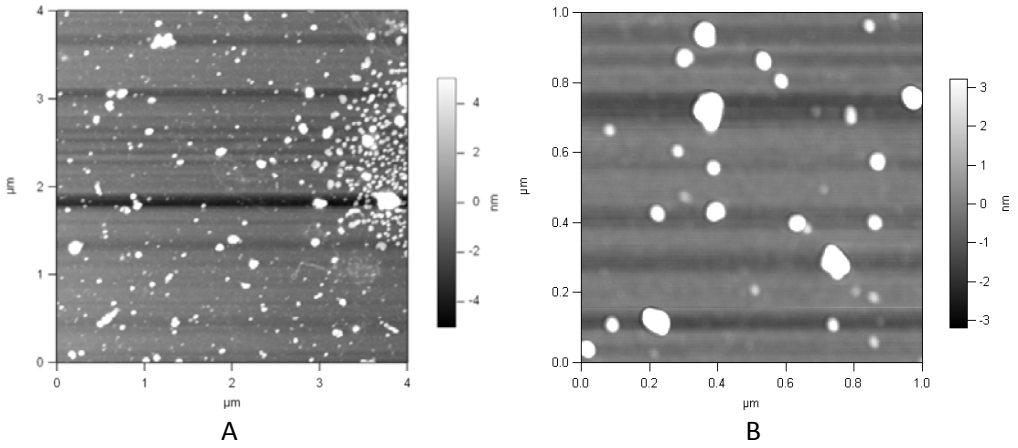

Figure 3-18. Tapping mode atomic force microscopy (AFM) images of unmodified chitosan nanoparticles. Scan areas were A) 4 and B) 1 µm. Chitosan/DS w/w ratio = 10 and N/P ratio = 35.

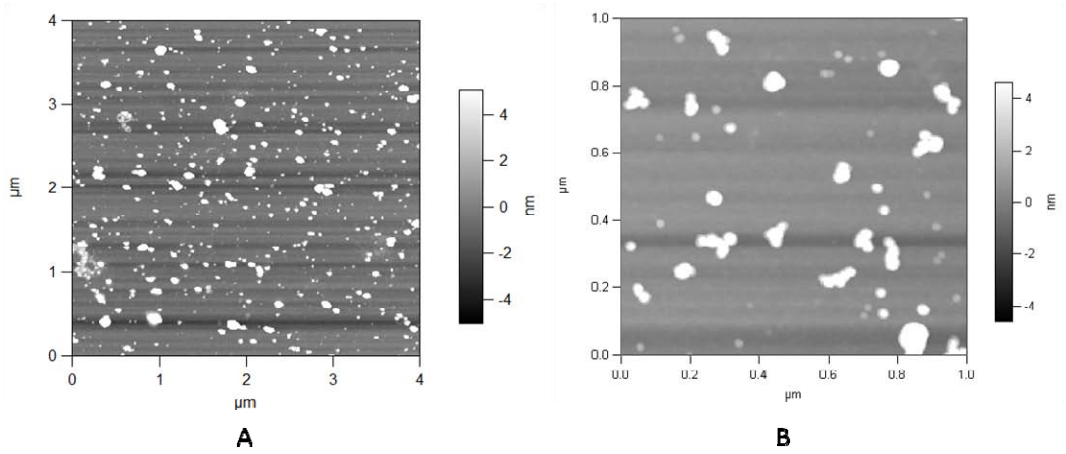

Figure 3-19. Tapping mode atomic force microscopy (AFM) images of RGD-modified chitosan nanoparticles prepared using method A. Scan areas were A) 4 and B) 1 µm. Added avidin = 60 µg/ml, chitosan/DS w/w ratio = 10 and N/P ratio = 35.

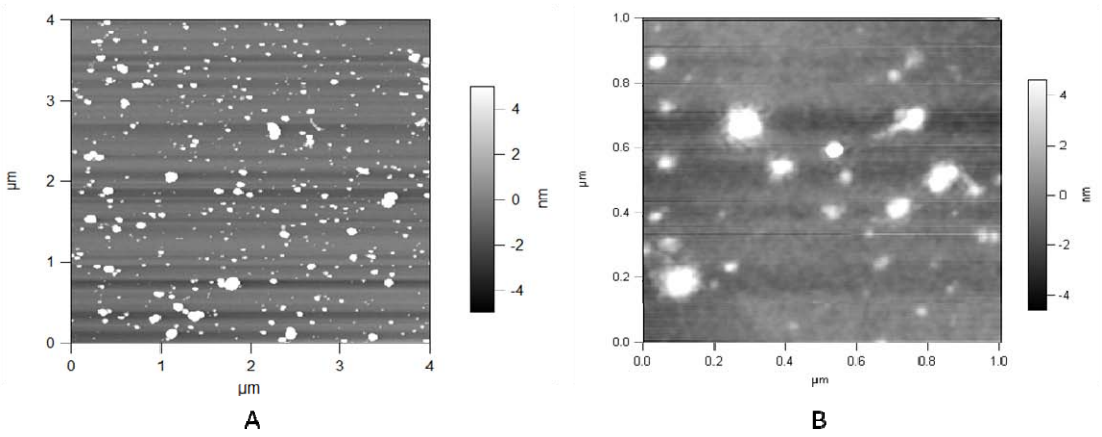

Figure 3-20. Tapping mode atomic force microscopy (AFM) images of PEG-modified chitosan nanoparticles prepared using method A. Scan areas were A) 4 and B) 1 µm. Added avidin = 60 µg/ml, chitosan/DS w/w ratio = 10 and N/P ratio = 35.

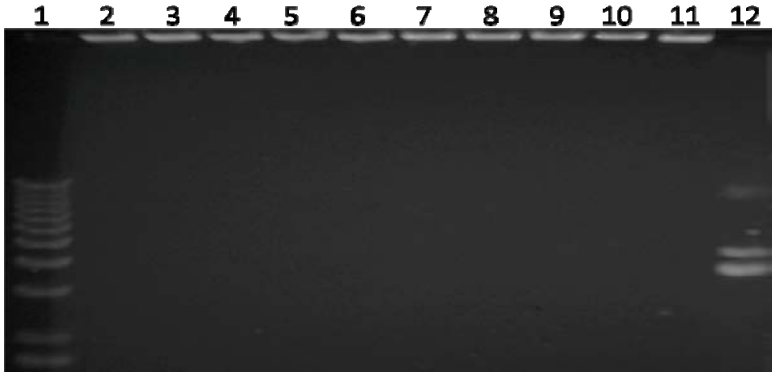

Figure 3-21. Agarose gel electrophoresis of chitosan-DS/DNA nanoparticles modified with RGD and PEG. (1) TrackIt™ 1 Kb DNA Ladder (Invitrogen™), (2) CS-RGD/DNA, N/P = 10 (3) CS-RGD/DNA, N/P = 15 (4) CS-RGD/DNA, N/P = 25 (5) CS-RGD/DNA, N/P = 35 (6) CS-RGD/DNA, N/P = 50 (7) CS-PEG/DNA, N/P = 10 (8) CS-PEG/DNA, N/P = 15 (9) CS-PEG/DNA, N/P = 25 (10) CS-PEG/DNA, N/P = 35.(11) CS-PEG/DNA, N/P = 50 (12) VR1255 naked pDNA.

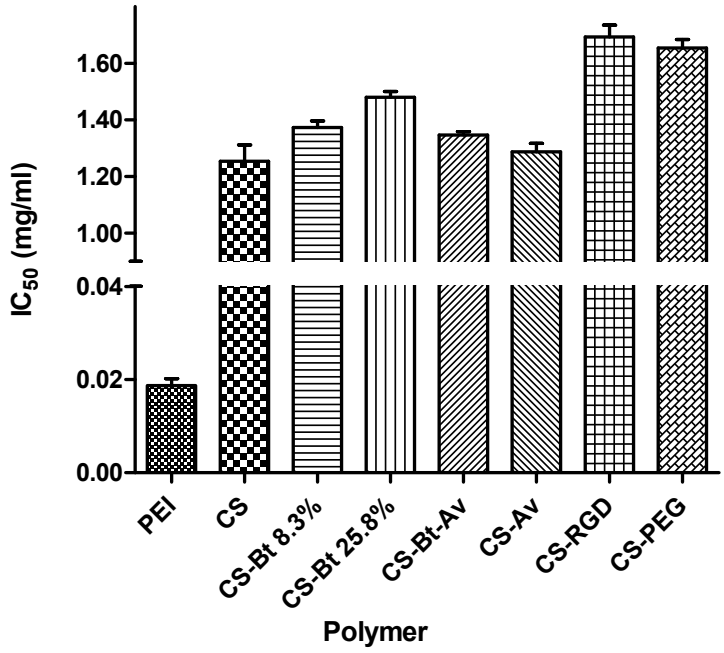

Figure 3-22. IC_{50} of VLM-HD chitosan (CS), Biotin modified chitosan at 8.3% and 25.8% biotinylation degrees (CS-Bt 8.3% and CS-Bt 25.8%, respectively), biotinylated chitosan modified with avidin (CS-Bt-Av), chitosan conjugated with avidin (CS-Av), RGD and PEG modified chitosan through avidin linker (CS-RGD and CS-PEG, respectively) in comparison to branched PEI. Cell viability was measured using MTT assay in HEK293 cells as described in the experimental section. Data are represented as the mean ± SD (n = 3).

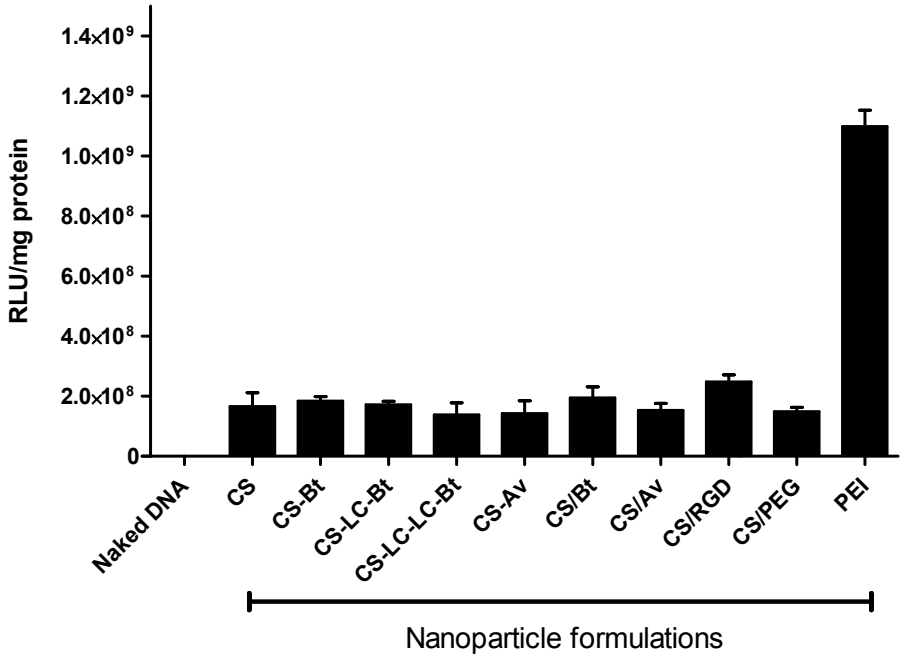

Figure 3-23. Transfection efficiencies in HEK293 using naked DNA, PEI and control chitosan nanoparticle formulations. Nanoparticles were fabricated with chitosans which were covalently modified with either biotin, LC-biotin, LC-LC-biotin or avidin, in addition to chitosans physically mixed with avidin, biotin, RGD or PEG. Data are represented as the mean ± SD (n = 3).

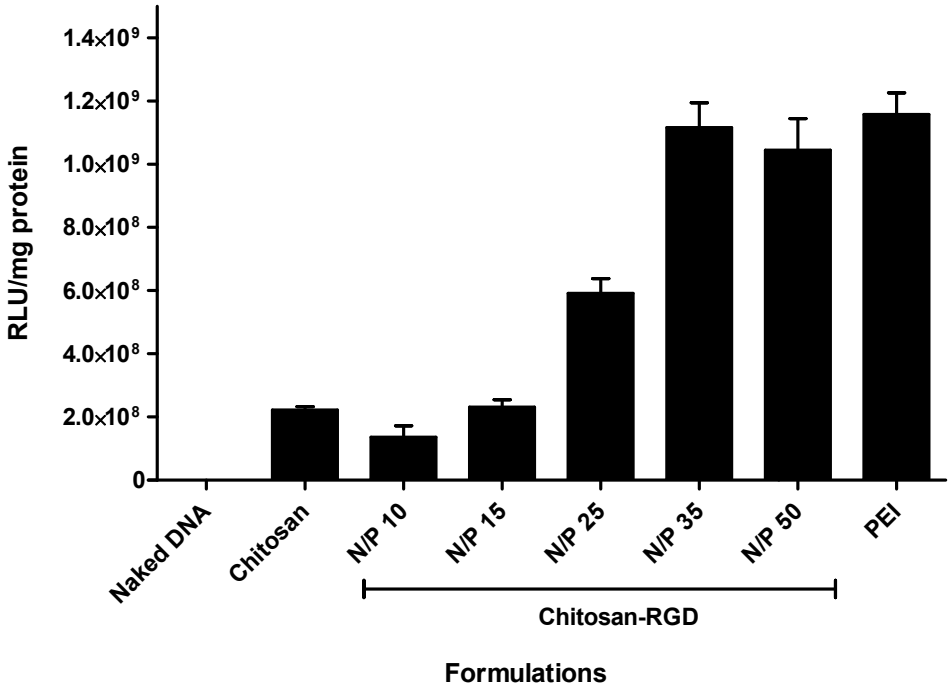

Figure 3-24. Transfection efficiencies of RGD modified chitosan nanoparticles (using method B) in HEK293 cells at different N/P ratios compared to naked DNA, unmodified chitosan and PEI nanoparticles. Data are represented as the mean ± SD (n = 3).

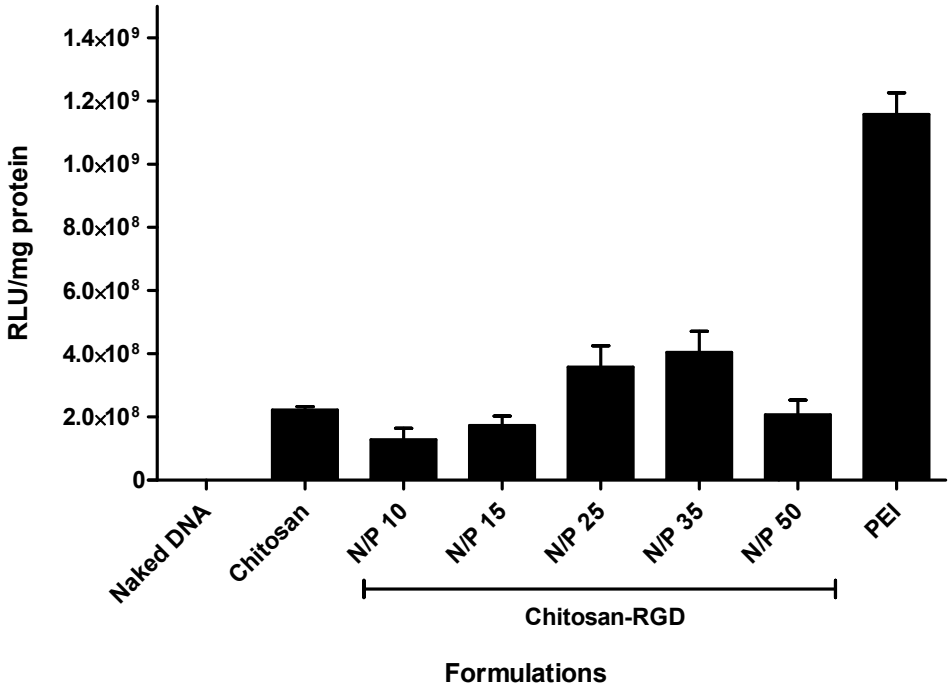

Figure 3-25. Transfection efficiencies of RGD modified chitosan nanoparticles (using method B) in HEK293 cells at different N/P ratios compared to naked DNA, unmodified chitosan and PEI nanoparticles. Data are represented as the mean ± SD (n = 3).

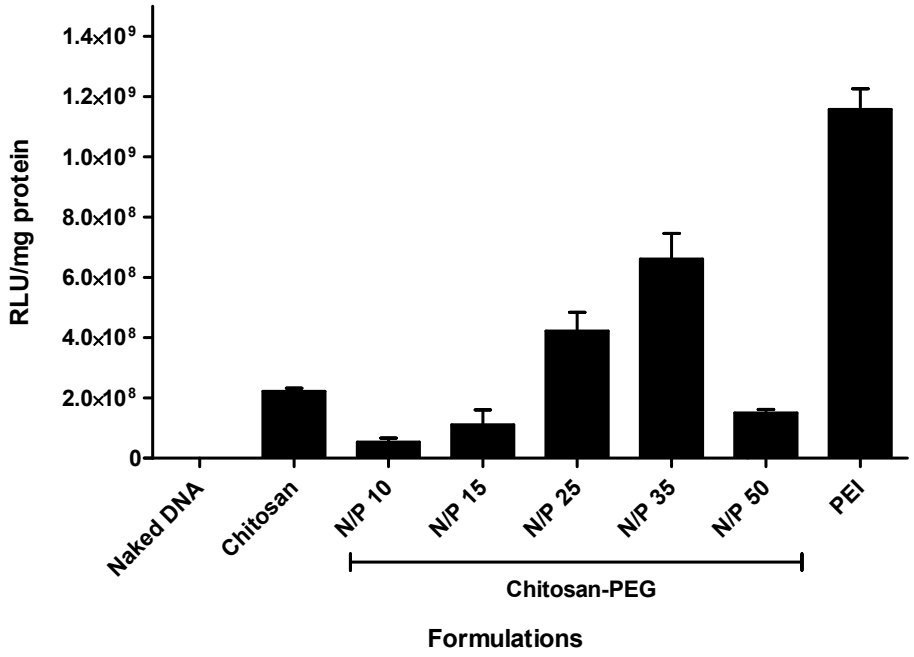

Figure 3-26. Transfection efficiencies of PEG modified chitosan nanoparticles (using method A) in HEK293 cells at different N/P ratios compared to naked DNA, unmodified chitosan and PEI nanoparticles. Data are represented as the mean ± SD (n = 3).

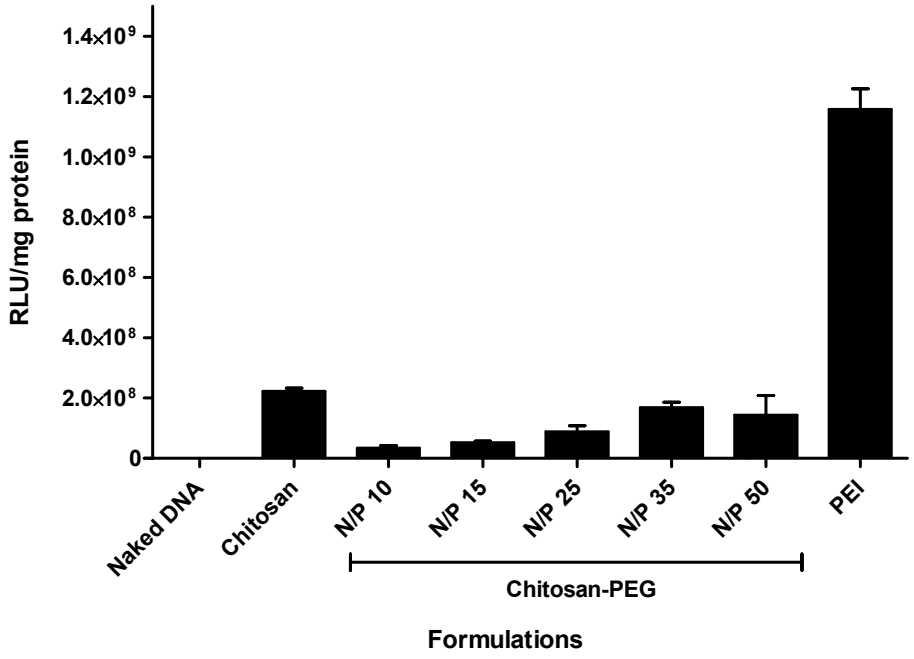

Figure 3-27. Transfection efficiencies of PEG modified chitosan nanoparticles (using method B) in HEK293 cells at different N/P ratios compared to naked DNA, unmodified chitosan and PEI nanoparticles. Data are represented as the mean ± SD (n = 3).

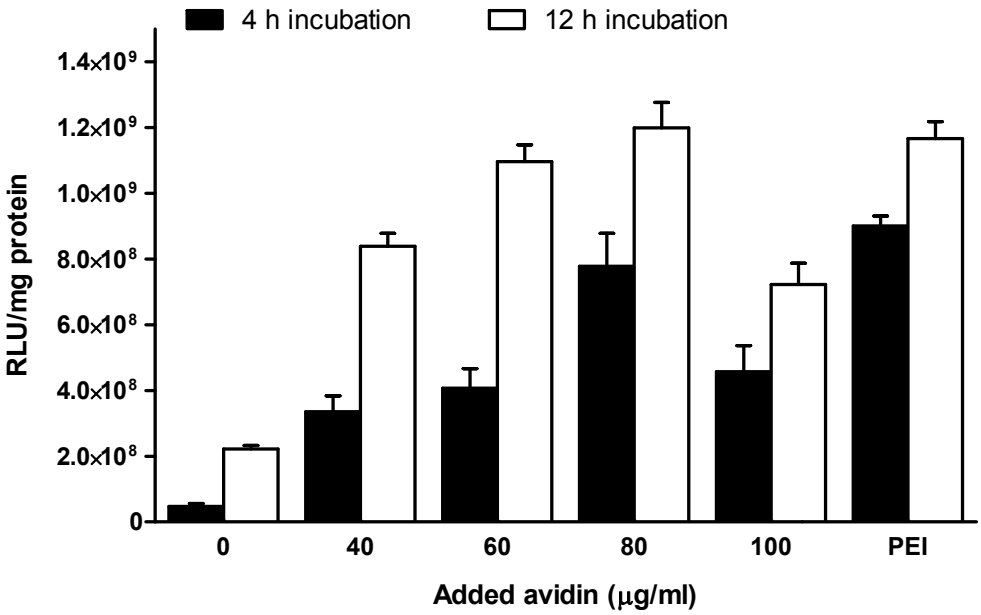

Figure 3-28. Transfection efficiencies of RGD modified chitosan nanoparticles (N/P 35) in HEK293 cells compared to PEI nanoparticles at increasing avidin content. Chitosan was biotinylated using NHS-biotin and ligand addition was controlled by the amount of added avidin. RGD ligand attachment was done using method A as described in the Materials and Methods section. Nanoparticles were incubated for either 4 or 12 h before changing the media and continuing incubation for another 44 and 36 h, respectively. Data are represented as the mean ± SD (n = 3).

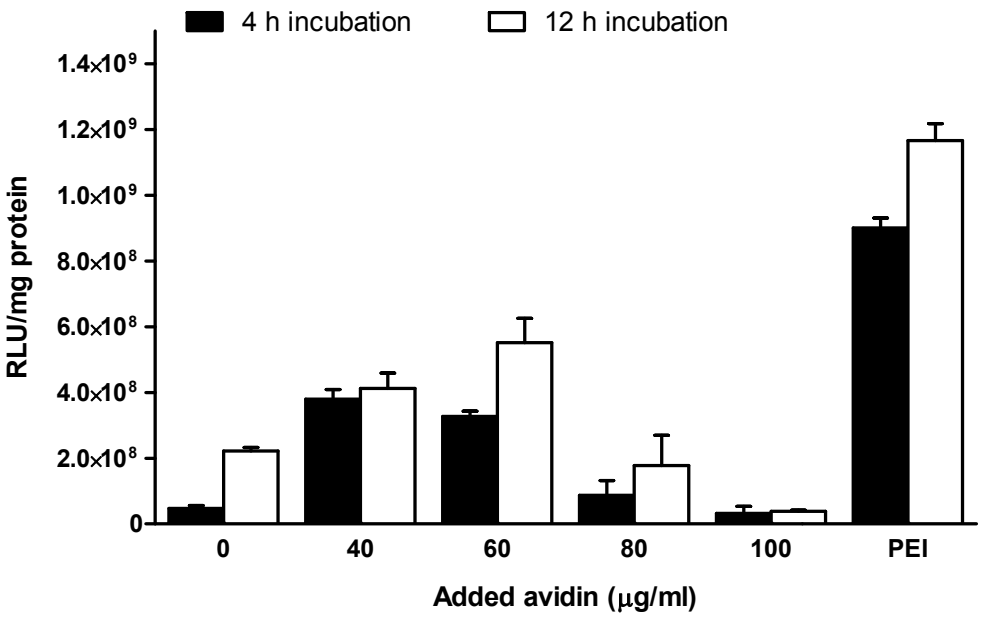

Figure 3-29. Transfection efficiencies of PEG modified chitosan nanoparticles (N/P 35) in HEK293 cells compared to PEI nanoparticles at increasing avidin content. Chitosan was biotinylated using NHS-biotin and ligand addition was controlled by the amount of added avidin. PEG ligand attachment was done using method A as described in the Materials and Methods section. Nanoparticles were incubated for either 4 or 12 h before changing the media and continuing incubation for another 44 and 36 h, respectively. Data are represented as the mean ± SD (n = 3).

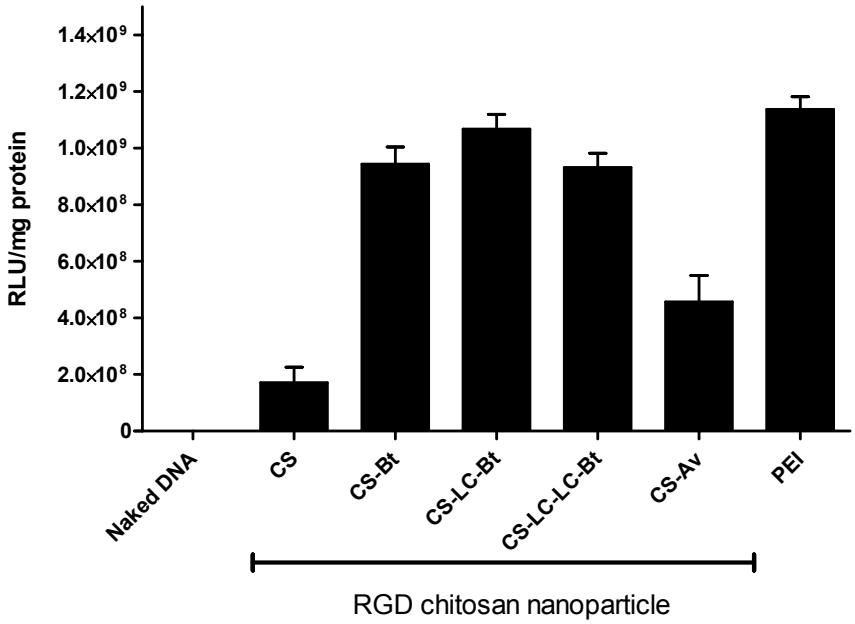

Figure 3-30. Transfection efficiencies of RGD modified chitosan nanoparticles using different linkers in HEK293 cells compared to naked DNA and PEI nanoparticles. Chitosan was covalently modified with either biotin, LC-biotin, LC-LC-biotin or avidin. RGD ligand attachment was done using method A as described in the Materials and Methods section. Data are represented as the mean ± SD (n = 3).

CHAPTER 4
CHITOSAN MODIFICATION USING AVIDIN-BIOTIN INTERACTION. PART II: APPLICATIONS IN ENZYME IMMOBILIZATION

4.1 Introduction

Enzymes exhibit a number of features that make their use advantageous compared to conventional chemical catalysts. Mainly, they possess a high level of catalytic efficiency, often far superior to chemical catalysts, and a high degree of specificity that allows them to discriminate not only between reactions but also between substrates (substrate specificity), similar parts of molecules (regiospecificity) and between optical isomers (stereospecificity).[222] However, a number of practical problems in the industrial use of enzymes exists. The high cost of isolation and purification of enzymes, the instability of their structures once they are isolated from their natural environments, and their sensitivity to both variation in process conditions and to trace levels of substances that can act as inhibitors represent some of these obstacles.[222]

Enzyme immobilization techniques are gaining more interest in enzyme technology, which is currently expanding in various fields such as bioorganic synthesis, biosensors and diagnostics, as well as in industrial processes. This is due to the success these techniques provide in overcoming some of the hurdles in utilizing the enzymes.[222,223] Advantages of immobilized enzymes include ease of separation, catalyst recycling and extended lifetimes. However, applications of immobilized enzymes are currently limited by diffusional or mass-transfer problems as well as conformational and environmental drawbacks, limiting catalytic processes on solid supports.[31] Micro and nano-scale materials have been applied for enzyme immobilization for their role in balancing the key factors that determine the efficiency of biocatalysis, including the mass transfer resistance, effective enzyme loading and surface area.[224]

The focus of this research is to apply ligand modification of chitosan developed previously in immobilization of a model enzyme, trypsin. This method avoids the use of harsh immobilization conditions, which can cause significant changes in the structure of enzymes and can affect the enzymatic activity dramatically.[32] Biotinylated chitosan nanoparticles and films were prepared and used for immobilizing trypsin through avidin bridged linkage. Enzyme activity and stability was measured at different enzyme reaction conditions.

4.2 Materials and Methods

4.2.1 Purification and preparation of chitosans

Chitosan was fully purified and prepared as discussed in the Materials and Methods section in Chapter 2. Briefly, high molecular weight and high degree of deacetylation (HM-HD), medium molecular weight and high degree of deacetylation (MM-HD) and low molecular weight and high degree of deacetylation (LM-HD) chitosans were obtained from Sigma®, MO. These chitosans were fully purified by first dissolving chitosan in 1% acetic acid solution and filtering the solutions to remove the insoluble particles. This was followed by decolorization and deproteinization in the presence of dithiothreitol and demineralization using ethylenediaminetetraacetic acid (EDTA). Viscosity average molecular weights were calculated from intrinsic viscosities using Mark–Houwink–Sakurada equation. Medium molecular weight and medium degree of deacetylation (MM-MD) and medium molecular weight and low degree of deacetylation (MM-LD) chitosans were prepared by heterogeneous reacetylation using acetic anhydride. Degrees of deacetylation were calculated based on first derivative UV spectrophotometry (1DUV) measurements.

4.2.2 Fabrication of chitosan nanoparticles and films

Chitosan solution (0.2 % w/v in 1 % (v/v) glacial acetic acid, Fisher Scientific, PA) was mixed with Tween 80 (polysorbate 80 or polyoxyethylene (20) sorbitan monooleate, Fisher Scientific, PA) at different w/v ratios for 10 min to ensure the formation of a uniform solution. Different polyanion solutions (10% w/v sodium sulfate, tripolyphosphate or dextran sulfate (5 kDa), Sigma®, MO) were added dropwise to the chitosan solution (50 ml in 100 ml glass beaker) under homogenization (6,500 rpm, Ultra Turrax T25 IKA®-WERKE basic homogenizer (IKA, NC)). Mixtures were homogenized for 20 min, after which the resulting solution was centrifuged at 12,500 rpm (Sorvall RC 26 Plus ultracentrifuge with SLA-1500 rotor (Thermo Scientific®, IL)) for 7 min to separate the particles which were washed twice with distilled water. The obtained pellets, composed of chitosan particles, were resuspended in distilled water and ultrasonicated for 2 min using a microtip probe sonicator set at level 2 (10 Watts) (Sonic Dismembrator Model 100, Fisher Scientific, PA), in order to break aggregates and redisperse the particles uniformly. Finally, chitosan particles were stored in the form of a colloidal suspension (1.6 mg/ml) in the refrigerator until used or lyophilized using a Labconco FreeZone 4.5 Liter Benchtop Freeze Dry System.

Particle sizes and zeta potential values were measured using Zetasizer Nano ZS particle analyzer (Malvern, UK). For size measurements, disposable low volume cuvettes (ZEN0117, Malvern, UK) were used, and for zeta potential measurements, disposable capillary cells (DTS1060) were used. Validation testing of the size and zeta potential measurements was done using polystyrene latex particles (PSL) with different uniform particle sizes and DTS1230 Malvern transfer standard which has a zeta potential of -68mV ± 6.8mV.

The yield of chitosan particles was determined by drying aliquots of the colloidal suspensions over night in a 65°C oven, followed by equilibrating at room temperature

and weighing. Percentage yield represents the percentage of obtained weight relative to the original weight in the formulation solution.

Films were fabricated by direct casting into 6-well flat-bottom tissue culture plates (Corning® Costar®, MA). Chitosan solution (5 ml of 1% (w/v) chitosan dissolved in 1% (v/v) acetic acid solution) was added into each well. Chitosan solutions were left to dry in a 65°C oven overnight. Chitosan films were then neutralized by adding 10 ml of 0.1 N NaOH solution for 15 min. After film biotinylation as mentioned below, chitosan films were cross-linked with 10% w/w glutaraldehyde in 50 mM phosphate buffer (pH 7.2) for 2 h to enhance their stability, followed by adding 1 M glycine buffer to quench the reaction. Films were extensively washed with distilled water and then air-dried.

4.2.3 Stability of chitosan nanoparticles and glutaraldehyde cross-linking

Chitosan nanoparticles prepared by coacervation with 0.1% sodium sulfate in 1% (v/v) Tween 80 were tested for their stability in different salts. Nanoparticle formulations, suspended in distilled water at 1.6 mg/ml, were diluted (1:3) in 1, 10 and 100 mM of sodium, potassium and magnesium sulfate to study the effect of buffers containing sulfate, the same counter-ion used to form chitosan nanoparticles. In addition particles were suspended in 1, 10 and 100 mM of sodium, potassium and magnesium chloride in order to see the effect of the same cationic species but with monovalent anion (chloride). Also formulations were diluted in Hanks' balanced salts (HBSS) in order to study the effect of glutaraldehyde cross-linking on particles suspended in a balanced salt solution used for cell culture media. HBSS contains calcium chloride•$2H_2O$ (0.185 mg/ml), anhydrous magnesium sulfate (0.09767 mg/ml), potassium chloride (0.4 mg/ml), anhydrous potassium phosphate monobasic (0.06 mg/ml), anhydrous

sodium phosphate dibasic (0.04788 mg/ml), D-glucose (1.0 mg/ml), sodium bicarbonate (0.35 mg/ml) and sodium chloride (8.0 mg/ml), pH adjusted to 7.4.

Glutaraldehyde (50 % w/w, Fisher Scientific, PA) was used as the cross-linking agent for chitosan nanoparticles (1.6 mg/ml) in order to improve their stability. Five different glutaraldehyde concentrations were added to cross-link the nanoparticulate formulations (20%, 30%, 40%, 50%, 60% and 100% w/w of glutaraldehyde to chitosan) for 2 h under magnetic stirring. At the end of reaction times, the reactions were quenched by adding 100 mM glycine buffer for 15 min. Chitosan particles were then centrifuged at 12,500 rpm for 7 min and washed twice with distilled water. The obtained pellets, composed of chitosan particles, were resuspended in distilled water and exposed to ultrasonication for 2 min using a microtip probe sonicator, set at level 2 (10 Watts), to redisperse the particles.

The degree of cross-linking was measured by fluorescamine assay. Fluorescamine reacts with the free amine group of chitosan to form a ring compound that exhibits fluorescence at an excitation wavelength of 390 nm and emission wavelength of 470 nm. After glutaraldehyde cross-linking, Schiff's bases form due to the reaction of amine groups of chitosan with glutaraldehyde. Consequently, the number of free amino groups on chitosan declines resulting in decreased fluorescence, which shows the success of the cross-linking process. Samples of cross-linked chitosan particles (100 µl) were added into 100 µL fluorescamine solution (3 mg/ml solution in dimethylsulfoxide (DMSO)) in a 96 well flat bottom microplate (Corning® Costar®, MA) and were mixed for 30 seconds on a plate vortex followed by taking the fluorescence readings.

The effect of glutaraldehyde cross-linking on the stability of chitosan nanoparticles was studied by measuring the difference in turbidity at 600 nm between formulations suspended in water and in HBSS. In addition, glutaraldehyde cross-linked and uncross-linked formulations were stored at room temperature for 1 week, followed

by measuring the change in size and zeta potential values. Also these formulations were exposed to ultrasonication to study particle stability after exposure to high shear.

4.2.4 Imaging of chitosan nanoparticles and films

Nanoparticle surface morphology was assessed by scanning electron microscopy (SEM, Hitachi S-4000). Nanoparticle suspensions were left to air-dry on silica wafers mounted on SEM specimen stubs. The specimen stubs were then sputter coated with approximately 5 nm of 60% gold 40% palladium ions by beam evaporation before examination in the SEM operated at 2 kV accelerating voltage.

An Asylum atomic force microscope (AFM) was used to study the topological features of chitosan films. Chitosan films were cast on clean and dry silica wafers by adding 1 ml of 1% (w/v) chitosan dissolved in 1% (v/v) acetic acid solution into each well of 48 well flat bottom cell culture plates (Corning® Costar®, MA) and leaving the film to dry in 65°C oven overnight. Films were then neutralized by adding 1 ml of 0.1 N NaOH solution for 15 min, followed by extensive washing with distilled water and then air-drying. Silica wafers, coated with chitosan films, were dislodged from the plates and glued on glass slides. Chitosan films were scanned using AFM cantilevers (MikroMasch, CA) which have spring constant of 46 N/m, and resonant frequency of 325 Hz. The scans were done using tapping mode AFM.

4.2.5 Biotinylation of chitosans and trypsins

Biotinylation of chitosan nanoparticles and films was performed using EZ-Link® NHS-biotin (N-hydroxysuccinimidobiotin, molecular weight: 341.38 Da, spacer arm length: 13.5 Å), NHS-LC-biotin (succinimidyl-6-(biotinamido)hexanoate, molecular weight: 454.54 Da, spacer arm length: 22.4 Å) and NHS-LC-LC-biotin (succinimidyl-6-(biotinamido)-6-hexanamido hexanoate, molecular weight: 567.70 Da, spacer arm length: 30.5 Å), all obtained from Thermo Scientific®, IL. Chitosan

biotinylation occurred by the formation of amide linkages between biotin and the free primary amines of the D-glucosamine units of chitosan.

Biotinylation reagents (100 mM) were dissolved in N,N-dimethylformamide (DMF). Biotinylation agents were added directly into stirred chitosan nanoparticles or films in amounts needed to yield 10 molar theoretical percentage of surface-conjugated biotin. Chitosan particles were suspended in 100 mM Na borate, pH 7.4, at a concentration of 1.6 mg/ml, whereas chitosan films casted in 6 well plates were immersed in 5 ml of the same buffer with shaking. The reactions were carried out overnight, after which chitosan nanoparticles were washed twice by centrifugation (12,500 rpm for 7 min) and resuspended in distilled water, and microplate wells were washed with distilled water and left to dry in a hood until further analysis.

Trypsin was biotinylated in HBSS (pH 7.4) using EZ-Link® NHS-biotin. NHS-biotin, dissolved in DMF that equals thirty molar excess of biotin to trypsin, was added to trypsin solution and incubated on ice for 2 h with shaking (30 rpm). The unreacted biotinylating agent was removed by dialysis against 50 mM sodium phosphate, pH 6.0, containing 0.02% NaN_3 and 20 mM $CaCl_2$.[225] Trypsin was freeze-dried using 10% (w/v) lactose as a cryoprotectant using a Labconco FreeZone 4.5 Liter freeze dry system.[226-228]

4.2.6 Quantification of the biotinylation degree and avidin content

The biotinylation degree was quantitatively assessed using HABA/avidin assay. Spectroscopy studies were completed on a SpectraMax Plus[384] plate reader (Molecular Devices, CA) operated by SoftMax PRO 1.3.4. LS software. HABA/avidin reagent (Sigma®, MO) was reconstituted in water to yield 0.3 mM HABA (4′-hydroxyazobenzene-2-carboxylic acid), 0.45 mg/ml avidin, 0.3 M NaCl, 0.01 M HEPES (N-2-hydroxyethylpiperazine-N'-2-ethanesulfonic acid, pKa = 7.5),

0.01 M $MgCl_2$ and 0.02% sodium azide. Standard calibration curves were plotted using D-biotin (Sigma®, MO) dissolved in distilled water at concentrations of 5, 10, 25, 35, 40 and 80 nmol/ml. Flat bottom 96 well plates (Corning® Costar®, MA) were used for HABA/avidin analysis by adding the assay solution (180 µl) to each of the wells used for biotin analysis followed by measuring the baseline absorbance at 500 nm. One hundred twenty microliters of biotin solutions, biotinylated nanoparticles (25 µg/ml) or films redissolved in 2% acetic acid (100 µg/ml) solution were added into the HABA/avidin assay solution and mixed well. Absorbance at 500 nm was measured again after 10 min incubation. The differences between the absorbance before and after the addition of biotinylated species were used to find the biotinylation degree against biotin calibration curves.

The percentage of avidin attachment on chitosan nanoparticles was measured using HABA dye. Avidin standard solutions were prepared in acetate buffer pH 5.5 and were diluted to concentrations between 20 – 80 µg/ml in flat-bottomed 96 well microplates. HABA dye, dissolved in the same buffer, was added to each standard or sample well for a final concentration of 0.34 mM and was mixed well and left covered for 15 min. The initial reading was taken at 500 nm, followed by adding biotin (0.04 mM) to saturate the avidin binding site and release HABA dye. Readings were again taken at 500 nm and subtracted from the initial readings.

4.2.7 Immobilization of trypsins using biotinylated chitosans

Biotinylated chitosans and biotinylated enzymes were linked via avidin molecules. In summary, biotinylated chitosan nanoparticles (10 mg) were suspended in HBSS and biotinylated chitosan films were immersed in 10 ml of HBSS. This was followed by the addition of excess avidin dissolved in water (0.5 mg/ml) into each nanoparticle formulation or well with shaking for 10 min. Unbound biotins were washed

off nanoparticles and films, followed by adding biotinylated trypsin solution for 30 min on ice with shaking. Finally, chitosan nanoparticles were washed with distilled water by centrifugation (12,500 rpm, 7 min) and films were rinsed gently but thoroughly with distilled water several times. Enzyme-chitosan films and nanoparticle suspensions were stored in 50 mM Bis-Tris buffer (pH 5.5) containing 0.02% sodium azide and 20 mM $CaCl_2$ at 4°C.

4.2.8 Immobilization of trypsins using avidin-conjugated chitosans

Coupling of chitosan to avidin was done by reductive amination. First, avidin, a glycoprotein, was oxidized to produce reactive aldehyde groups. Avidin (10 mg) was dissolved in 20 ml of phosphate buffered saline (PBS) and sodium meta-periodate was added in a concentration of 10 mM, which is sufficient for general carbohydrate oxidization with minimum risk of oxidizing amino acids. The oxidation reaction was incubated for 30 min over ice protected from light. Glycerin was added to quench the reaction and the oxidizing agent was removed using PD-10 desalting column (GE Healthcare Bio-Sciences, NJ), pre-equilibrated with PBS. The eluted oxidized avidin was added to chitosan films. Fresh solution of 50 mM sodium cyanoborohydride ($NaCNBH_3$) in 1 M NaOH was added to the avidin/chitosan conjugation mixture as a reductant solution and left over night in the refrigerator. Non-reacted aldehyde sites were blocked by adding 50 mM ethanolamine, pH 9.6, onto the conjugation solution for 30 min at room temperature. Finally, chitosan films were washed from excess reactants using 50 mM phosphate buffer (pH 7.2). Biotinylated trypsin was added onto chitosan films and the enzyme-chitosan films were stored in 50 mM Bis-Tris buffer (pH 5.5) containing 0.02% sodium azide and 20 mM $CaCl_2$ at 4°C.

4.2.9 Immobilization of trypsins on chitosan using glutaraldehyde activation

For comparison, trypsin was covalently immobilized on chitosan films using glutaraldehyde activation.[229,230] Chitosan films were activated by reacting with glutaraldehyde (5% weight ratio of glutaraldehyde to chitosan) for 1 h in 50 mM sodium phosphate buffer (pH 6.0). The films were washed with water followed by phosphate buffer. Trypsin, dissolved in 100 mM borate buffer (pH 7.4) containing 20 mM $CaCl_2$, was added to chitosan films and incubated for 2 h at 4°C. This was followed by adding sodium borohydride (10 mg/ml) for reduction of the resulting Schiff's bases for 30 min. Films were then incubated with glycine buffer (100 mM, pH 8.0) in order to quench excess aldehyde groups. Washing of chitosan films was performed thoroughly and the enzyme-chitosan conjugates were stored in 50 mM Bis-Tris buffer (pH 5.5) containing 0.02% sodium azide and 20 mM $CaCl_2$ at 4°C.

4.2.10 Enzyme activity assay

Activities of immobilized and native enzyme preparations were determined using casein as a substrate. Trypsin hydrolyzes casein into products that are soluble in trichloroacetic acid, and the enzyme activity was assessed by measuring the optical density at 280 nm.[231] Casein (1 g) was dissolved in 100 ml of 0.1 M phosphate buffer (pH 7.6) in a boiling water bath for 15 min until all casein is dissolved. This solution was stored at temperature less than 4^oC for a maximum of one week. Enzymatic activity was studied in either Eppendorf centrifuge tubes (for chitosan nanoparticles) or directly onto chitosan films cast in 6 well plates. Trypsin (MP Biomedicals LLC, Ohio) was dissolved in 0.001 N HCl at concentration of 0.1 mg/ml and then diluted using 0.1 M phosphate buffer to the required concentrations. Equal volumes of enzyme solution and pre-warmed substrate solutions were mixed and left in a water bath shaker (30 rpm) for exactly 20 min. The reaction was stopped by the addition of 5% trichloroacetic acid and allowed

to stand for 30 min at room temperature. Blank solutions were prepared by first mixing the substrate and trichloroacetic acid solutions then adding the enzyme solutions diluted in phosphate buffer and allowing the mixtures to stand for 30 min at room temperature. In order to measure the trichloroacetic acid-soluble hydrolysis products, the reaction mixtures were centrifuged at room temperature (3000 *g*) for 30 min and the supernatant optical density was read at 280 nm using a UV-Visible spectrophotometer (NanoDrop 2000 Spectrophotometer (Thermo Scientific®, IL)) after subtraction of the blank readings. The enzyme activity was expressed in trypsin enzyme units (TU^{Cas}). One TU^{Cas} is defined as the amount of trypsin under the defined conditions (incubation at 37°C for 20 min, pH 7.6) which liberates sufficient trichloroacetic acid-soluble hydrolysis products so that the optical density at 280 nm increases by 1.00 unit in 1 min. Specific activity is defined as the trypsin enzyme units per unit weight of the protein (TU^{Cas} /mg enzyme).[232] The concentration of immobilized enzyme was calculated by subtracting enzyme concentration found in the immobilization solution after the incubation time from the original added concentration. Trypsin concentration was determined using Pierce® micro BCA protein assay kit (Thermo Scientific®, IL) against a trypsin standard calibration curve.

4.2.11 Thermal and pH stability and reusability of trypsins

The thermal stability of native trypsin and trypsin immobilized on chitosan nanoparticles and films was determined by incubation of the stock enzyme solutions or enzyme preparations for different periods ranging from 20 to 300 min at 55°C in 0.001 N HCl containing 20 mM $CaCl_2$ to minimize autoproteolysis. After incubation at each given time, the enzyme preparations were left for 15 min at room temperature to cool down before dilution or immersing in 50 mM phosphate buffer, pH 8.2, followed by performing the standard enzyme activity assay. The average activity of trypsin at 37°C obtained for a fresh enzyme not exposed to heat was assigned a value of 100%.

The effect of pH on the enzymatic activity was studied using a range of buffers prepared at a concentration of 50 mM and ionic strength of 154 mM, adjusted by adding NaCl. Studied buffers were phosphate (pH 6.2, 7.2 and 8.2) and carbonate (pH 9.25 and 10.25).

Reusability and recovery of trypsin were studied using LC-biotin modified chitosan films and nanoparticles. Chitosan films were washed with 50 mM phosphate buffer, pH 8.2, after each run and reused with fresh casein. Nanoparticles were centrifuged and washed with 50 mM phosphate buffer, pH 8.2, twice before the addition of fresh substrate. For comparison reasons, native trypsin solutions used for casein proteolysis were subjected to ammonium sulfate precipitation at 40% saturation.[233] The precipitate was collected by centrifugation (5,000 rpm for 5 min at 4°C), followed by re-dissolving in fresh substrate solution. Reusability was tested by performing the enzymatic analysis for three consecutive times.

4.2.12 Statistical analysis

Group data are reported as mean+/-SD. Differences between groups were analyzed by one way analysis of variance with a Tukey's post-test analysis. Levels of significance were accepted at the $\rho < 0.05$ level. Statistical analyses were performed using Prism 5.02 software (GraphPad Software, Inc., CA).

4.3 Results and Discussions

Enzyme immobilization has expanded the range of potential applications for enzyme technology. This is possible because of the substantial improvement in overcoming some of the practical drawbacks in utilizing enzymes. These include the high cost of isolation and purification of enzyme and sensitivity to process condition. Some of the properties of the ideal support systems for enzymes are the availability of reactive functional groups for chemical modification, rigidity, mechanical strength, ease of fabrication and minimal interaction with enzyme activity.[222] Chitosan, a product of the partial deacetylation of chitin (β (1 → 4) *N*-acetyl-2-amino-deoxy-D-glucose polymer), has been studied as enzyme support in both films and particulate forms.[229,234-236] In our study, chitosan was utilized for immobilizing a model enzyme, trypsin. Trypsin, an important proteolytic enzyme, has wide research applications, such as in different tissue culture protocols, and industrial applications, such as dairy products.[237]

4.3.1 Fabrication of chitosan nanoparticles

Table 4-1 shows the different grades of chitosan used in particle preparation and enzyme immobilization. Namely, high molecular weight and high degree of deacetylation (HM-HD), medium molecular weight and high degree of deacetylation (MM-HD), low molecular weight and high degree of deacetylation (LM-HD), medium molecular weight and medium degree of deacetylation (MM-MD) and medium molecular weight and low degree of deacetylation (MM-LD) chitosans.

Chitosan particles were prepared using coacervation/precipitation method. This method enables the fabrication of chitosan nano- to micro-sized particles by precipitation of chitosan from solution using strong electrolytes, followed by coacervation by fusion of aqueous shells of several particles.[238] In this study, different parameters affecting chitosan nano/microparticle fabrication were studied. These include the mixing technique, surfactant use, chitosan degree of deacetylation and molecular weight,

chitosan concentration, pH of the preparation, equilibration time, type and concentration of the polyanion, the effect of lyophilization and the use of cryoprotectant and formulation stability in various salts upon cross-linking of the nanoparticles.

Shear forces are substantial for the formation of chitosan complexes with polyanions.[239] In this study, stirring (~800 rpm), homogenization (6,500 rpm) and ultrasonication (10 W) were used in the process of formation of chitosan particles (Table 4-2). It was found that high shear mixing created intense and concentrated energy inputs that can disperse particles significantly more quickly than traditional mixing methods, as shown by the difference in the sizes of particles fabricated by mixing and homogenization (1498.3 ± 218.7 nm and 639.9 ± 31.2 nm, respectively). Zeta potential values were positive and approximately 29 mV for the three studied methods of dispersing. Ultrasonication resulted in more homogeneous and uniformly distributed particles, and displayed the least change in size after particle washing (only 3% change). However, the yield when using sonication (47.1%) was much lower than when using the homogenization method (62.5%). Hence, homogenization was selected to be the method of choice for formation of the particles, for it was satisfactory in producing uniform particle sizes, relatively high zeta potential values and good yield.

Surfactants were added to chitosan solutions in the process of fabrication of nanoparticles in order to prevent particle clumping during polymer coacervation and to serve as anti-aggregating excipients for storing the particles in solution. Tween 80, polyoxyethylene-sorbitan monooleate, is a nonionic surfactant that has been well studied for chitosan particle formulation using water in oil emulsification method,[240] and therefore was chosen for preparing chitosan nanoparticles designed for enzyme immobilization. The effectiveness of adding Tween 80 in formulating chitosan nanoparticles using the coacervation/precipitation method was shown by the smaller and more homogeneous particle sizes (Table 4-3). The Z-average particle size obtained after centrifugation and washing of the particles formed with sulfate as the counter-ion was

636.0 ± 28.0 nm using 2% (v/v) Tween 80, compared to 1009.1 ± 99.4 nm without surfactant. Similarly, the polydispersity index went down from 0.447 without using Tween 80 to 0.282 for formulation that included 2% of the surfactant. Surprisingly, the yield of chitosan particles obtained after centrifugation and washing has increased from 37.4% to 63.8% when using 2% Tween 80. This indicates that, similar to the emulsification method, adding surfactant while gelation of the polymer aided in the formation of the particles, possibly by replacing the water layer surrounding the hydrophobic parts of the coacervation system. In addition, resuspendability of chitosan particles has improved and their size change after centrifugation was minimized. This was shown by the small increase in particle sizes when using Tween 80 compared to formulations without surfactant (5% increase compared to 49%). Also, it was noticed that formulations containing 1% and 2% Tween 80 were not significantly different in particle sizes, PDI and yield. Therefore, adding 1% Tween 80 during fabrication of chitosan nanoparticles was chosen for the satisfactory yields and uniformity in particle sizes gained upon using this percentage. Observing the difference in zeta potential values before and after washing of the particles, it can be also concluded that the two washing cycles were sufficient to remove most of the residual surfactant on the surface of chitosan nanoparticles. This leads to minimization of unwanted interaction between Tween 80 and added biomolecules that can interfere with the intended use of the nanoparticles. However, if the experimental design for using the nanoparticulate formulations requires the avoidance of surfactant use, it was found that longer ultrasonication time after washing and collecting chitosan particles was adequate to separate aggregates and resulted in reasonably uniform particles that were readily resuspendable (after 8 min sonication, the Z-average particle size was 788.3 ± 69 nm and PDI was 0.293).

Table 4-4 shows the effect of chitosan molecular weight and degree of deacetylation on particle Z-average sizes and zeta potential values. Molecular weight variation showed less substantial effect compared to the degree of deacetylation. High

molecular chitosans yielded particle sizes of approximately 715 nm with the highest zeta potential values (30.0 ± 1.2 mV). Using medium molecular weight chitosan (91% deacetylated) resulted in smaller particles and lower PDI values, indicating narrower particle distribution. When chitosan molecular weight was decreased further (LM-HD) but the degree of deacetylation was kept constant, the particle sizes started to increase again and the zeta potential decreased slightly further (668.9 ± 52.4 nm and 27.8 ± 0.7 mV). Medium and low degree of deacetylated chitosans showed significantly higher particle sizes and PDI values and lower zeta potential values (as low as 23 mV), as a result of less ionizable groups on chitosan chains and less efficient complexation process. Generally, all chitosan grades formed particles in a size range suitable for the intended purpose of enzyme immobilization.

MM-HD chitosan was selected for performing the rest of the formulation study and a range of chitosan concentrations was investigated (Table 4-5). It was observed that at 0.4% (w/v) chitosan concentration, the particles were significantly larger compared to lower concentrations and the PDI was high and at the critical edge of acceptable laser diffraction methodology criteria. This wide particle size distribution resulted from the effect of high viscosity of medium molecular weight chitosan solutions at this concentration, which can hinder efficient interaction between the polycationic polymer and the added polyanion. Decreasing chitosan concentration caused concentration dependent decline in particle sizes. This shows that this method can be used effectively for preparing chitosan nanoparticles with sizes that can be simply controlled by changing some of the formulation parameters. A chitosan concentration of 0.2% (w/v) was selected because it resulted in a high yield and uniform particles.

Since coacervation/precipitation method depends on the ionization status of the polymer used, the pH of the formulation solution is of a significant importance. All the above mentioned formulations were prepared in chitosan solvent (1% (v/v) acetic acid, pH ~ 2.8). When the pH of the chitosan solution was adjusted to 5.5 with NaOH, no

particles were formed (Table 4-6). This is possibly due to lack of sufficient positive charges on chitosan chains because of incomplete protonation (pKa of chitosan is approximately 6-6.5). Conversely, at a lower pH values, chitosan can be assumed to be completely ionized and protonated, favoring particle formation. It was found that the optimum solvent for chitosan for the fabrication of nanoparticles is 1% (v/v) acetic acid, resulting in particles having the highest zeta potential values (29.5 mV) and smallest sizes (639.9 nm). Higher pH buffers can be used for preparing larger particles when needed (pH 3.5 and 4.5, resulted in 1040.1 and 2769.5 nm particles, respectively), but aggregation problems would be expected upon storage.

Polyanions are essential components to form microparticles from chitosan using the coacervation/precipitation method. Therefore, types and concentrations of counter-ions were studied. Table 4-7 shows the particle sizes and zeta potential values for chitosan particles formulated using sulfate as the counter-ion. As expected, it was found that the concentration of sodium sulfate and the ratio of chitosan to sodium sulfate are extremely important. At a low concentration of sodium sulfate (0.01% w/v), the complexation process between chitosan and sulfate was insufficient to produce definite particles, resulting in massive suspended aggregates. Increasing the concentrations up to 0.2% w/v resulted in the formation of chitosan particles in size range of ~ 500-900 nm as shown in Table 4-7. The most robust formulation which has the narrowest particle size range was obtained using sodium sulfate at a concentration of 0.1%. (w/v) (648.2 ± 63.0 nm particles with 0.221 PDI), which was considered suitable for the purpose of this study. Increasing the concentration of sodium sulfate to more than 0.1% (w/v) resulted in increasing the particle size and size distribution and decreasing the zeta potential values as a result of having excess of the sulfate ions, saturating chitosan cationic binding sites.

In order to study the effect of polyanion's type, tripolyphosphate (TPP) and dextran sulfate (DS) were used as counter-ions in the formation of chitosan nanoparticles

and compared to using sodium sulfate. Tables 4-8 and 4-9 show that using low concentrations of TPP and DS (0.05% w/v), prevented the formation of particles, similar to sodium sulfate, and using higher concentrations (1% w/v and higher) caused the formation of non-uniform large aggregates. PDI values for chitosan-TPP and chitosan-DS nanoparticles were in the unacceptable range (more than 0.5) for all formulations except at 0.2% w/v and 0.1% w/v polyanion concentration, respectively. Surprisingly, the zeta potential values for chitosan-TPP and chitosan-DS formulations were significantly higher than chitosan-sodium sulfate, which can be useful for specific applications. The variation of results compared to using sodium sulfate is indicative of the complexity of the interaction between polycationic polymers, such as chitosan, and other polyanions, in forming microparticulate systems.

Sodium sulfate was selected as the polyanion of choice since it resulted in stable and robust nanoparticulate formulations. These formulations were tested for the effect of freeze-drying and using different cryoprotectants on the formulation stability. Table 4-10 shows the increase in particle sizes and the decrease in zeta potential values after freeze-drying for chitosan-SS formulations protected by adding 7.5% w/v of sucrose, mannitol or sorbitol, compared to the original formulation. It was observed that freeze-drying chitosan nanoparticles without cryoprotectant resulted in more than 100% increase in size and significant decrease in zeta potential, indicating particle aggregation and possible major alteration in the complex polymeric interactions. Adding mannitol and sorbitol resulted in 37.2% and 16.8% increase in particle sizes, and 14.8% and 6.1% decrease in zeta potential values, respectively, which are considered significant deviations. On the other hand, addition of sucrose as a cryoprotectant resulted in free-flowing powder and stable particles with minimal change in sizes and zeta potential values upon freezing and storage, hence, sucrose was the cryoprotectant of choice. The ability to lyophilize these nanoparticulate formulations is important for the practicality of the developed method.

From the above studies, it can be concluded that the coacervation/precipitation technique is a good and simple method to fabricate chitosan particles which avoids the use of organic solvents and lengthy procedures. Controlling formulation parameters, such as using surfactants and the concentrations and types of chitosans and polyanions, resulted in uniformly dispersed particles with desirable zeta potential values and particle sizes.

4.3.2 Stability of chitosan nanoparticles

Chitosan nanoparticles were formulated with the optimized parameters as discussed above (0.2 % w/v MM-HD chitosan, 1% v/v Tween 80 and 0.1% w/v sodium sulfate). When chitosan nanoparticle formulations were suspended in HBSS, immediate disintegration of particles occurred. HBSS was used for suspending the particles because of its similarity to the physiological salt content and because it was used for biotinylating and preserving trypsin. The presence of salts in the suspending solution exerted a detrimental destabilizing effect on chitosan particles causing them to breakdown and solubilize instantaneously. In contrast, upon suspending chitosan nanoparticles in 5% dextrose, the particles did not show any significant change in size and no solubilization effect was visible. This was attributed to the fact that dextrose is non-ionic in nature and therefore it did not interfere with the complexation of chitosan with polyanions.

In order to study this phenomena more, the effect of the presence of salts bearing the same counter-ion (sulfate) used for the formulation of nanoparticles on the stability of chitosan nanoparticles was studied (Table 4-11). At lower concentrations of sodium, magnesium and potassium sulfate salts (1 and 10 mM), the sulfate ion concentrations were not high enough to destabilize the particles. However, at higher salt concentrations (100 mM), the excess sulfate caused inter-particulate cross-linking, resulting in particle growth and visible sedimentation, leading to high PDI readings and making particle size

analysis inaccurate. This effect of salts on stability of chitosan nanoparticles was similar for all the salts carrying the same anion but different cations (sodium, potassium or magnesium salts).

In the presence of salts containing different counter ions (sodium, potassium and magnesium chloride), immediate solubilization of the particles occurred. This can be attributed to the equilibrium exchange between the chloride from the salts and sulfate anions inside the nanoparticles. It was noticed that this equilibrium occurred rapidly because of the high affinity of cationic species of all the three salts (sodium, potassium and magnesium) for the sulfate ion present inside the particles and due to the relatively smaller size of chloride ions compared to sulfate, allowing access to the inside of the particles. The instant destabilization of chitosan nanoparticles due to sulfate exchange with the monovalent anion, chloride, caused chitosan's chain relaxation and solubilization (pH of the solution was 4.5-5.5), resulting in a clear solution. At high salt concentrations (100 mM), a reaction similar to above takes place instantaneously resulting in solubilization, but was followed by the formation of large aggregates and by increasing the turbidity of the nanoparticle suspensions due to precipitation of chitosan.

Hence, it can be concluded that upon exposure to high concentration of the common sulfate counter-ions in the suspending solutions and to any concentration of other counter-ions, chitosan nanoparticles fabricated by coacervation/precipitation method disintegrate. This fact was not addressed properly by many studies using this method in preparation of chitosan nanoparticles, although these formulations were intended to be used *in vivo*, where a high concentration of different salts is expected.

4.3.3 Glutaraldehyde cross-linking of chitosan nanoparticles

In order to improve the stability of chitosan nanoparticles, glutaraldehyde was used to form interparticle cross-linkages. Fluorescamine assay was performed to assess

the efficiency of the cross-linking reactions. Figure 4-1 shows the calibration curve of glucosamine using fluorescamine assay which shows the effectiveness of this assay in detecting any changes in the free amine contents of chitosan, since glucosamine is the basic building unit in chitosan chains which is the unit susceptible to reaction with glutaraldehyde.

As shown in Figure 4-2, reacting chitosan with glutaraldehyde caused reduction in the available amine groups on the surface of chitosan nanoparticles. The relation between glutaraldehyde concentration and % relative fluorescence was inversely proportional and linear ($r^2 = 0.9980$). This confirmed the efficiency of cross-linking using glutaraldehyde.

Glutaraldehyde cross-linking of chitosan-sodium sulfate nanoparticles showed significant effect on particle size and zeta potential values, especially at higher percentage of cross-linking (Figure 4-3). Whereas at 50% (glutaraldehyde/chitosan w/w %), there was only 15% increase in Z-average particle size and 11% decrease in zeta potential value, at 100% glutaraldehyde ratio, there was 46% increase in particle sizes and 43% decrease in zeta potential. This again proves the efficiency of the cross-linking reaction and shows the effect it exerts on particles.

The effect of glutaraldehyde cross-linking on the stability of chitosan nanoparticles was assessed by measuring the difference in nanoparticulate suspension turbidity at 600 nm after the addition of HBSS in comparison to the addition of water, as shown in Figure 4-4. Whilst the turbidity of uncross-linked particles has decreased 75% after addition of HBSS, the turbidity change of 60% glutaraldehyde cross-linked particles was only 8.65%. The relation between the decrease in turbidity and the degree of cross-linking was also linear ($r^2 = 0.9982$). This indicates that cross-linking improves chitosan nanoparticle formulation's stability and resistance to disintegration. In addition, glutaraldehyde cross-linking enhanced particles resuspendability, requiring minimum force to disperse the nanoparticles, and hindered aggregations upon storage, as shown by Table 4-13. It was found that uncross-linked chitosan nanoparticles increased 76% in

particle size and decreased 18% in zeta potential upon storage for 1 week at room temperature. On the other hand, chitosan nanoparticles cross-linked with glutaraldehyde (60%) changed only insignificantly in size and zeta potential values (3.5% and 5%, respectively).

Furthermore, the effect of post-washing sonication time, using sonic dismembrator at 10 W setting, on the size reduction of chitosan-sodium sulfate nanoparticles was investigated (Figure 4-5). All preparations contained 0.2 % (w/v) chitosan 1% (v/v) Tween 80 in 1% (v/v) acetic acid solution and 0.1% (w/v) sodium sulfate. In method I, formulation solution was homogenized for 20 min and then cross-linked with 60% (w/w) glutaraldehyde, followed by centrifugation and washing. Method II the order of particle washing and cross-linking was reversed. In method III, stirring for 3 h was done followed by cross-linking with 60% (w/w) glutaraldehyde. Finally, in method 1V, homogenization was used but without cross-linking. It was noticed that the order of cross-linking and washing of the particles had only a slight effect on particle sizes and zeta potential values. Initial particle sizes were in the order of method III > IV > II > I. Sonication caused dissociation of chitosan particles because of the high shear, which exerted strong effect on uncross-linking particles, shown by the progressive decrease in particle sizes with sonication, but insignificant effect on glutaraldehyde cross-linked particles. Also it was found that glutaraldehyde cross-linking of particles formed by stirring was inefficient in stabilizing the particles against mechanical disintegration, due to the ineffective particle formation using stirring. The initial sizes of particles formed by stirring were more than 3 fold higher than particles formed by homogenization. The formation of larger particles using stirring can be attributed to the lack of sufficient shear needed for the coacervation process. It was noticed that at each consecutive time point, particle sizes of uncross-linked formulations and formulations made by stirring decreased significantly following sonication, however the overall size always remained higher than particles cross-linked with glutaraldehyde.

The above results indicate that chitosan particles can be stabilized by glutaraldehyde cross-linking via Schiff's base. In this method, intra-particle covalent linking occurred, providing more resistance to changes in surrounding environment compared to physical complexation, hence, the particles are less susceptible to breakdown in the presence of salts such as HBSS, or upon exposure to mechanical forces. Additionally, as the concentration of glutaraldehyde cross-linking increased, the stability of the particles increased, with 60% glutaraldehyde resulting in almost complete protection from disintegration.

4.3.4 Morphology of nanoparticles and film imaging

The morphology of chitosan nanoparticles were studied using SEM. Figure 4-6 shows the images of uncross-linked chitosan-sodium sulfate nanoparticles prepared by homogenization of 0.2% chitosan, 1% Tween 80 and 0.1% sodium sulfate as described previously. Figure 4-7 shows the effect of cross-linking on these particles. It was noticed that cross-linked particles have more surface protrusions and appeared more porous. Particle sizes correlated with Z-average sizes obtained by laser diffraction measurements.

Figure 4-8 shows the AFM imaging of chitosan film. It was noticed that neutralized chitosan film consisted of interconnected nanoparticulate spheres forming fiber-like networks.

4.3.5 Biotinylation of chitosans and trypsins

The N-hydroxysulfosuccinimide (NHS) ester groups on NHS-biotin, NHS-LC-biotin or NHS-LC-LC-biotin reagents react with ε-amine of lysine residues of trypsin and with chitosan amino groups at the C-2 position, producing stable biotinylated products. In addition, α-amine groups present on the N-termini of peptides react with NHS esters, but are significantly less accessible for conjugation. NHS esters react with primary amines in the deprotonated form and, therefore, typically the reaction requires

neutral to basic pH values to proceed. Primary amines react with NHS esters by nucleophilic attack and N-hydroxysuccinimide is released as a byproduct.

Biotinylation degrees of chitosan and trypsin were quantified using HABA/avidin assay. Surface biotinylation degree for chitosan nanoparticles was 23.45 ± 1.84 nmol biotin/mg chitosan and for films was 21.21 ± 1.63 nmol biotin/mg chitosan. Trypsin biotinylation degree was 142% (moles of biotin/moles of trypsin) at 65.35 ± 4.78 nmol biotin/mg trypsin. Avidin was immobilized on the surface of chitosan nanoparticles and films in amounts adjusted to have approximately the same final content of 12-14 μg avidin/preparation among all samples.

Particle sizes and zeta potential values of the biotinylated, avidin modified and trypsin immobilized nanoparticles were measured (Table 4-14). In comparison to cross-linked unmodified chitosan-sodium sulfate nanoparticles, slight increase in particle sizes were noticed in the following order; trypsin-modified chitosan > avidin-modified chitosan > biotin-modified chitosan nanoparticles. PDI for all formulations were within the acceptable limits (< 0.5). Zeta potential values progressively decreased with each modification step, but stayed above 20 mV.

4.3.6 Enzyme immobilization and activity

Trypsin immobilization on chitosan nanoparticles was performed using LC-biotin modified chitosan. NHS-LC-biotin was chosen because it was found previously that chitosan-LC-biotin nanoparticles yielded the best transfection when modified with RGD ligands. This was hypothesized to be due to providing the optimum distances from chitosan surfaces required for successful ligand attachment and activity.

In order to study the effect of immobilization on the use of trypsin, two factors were studied simultaneously; the percentage of immobilization, as measured by quantifying unattached enzymes in the enzyme immobilization solution after the incubation time, and the percentage enzyme activity, which is the percentage of specific

activity (TU^{Cas}/μg trypsin) of the immobilized enzyme relative to the soluble enzymes at 37°C.

The effects of degree of deacetylation and molecular weight of chitosan used for the preparation of chitosan nanoparticles on trypsin immobilization via avidin linker are shown in Figure 4-9. It was observed that using MM-HD chitosan resulted in the highest immobilization efficiency, followed by LM-HD chitosan and then the highest molecular weight. LM-HD chitosans had the highest specific trypsin activity, followed by MM-HD then HM-HD chitosans. The effect of chitosan's molecular weight on the enzymatic activity and enzyme immobilization can be explained by the condensation efficiency of different grades. As discussed above regarding the size measurements of chitosan nanoparticles, it was found that medium molecular weight chitosans resulted in the most compact and smallest size structures, followed by LM-HD and then HM-HD chitosans. The complexation of chitosan chain pattern of with polyanions and particle sizes affects the availability of ligand-binding sites and total surface area, which increase with decreasing particle sizes, and the type of interaction between chitosan and amino acids of enzymes. The effect of changing the degrees of deacetylation of chitosan showed more prominent effects compared to varying the molecular weight. Low degree of deacetylated chitosans resulted in the lowest trypsin activity and immobilization. The effect of degree of deacetylation on enzyme immobilization stemmed from the unfavorable effect of reducing the charges on the surface of particles on the stability of the enzyme supports, which increased the tendency for more aggregation.

Trypsin immobilization on chitosan films was achieved through three methods; adsorption on chitosan surfaces, conjugation with chitosan using glutaraldehyde or using avidin linkers, either conjugated directly to chitosan or attached onto biotinylated chitosan. Figure 4-10 shows that the highest immobilization efficiency was obtained for chitosan films that were biotinylated by the longest arm linker, LC-LC-biotin (99.35%), followed in order by the shorter arm biotins. However, the order of enzyme activity was

chitosan-LC-biotin > chitosan-LC-LC-biotin > chitosan-biotin (96.43%, 91.58% and 86.48%, respectively). The relative specific activities of trypsin immobilized through avidin linker on biotinylated chitosans were higher than using avidin conjugated chitosans due to the spatial hindrance caused by conjugating avidin directly onto chitosan surfaces without a spacer. This hindrance reduces the efficiency of avidin-biotin interaction in the presence of biotinylated macromolecules, such as trypsin. Covalently conjugating trypsin onto chitosan films showed high immobilization efficiency, but the enzyme activity was significantly lower than any of the avidin-biotin methods (69.46%), as a result of trypsin denaturation during conjugation procedures. Adsorbed trypsin showed both low immobilization and low relative specific activity. Physical interactions between enzymes and support in close proximity can affect the enzymatic performance and limit access of substrates. Also, adsorbed enzymes have the potential of being desorbed from support surfaces.

In comparison to enzyme immobilization onto films, immobilization of trypsin on chitosan nanoparticles using LC-biotin was as efficient as using LC-LC-biotin on chitosan films, as shown in Figure 4-10. In fact, chitosan nanoparticles showed specific activity that was slightly higher than the soluble enzyme control (102.84%), indicating high substrate accessibility.

Native and immobilized trypsins were incubated for different times at 55°C in order to study the effect of temperature on enzyme activity. Figure 4-11 shows that, compared to free native enzymes, immobilized enzymes by different methods showed significant thermal stability against heat denaturation, which is in accordance with other reports.[230,232] It was noticed that trypsins immobilized through avidin linker on LC-biotin modified chitosan nanoparticles and films showed the highest thermal stability with less than 20% loss in enzymatic activity after 5 h incubation at 55°C. Trypsins immobilized on chitosan films through conjugated avidin and conjugated enzyme resulted in preserving 63% and 73% of enzyme activity, respectively, at the end of 5 h experiment.

On the other hand, native enzymes showed 65% decrease in activity after 5 h, with abrupt decline starting at 60 min of incubation. All samples showed higher variations after 5 h incubation at 55°C due to the effect of temperature on denaturation of enzymes. It can be concluded from the thermal stability results that immobilization of enzymes improves thermal resistance to denaturation and conserves high enzymatic activity. Immobilization using LC-biotin through avidin linker showed the best retention of activity after long exposure to heat. Hence formulations utilizing LC-biotin were used to study pH stability of enzymes.

Figure 4-12 shows the effect of pH of the reaction solution (pH range from 6-10) on trypsin activity. Similar to native enzymes, it was found that the peak enzymatic activity was at pH 8.2 for immobilized enzymes using chitosan nanoparticles and films. At lower pH values, however, the activity of soluble enzymes decreased dramatically, losing 79% of its activity at pH 6.2 relative to activity at pH 8.2. On the other hand, immobilized enzymes on chitosan nanoparticles showed double the activity of soluble enzymes at pH 6.2. Immobilized enzymes on chitosan films also showed improved resistance to lower pH values but to a lesser degree compared to chitosan nanoparticles. At higher pH values, soluble trypsins showed a decline in activity but not as prominent as the decline in activity at lower pH values. Chitosan films showed superior effect on the stability and activity of trypsins at higher pH value compared to nanoparticles and soluble enzymes. At pH 10.2, enzymes immobilized on chitosan films showed 90.8% retention in activity, whereas chitosan nanoparticles resulted in 82.9% retention. Soluble trypsin showed the least resistance to high pH values, resulting only in 72.2% of the activity at pH 8.2. The superiority of chitosan films at higher pH values was due to the stability of films at these pH values. High pH values caused reduction in the zeta potential of chitosan nanoparticles, leading to more aggregation and negatively affecting enzymatic activity. It can be concluded that immobilization of trypsin on chitosan supports improves its activity and stability in a wide range of pH values.

Finally, the ability to recover and reuse immobilized trypsins was compared to the recovery of the soluble native enzymes by ammonium sulfate precipitation. Figure 4-13 shows the reusability results of chitosan films and nanoparticles modified with LC-biotin and linked to trypsin via avidin. Immobilized enzymes on chitosan supports were compared to native enzymes recovered through ammonium sulfate precipitation at 40% saturation. It was found that chitosan films resulted in the best retention of activity after the third use (87.6%), compared to 77.1% for chitosan nanoparticles and 5.9% for precipitated native enzyme. This superiority of chitosan films happened due to the high stability of the construct and the lower susceptibility to washing effects. Chitosan nanoparticles were susceptible to loss during centrifugation and washing, in addition to the possibility of disintegration with repeated washing steps. It can be concluded that both chitosan films and nanoparticles are suitable support systems for enzyme immobilization, providing superior reusability and recovery, which are key factors in large scale industrial processes to reduce the cost of production.

4.4 Conclusions

This study was a continuation of our previous work and others that shows that chitosan is a promising polymer that has a great potential for biomedical applications, including enzyme immobilization.[222,235,236] Formulation techniques for chitosan nanoparticles were optimized to fabricate chitosan nanoparticles suitable for enzyme immobilization and other applications. Chitosan nanoparticles were prepared by coacervation/precipitation method, followed by cross-linking with glutaraldehyde to improve stability of particles. Trypsin, a model enzyme, was immobilized on chitosan nanoparticles and films through relatively facile and rapid method that avoids the use of harsh conjugation environments. This method is based on the strong avidin-biotin interaction and the ability of chitosan to be biotinylated in a controlled fashion. It was found that immobilization of trypsin onto the surface of chitosan nanoparticles and films

resulted in significant improvement in enzymatic activity upon exposure to high temperature and pH extremes. In addition, immobilizing trypsin on chitosan supports allowed for reusing the enzyme with minimum loss of activity. These findings show that the biotin/avidin ligand modification method can be used to modify chitosan nanoparticles and films with enzymes, enabling the most efficient utilization of enzymes and the potential for large scale enzymatic usage at lower costs.

4.5 Figures and Tables

Table 4-1. Degrees of deacetylation as measured by first derivative UV spectrophotometry and viscosity average molecular weights of different grades of chitosan.

Chitosan grade	Measured degree of deacetylation	Viscosity average molecular weight (M_v)
HM-HD	91.28%	181686
MM-HD	90.92%	144760
MM-MD	84.02%	132578
LM-HD	92.10%	102017
MM-LD	74.36%	140708

Table 4-2. The effects of chitosan-nanoparticle fabrication techniques on the yields, particle sizes and zeta potential values before and after centrifugation and washing.

Technique	Yield (%)	Before washing			After washing		
		Particle size Z-average (nm) ± SD	PDI	Zeta potential average (mV) ± SD	Particle size Z-average (nm) ± SD	PDI	Zeta potential average (mV) ± SD
Stirring (2 h)	42.5	1162.1 ± 169.6	0.516	23.2 ± 0.8	1498.3 ± 218.7	0.640	28.8 ± 1.0
Homogenization (20 min)	62.5	598.9 ± 30.1	0.214	18.1 ± 0.9	639.9 ± 31.2	0.271	29.5 ± 1.1
Ultrasonication (20 min)	47.1	659.2 ± 24.4	0.186	21.1 ± 1.0	683.2 ± 19.2	0.224	29.3 ± 0.8

Note: Formulation parameters were: 0.2% (w/v) chitosan, 1% (v/v) Tween 80 and 0.1% (w/v) sodium sulfate.

Table 4-3. The effects of Tween 80 concentrations on the yields, particle sizes and zeta potential values before and after centrifugation and washing.

Tween 80 concentration (% w/v)	Yield (%)	Before washing			After washing		
		Particle size Z-average (nm) ± SD	PDI	Zeta potential average (mV) ± SD	Particle size Z-average (nm) ± SD	PDI	Zeta potential average (mV) ± SD
0	37.4	679.0 ± 22.7	0.421	31.3 ± 2.4	1009.1 ± 99.4	0.447	30.0 ± 1.1
0.2	45.3	650.0 ± 75.7	0.287	19.9 ± 0.7	762.7 ± 54.4	0.404	30.6 ± 1.2
1.0	62.5	598.9 ± 30.1	0.231	18.1 ± 0.9	639.9 ± 31.2	0.271	29.5 ± 1.1
2.0	63.8	608.3 ± 37.4	0.255	18.2 ± 0.6	636.0 ± 28.0	0.282	28.4 ± 0.7

Note: Formulation parameters were: 0.2% (w/v) chitosan and 0.1% (w/v) sodium sulfate using homogenization.

Table 4-4. The effects of chitosan grades on the particle size and zeta potential values of chitosan-SS nanoparticles.

Chitosan grade	Particle size Z-average (nm) ± SD	PDI	Zeta potential average (mV) ± SD
HM-HD	715.3 ± 23.1	0.258	30.0 ± 1.2
MM-HD	648.2 ± 63.0	0.221	28.7 ± 1.2
LM-HD	668.9 ± 52.4	0.357	27.8 ± 0.7
MM-MD	756.7 ± 38.5	0.414	25.3 ± 1.4
MM-LD	792.1 ± 47.7	0.438	23.9 ± 1.3

Note: Formulation parameters were: 0.2% (w/v) chitosan, 1% (v/v) Tween 80 and 0.1% (w/v) sodium sulfate using homogenization.

Table 4-5. The effects of chitosan concentrations on particle sizes and zeta potential values of chitosan particles.

Chitosan concentration (% w/v)	Particle size Z-average (nm) ± SD	PDI	Zeta potential average (mV) ± SD
0.01	329.6 ± 27.2	0.254	28.5 ± 1.0
0.1	418.2 ± 32.0	0.294	29.1 ± 0.8
0.2	639.9 ± 31.2	0.271	29.5 ± 1.1
0.4	758.7 ± 62.2	0.504	30.8 ± 1.6

Note: Formulation parameters were: 1% (v/v) Tween 80 and 0.1% (w/v) sodium sulfate using homogenization.

Table 4-6. The effects of the pH of the preparation solutions on particle sizes and zeta potential values of chitosan-SS nanoparticles.

pH	Particle size Z-average (nm) ± SD	PDI	Zeta potential average (mV) ± SD
2.8	639.9 ± 31.2	0.271	29.5 ± 1.1
3.5	1040.1 ± 73.7	0.319	25.7 ± 0.5
4.5	2769.5 ± 224.5	0.442	15.0 ± 1.8
5.5	Large aggregates were formed		

Note: Formulation parameters were: 0.2% (w/v) chitosan, 1% (v/v) Tween 80 and 0.1% (w/v) sodium sulfate using homogenization.

Table 4-7. The effects of sodium sulfate (SS) concentrations on particle sizes and zeta potential values.

SS concentration (% w/v)	Particle size Z-average (nm) ± SD	PDI	Zeta potential average (mV) ± SD
0.01	No Particles		
0.05	544.7 ± 107.5	0.398	29.6 ± 1.8
0.1	648.2 ± 63.0	0.221	28.6 ± 1.4
0.2	737.0 ± 159.9	0.454	27.2 ± 0.5
1.0	4231.8 ± 693.4	1.000	21.9 ± 1.2
2.0	26460.8 ± 2811.2	1.000	4.0 ± 2.4

Note: Formulation parameters were: 0.2% (w/v) chitosan and 1% (v/v) Tween 80 using homogenization.

Table 4-8. The effects of sodium tripolyphosphate (TPP) concentrations on particle sizes and zeta potential values.

TPP concentration (% w/v)	Particle size Z-average (nm) ± SD	PDI	Zeta potential average (mV) ± SD
0.05	No Particles		
0.1	568.1 ± 64.8	0.664	53.4 ± 2.1
0.2	257.9 ± 12.1	0.257	44.0 ± 3.2
0.5	353.6 ± 23.6	0.607	38.4 ± 1.1
0.8	462.8 ± 42.8	0.522	27.7 ± 3.1
1.0	5486.1 ± 1325.5	1.000	15.9 ± 3.5
2.0	25868.7 ± 3542.3	1.000	6.6 ± 3.0

Note: Formulation parameters were: 0.2% (w/v) chitosan and 1% (v/v) Tween 80 using homogenization.

Table 4-9. The effects of dextran sulfate (DS) concentrations on particle sizes and zeta potential values.

DS concentration (% w/v)	Particle size Z-average (nm) ± SD	PDI	Zeta potential average (mV) ± SD
0.05	No Particles		
0.1	935.3 ± 79.4	0.426	58.6 ± 0.7
0.2	1732.2 ± 299.5	0.609	56.2 ± 1.2
1.0	3245.2 ± 1151.7	0.984	54.7 ± 1.4

Note: Formulation parameters were: 0.2% (w/v) chitosan and 1% (v/v) Tween 80 using homogenization.

Table 4-10. The effects of freeze-drying in the presence of different cryoprotectants on particle sizes and zeta potential values of chitosan-SS nanoparticles.

Cryoprotectant (7.5 % w/v)	**Increase in particle size (%)**	**Decrease in zeta potential (%)**
No cryoprotectant	108.7%	24.4%
Sucrose	5.3%	1.6%
Mannitol	37.2%	14.8%
Sorbitol	16.8%	6.1%

Note: Formulation parameters were: 0.2% (w/v) chitosan, 1% (v/v) Tween 80 and 0.1% (w/v) sodium sulfate using homogenization.

Table 4-11. The effects of resuspending chitosan-SS nanoparticles in salt solutions containing sulfate ions.

Salt type	Concentration (mM)	Relative particle size (%)
Sodium sulfate	1	95.1%
	10	98.9%
	100	large aggregates
Magnesium sulfate	1	93.7%
	10	103.6%
	100	large aggregates
Potassium sulfate	1	105.9%
	10	103.3%
	100	large aggregates

Note: Formulation parameters were: 0.2% (w/v) chitosan, 1% (v/v) Tween 80 and 0.1% (w/v) sodium sulfate using homogenization.

Table 4-12. The effect of resuspending chitosan-SS nanoparticles in salt solutions containing chloride ions.

Salt type	Concentration (mM)	Effect
Sodium chloride	1	Particles disintegrated
	10	Particles disintegrated
	100	Particles instantaneously disintegrated but within seconds slight turbidity developed
Potassium chloride	1	Particles disintegrated
	10	Particles disintegrated
	100	Particles instantaneously disintegrated but within seconds slight turbidity developed
Magnesium chloride	1	Particles disintegrated
	10	Particles disintegrated
	100	Particles instantaneously disintegrated but within seconds slight turbidity developed

Note: Formulation parameters were: 0.2% (w/v) chitosan, 1% (v/v) Tween 80 and 0.1% (w/v) sodium sulfate using homogenization.

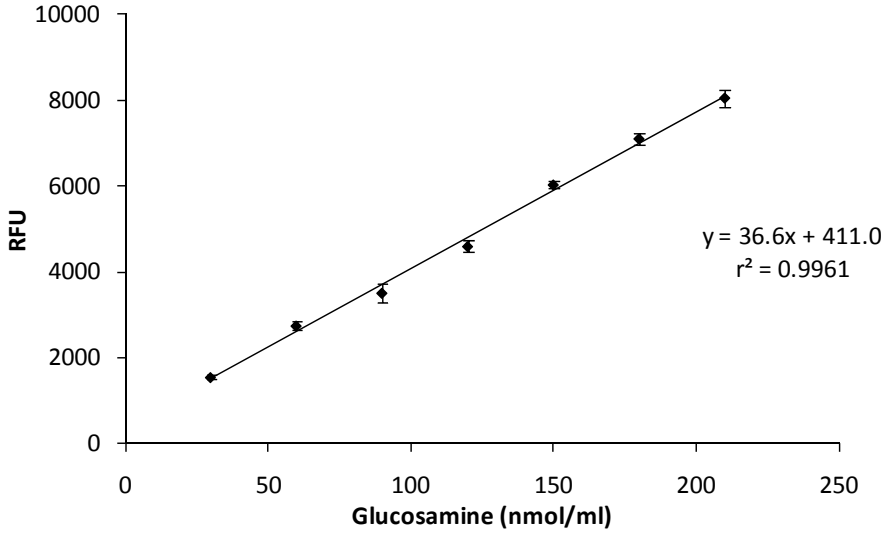

Figure 4-1. Standard calibration curve of glucosamine using fluorescamine assay.

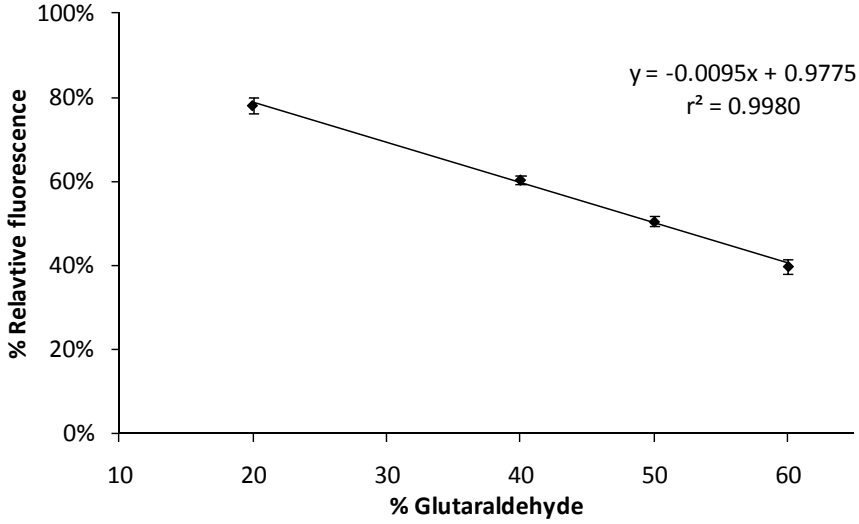

Figure 4-2. The effect of glutaraldehyde on decreasing the available free amine groups on the surface of chitosan-SS nanoparticles due to cross-linking, detected by fluorescamine assay.

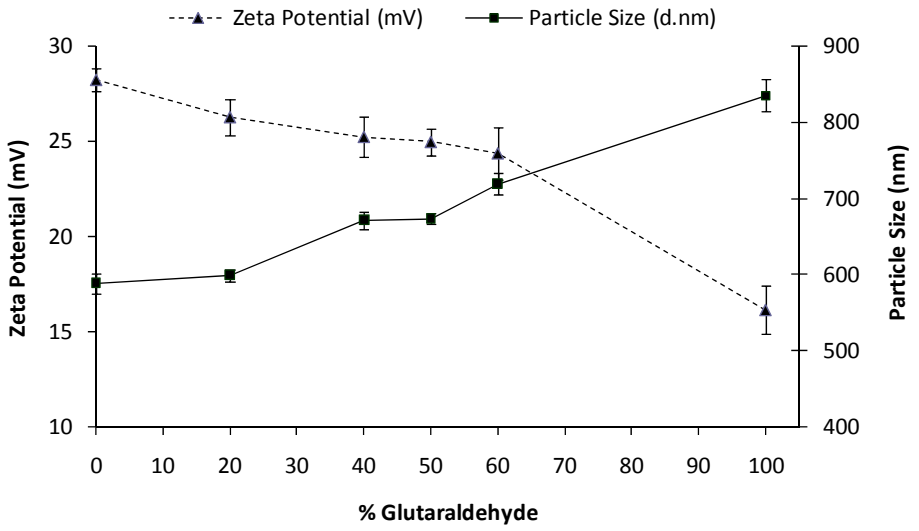

Figure 4-3. The effect of glutaraldehyde cross-linking on particle sizes and zeta potential values of chitosan-SS nanoparticles.

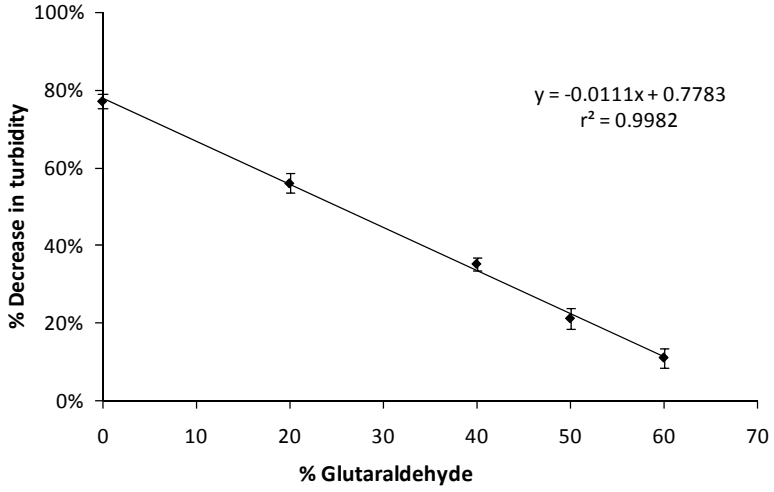

Figure 4-4. The effect of glutaraldehyde cross-linking on the stability of chitosan-SS nanoparticles as shown by turbidity measurement at 600 nm in Hanks' balanced salts (HBSS) relative to water.

Table 4-13. The effect of glutaraldehyde cross-linking on the stability of chitosan-SS nanoparticles stored for 1 week at room temperature.

GA (% w/v)	Initial			1 week		
	Particle size Z-average (nm) ± SD	PDI	Zeta potential average (mV) ± SD	Particle size Z-average (nm) ± SD	PDI	Zeta potential average (mV) ± SD
0	585.1 ± 13.3	0.184	28.2 ± 0.6	1030.8 ± 115.0	0.279	23.1 ± 2.1
20	599.2 ± 7.6	0.223	26.3 ± 0.9	637.9 ± 22.9	0.299	26.0 ± 1.1
40	681.8 ± 11.4	0.265	25.2 ± 1.1	705.4 ± 22.2	0.319	24.0 ± 1.1
60	715.8 ± 14.3	0.238	24.4 ± 1.4	740.6 ± 23.4	0.340	23.1 ± 0.9

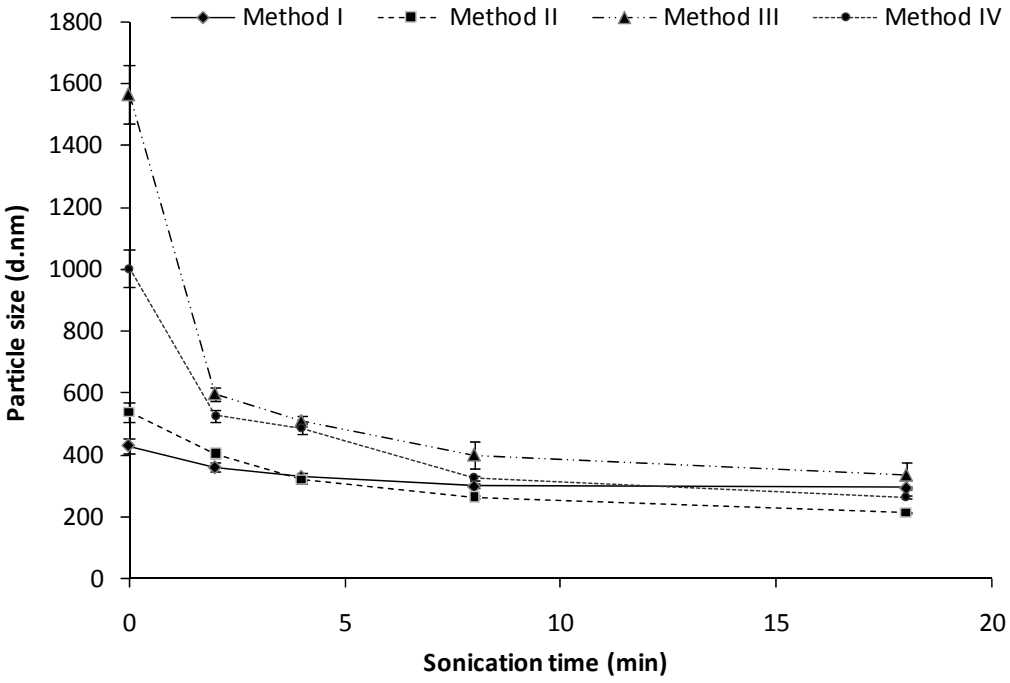

Figure 4-5. The effect of sonication time on particle sizes of chitosan-SS nanoparticles. All preparation methods contained 0.2 % (w/v) chitosan 1% (v/v) Tween 80 in 1% (v/v) acetic acid solution and 0.1% (w/v) sodium sulfate. In method I, formulation solutions were homogenized for 20 min and then cross-linked with 60% (w/w) GA, followed by centrifugation and washing. In method II, the order of particle washing and cross-linking was reversed. In method III, stirring for 3 h was done followed by cross-linking with 60% (w/w) GA. In method 1V, homogenization was done but without cross-linking. Sonication was done using Fisher Sonic Dismembrator Model 100 at 10 W.

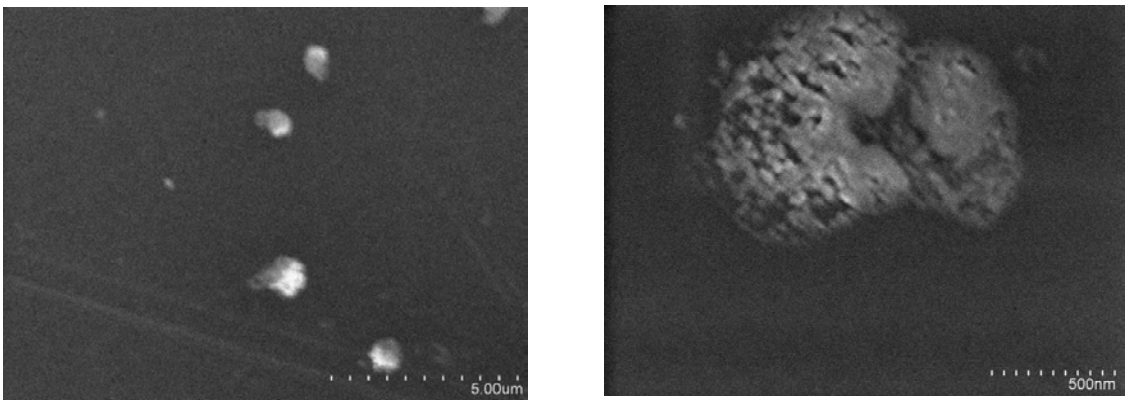

Figure 4-6. Micrographs of uncross-linked chitosan-SS nanoparticles. Images were taken using Hitachi S-4000 scanning electron microscope at A) low and B) high magnifications.

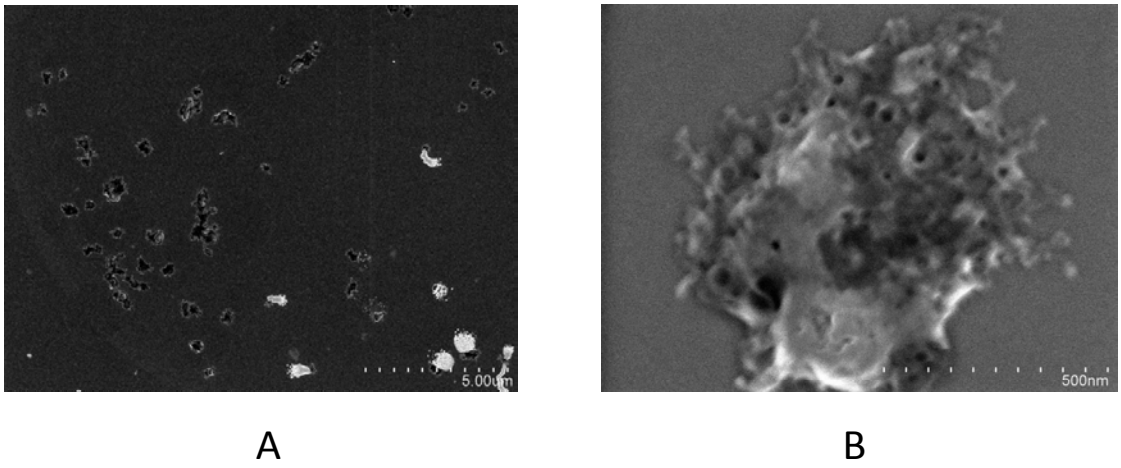

Figure 4-7. Micrographs of 40% glutaraldehyde cross-linked chitosan-SS nanoparticles. Images were taken using Hitachi S-4000 scanning electron microscope at A) low and B) high magnifications.

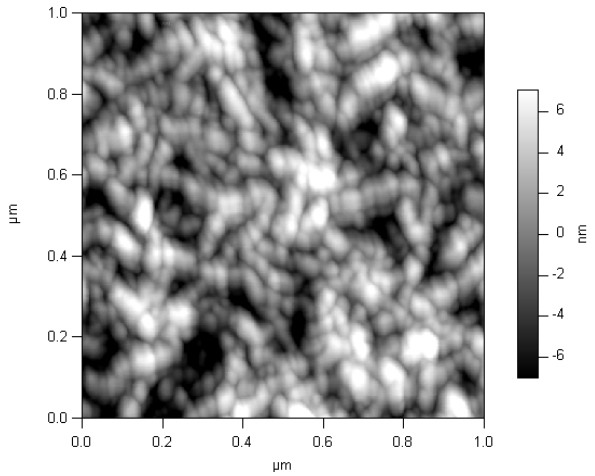

Figure 4-8. Image of a MM-HD chitosan film using Asylum atomic force microscope.

Table 4-14. Z-average particle sizes and zeta potential values of chitosan formulations.

Formulation	**Particle size Z-average (nm) ± SD**	**PDI**	**Zeta potential average (mV) ± SD**
Unmodified nanoparticles	720.8 ± 36.5	0.308	24.3 ± 1.4
Bt-modified nanoparticles	696.7 ± 68.5	0.298	23.7 ± 1.6
Av-Bt-modified nanoparticles	733.8 ± 85.4	0.377	23.7 ± 2.0
Tp-Av-Bt-modified nanoparticles	802.5 ± 109.8	0.412	21.2 ± 1.2

Note: Chitosan formulations were prepared using unmodified chitosan, biotin-modified chitosan (Bt), avidin-biotin-modified chitosan (Av-Bt) and trypsin-modified chitosan via avidin-biotin interaction (Tp-Av-Bt).

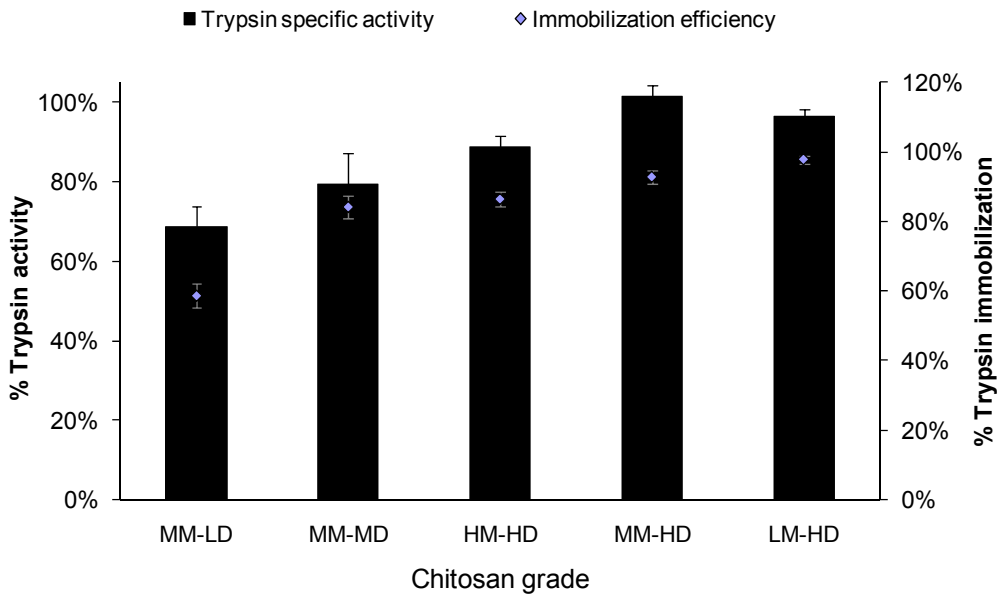

Figure 4-9. Trypsin activities and immobilization efficiencies via avidin-biotin linkers on chitosan nanoparticles fabricated using different chitosan grades. The following chitosan grades were used: high molecular weight and high degree of deacetylation (HM-HD), medium molecular weight and high degree of deacetylation (MM-HD), low molecular weight and high degree of deacetylation (LM-HD), medium molecular weight and medium degree of deacetylation (MM-MD) and medium molecular weight and low degree of deacetylation (MM-LD) chitosans.

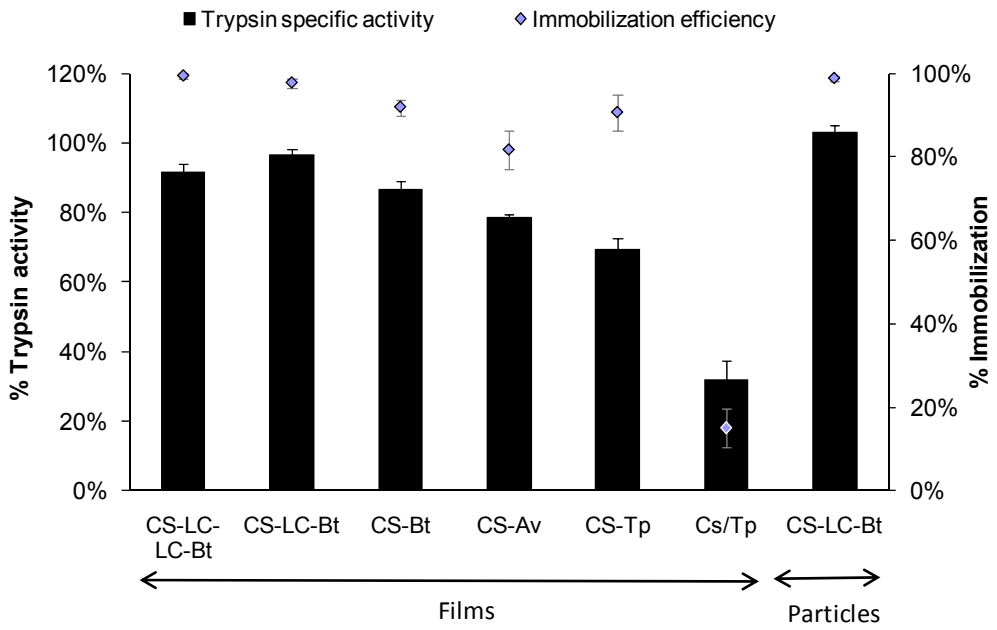

Figure 4-10. The percentages of trypsin activity and immobilization by different methods on chitosan films and nanoparticles. Trypsin immobilization was done using avidin linkages on chitosan-modified biotin (CS-Bt), chitosan-modified LC-biotin (CS-LC-Bt), chitosan-modified LC-LC-biotin (CS-LC-LC-Bt), chitosan-conjugated avidin (CS-Av), chitosan-conjugated trypsin (CS-Tp) and chitosan-adsorbed trypsin (CS/Tp).

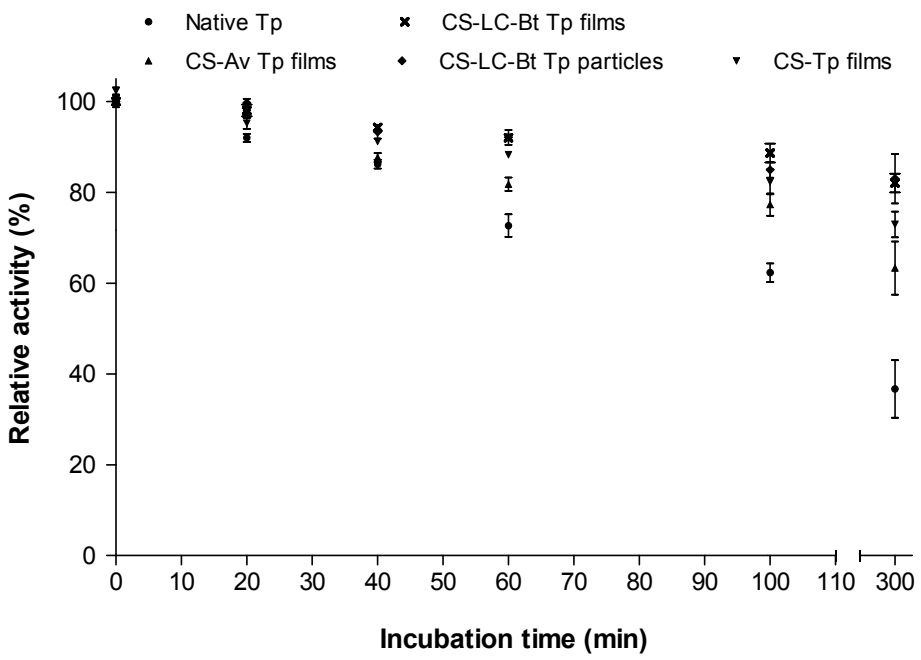

Figure 4-11. The effect of higher temperatures on the enzymatic activities of native trypsins and trypsins immobilized on chitosan nanoparticles. Trypsin was immobilized via avidin-biotin linker, avidin-LC-biotin linker, avidin-conjugated chitosan linker and glutaraldehyde activated chitosan conjugation. All enzymes were incubated for different times at 55°C.

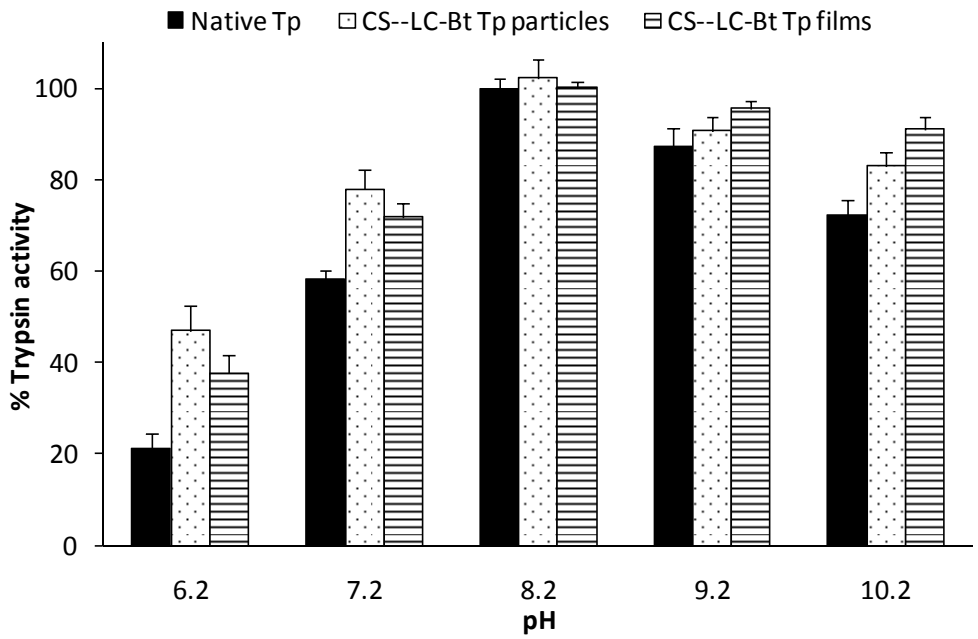

Figure 4-12. The effect of pH on enzymatic activities of native trypsins and trypsins immobilized on chitosan films via avidin-LC-biotin linker. The activity was plotted relative activity of the soluble enzyme at pH 8.2.

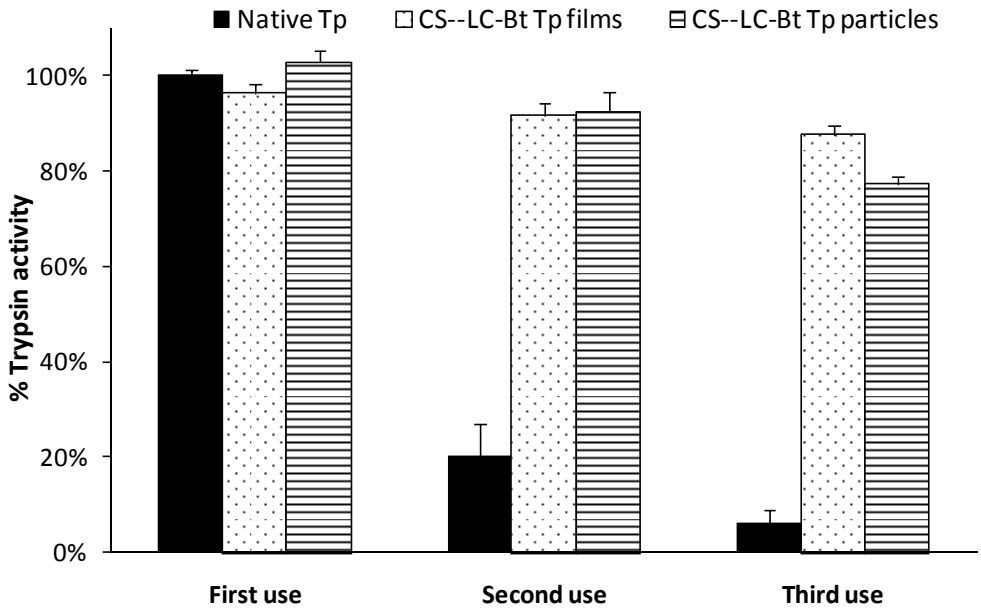

Figure 4-13. The reusability of trypsins immobilized on chitosan films and nanoparticles via avidin-LC-biotin linker compared to native enzymes recovered by precipitation.

CHAPTER 5
CHITOSAN MODIFICATION USING AVIDIN-BIOTIN INTERACTION. PART III: APPLICATIONS IN TISSUE ENGINEERING

5.1 Introduction

Tissue engineering is an emerging interdisciplinary field that applies the principles of biology and engineering for developing viable substitutes to restore, maintain, or improve the function of human tissues.[241] Tissue engineering, or regenerative medicine, is becoming a focus of biomaterial research due to the increasing demand for alternative therapies in the treatment of end-stage organ failure and replacement of lost organs or tissues.[242]

A promising approach to the regeneration of tissues has been the use of a support matrix or a scaffold for cell seeding or induction. Materials used in the formation of scaffolds must be compatible and bioresorbable, ensuring their transient degradation while allowing regeneration of tissues without any reminiscent foreign material. A successful scaffold also should be able to directly influence the behavior of the incorporated cells, control cellular infiltration and regulate the release of the bioactive materials.[243] One of the techniques utilized in achieving these goals is the incorporation of biomolecules within scaffolds, providing environments that direct progenitor cell differentiation, biological activity and subsequent organization into functional tissues.[244]

Recently, the attention of tissue engineering matrices was geared toward using natural polymers such as chitosan.[245] Chitosan has a set of unique characteristic which makes it an excellent candidate to be used as scaffold for tissue regeneration purposes. In addition to being biodegradable and non-immunogenic, chitosan supports the attachment and the subsequent proliferation and growth of different kind of cells, such as chondrocytes[75,76] and mesenchymal cells,[72] which is attributed to the cationic nature of

chitosan.[78] Also chitosan exhibits a number of favorable biological activities, which include stimulation of cellular growth[73] and maintenance of the chondrogenic phenotype.[74]

In order to improve on chitosan's ability to modulate the adhesion and growth of cells, several methods for engineering of chitosan surfaces with different ligands and biofactors, such as transforming growth factor-β1, have been investigated,[42] using covalent attachment, adsorption and physical entrapment. These methods can result in reduced biomolecule activity, which can be detrimental to the bioactivity of chitosan or its ability to support cellular growth. Generally, the proteins need to be firmly anchored onto surfaces without adversely affecting their activity. Covalent binding often involves harsh reaction conditions such as the use of solvents that can denature proteins and reduce biomolecule activity.[203] Adsorption, on the other hand, is usually reversible and can result in protein denaturation, especially when the proteins or biomolecules are bound directly to the substrate without a spacer. Finally, physical entrapment can mask active components of molecules within the bulk substrate and yields inefficient loading. This research focused on applying a new technique for modification of chitosan surfaces with various types of ligands utilizing avidin-biotin interaction for modifying chitosan films with cell attachment and cell repelling ligands.

5.2 Materials and Methods

5.2.1 Purification and preparation of chitosans

Chitosan was fully purified and prepared as discussed in the Materials and Method section in Chapter 2. Briefly, high molecular weight and high degree of deacetylation (HM-HD), medium molecular weight and high degree of deacetylation (MM-HD) and low molecular weight and high degree of deacetylation (LM-HD) chitosans were obtained from Sigma®, MO. These chitosans were fully purified by first dissolving chitosan in 1% acetic acid solution and then filtering the solutions to remove

the insoluble particles. This was followed by decolorization and deproteinization in the presence of dithiothreitol and demineralization using ethylenediaminetetraacetic acid (EDTA). Viscosity average molecular weights were calculated using Mark–Houwink–Sakurada equation from intrinsic viscosities. Medium molecular weight and medium degree of deacetylation (MM-MD) and medium molecular weight and low degree of deacetylation (MM-LD) chitosans were prepared by heterogeneous reacetylation using acetic anhydride. Degrees of deacetylation were calculated based on first derivative UV spectrophotometry (1DUV) measurements.

5.2.2 Preparation and cross-linking of chitosan films

Chitosan films were prepared by solvent-casting 1% (w/v) chitosan solution (dissolved in 1% v/v acetic acid) onto 96 well tissue culture plates (TCP, Costar® Corning®, NY). Two hundred microliters of this solution was pipetted into each well and degassed for 2 min by sonication and then left to heat-dry in the oven at 65°C for 12 h. The TCPs were left to cool under vacuum at room temperature before neutralizing with 0.1N NaOH for 30 min, followed by extensive washing with Nanopure water until the pH of the rinse solution became similar to the pH of the water. Chitosan surfaces were disinfected by immersing films in 70% ethanol for 12 h in the laminar flow hood, followed by 30 min UV exposure and finally washing with sterile phosphate buffered saline (PBS).

Glutaraldehyde (50 % w/w, Fisher Scientific, PA) was used as the cross-linking agent for chitosan films in order to improve their mechanical and physicochemical characteristics. Three different methods for cross-linking chitosan films were investigated; incorporating glutaraldehyde in the chitosan casting solutions (method I), preparing films from the already cross-linked chitosans (method II) or *in situ* cross-linking on the formed and neutralized film surfaces (method III). In method I, 0.1, 1 and 10% w/w ratios of glutaraldehyde to chitosan were mixed with 1% w/v chitosan

solutions and left to dry in the oven before washing and neutralizing with 0.1 N NaOH. In method II, chitosan solutions were cross-linked with 10% glutaraldehyde at different pH values using 100 mM buffer solution (acetate (pH 4.2 and 5.2), phosphate (pH 6.2, 7.2 and 8.2) or carbonate (pH 9.2, 10.2 and 11.2) for 2 h. This was followed by quenching the excess aldehyde groups by adding 100 mM glycine buffer. Cross-linked chitosans were then dialyzed and lyophilized. In method III, 10% w/w glutaraldehyde was added into the already formed chitosan films that have been neutralized. The cross-linking reaction was allowed to proceed for 2 h on a shaker before washing. Cross-linked chitosan films were then incubated with 100 mM phosphate, glycine, ethanolamine or Tris buffers to quench the free aldehydes, followed by film washing and drying.

The degree of cross-linking was quantified by measuring the free surface amine groups using the fluorescamine assay. Fluorescamine reacts with the free amine group of chitosan to form ring compounds that exhibit fluorescence at an excitation wavelength of 390 nm and emission wavelength of 470 nm. Fluorescamine solutions were added into wells containing chitosan films cast in 96 well flat bottom TCPs (100 µl of 3 mg/ml solution in dimethylsulfoxide (DMSO) per well). TCPs were mixed for 30 s on a plate vortex (VWR) before taking the fluorescence readings using SpectraMax Plus^{384} (Molecular Devices, CA).

Stability of chitosan films, cross-linked and uncross-linked, were studied by testing their solubility and degradation. Solubility of chitosan films was studied by soaking 25-35mg chitosan films, weighed exactly using a Mettler Toledo microbalance, in 50 ml 0.5% acetic acid solution for 15 min. Film degradation was studied by incubating 25-35 mg chitosan films in 50 ml phosphate buffered saline (PBS) with or without 5 mg/ml lysozymes (Sigma®, MO) in 37°C shaker for 1, 5, 15 and 30 days. At each time point, films were taken out, washed and lyophilized, then weighed. The difference between the weights of chitosan films initially and after each time point was plotted against film's treatment.

MFP-3D Asylum atomic force microscope (AFM, Asylum Research, CA) was used to study the topological features of chitosan films. Chitosan films were cast on clean and dry silica wafers by adding 1 ml of 1% (w/v) chitosan dissolved in 1% (v/v) acetic acid solution into 48 well flat bottom TCPs (Corning® Costar®, MA) and leaving the film to dry in 65°C oven overnight. Chitosan films were then neutralized by adding 1 ml of 0.1 N NaOH solution for 15 min, followed by extensive washing with distilled water and then air-drying. Silica wafers, coated with chitosan films, were dislodged from the plates and glued on a glass slide. Chitosan films were scanned using AFM cantilevers (MikroMasch, CA) which have spring constant of 46 N/m, and resonant frequency of 325 Hz using tapping mode AFM. Scans of 5 μm and 1 μm were performed at a scan rate of 1 Hz. The root mean square of roughness (R_{RMS}), average deviation, skewness and kurtosis values of the scans were calculated using the Asylum Research analysis program (MFP-3D Xop V.28) in Igor Pro 6.2 software (WaveMetrics, OR).

5.2.3 Biotinylation of chitosans

Biotinylation of chitosan films was performed using EZ-Link® NHS-LC-biotin (succinimidyl-6-(biotinamido)hexanoate, molecular weight: 454.54 Da, spacer arm length: 22.4 Å (Thermo Scientific®, IL)). Biotinylation occurred by the formation of amide linkages between biotin and the free primary amines of the D-glucosamine units of chitosan. Biotinylation reagent was dissolved in N,N-dimethylformamide (DMF) at 100 mM concentration. The calculated volumes from the biotinylation agent solutions to yield 2.5, 5, 10 and 20% molar percentage of surface-conjugated biotin to total chitosan glucosamine units were added directly onto chitosan films in 96 well plates immersed in 0.2 ml of different buffers (100 mM acetate (pH 4.2 and 5.2), phosphate (pH 6.2, 7.2 and 8.2) and carbonate (pH 9.2, 10.2 and 11.2) buffer solutions. The reaction plates were left on a shaker overnight. Chitosan wells were then washed with distilled water and left to air dry in the hood. Films were stored in a refrigerator until further analysis.

The biotinylation of chitosan films was visually tested using rhodamine-labeled avidin. Two hundred microliters of rhodamine-avidin solution in PBS (2 mg/ml, Sigma®, MO) was added to each of the chitosan film wells prepared in a 48 well TCP. The plate was left covered in the shaker overnight at room temperature. After the incubation period, the plate was washed extensively and viewed under a fluorescence microscope (Olympus CKX41 microscope equipped with epifluorescence optics, Leeds Precision Instruments, Minneapolis, MN), using green wavelength excitation in the range 480-550 nm and a barrier filter at 590 nm. Control and biotinylated films were exposed to fluorescence for the same time period and under the same intensity.

The biotinylation degree was quantitatively assessed using HABA/avidin assay. Spectroscopy studies were completed on a SpectraMax Plus^{384} plate reader (Molecular Devices, CA). HABA/avidin reagent (Sigma®, MO) was reconstituted in water to yield a concentration of 0.3 mM HABA. One hundred eighty microliters of fresh HABA/avidin solution was added to each well that contained biotinylated and unbiotinylated films (control), followed by measuring the absorbance at 500 nm after 10 min incubation. The difference in absorbance at 500 nm between samples and control films were measured against biotin standard calibration curve in order to find the concentration of attached biotin.

5.2.4 Cell adhesion

Human Embryonic Palatal Mesenchymal cells (HEPM) and Human Embryonic Kidney cells (HEK293) were purchased from American Type Culture Collection (ATCC®, MD). The cells were maintained in 75 cm^2 tissue culture flasks (Corning® Costar®, MA) and supported with Modified Eagle's Minimum Essential Media (EMEM) (MEM modified to contain Earle’s balanced salt solution, non-essential amino acids, 2 mM L-glutamine, 1 mM sodium pyruvate, and 1500 mg/l sodium bicarbonate) supplemented with 10% fetal bovine calf serum (FBS) (Gibco™ Invitrogen™ corporation,

NY), antibiotic-antimycotic (ABAM) that consists of 0.5% penicillin and 0.5% streptomycin (Sigma®, MO) and 1% L-glutamine in a humidified incubator at 37°C at 5% CO_2. Subcultivation was done in a ratio of about 1:6 every 5 days when 90% confluence was reached.

For the cell adhesion study on chitosan films, stock cell suspensions containing between 5–12×10^5 cells/ml were prepared. The number of cells was counted using a hemocytometer (Fisher Scientific, PA) after staining the cells with trypan blue (Biowhittaker, MD). Aliquots of cell suspension were pipetted into each well containing pre-warmed media and the plates were incubated at 37°C in a humidified 5% CO_2 incubator for the specified period. Cell passage numbers used in the attachment experiments were between 5 and 18.

In order to estimate the viability and the number of cells attached to chitosan films, MTT assay was performed. MTT salts were reconstituted in phenol red-free and serum-free medium to yield yellow solutions (1 mg/ml) which were filtered to remove insoluble particles. TCPs containing the casted chitosan films, with the incubated cells, were washed gently with PBS and 100 µl of pre-warmed and fresh MTT solution was added. The plates were wrapped and returned to the incubator for 2 h. After the end of the incubation time, formazan crystals were dissolved in acidified isopropanol containing Triton X-100 (polyoxyethylene octyl phenyl ether), a nonionic surfactant that facilitated lysis of the cells. Trituration by gently pipetting assay solution in and out was needed to make sure that all the crystals were dissolved. The absorbance of the resulting purple solutions were spectrophotometrically measured using a microplate reader (SpectraMax Plus^{384}, Molecular Devices, CA) at a wavelength of 570 nm. The background absorbance of the multi-well plates was measured at 690 nm, and this value was subtracted from absorbance at 570 nm.

Cell proliferation of HEK293 cells after 48 h incubation was studied using MTT assay by inoculating 2, 3, 4 and 5×10^4 cells per well onto chitosan films casted in

96 well TCPs. Proliferation on glutaraldehyde cross-linked chitosan surfaces were studied by inoculating 5×10^4 cells per well and studying the cell viability after 48 h incubation.

Cell adhesion studies were performed on biotinylated and cross-linked chitosan films. Some of the films were ligand modified using avidin-biotin interaction (as discussed below). Chitosan films were inoculated with 5×10^4 cells per well and incubated for 2 h at 37°C in a humidified 5% CO_2 incubator. After that, the films were washed gently with pre-warmed PBS and MTT assay was performed.

5.2.5 Ligand attachment on chitosan surfaces

Avidin from egg white (Sigma®, MO), dissolved in phosphate buffer saline, was added to the 2.5%, 5% and 10% biotinylated chitosan film wells in excess (10 μg/cm^2) and incubated overnight, followed by washing the TCP with sterile PBS. Then biotinylated ligands were added to the avidin-modified films. Biotin-polyethylene glycol (biotin-PEG), molecular weight of circa 5 kDa prepared as discussed in Chapter 3, and biotin-G11GRGDS (biotin-RGD), obtained from Sigma-Genosys®, were added to the biotinylated chitosan wells (0.5, 1.0 and 2.0 μmol/cm^2 in 2.5%, 5% and 10% biotinylated chitosan film wells, respectively) and incubated overnight. Figure 5-9 summarizes the process of biotinylation and ligand attachment.

5.2.6 Statistical analysis

Group data are reported as mean+/-SD. Differences between groups were analyzed by one way analysis of variance with a Tukey's post-test analysis. Levels of significance were accepted at the $\rho < 0.05$ level. Statistical analyses were performed using Prism 5.02 software (GraphPad Software, Inc., CA).

5.3 Results and Discussions

5.3.1 Fabrication and cross-linking of chitosan films

Different grades of chitosan have been prepared and characterized as shown in Table 5-1. Chitosan films were prepared by solvent-casting in tissue culture plates. A key step in chitosan film formation was neutralizing the remaining acetic acid entrapped within the chitosan chains. As shown in Figure 5-1, morphology of chitosan films changed dramatically after neutralizing with a strong base (NaOH). Before neutralizing, the films exhibited smeared appearance and were susceptible to swelling upon exposure to water or buffer. After adding the base, the morphology of chitosan films changed into interconnected nodular structures, in the nanometer size range, which became resistant to environmental changes. In addition to the structural changes, adding NaOH caused a significant decline in the root mean square roughness (R_{RMS}) (as shown in Table 5-2). The R_{RMS} decreased from 13.7 to 3.8 after neutralization, indicating a flattening in the surface.

Chitosan cross-linking is an important factor for the preparation of chitosan scaffolds and films, modifying their swelling rate, drug release, mechanical properties such as tensile strength and adjusting chitosan's biodegradability.[186,246] Cross-linking of chitosan films using glutaraldehyde was performed by three methods. At 0.1% w/w glutaraldehyde concentration and exposing chitosan to the cross-linking agent during film casting (method I), the general structural appearance of chitosan film was not significantly different than uncross-linked films (Figure 5-2A), but the film roughness increased from 5.0 for uncross-linked films to 6.8 (Table 5-3). At 1% w/w glutaraldehyde cross-linking, film appearance started to change substantially and the film roughness increased significantly to 10.5. Using higher glutaraldehyde concentrations (10% or more) in method I was found to have detrimental effects on chitosan films. Figure 5-2C shows a chitosan film cross-linked with 10% glutaraldehyde by method I, revealing the

breaks in the continuity of film coverage and the structural changes from nano-sized nodules to chunky aggregates that occurred. R_{RMS} of 10% cross-linked film was 88.6 as shown in Table 5-3.

Using method II, chitosans were initially cross-linked with glutaraldehyde in solutions of different pH values. Purified and lyophilized cross-linked polymers were re-dissolved in acetic acid solutions and used for casting the films. Chitosan polymers that were cross-linked at pH values of 6 to 8, failed to form films. Cross-linking at pH values of 9.2, 10.2 and 11.2 formed continuous films, but with less distinctive nodular features compared to the uncross-linked films (Figure 5-3). The film roughness increased with increasing the pH of biotinylation as shown in Table 5-4.

At pH values of 7.2 and higher, method III was found to yield the mildest changes in chitosan films, as shown in Figure 5-4. In comparison, cross-linking chitosan films at pH value of 6.2 caused significant cross-linking, as shown by the merged and swollen nodular structures. Also surface roughness has increased more than threefold (17.6), compared to uncross-linked chitosan films (Table 5-5). Flattening of chitosan films occurred at higher pH values, as indicated by the decrease in roughness with increasing pH values when comparing the R_{RMS} of the masked images, which represent manually selected 1 μm areas of continuous and gap-free film coverage. Cross-linking at pH values less than 6 resulted in extremely strong cross-linking reactions and successful film formation. However, these films were hard and brittle, as a result of high degree of cross-linking, rendering them difficult to handle for AFM imaging. In conclusion, by controlling the pH of the cross-linking solutions, method III was found to be the most suitable for preparing cross-linked chitosan films used for supporting cellular adhesion.

The effect of glutaraldehyde on chitosan films was detected by fluorescamine assay. This assay measures the free C2 amino groups on the surface of chitosan films by the formation of ring structure upon reacting with the free amine. This structure has a maximum excitation and emission at 390 and 470 nm, respectively. Figure 5-5 shows the

% relative fluorescence of chitosan films cross-linked by glutaraldehyde using method III, relative to untreated films. It was found that the highest degree of cross-linking occurred at pH 6.2, with approximately 40% decrease in fluorescence intensity, followed by cross-linking at higher pH values in order. These results confirm the observation of chitosan film images using AFM, in which the most structural deviation was observed at pH 6.2. Glutaraldehyde cross-linking was studied further by measuring the effect of glutaraldehyde concentration on the reduction of relative fluorescence using fluorescamine assay (Figure 5-6). As expected, it was found that surface free amines decreased with increasing the added glutaraldehyde as the result of cross-linking. At 50% w/w glutaraldehyde concentration, 53.8% of the amine groups were cross-linked with high variation between samples.

One of the advantages of cross-linking chitosan films is improving their resistance to dissolution. Dissolution of chitosan films causes these films to lose their surface functionalities and cause uncontrollable degradation. Figure 5-7 shows the effect of dissolving cross-linked and uncross-linked films in 0.5% acetic acid solution. Solubility of chitosan films decreased significantly with increasing the degree of cross-linking. At 10% w/w glutaraldehyde, the weight loss of chitosan films was 25.6% ± 7.1%, whereas uncross-linked films showed 73.0% ± 9.7% weight loss after 15 min incubation. In addition, the degradation of chitosan films in phosphate buffered saline (PBS) with and without lysozymes was hindered upon cross-linking, as shown in Figure 5-8. After 30-day incubation in PBS containing 5 mg/ml lysozymes, chitosan films which were cross-linked with 10% w/w glutaraldehyde at pH 7.2 showed only 34.5% weight loss. In comparison, uncross-linked films showed 73.7% weight loss after 30 days. This indicates the importance of film cross-linking in controlling the biodegradability of chitosan films and tailoring them to the intended use.

5.3.2 Biotinylation of chitosan and avidin addition

Avidin-biotin interaction is the strongest known non-covalent, biological interaction between a protein and a ligand (K_d for avidin-biotin complex $=10^{-15}M^{-1}$). Bond formation is very rapid and, once formed, is unaffected by wide extremes of pH, temperature, organic solvents and other denaturing agents. The avidin-biotin complex is also resistant to enzymatic proteolysis.[154] This strong biological interaction was utilized in this research to modify chitosan with targeting ligands of choice for tissue engineering purposes in the simple and facile method shown in Figure 5-9.

Biotinylation of chitosan was performed using N-hydroxysulfosuccinimide (NHS) chemistry. NHS esters of NHS-LC react with primary amines in the deprotonated form to produce stable biotinylated products and, therefore, the reaction typically requires neutral to basic solutions to proceed. Primary amines reacted with NHS esters by nucleophilic attack and N-hydroxysuccinimide groups were released as byproducts. However, hydrolysis of the NHS-ester competed with the biotinylation reaction in aqueous solution. Hydrolysis in aqueous solutions occurs in a higher rate with increasing the pH values.

Avidin-rhodamine tests clearly showed that the biotin-addition reaction was successful. Figure 5-10A and 10B shows the biotinylated and the unbiotinylated films, respectively, after addition of avidin-rhodamine. The biotinylated films showed significantly higher fluorescence in the scanned region, which indicated the efficiency of avidin attachment and the presence of biotin on the treated chitosan.

HABA/avidin assay was used to quantitatively determine the degree of biotinylation of chitosan surfaces. Figure 5-11 shows the biotinylation efficiency (theoretical calculated biotinylation percentage vs. actual biotinylation percentage) of NHS-LC-biotin measured by HABA/avidin assay as a function of concentration of biotinylation agent. Chitosan-conjugated biotin content was measured as nmol biotin/mg chitosan and the biotinylation percentage was calculated relative to the number of moles of glucosamine units of chitosan. It was observed that chitosan film biotinylation curve

relative to the theoretical biotinylation percentage followed the same pattern as biotinylation in solution (shown previously in Chapter 3). The maximum achieved biotinylation per unit surface area was approximately 500 nmol/cm^2 at theoretical biotinylation of 10% molar ratio, which corresponds to 1.34% actual biotinylation. After that, a plateau in biotinylation curve was attained, indicating saturation in available biotin sites on chitosan surfaces.

The effect of the pH of biotinylation buffer on the biotinylation efficiency was studied at pH values ranging from 4.2 to 11.2 (Figure 5-12). It was found that the maximum biotinylation was obtained at pH ranges of 6.2 to 8.2, with no significant differences between the biotinylation between pH 6.2, 7.2 and 8.2. At higher pH values, the degradation of the biotinylation reagents was the rate limiting step in the biotinylation reaction, decreasing the biotinylation efficiency, whereas at low pH values, the deprotonation of amine groups limited of the biotin addition reaction. From this, it was concluded that biotinylation of chitosan surfaces can be done in a facile and rapid method using NHS chemistry and that the degree of biotinylation can be controlled by controlling the pH of biotinylation and the concentration of the biotinylating agent, among other factors.

5.3.3 Cell adhesion on chitosan films

Two cell lines, HEPM and HEK293, were tested for their adhesion on chitosan films. Interestingly, cell adhesion on chitosan films showed batch-to-batch variations, whereas some batches of chitosan films resulted in cell aggregation once the suspended cells are added onto chitosan films with no notable cell attachment and finally cell death, whereas other batches yielded good cell attachment on the films. However, this problem was solved by exhaustively purifying chitosan, removing heavy metals, proteins and other impurities. This lead to comparable cellular attachment results for chitosan grades characterized with the same degree of deacetylation and molecular weight.

HEPM cells were observed to spread well on the chitosan surfaces, similar to tissue culture plates (TCP), especially treated to enhance cellular attachment, and demonstrated the typical phenotypic morphology of fibroblasts. HEPM cells adopted stellate morphology with a few filopedia-like protrusions, extending from the cell periphery (Figure 5-13). Similarly, HEK 293 showed typical spreading on chitosan films as shown in Figure 5-14.

Cell adhesion and viability were tested by the MTT assay. MTT or 3-[4,5- dimethylthiazol-2-yl]-2,5-diphenyltetrazolium bromide is a monotetrazolium salt that is widely used to detect the biological redox systems and viability of cells in order to measure cell proliferation and cytotoxicity.[187,188] The MTT measures the activity of living cells mainly via mitochondrial dehydrogenases, which is supported by NADH-linked mitochondrial substrates, such as malate, glutamate or pyruvate. Mitochondrial dehydrogenases of viable cells cleave the tetrazolium ring of MTT, yielding purple formazan crystals which are insoluble in aqueous solutions. The exocytosis of the intracellular formazan-containing vesicles gives rise to needle-like formazan crystals at the cell surface, which can be solubilized and measured spectrophotometrically.[187] An increase or decrease in attached cell number results in a concomitant change in the amount of formazan formed. The MTT assay is simple, accurate and yields reproducible results.

The effect of molecular weight and degree of deacetylation of chitosan on the cellular adhesion was done using HEK293 cell line. Figure 5-15 shows that low molecular weight chitosans (102 kDa) had the greatest cell adhesion after 48 h inoculation, followed in order by the higher molecular weight chitosans. Among medium molecular weight chitosans, significant decrease in cell adhesion was obtained by decreasing the degree of deacetylation (MM-HD > MM-MD > MM-LD). The higher the degree of deacetylation of chitosan, the higher the amount of free amino groups ($-NH_2$), which in turn, can become protonated to form cationic amine groups ($-NH_3^+$) producing

positively charged surfaces. This polycationic nature of chitosan helped in the interaction between the chitosan surface and the negatively charged cells. Therefore, chitosans with a higher extent of deacetylation facilitated cell adhesion.[84] Interestingly, all chitosan grades, but MM-LD, showed higher cell attachment compared to TCP, confirming the ability of chitosan to support the spreading, growth and normal biochemical activities of attached cells.

Cross-linking of chitosan films with glutaraldehyde was studied for their effect on cell viability. Figure 5-16 shows the effect of glutaraldehyde on three grades of chitosan; MM-MD, HM-HD and MM-HD. It was found that at 10% w/w glutaraldehyde, MM-HD chitosans had the greatest decline in cell viability upon cross-linking (48.6% decrease), whereas MM-MD chitosan films showed the least difference (22.1% decrease). The toxic effect of glutaraldehyde on attached cells resulted from the residual aldehyde groups on chitosan and residual glutaraldehyde adsorbed onto the film surfaces. Also the decrease in positive charges of chitosan as a result of cross-linking between amine groups has potentially affected the viability of cells. In order to surmount the effect of glutaraldehyde on chitosan films, ethanolamine (EA), glycine (Gly) and Tris (tris(hydroxymethyl)aminomethane) were used to quench the glutaraldehyde reaction. It was found that the three neutralizing agents caused recovery of the intrinsic property of chitosan in supporting cell growth, and the addition of ethanolamine had the greatest effect in neutralizing the toxic effects of glutaraldehyde. Therefore, for the cell adhesion study, biotinylated chitosan films were cross-linked with 10% w/w glutaraldehyde followed by neutralizing the films with 100 mM ethanolamine.

The spatial distribution of cells plays a significant role in the organization of tissues.[247,248] In order to obtain precise control of protein adsorption and cellular interactions, cell-resistant polymers such as poly(ethylene glycol) (PEG), poly(vinyl alcohol), polyacrylamide and some polysaccharides such as dextran have been used.[249,250] PEG has been incorporated onto biomaterial surfaces via various methods,[251]

including simple primary adsorption,[252] secondary adsorption ,[253] grafting [254,255]or bulk incorporation via cross linking[256] or block copolymerization.[257] PEG hydrophilic and electrically neutral properties and chain mobility render it effective in repelling cells from bioactive surfaces.

On the other hand, approaches to promote the specific binding of cells and biomaterial have focused on the enrichment of the biomaterial surface with extracellular matrices (ECMs) components such as RGD (arginine-glycine-aspartic acid),[58] which is a sequence contained in a large number of proteins, including fibronectin.[258]

In this study, biotinylated and cross-linked chitosan films were used for studying cellular adhesion upon chitosan modification with RGD and PEG through an avidin linker. Biotinylated RGD with a spacer arm, biotin-G_{11}GRGDS, was used to modify chitosan's cell adhesion properties. The selection of longer linker arm is important to overcome the topological variations of different surfaces. In the literature, it was reported that using peptide adhesive moieties that contain spacer arms, such as G_{11}GRGDS, instead of using short peptides, enhanced cell attachment and spreading, compared to directly grafting short peptide sequences onto biomaterial surfaces.[207,208] Biotinylated PEG polymers with molecular weights of ~ 5 kDa were prepared as mentioned previously, and biotin conjugation was confirmed using ^{1}H-NMR.

Cell attachment and cell viability on RGD and PEG engineered chitosan substrates have been tested using MTT assay. Figure 5-18 shows the effect of RGD and PEG modification of chitosan surface on the cellular adhesion of on HEK293 cells after 2 h incubation. It was found that HEK293 cells which were grown on chitosan films showed immobilized RGD concentration-dependent cell adhesion. At 10% biotinylation, corresponding to 2 μg/ml immobilized ligands, the efficiency of cellular adhesion was 260.8% ± 13.7% of the cellular adhesion on TCP. Similar results were obtained for HEPM cell line (Figure 5-19), but with slightly less efficiency for RGD in improving cell adhesion on chitosan films compared to HEK293 cells (229.9% ± 20.2%). This

significant improvement in cell adhesion upon immobilization of extracellular matrix components, such as RGD, is important for the design of efficient tissue regeneration systems.

On the other hand, PEG immobilized on chitosan films caused significant decrease in cell adherence as a result of the cell repellant properties of this hydrophilic polymer. At 10% biotinylation, PEG immobilized chitosan films showed insignificant number of adhered HEK293 cells and only 24.4% adhered of HEPM cells relative to TCPs. It was noticed that adding the ligand on unbiotinylated chitosan films caused only slight modification the cellular adhesion, which is caused by adsorption of the ligands, showing that immobilization of ligands using avidin was successful.

5.4 Conclusions

In this research, the high affinity avidin-biotin receptor-ligand interaction has been exploited to form arrays of avidin molecules onto a polymeric substrate expressing biotin moieties. This creates a generic technique by which any biotinylated species can be immobilized into defined patterns. The selection of RGD and PEG was based on the thoroughly studied applications of these two molecules in modifying surfaces for use in tissue engineering. In this study, specific receptor-ligand mediated cellular response has been achieved using RGD and PEG, which served as model molecules for spatially controlling cell attachment and distribution. Such spatial control has been shown to be essential for producing healthy functional tissues.[259]

5.5 Figures and Tables

Table 5-1. Degrees of deacetylation as measured by first derivative UV spectrophotometry and viscosity average molecular weights of different grades of chitosan used in studying cellular adhesion.

Chitosan grade	Measured degree of deacetylation	Viscosity average molecular weight (M_v)
HM-HD	91.28%	181686
MM-HD	90.92%	144760
MM-MD	84.02%	132578
LM-HD	92.10%	102017
MM-LD	74.36%	140708

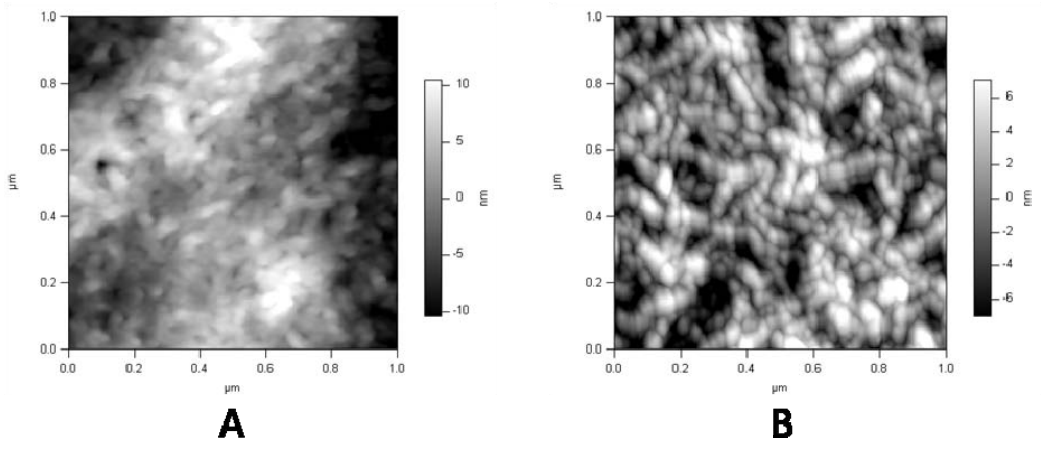

Figure 5-1. AFM height images of uncross-linked chitosan films. (A) A chitosan film before neutralization and (B) after neutralization with NaOH.

Table 5-2. Surface characterization of uncross-linked chitosan films before and after neutralization.

	Before neutralization		After neutralization	
	Full image	**Masked image**	**Full image**	**Masked image**
R_{RMS}	16.5	6.9	5.0	3.7
Average deviation	13.7	5.3	3.8	2.9
Skewness	0.05	0.36	0.11	0.01
Kurtosis	-0.64	-0.73	1.46	-0.19

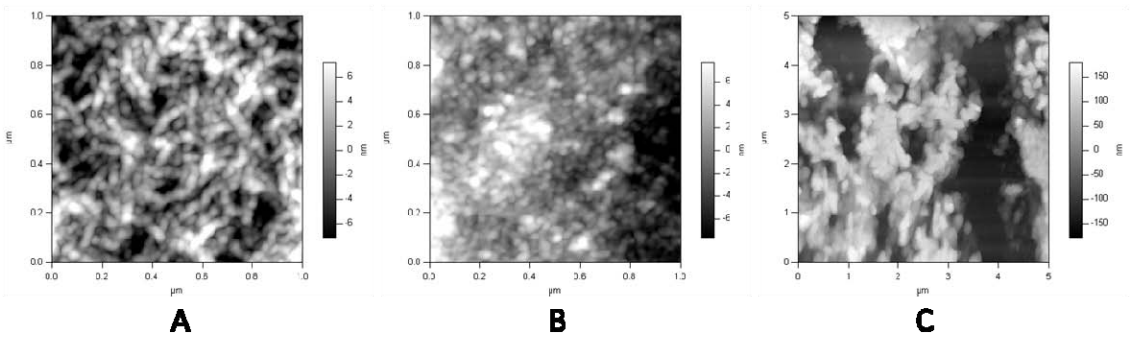

Figure 5-2. AFM height images of glutaraldehyde cross-linked films using method I as a function of glutaraldehyde concentration. Glutaraldehyde ratio relative to chitosan was (A) 0.1%, (B) 1% and (C) 10% (w/w) ratios.

Table 5-3. Surface characterization of glutaraldehyde cross-linked films using method I as a function of glutaraldehyde concentration. Glutaraldehyde ratio relative to chitosan was 0.1%, 1% or 10% (w/w).

	0.1% GA		1% GA		10% GA	
	Full image	**Masked image**	**Full image**	**Masked image**	**Full image**	**Masked image**
R_{RMS}	6.8	4.0	10.5	4.8	88.6	88.2
Average deviation	5.2	3.1	8.1	2.1	78.3	51.0
Skewness	0.23	0.03	0.57	0.58	-0.02	-0.14
Kurtosis	0.76	-0.04	1.52	0.44	-1.29	-0.66

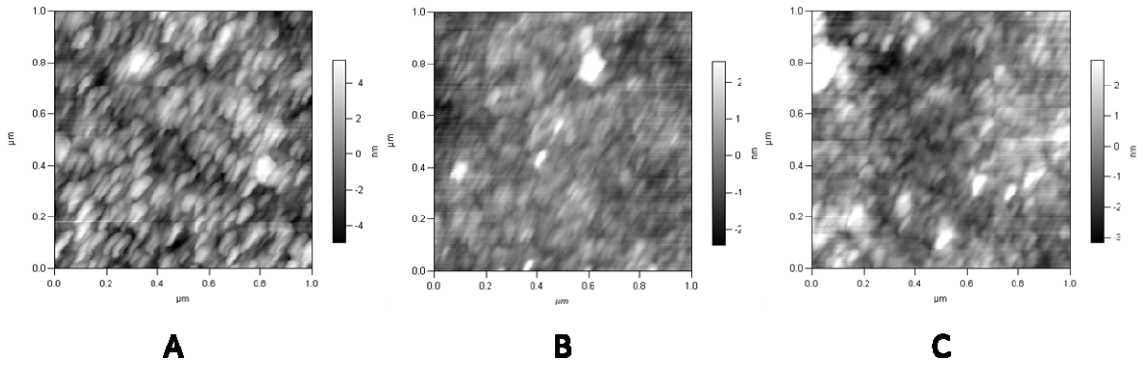

Figure 5-3. AFM height images of glutaraldehyde cross-linked films using method II as a function of pH of the cross-linking solution. pH of the buffers were (A) 9.2 (B) 10.2 or (C) 11.2.

Table 5-4. Surface characterization of glutaraldehyde cross-linked films using method II as a function of pH of the cross-linking solution.

	pH 9.2		pH 10.2		pH 11.2	
	Full image	**Masked image**	**Full image**	**Masked image**	**Full image**	**Masked image**
R_{RMS}	3.5	4.5	8.0	5.6	14.9	4.1
Average deviation	2.7	2.1	6.0	0.7	8.9	1.2
Skewness	0.57	0.14	1.48	-0.19	3.01	0.75
Kurtosis	0.98	-0.49	3.01	0.45	14.50	0.80

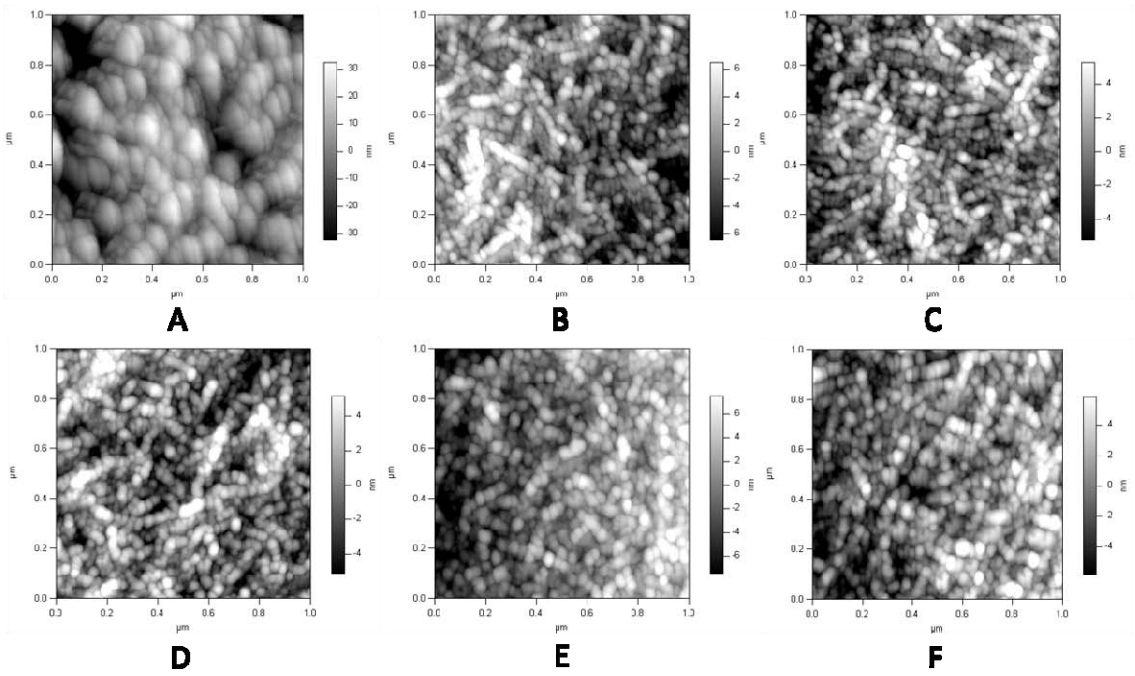

Figure 5-4. AFM height images of glutaraldehyde cross-linked chitosan films using method III as a function of pH of the cross-linking solution. pH of the buffers were (A) 6.2 (B) 7.2 (C) 8.2 (D) 9.2 (E) 10.2 or (F) 11.2.

Table 5-5. Surface characterization of glutaraldehyde cross-linked films using method III as a function of pH of the cross-linking solution.

	pH 6.2		pH 7.2		pH 8.2		pH 9.2		pH 10.2		pH 11.2	
	Full image	**Masked image**	**Full image**	**Masked image**	**Full image**	**Masked image**	**Full image**	**Masked image**	**Full image**	**Masked image**	**Full image**	**Masked image**
R_{RMS}	17.6	13.0	3.0	3.1	3.6	2.8	3.1	2.7	3.3	2.9	2.8	2.7
Average deviation	13.7	10.3	2.4	2.5	2.5	2.1	2.4	2.1	2.5	2.1	2.2	2.0
Skewness	-0.60	-0.22	0.24	0.21	1.96	0.12	-0.15	0.13	0.45	0.39	0.31	0.07
Kurtosis	0.40	0.17	0.01	-0.13	10.20	-0.20	1.87	-0.15	3.31	0.11	0.22	-0.14

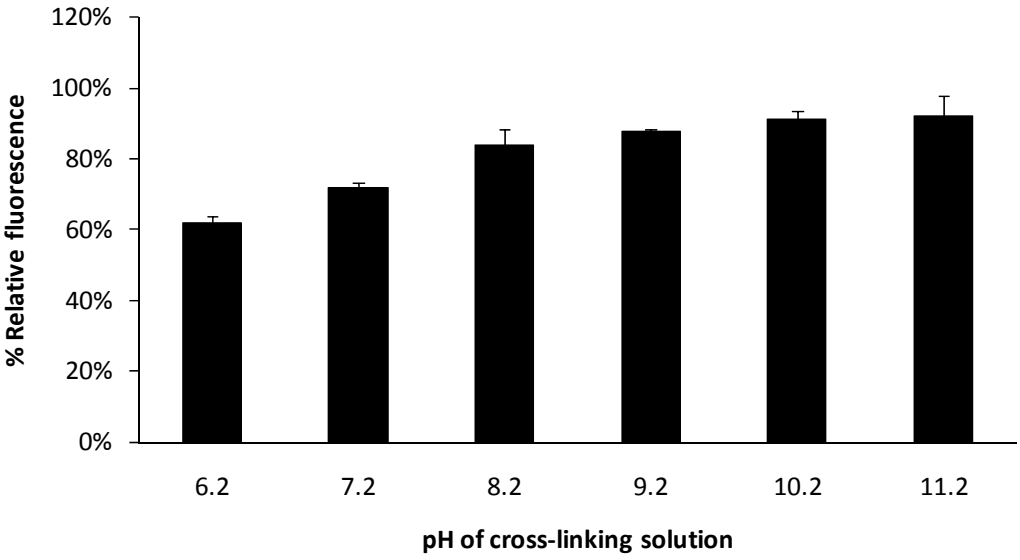

Figure 5-5. Fluorescamine assay results of glutaraldehyde cross-linked chitosan films relative to untreated films at different pH values.

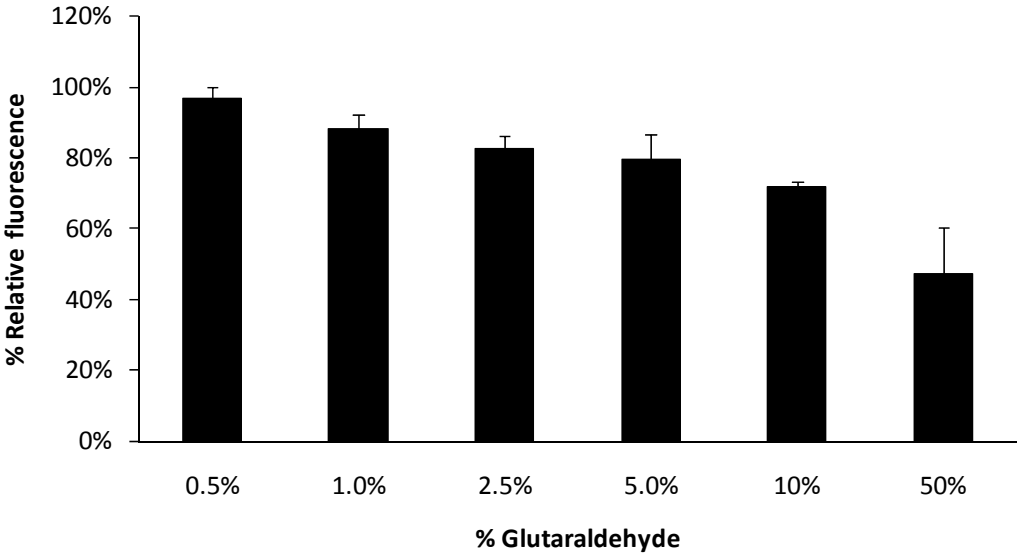

Figure 5-6. Relative fluorescence of glutaraldehyde cross-linked chitosan films to untreated films at different glutaraldehyde w/w% as measured by fluorescamine assay. Cross-linking was carried out in 100 mM phosphate buffer, pH 7.2.

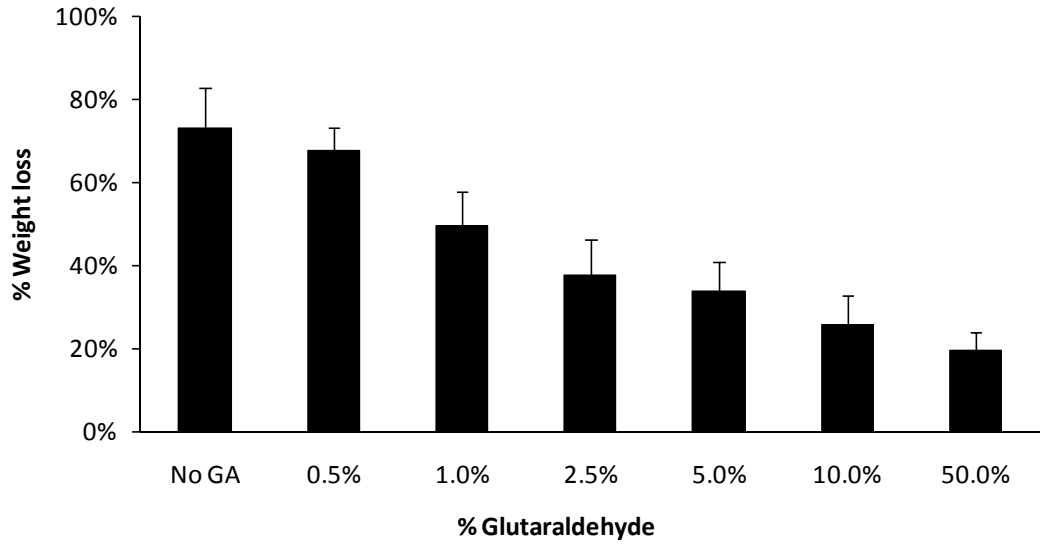

Figure 5-7. Solubility of chitosan films in 0.5% v/v acetic acid solutions as a function of the percentage of glutaraldehyde (w/w%).

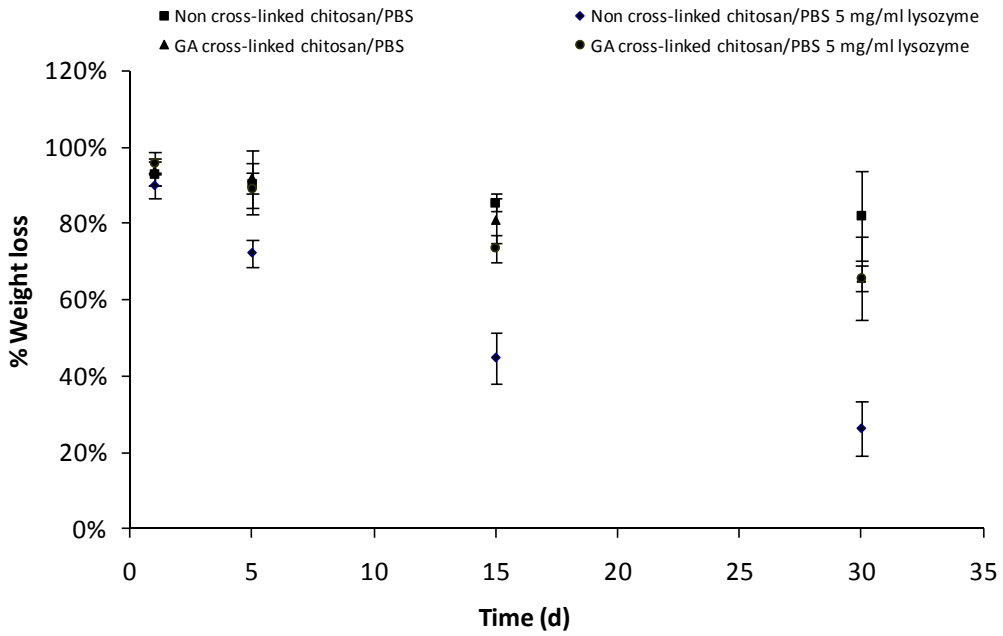

Figure 5-8. Degradation of chitosan films in phosphate buffered saline with and without lysozymes at 37°C.

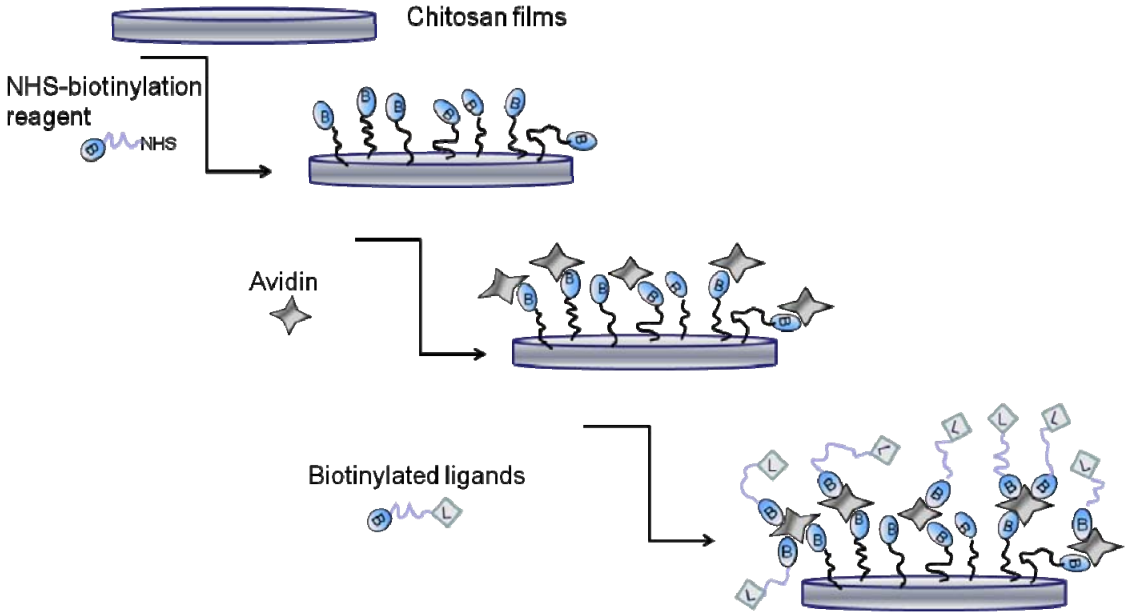

Figure 5-9. Schematic of ligand modification of chitosan films via the avidin-biotin linker.

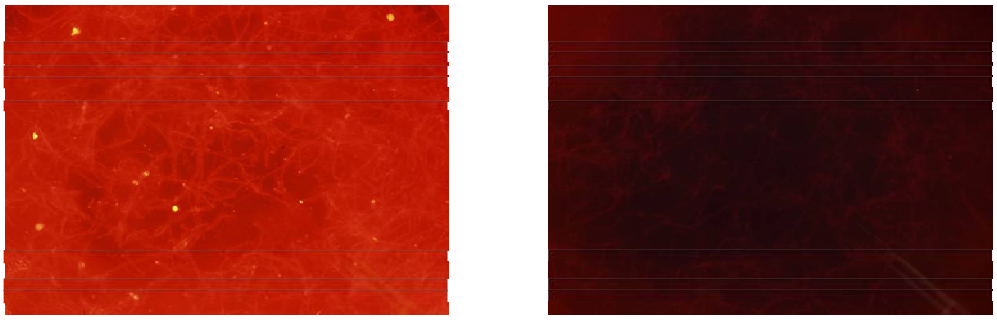

Figure 5-10. Avidin-rhodamine fluorescence. (A) Biotinylated and (B) control chitosan films.

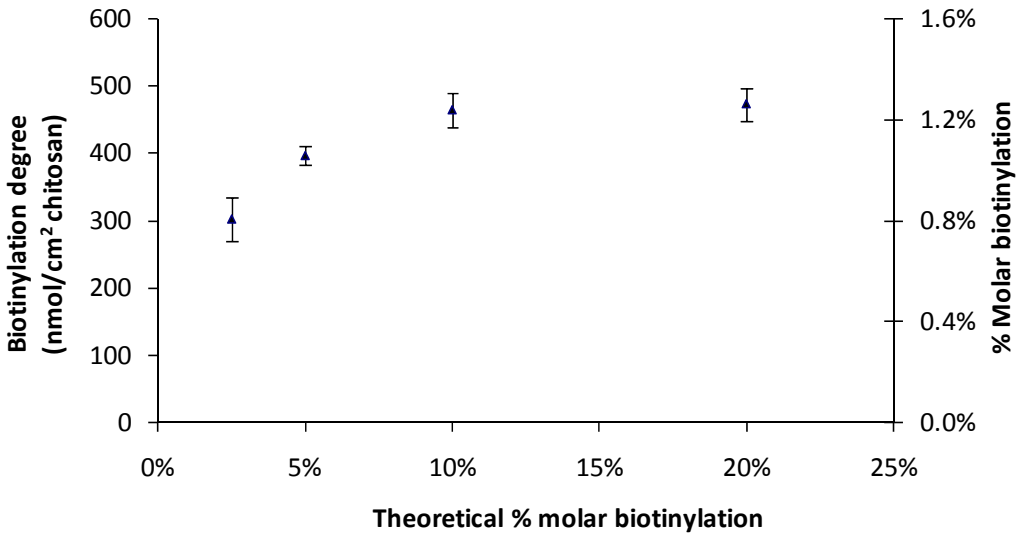

Figure 5-11. The effect of biotin concentration on the biotinylation efficiency of chitosan films.

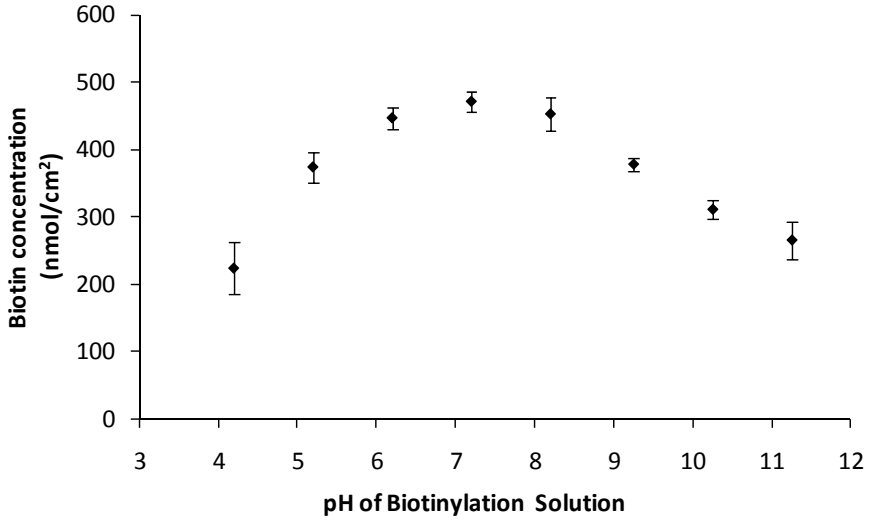

Figure 5-12. The effect of pH on the biotinylation efficiency of chitosan films.

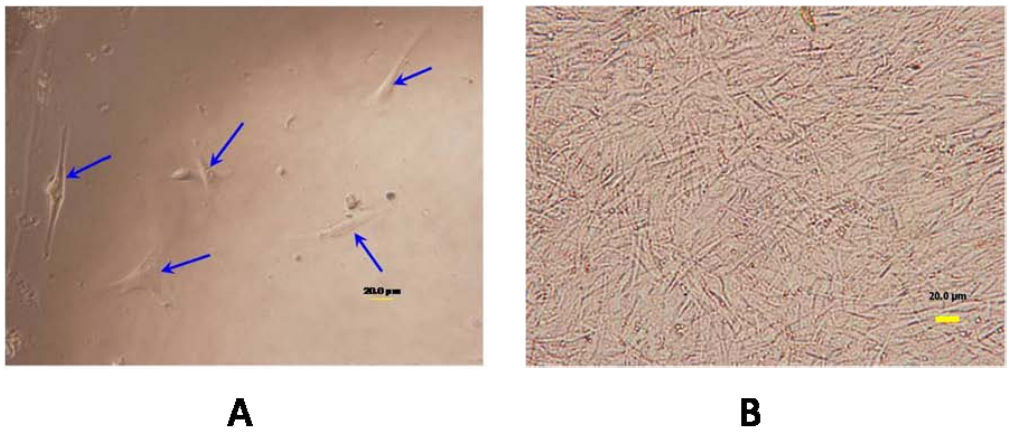

Figure 5-13. Chitosan films showing HEPM cell adhesion. (A) Initially (after 4 h) and (B) at confluence (after 5-day incubation). The arrows point to attached cells.

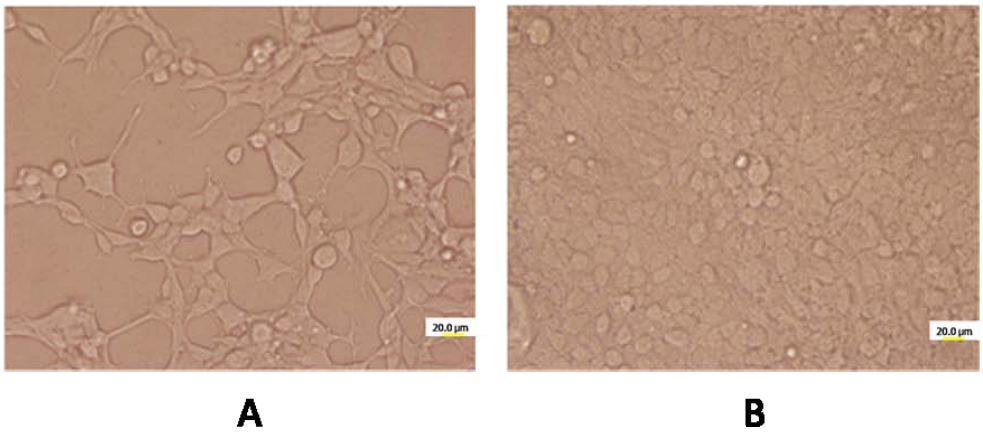

Figure 5-14. Chitosan films showing HEK293 cell adhesion. (A) Initially (after 4 h) and (B) at confluence (after 5-day incubation).

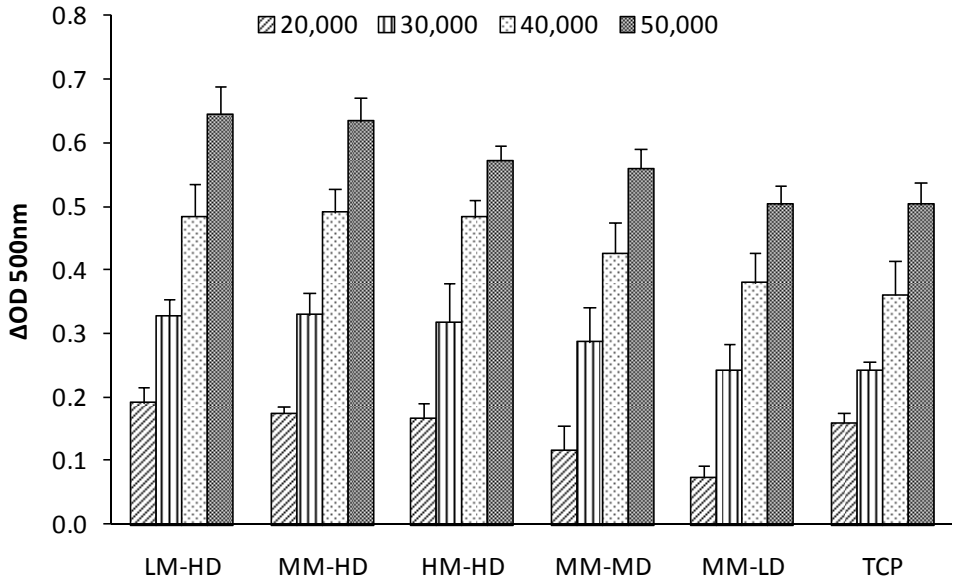

Figure 5-15. The effect of the chitosan grades on the cellular viability of HEK293 cells inoculated on chitosan films. Chitosan films were fabricated from high molecular weight and high degree of deacetylation (HM-HD), medium molecular weight and high degree of deacetylation (MM-HD), low molecular weight and high degree of deacetylation (LM-HD), medium molecular weight and medium degree of deacetylation (MM-MD) and medium molecular weight and low degree of deacetylation (MM-LD) chitosans.

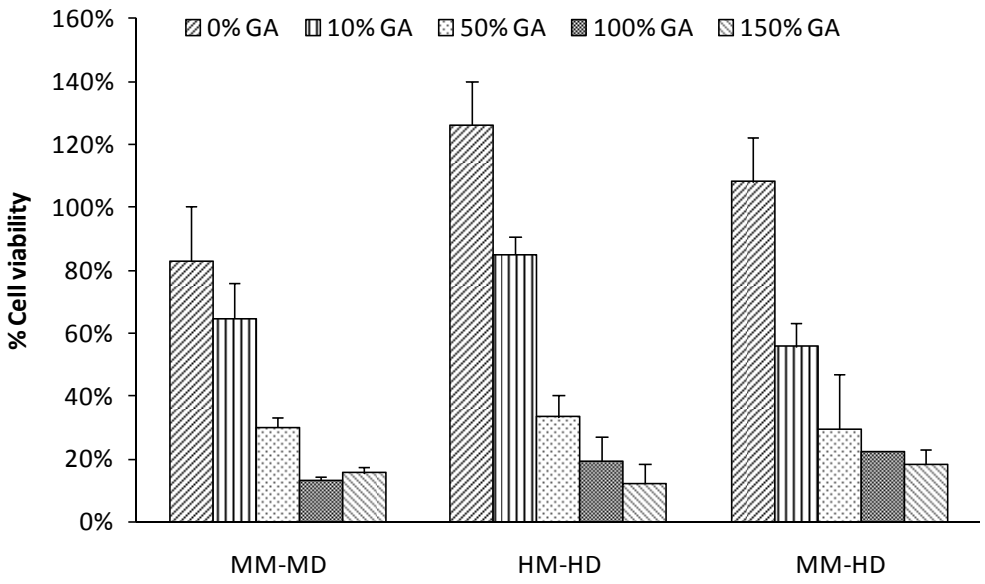

Figure 5-16. The effect of the percentage of glutaraldehyde cross-linking on the cellular viability of HEK293 cells inoculated on chitosan films. Films were made of high molecular weight and high degree of deacetylation (HM-HD), medium molecular weight and high degree of deacetylation (MM-HD) and medium molecular weight and medium degree of deacetylation (MM-MD) chitosans.

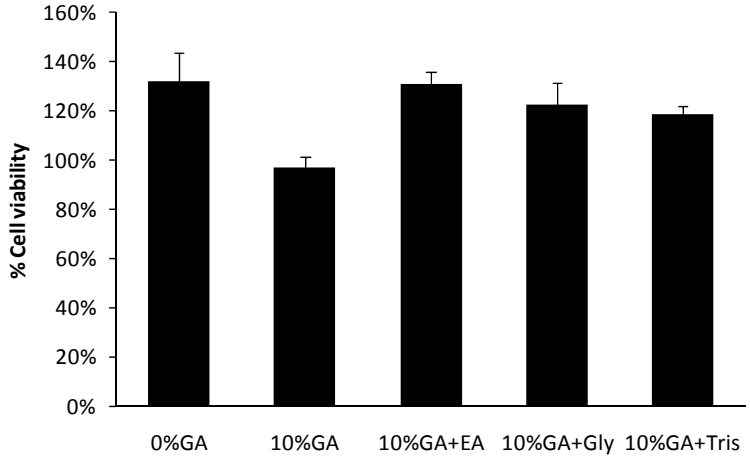

Figure 5-17. The effect of glutaraldehyde cross-linking and the subsequent quenching of the reaction using ethanolamine (EA), glycine (Gly) or Tris (tris(hydroxymethyl)aminomethane) on the viability of HEK293 cells on chitosan films.

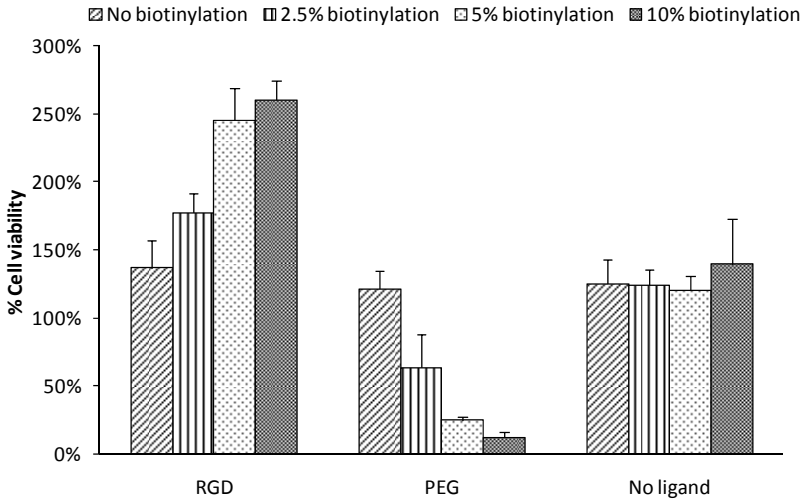

Figure 5-18. The effects of RGD and PEG ligand modification on HEK293 cell adhesion measured by the MTT assay. Biotinylation percentage was used as a measure of the degree of ligand attachment.

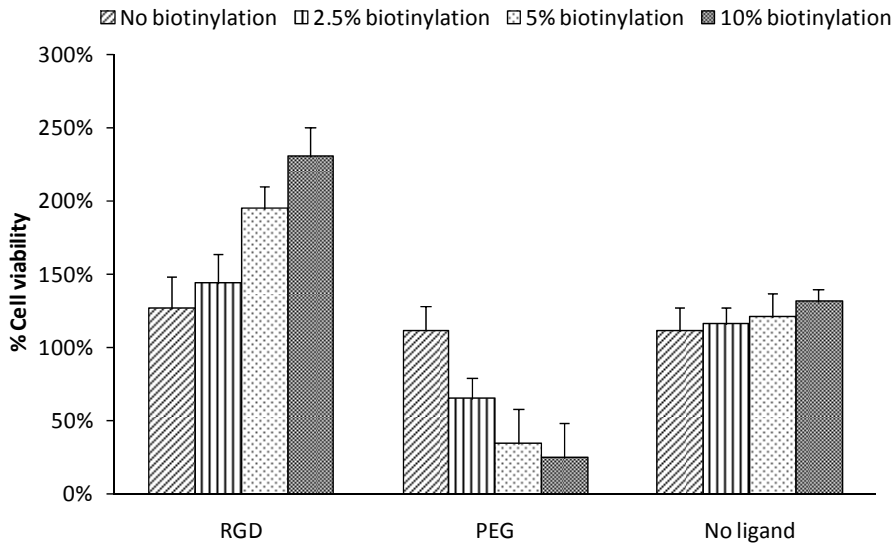

Figure 5-19. The effect of RGD and PEG ligand modification on HEPM cell adhesion, measured by the MTT assay. Biotinylation percentage was used as a measure of the degree of ligand attachment.

CHAPTER 6

CONCLUSIONS AND FUTURE PERSPECTIVE

6.1 Conclusions

This research focused on modifying and optimizing chitosan for applications in gene delivery, enzyme immobilization and tissue engineering. Firstly, polyelectrolyte complexes (PECs) made of chitosan with different polyanions, especially dextran sulfate, were studied for gene delivery purposes. It was found that chitosan PECs resulted in spherical nano-sized particles and were able to condense plasmid DNA (pDNA) effectively. In addition, these particles were able to protect DNA from degradation by DNase I. Physicochemical properties of particles, such as particle sizes and charges, as well as gene and drug delivery properties, such as transfection efficiencies, were largely dependent on chitosan's molecular weight and degree of deacetylation, type of polyanions, chitosan to polyanion weight ratio and chitosan to pDNA charge ratio. Inclusion of dextran sulfate into chitosan particles resulted in superior particle stability and high exogenous protein expression, compared to using other polyanions. These formulations were tested as DNA vaccine delivery vehicles and were found to effectively induce the immune response when combined with antigens and immune-adjuvants.

Optimized chitosan nanoparticulate formulations using dextran sulfate were modified further with two ligands, polyethylene glycol (PEG) and G_{11}GRGDS peptide sequence (RGD), through avidin-biotin linkers. It was found that this method was successful in immobilizing these ligands on the surface of chitosan nanoparticles or within the particles. The first step in this technique was to biotinylate chitosan and the studied ligands using N-hydroxysuccinimide chemistry, utilizing the free primary amine groups of the deacetylated chitosans. Biotinylation reaction was studied thoroughly using different pH buffers and at different concentrations of chitosan and biotinylation agents. It was found that the biotin conjugation reaction was dependent on all these factors, in

addition to the degree of deacetylation of chitosan and the physical status of chitosan during cross-linking (suspended, dissolved or solid). After biotinylating chitosan efficiently, avidin was added, followed by the addition of the biotinylated ligands. PEG and RGD served as model ligands on chitosan chains, with the possibility of adding various types of ligands based on the needed applications. In this study, RGD unique property of enhancing the cellular uptake of particulate systems was utilized for chitosan particles used for gene delivery and the degree of gene expression after introducing chitosan nanoparticles into HEK293 cells was detected. PEG was used to enhance the stability of chitosan nanoparticles and to reduce protein adsorption. Indeed, it was found that chitosan vectors modified with RGD or PEG exhibited improved transfection capabilities, with transduced protein expression as high as the positive control, polyethylene amine (PEI). Surface immobilization of ligands was feasible and significantly more efficient compared to immobilization of ligands along all chitosan chains before particle formation.

Modification of chitosan via avidin linkers was implemented further in enzyme immobilization. Trypsin was used as a model enzyme to be immobilized on both chitosan films and particles. Trypsin itself has a number of industrial, research and biomedical applications and immobilizing it is essential for the practical use of this enzyme. Biotinylation of the enzyme was efficiently accomplished by the same mechanism as biotinylation of chitosan. Formulations of chitosan nanoparticle were optimized to yield stable and consistent particles. Particle stabilization was achieved through chemical cross-linking with glutaraldehyde. Trypsin activity was measured using casein as a substrate and it was found that immobilization via avidin-biotin mechanism is an efficient method that retain the enzymatic activity. Moreover, it was found that immobilized trypsin on chitosan supports improved the enzymatic resistance to pH changes and high temperature denaturation.

Chitosan has been proposed as a tissue engineering material for its biodegradability and biocompatibility. In this study, chitosan films were fabricated through dry-casting method and the films were cross-linked with glutaraldehyde to increase their stability and reduce their degradation. Cytotoxicity of glutaraldehyde was minimized with the neutralization of surface aldehyde using amine containing buffers such as glycine. This was followed by surface engineering of chitosan films using RGD, to enhance cell adhesion, or PEG, to repel cells from chitosan surfaces, via the same mechanism discussed above. It was found that these ligands effectively modulated the cellular adhesion and growth on chitosan films in ligand-concentration dependent manner and that this method of ligand immobilization is suitable for surface engineering of chitosan films and scaffolds.

These results shows that chitosan has a great potential in a variety of biomedical applications and that chitosan's physicochemical and mechanical properties utilized in fabricating particles and films can be modulated for specific purposes. In addition, chitosan, having both amine and hydroxyl groups, can be modified with various ligands. We found that adding ligands to chitosan for different purposes can be easily done in mild conditions using avidin-biotin interaction. Moreover, avidin provides multiple binding sites for one or more types of biotinylated ligands to be attached concurrently.

6.2 Future perspectives

Chitosan nanoparticles prepared with dextran sulfate showed great potential for gene and protein delivery, especially for DNA vaccines. Also, RGD and PEG modified nanoparticles yielded considerably high *in vitro* transfection. These vehicles need further evaluation for their pharmacokinetics, pharmacodynamic and transgene expression *in vivo*. Also, the selection of route of administration of these particles should be addressed, especially pulmonary and nasal routes.

Specific labeling of enzymes with biotin to produce site-specific immobilization on avidin bridged novel biotinylated chitosan nanoparticles should be tested. Enzyme oriented immobilization can be done through preparing enzymes with biotin using expressed protein ligation (EPL), also named intein-mediated protein ligation, which represents an excellent tool with which to introduce chemical modifications selectively.[260-262] An example of a model enzyme to be immobilized on chitosan surfaces is human aldo/keto reductase (AKR1A1), an ideal enzyme for biosensor applications.[263-266]

Current work in tissue engineering is focused on two-dimensional chitosan substrates. Future work will aim to prepare and test three-dimensional porous scaffolds prepared from chitosan by freeze-extraction and freeze-gelation methods.[267] Different ligands, such as growth factors and cell adhesion moieties, will be used to modify chitosan through the developed avidin-biotin mechanism. In addition, chitosan scaffolds will be synthesized using a novel method which utilizes the success in the biotinylation of chitosan and the fabrication of plasmid DNA loaded chitosan particles. Upon exposure to avidin, the biotinylated chitosan particles are expected to crosslink forming an interconnected network that can be the basis of *in situ* scaffolds.[268,269] Future studies are needed to be done to determine the efficiency of chitosan films to support the differentiation of the preosteoblasts, that include performing alkaline phosphatase (ALP) specific assay, studying 1,25 (OH_2) D_3 stimulated osteocalcin production and measuring mRNA steady-state expression for bone-related genes.[270,271]

APPENDIX

A.1 Degree of deacetylation of chitosan

As discussed previously, heterogeneous chitosan reacetylation was carried out using acetic anhydride. For the theoretical stoichiometric calculation of the required amount of acetic anhydride, the total number of moles of chitosan monomers was calculated using the following equation:

$$Sample\ weight = 162\ \times DD\ \times Z\ + 203\ \times (1 - DD) \times Z$$

In which *DD* is the degree of deacetylation of the starting material to be reacetylated, *Z* is the number of moles of chitosan monomers, 203 Da is the molecular weight of the acetylated monomers calculated by subtracting the molecular weights of a hydroxyl group and a hydrogen atom (removed due to polymerization) from that of N-acetyl glucosamine (221-17-1) and 162 Da is the molecular weight of the deacetylated monomers calculated by subtracting the molecular weights of a hydroxyl group and a hydrogen atom from the molecular weight of glucosamine (179-17-1).

After obtaining *Z*, the following equations were applied to find the needed volume of acetic anhydride:

$$Required\ moles\ of\ acetic\ anhydride = (original\ DD - target\ DD) \times Z$$

$$Required\ volume\ of\ acetic\ anhydride = 102.09\ \times Z\ \div 1.0825$$

Where 102.09 is the molecular weight of acetic anhydride and 1.0825 g/ml is its density.

The same calculations above were used for finding the molarity of protonable nitrogen-containing repeating units in chitosan as following:

$$Molecular\ weight\ per\ glucosamine\ unit = 1/(\mathrm{DD}\ \times Z\ )$$

In order to find the degree of deacetylation of chitosan, many analytical methods have been used,[183] such as UV-spectroscopy,[272,273] first derivative UV-spectroscopy (1DUVS),[182] colloidal titration,[274] linear potentiometric titration,[275] X-ray powder

diffraction,[276] enzymatic determination,[277] infrared spectroscopy (IR),[278] near infrared spectroscopy,[279] nuclear magnetic resonance,[280] ninhydrin test[281] and circular dichroism.[282]

1DUVS shows an enhanced ability to detect minor spectral features by plotting the first derivative of absorbance versus wavelengths, especially in the presence of interfering peaks that are broader by at least a factor of two than the analyte peaks.[283] This technique has been used quantitatively for analyzing the obstruction of chitosan's peaks by the overlapping peaks of the solvent (acetic acid).[283] 1DUVS provides simple, convenient, rapid, precise and non-destructive determination of the acetyl content of chitin/chitosan with minimal interference from protein contamination.[182,183] The theory behind 1DUVS is explained below.

In case of having two substances which absorb in the same spectral region, such as acetic acid and the acetylated units of chitosan monomers, and assuming that the absorbance is additive and each follows Beer's Law:

$$A = \varepsilon bC$$

$$A = A_x + A_y$$

$$P = P_0 10^{-A}$$

Where A is the absorbance, ε is the absorptivity in units of liter mole^{-1} cm^{-1}, b is the path length in cm, C is the molar concentration, P is the radiant power of the transmitted unabsorbed radiation that emerges from the absorbing medium at x=b and P_o is the radiant power at X=0.

Taking the first derivative relative to λ, the wavelength in nm;

$$\frac{dP}{d\lambda} = 10^{-A}\frac{dP_0}{d\lambda} - 2.303P_0 10^{-A}\left[bC_x\left(\frac{d\varepsilon}{d\lambda}\right)_x + bC_y\left(\frac{d\varepsilon}{d\lambda}\right)_y\right]$$

If P_o does not vary much with λ in the spectral region of interest, $dP_o/d\lambda$ can be neglected. In addition, if the molar absorptivity of one component, such as ε_y, varies

slightly in the spectral region under investigation, $bC_y(d\varepsilon/d\lambda)_y$ can be neglected as well, which results in the following equation:

$$\frac{dP}{d\lambda} = -2.303PbC_x\left(\frac{d\varepsilon}{d\lambda}\right)_x$$

This leads to:

$$\frac{dA}{d\lambda} = bC_x\left(\frac{d\varepsilon}{d\lambda}\right)_x$$

Therefore, there is a direct relationship between first derivative of the absorbance and molar concentration.

To measure the degree of deacetylation of chitosan, first derivative calibration curves of N-acetylglucosamine (NAG, Sigma®, MO) dissolved in 0.01 M acetic at concentrations of 0.0125, .0.025, 0.050 and 0.075 mg/ml were plotted. In addition, a plot of three different concentrations (0.01, 0.02 and 0.03 M) of acetic acid was constructed to find the zero crossing point (ZCP), which is the point where the three concentrations intersect in the first derivative absorption spectrum. The height (H) was calculated by calculating the vertical distance between ZCP and the corresponding points of the chitosan's first derivative spectra. ZCP was used as a reference point since at ZCP the effect of acetic acid on the absorbance of chitosan is expected to be minimal. Plotting H versus NAG concentrations resulted in a linear relation which was used to calculate the concentrations of NAG units in the chitosan samples. The number of moles of NAG units can then be easily obtained and used in the following equation to obtain the DD of the sample;

$$DD = \left(100 - M/(M + \frac{W - 203 \times M}{162})\right) \times 100\%$$

Where M is the calculated number of moles of NAG monomers in the chitosan sample, W is the weight of chitosan sample, 203 Da is the molecular weight of NAG

monomers in chitosan polymer and 162 Da is the molecular weight of glucosamine monomers in chitosan polymer.

Figure A-1 shows an example of the UV spectra of acetic acid solutions and N-acetylglucosamine standards. When converting acetic acid curves into their 1DUV spectra (Figure A-2), the ZCP was found to be at 203 nm. The heights (H) were calculated from the distance between the ZCP to the corresponding N-acetylglucosamine standard 1DUV spectra (Figure A-3) and the standard curve of N-acetylglucosamine concentration vs. H was plotted (Figure A-4). Similar approach was followed for all chitosan samples and the degrees of deacetylation were calculated according to the equations above.

A.2 Molecular weight of chitosan

Viscosity average molecular weights of different chitosan grades were calculated from intrinsic viscosities, which were determined using Ostwald 100 viscometer (Fisher Scientific, PA). Chitosans were dissolved in 0.25 mM acetate buffer at range of diluted concentrations (0.05-0.3 g/dl) and 7 ml of each of these solutions were pipetted into the viscometer and left to equilibrate in a 25°C water bath. Polymer solutions inside the viscometer were sucked up using vacuum until the meniscus troughs reached the upper marked line, after which solutions were left to move down freely under the influence of gravity until they reached the lower marked line. The time intervals for the added solutions to move between the two marks were recorded in triplicate. The following equations were utilized:

$$\textit{Relative viscosity}\ (\eta_r) = \frac{\eta}{\eta_0} = \frac{t}{t_0}$$

$$\textit{Specific viscosity}\ (\eta_{sp}) = \frac{\eta - \eta_0}{\eta_0} = \eta_r - 1$$

$$Inherent\ viscosity\ (\eta_i) = \frac{\ln \eta_r}{c}$$

$$Reduced\ viscosity\ (\eta_{red}) = \frac{\eta_{sp}}{c}$$

Intrinsic viscosities were obtained from the y-intercept of the concentration vs. reduced viscosity plots.

Viscosity average molecular weights were calculated using Mark–Houwink–Sakurada equation:

$$[\eta] = KM_v^a$$

Where $[\eta]$ is the intrinsic viscosity, K and a are experimentally determined constants for each specific system and M_v is the viscosity-average molecular weight. For chitosan dissolved in 0.25 mM acetate buffer at 25°C, $K = 1.4 \times 10^{-4}$ and $a = 0.83$.[174]

Average viscosity molecular weights of chitosans dissolved in 0.25 mM acetate buffers were determined using Ostwald viscometer at 25°C. Figures A-5 to A-8 show reduced viscosities (η_{red}, left y-axis) and (ln η_{rel})/C (right y-axis) vs. concentration for MM-HD, HM-HD, LM-HD and MM-MD chitosans. Figures A-9, 10, 11 and 12 show the reduced viscosity curves for LM-MD chitosans oxidatively fragmented at 1%, 1.5%, 2% and 4% sodium nitrite w/w ratios, respectively.

A.3 Zeta potential theory

Zeta potential is the potential that exists at the boundaries of the outer diffuse layer surrounding charged particles. Zeta potential is important since it plays a major role in the stability of colloidal systems. If suspended particles have large negative or positive zeta potential values, they tend to repel each other, minimizing flocculation. Generally, particles which have zeta potential greater than +30mV or less than -30 mV are considered stable.

The Zetasizer Nano ZS particle analyzer calculates zeta potential by determining the electrophoretic mobility and then applying Henry's equation.

$$U_e = \frac{2\varepsilon z f(Ka)}{3\eta}$$

Where z is the zeta potential, U_e is electrophoretic mobility, ε is dielectric constant, η is viscosity and $f(Ka)$ is Henry's function.

Electrophoretic mobility, the velocity of a particle in an electrical field, depends on the strength of the applied electrics field or voltage gradient, the dielectric constant of the medium, the viscosity of the medium and the zeta potential. The electrophoretic mobility is obtained by performing an electrophoresis experiment on samples and then measuring the velocity of the particles using laser Doppler velocimetry (LDV).

A.4 Particle size theory

Biodistribution studies demonstrated that the particle size and route of administration exhibit great effect on the localization site of injected nano and micro-sized particles.[284] Particle sizes of the drug carrier systems are considered the basis of passive drug targeting and also determine the first-order distribution. Carrier systems larger than 400 nm in diameter are exposed to nonspecific scavenging by the reticuloendothelial systems (RES), which reduces the circulation time in the bloodstream and usually leads to inefficient delivery of therapeutic agents.[285] In contrast, carriers with particle sizes of less than 200 nm have a relatively long circulation time and therefore are used for targeted drug delivery. When particles are smaller than 10 nm, renal filtration becomes the dominant mechanism of clearance, causing a reduction in circulation time.[286]

The Zetasizer Nano ZS particle analyzer performs size measurements using a process called dynamic light scattering (DLS). DLS, also known as photon correlation spectroscopy (PCS) or quasi elastic light scattering (QELS), utilizes the Brownian motion to calculate the sizes of particles. This is done by illuminating the particles with a laser and analyzing the intensity fluctuations in the scattered lights at the same spot within

nano- to micro-seconds using a correlator. The relationship between the size of a particle and its speed due to Brownian motion is defined in the Stokes-Einstein equation. Larger particles move slowly, and consequently the intensity of the speckle pattern will also fluctuate slowly. With smaller particles, the intensity of the speckle pattern will fluctuate quickly since these particles move quickly. Special algorithms are used to extract the decay rates from which size distributions are produced.[176,287] DLS has been used in literature as the method of choice to measure the size of chitosan-DNA complexes[123] and it was found to be complimentary to microscopic methods such as AFM.[288]

A.5 Ethidium bromide competition binding assay

Since fluorometry is considered the most sensitive detection technique, it has been utilized widely for detecting the concentration of nucleic acids.[289] Ethidium bromide, PicoGreen®, SYBR Green I and Hoechst 33258 are examples of fluorophores that have been used in this field. Ethidium bromide (EtBr, Figure A-13), a widely used dye in gel electrophoresis staining, intercalates preferentially with double stranded DNA molecules (dsDNA). Although EtBr is toxic and mutagenic,[289] but when it is handled with caution and its assay is optimized, it can detect DNA with high degree of sensitivity and low limit of detection in a high throughput screening.[185,290]

Intercalation of EtBr within the DNA double strands in the competition binding assay (also called ethidium bromide exclusion assay) increases the fluorescence quantum yield of the dye. Upon DNA compaction, EtBr is expelled from the DNA-EtBr complex, causing a decrease in the fluorescence signal. Conversely, destabilization of the DNA condensates is expected to cause a recovery of the fluorescence signal.[291] The complexation of DNA with chitosan was studied by recording the fluorescence obtained with the fluorescent probe EtBr (Sigma®, MO) in 96 well flat bottom polypropylene cell culture plates (Corning® Costar®, MA) using SpectraMax® M5 multi-mode microplate reader (Molecular Devices, CA). EtBr (stock solution of 0.05 mg/ml) was added to each

well at different dye/DNA ratios and was mixed with DNA solutions. Various concentrations of EtBr and DNA were studied. The excitation wavelength was 519 nm and the emission spectra from 580 to 630 nm were recorded. The maximum fluorescence intensity within the wavelengths of 580-630 nm was obtained from each spectrum and the fluorescence intensities were normalized relative to the fluorescence signals of DNA-EtBr, without subtracting the background fluorescence. Results from 3 independent experiments were averaged.[291]

In order to validate the ethidium bromide exclusion assay for chitosan systems, different parameters were adjusted. First, the fluorescence intensities at increasing concentrations of EtBr (corresponding to decreasing w/w ratio of DNA/EtBr) and fixed concentrations of DNA were studied (Figure A-14). It was found that fluorescence intensities are linearly proportional to the concentration of EtBr at low concentrations of EtBr. At higher concentrations of EtBr, the fluorescence intensity's curve reached a plateau, followed by a decline. Figure A-15 shows the linear relation between EtBr concentrations up to 0.01 mg/ml at fixed DNA concentrations vs. relative fluorescence intensities at maximum wave length. This range represents DNA/EtBr ratios of 2 to 40 ($r^2 = 0.9979$). Therefore, lower DNA/EtBr ratios were selected for better DNA detection.

This was followed by studying the fluorescence intensities of DNA-EtBr complex at three fixed concentrations of EtBr; 0.5, 2.5 and 5.0 μg/ml. Figure A-16 shows DNA-EtBr curve at EtBr concentration of 0.5 μg/ml. It was noticed that for the three studied EtBr concentrations, DNA-EtBr calibration curve changes slope at DNA concentration of ~ 0.02 mg/ml. The lowest concentration of EtBr (0.5 μg/ml) has shown the best r^2 value at lower DNA concentrations, but it failed to give acceptable detection at higher DNA concentrations (Figures A-17 and A-18, respectively). In comparison, the highest EtBr concentration (5.0 μg/ml) showed better detection at higher DNA concentrations (Figure A-21) and did not show satisfactory detection at low concentrations of DNA (Figure A-22). Therefore, EtBr concentrations of 2.5 μg/ml was selected for detecting

chitosan ability to compact with DNA since it showed optimum detection results regarding linearity and limit of detection of DNA as shown in Figures A-19 and A-20.

A.6 The MTT assay

Tetrazolium salts are large group of heterocyclic organic compounds that change to highly colored and insoluble formazan salts upon reduction.[187]

MTT (3-[4,5- dimethylthiazol-2-yl]-2,5-diphenyltetrazolium bromide) is a monotetrazolium salt that is widely used to detect the biological redox systems and viability of cells as indication of cellular proliferation and cytotoxicity of different materials.[187,188] MTT measures the activity of living cells mainly via mitochondrial dehydrogenases, which are supported by NADH-linked mitochondrial substrates, such as malate, glutamate or pyruvate (Figure A-23). Mitochondrial dehydrogenases of viable cells cleave the tetrazolium ring of MTT, yielding purple formazan crystals which are insoluble in aqueous solutions. The exocytosis of the intracellular formazan-containing vesicles gives rise to needle-like formazan crystals at the cell surface, which can be solubilized and measured spectrophotometrically.[187] An increase or decrease in cell number results in a concomitant change in the amount of formazan formed, indicating the degree of cytotoxicity caused by the test materials. MTT assay is simple, accurate and yields reproducible results.

A.7 The HABA/avidin assay

4-Hydroxyazobenzene-2-carboxylic acid (HABA) is a dye that binds weakly to strept(avidin). When bound to strept(avidin), HABA dye loses its planarity and exists in twisted conformer along the N-N bond, which is a hydrazone tautomer and changes color from orange to red. HABA and biotin share common binding sites in strept(avidin). However, HABA is easily displaced by biotin because of the stronger affinity of the latter to avidin, and hence, the orange color is restored. This enables the spectrophotometric measurement of biotin levels by detecting the decrease in absorbance at 500 nm as a

result of the release of the dye.[292-294] Additionally, HABA can be used to quantify avidin activity. Figures A-24 and A-25 show the standard calibration curves of avidin and biotin, respectively.

A.8 Figures and Tables

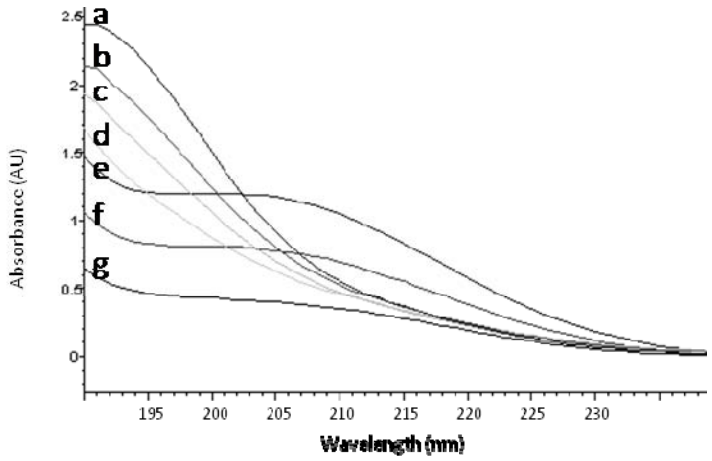

Figure A-1. UV absorbance of 0.01 0.02 0.03 M acetic acid and 0.0125, 0.025, 0.050 and 0.075 M NAG standards (g, f, e, d, c, b and a, respectively).

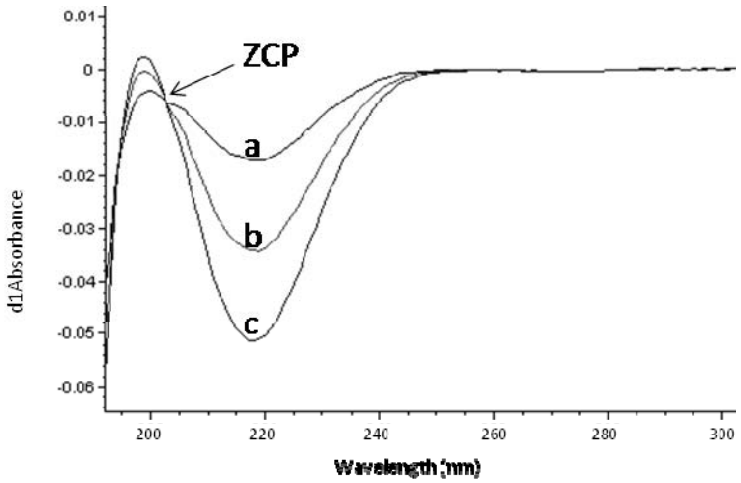

Figure A-2. UV first derivative spectrum showing the zero crossing point (ZCP) of 0.01 0.02 0.03 M acetic acid (a, b and c, respectively).

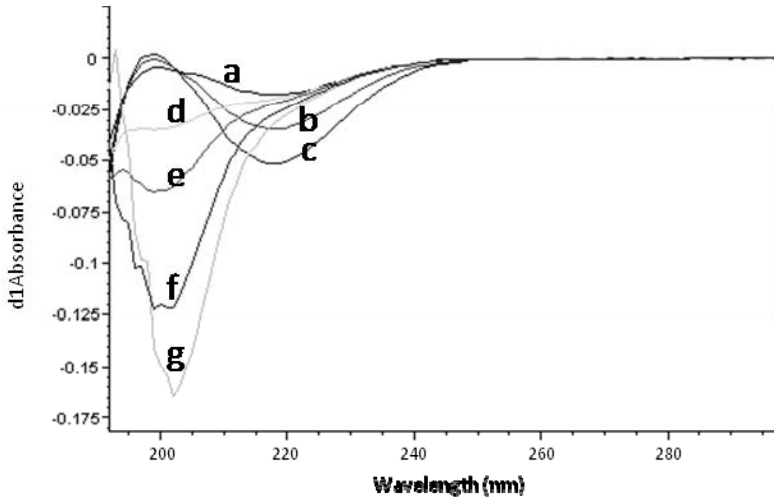

Figure A-3. UV first derivative spectrum of 0.01 0.02 0.03 M acetic acid solutions (a, b and c, respectively), and 0.0125, 0.025, 0.050 and 0.075 M N-acetylglucosamine standards (d, e, f and g, respectively).

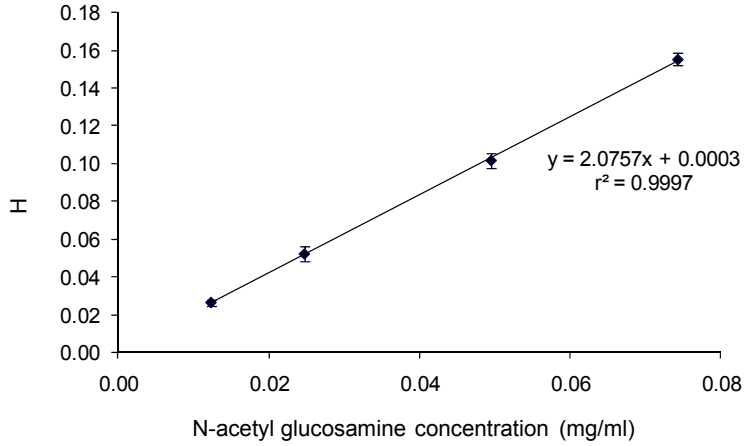

Figure A-4. N-acetyl glucosamine calibration curve showing the height (H), the absolute distance between acetic acid and first derivative curves, versus N-acetyl glucosamine concentration.

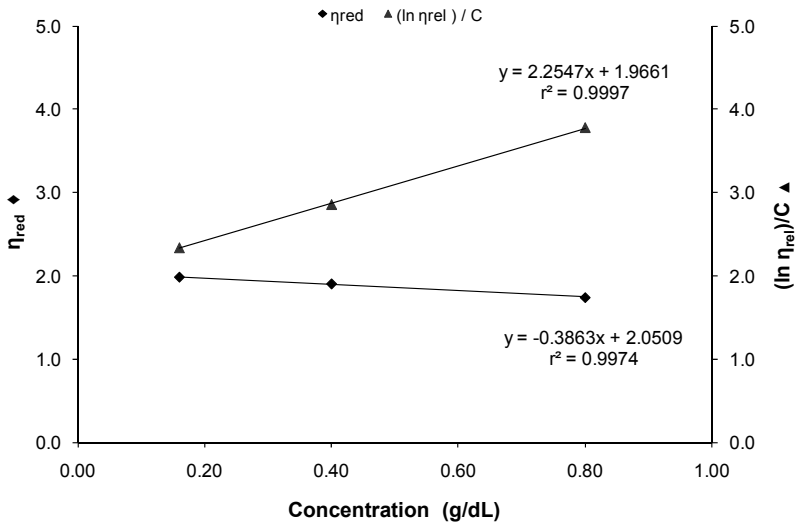

Figure A-5. Reduced viscosity (η_{red}, left y-axis) and (ln η_{rel})/C (right y-axis) vs. concentration of MM-HD chitosan.

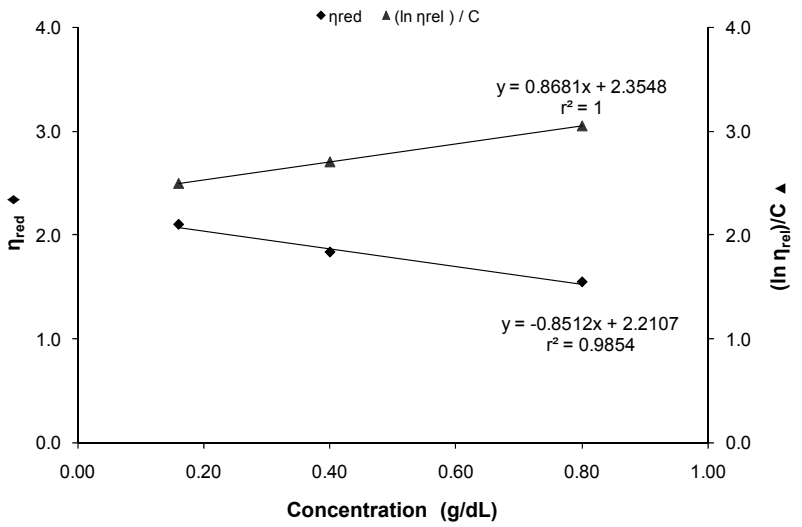

Figure A-6. Reduced viscosity (η_{red}, left y-axis) and (ln η_{rel})/C (right y-axis) vs. concentration of HM-HD chitosan.

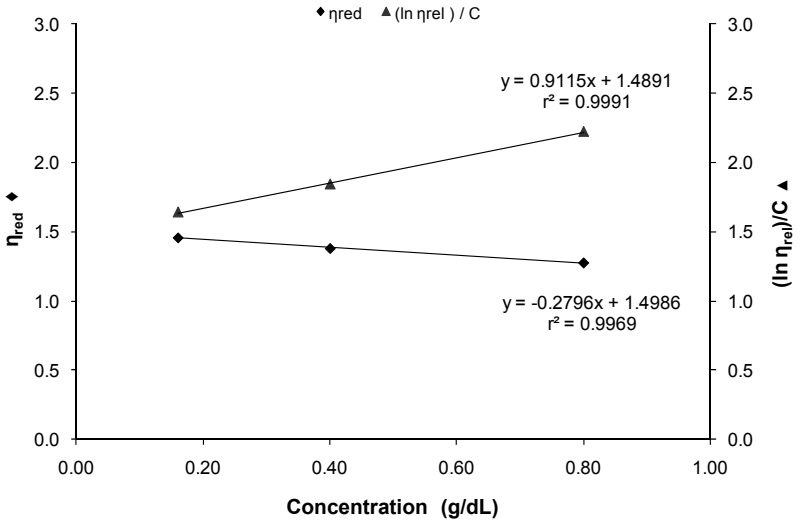

Figure A-7. Reduced viscosity (η_{red}, left y-axis) and (ln η_{rel})/C (right y-axis) vs. concentration of LM-HD chitosan.

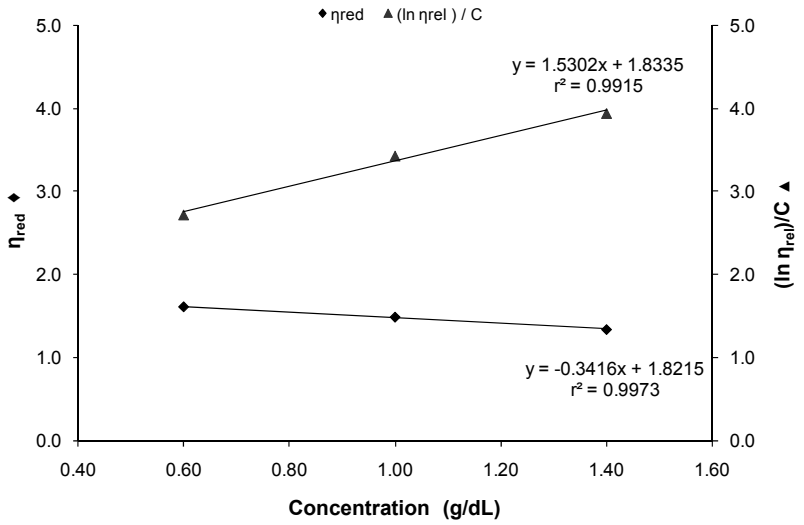

Figure A-8. Reduced viscosity (η_{red}, left y-axis) and (ln η_{rel})/C (right y-axis) vs. concentration of MM-MD chitosan.

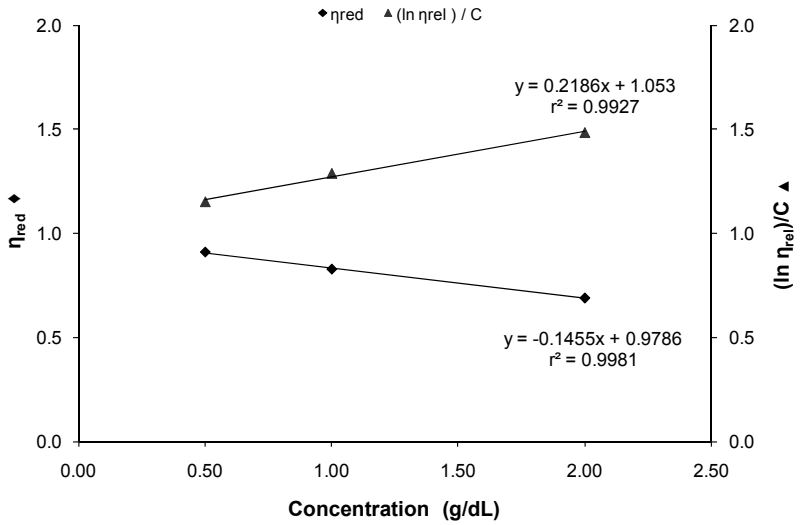

Figure A-9. Reduced viscosity (η_{red}, left y-axis) and (ln η_{rel})/C (right y-axis) vs. concentration of LM-HD OF1% chitosan.

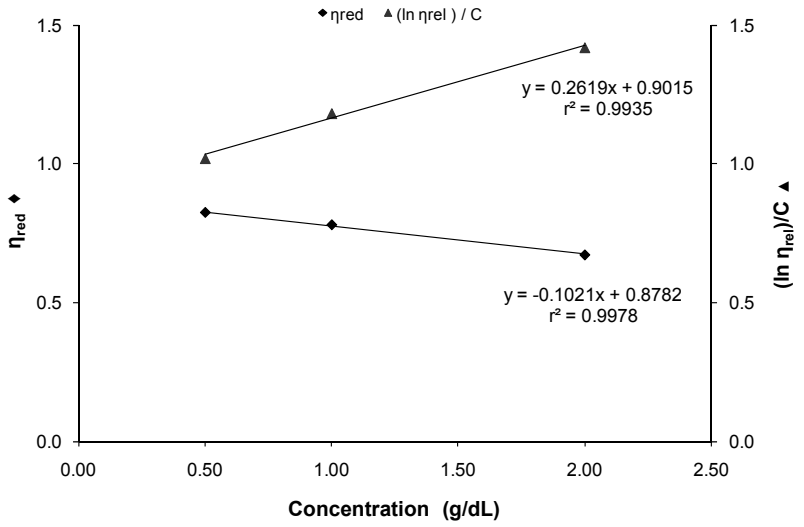

Figure A-10. Reduced viscosity (η_{red}, left y-axis) and (ln η_{rel})/C (right y-axis) vs. concentration of LM-HD OF1.5% chitosan.

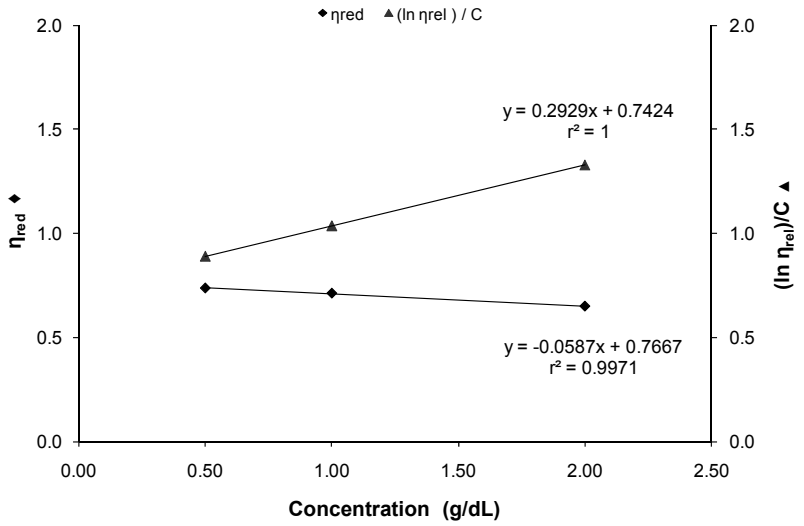

Figure A-11. Reduced viscosity (η_{red}, left y-axis) and (ln η_{rel})/C (right y-axis) vs. concentration of LM-HD OF2% chitosan.

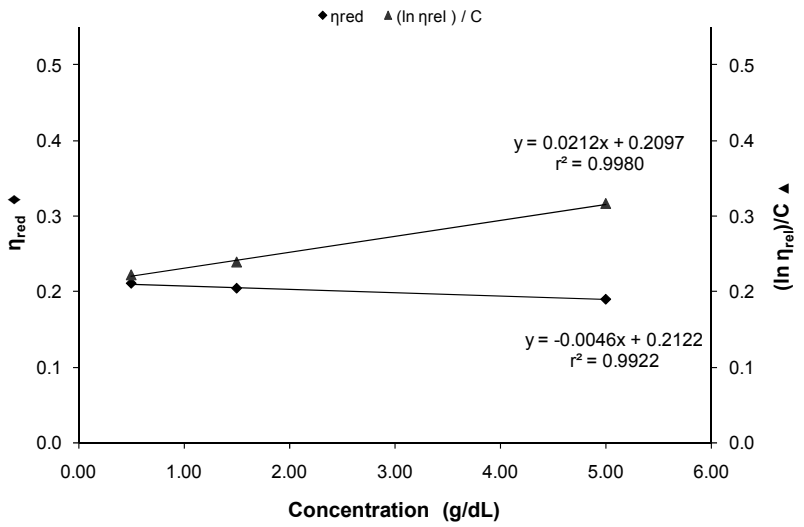

Figure A-12. Reduced viscosity (η_{red}, left y-axis) and (ln η_{rel})/C (right y-axis) vs. concentration of LM-HD OF4% chitosan.

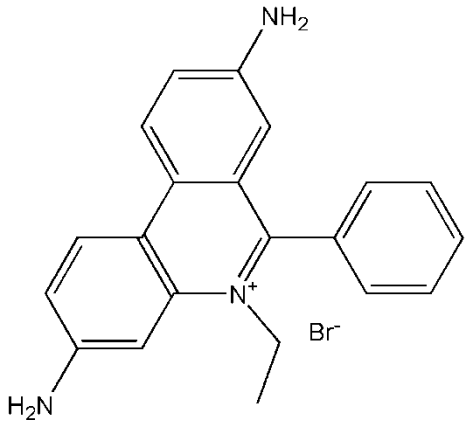

Figure A-13. Molecular structure of ethidium bromide (EtBr).

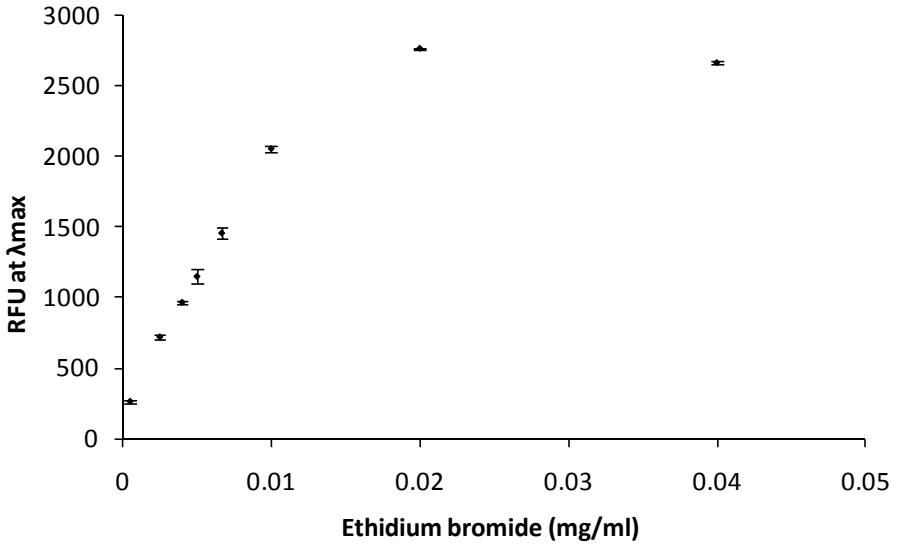

Figure A-14. The effect of ethidium bromide concentration on the relative fluorescence at maximum wave length. DNA concentration was 20.0 µg/ml.

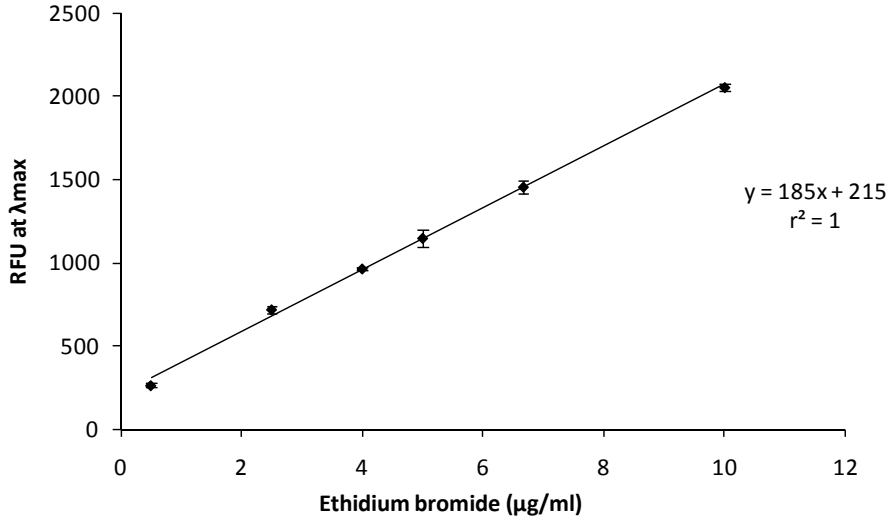

Figure A-15. Linear regression of ethidium bromide concentration vs. relative fluorescence at maximum wave length. DNA concentration was 20.0 µg/ml.

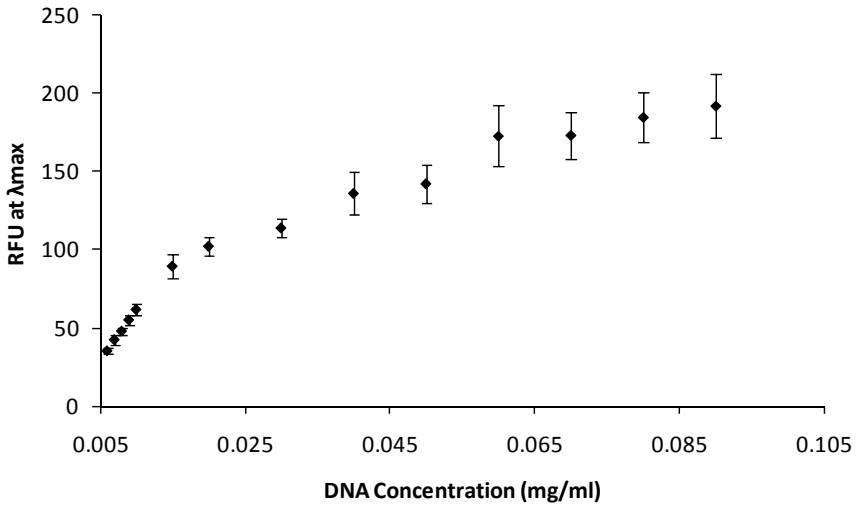

Figure A-16. Calibration curve of the maximum fluorescence intensities of DNA-ethidium bromide at increasing DNA concentrations. Ethidium bromide concentration was 0.5 µg/ml.

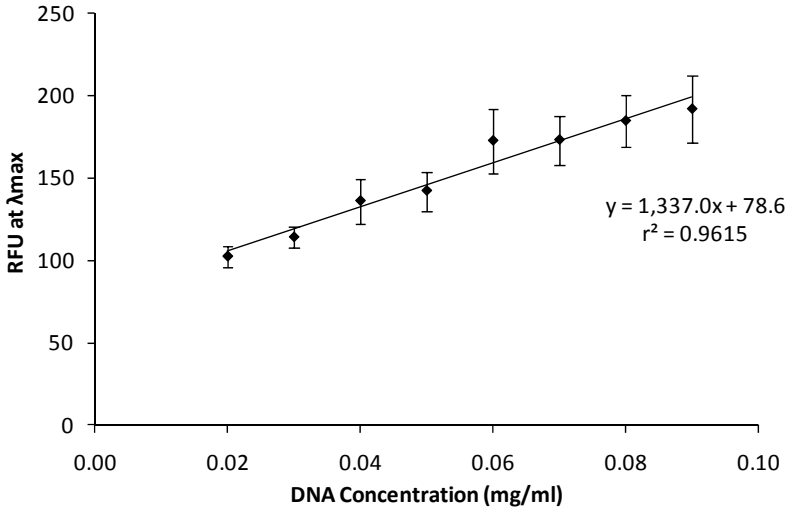

Figure A-17. Linear regression of the calibration curve of the maximum fluorescence intensities of DNA-ethidium bromide at higher concentrations of DNA. Ethidium bromide concentration was 0.5 µg/ml.

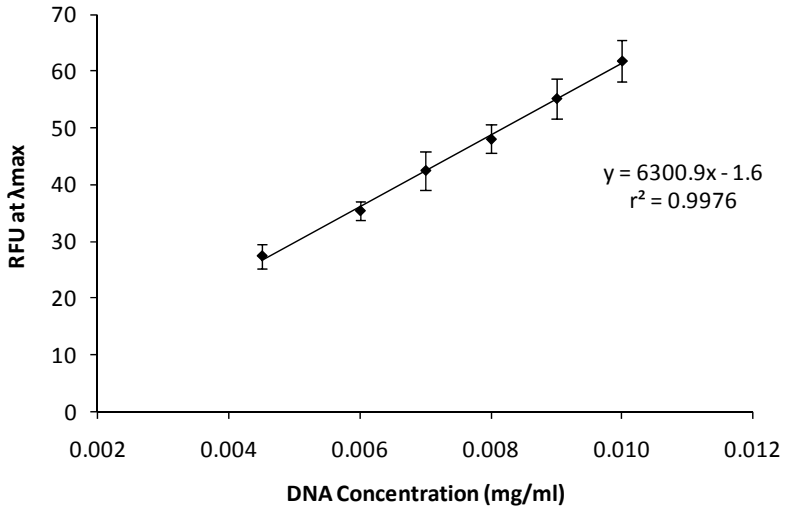

Figure A-18. Linear regression of the calibration curve of the maximum fluorescence intensities of DNA-ethidium bromide at lower concentrations of DNA. Ethidium bromide concentration was 0.5 µg/ml.

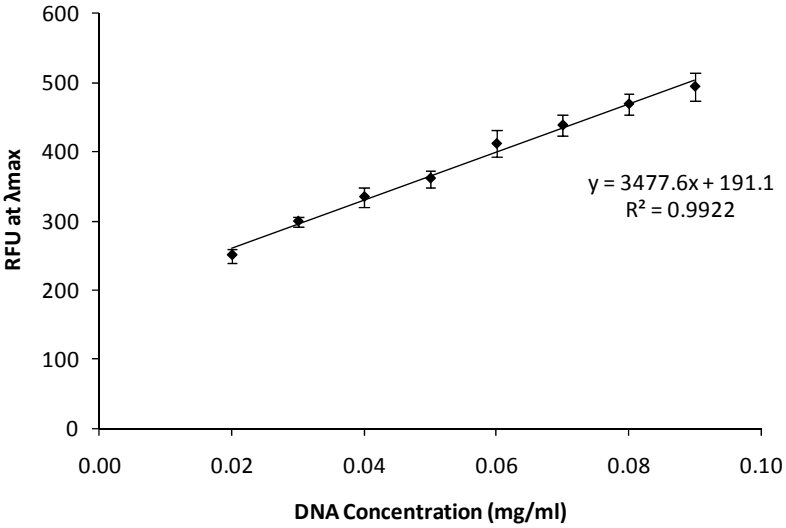

Figure A-19. Linear regression of the calibration curve of the maximum fluorescence intensities of DNA-ethidium bromide at higher concentrations of DNA. Ethidium bromide concentration was 2.5 µg/ml.

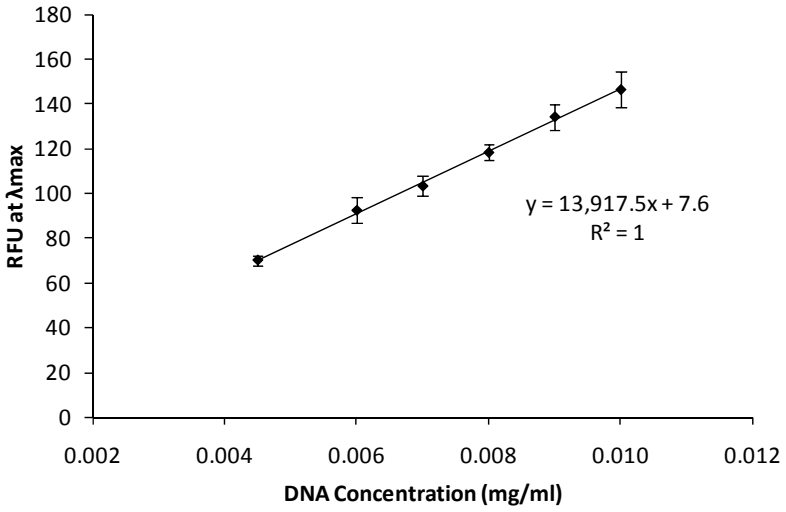

Figure A-20. Linear regression of the calibration curve of the maximum fluorescence intensities of DNA-ethidium bromide at lower concentrations of DNA. Ethidium bromide concentration was 2.5 µg/ml.

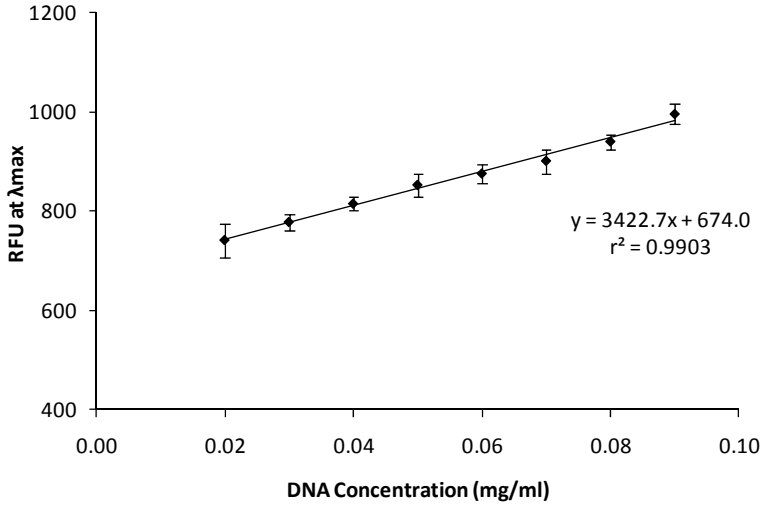

Figure A-21. Linear regression of the calibration curve of the maximum fluorescence intensities of DNA-ethidium bromide at higher concentrations of DNA. Ethidium bromide concentration was 5.0 µg/ml.

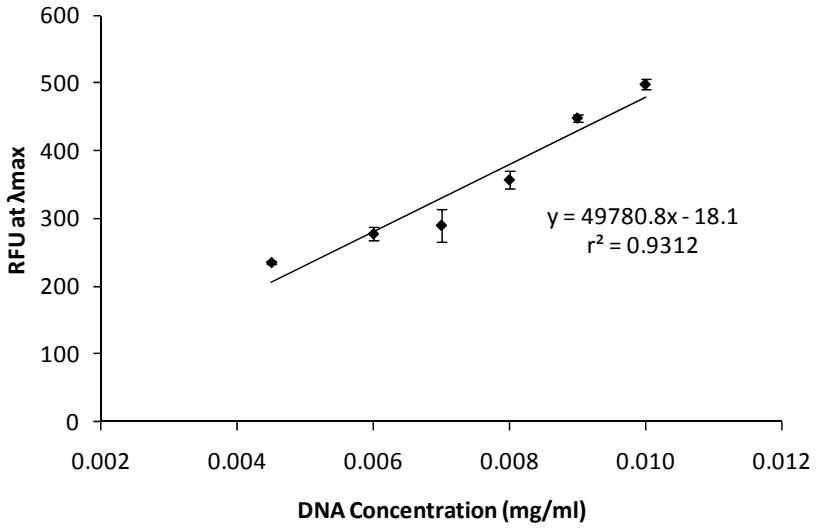

Figure A-22. Linear regression of the calibration curve of the maximum fluorescence intensities of DNA-ethidium bromide at lower concentrations of DNA. Ethidium bromide concentration was 5.0 µg/ml.

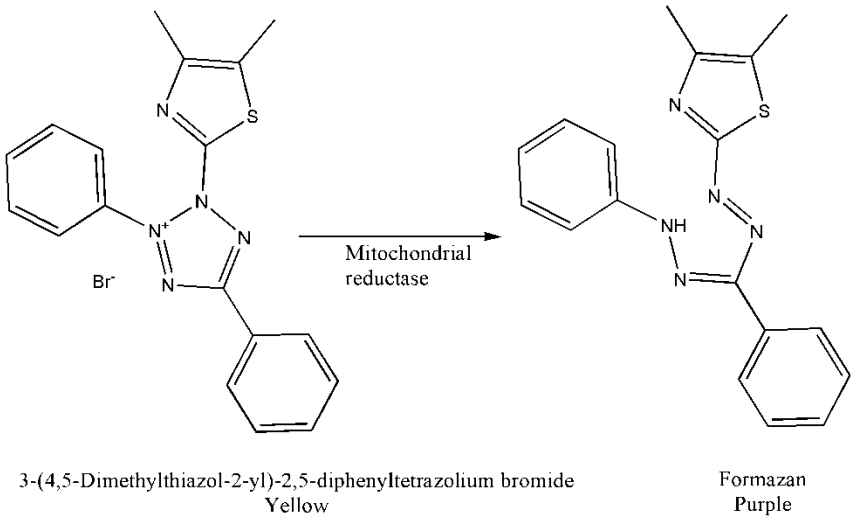

Figure A-23. A scheme representing MTT reduction by mitochondrial reductase.

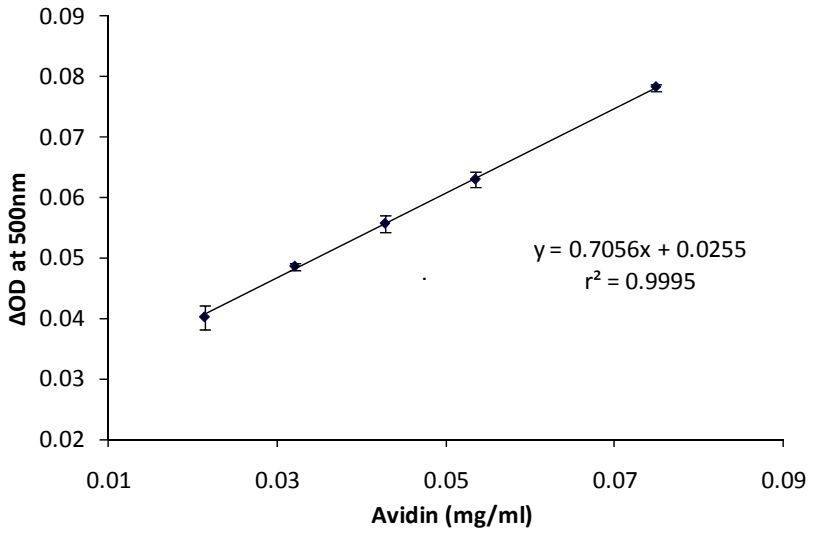

Figure A-24. Avidin activity calibration curve using HABA dye.

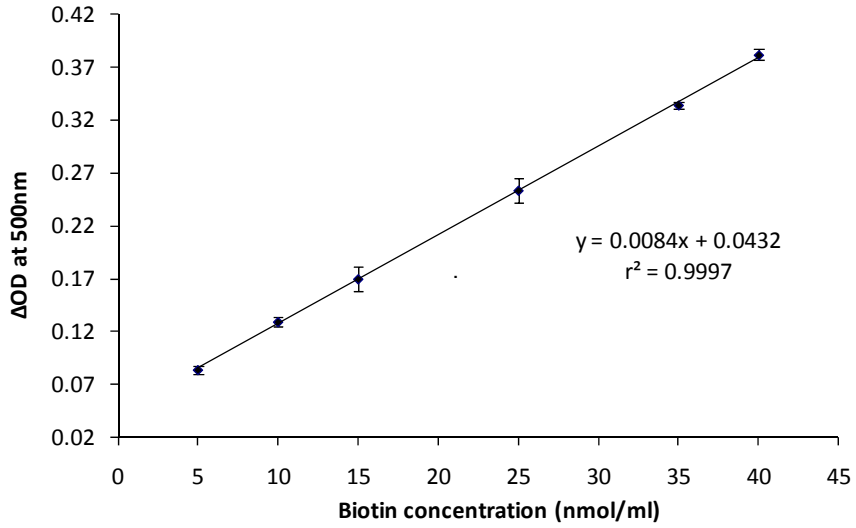

Figure A-25. Biotin activity calibration curve using the HABA/avidin assay.

REFERENCES

1 Scanlon, K.J. (2004) Cancer gene therapy; Challenges and opportunities. *Cancer Gene Therapy* 11 (12), S2

2 Terence, R.F. (2007) Gene therapy: The first two decades and the current state-of-the-art. *Journal of Cellular Physiology* 213 (2), 301-305

3 Anderson, W.F. (1998) Human gene therapy. *Nature* 392 (6679), 25-30

4 Templeton, N.S. (2009) *Gene and cell therapy : Therapeutic mechanisms and strategies*, CRC Press

5 Boulaiz, H. et al. (2005) Non-viral and viral vectors for gene therapy. *Cellular and Molecular Biology* 51 (1), 3-22

6 Maurya, S.K. et al. (2009) Retroviral vectors and gene therapy: An update. *Indian Journal of Biotechnology* 8 (4), 349-357

7 Fukazawa, T. et al. (2010) Adenovirus-mediated cancer gene therapy and virotherapy (Review). *International Journal of Molecular Medicine* 25 (1), 3-10

8 Tang, Y. et al. (2010) AAV-directed muscular dystrophy gene therapy. *Expert Opinion on Biological Therapy* 10 (3), 395-408

9 Yeomans, D.C. and Wilson, S.P. (2009) Herpes virus-based recombinant herpes vectors: gene therapy for pain and molecular tool for pain science. *Gene Therapy* 16 (4), 502-508

10 Nemunaitis, J. (2005) Cancer gene therapy with vaccinia virus. *Minerva Biotecnologica* 17 (2), 77-92

11 Lu, Y. and Madu, C.O. (2010) Viral-based gene delivery and regulated gene expression for targeted cancer therapy. *Expert Opinion on Drug Delivery* 7 (1), 19-35

12 Kohn, D.B. et al. (2003) Occurrence of leukaemia following gene therapy of X-linked SCID. *Nature Reviews Cancer* 3 (7), 477

13 Schmidt-Wolf, G.D. and Schmidt-Wolf, I.G.H. (2003) Non-viral and hybrid vectors in human gene therapy: an update. *Trends in Molecular Medicine* 9 (2), 67-72

14 Gao, X. et al. (2007) Nonviral gene delivery: What we know and what is next. *AAPS Journal* 9 (1), E92-E104

15 Jong, Y. et al. (1997) Controlled release of plasmid DNA. *Journal of Controlled Release* 47 (2), 123-134

16 Al-Dosari, M.S. and Gao, X. (2009) Nonviral gene delivery: Principle, limitations, and recent progress. *AAPS Journal* 11 (4), 671-681

17 Ward, C.M. et al. (2001) Systemic circulation of poly(L-lysine)/DNA vectors is influenced by polycation molecular weight and type of DNA: differential circulation in mice and rats and the implications for human gene therapy. *Blood* 97 (8), 2221-2229

18 Choosakoonkriang, S. et al. (2003) Biophysical characterization of PEI/DNA complexes. *Journal of Pharmaceutical Sciences* 92 (8), 1710-1722

19 Seib, F.P. et al. (2007) Comparison of the endocytic properties of linear and branched PEIs, and cationic PAMAM dendrimers in B16f10 melanoma cells. *Journal of Controlled Release* 117 (3), 291-300

20 Hirko, A. et al. (2003) Cationic lipid vectors for plasmid DNA delivery. *Current Medicinal Chemistry* 10 (14), 1185-1193

21 Panke, S. and Wubbolts, M.G. (2002) Enzyme technology and bioprocess engineering. *Current Opinion in Biotechnology* 13 (2), 111-116

22 Guisan, J.M. (2006) *Immobilization of enzymes and cells*, Humana Press

23 Sheldon, R.A. (2007) Enzyme immobilization: The quest for optimum performance. *Advanced Synthesis & Catalysis* 349 (8-9), 1289-1307

24 Mateo, C. et al. (2007) Improvement of enzyme activity, stability and selectivity via immobilization techniques. *Enzyme and Microbial Technology* 40 (6), 1451-1463

25 Xie, T. et al. (2009) Recent advance in the support and technology used in enzyme immobilization. *African Journal of Biotechnology* 8 (19), 4724-4733

26 Kim, J.B. et al. (2008) Nanobiocatalysis and its potential applications. *Trends in Biotechnology* 26 (11), 639-646

27 Kim, J. et al. (2006) Nanostructures for enzyme stabilization. *Chemical Engineering Science* 61 (3), 1017-1026

28 Bora, U. et al. (2006) Photoreactive cellulose membrane - A novel matrix for covalent immobilization of biomolecules. *Journal of Biotechnology* 126 (2), 220-229

29 Tanaka, Y. et al. (2007) Exploring enzymatic catalysis at a solid surface: a case study with transglutaminase-mediated protein immobilization. *Organic & Biomolecular Chemistry* 5 (11), 1764-1770

30 van Langen, L.M. et al. (2002) Active site titration as a tool for the evaluation of immobilization procedures of penicillin acylase. *Biotechnology and Bioengineering* 79 (2), 224-228

31 Kobayash.T and Laidler, K.J. (1973) Kinetic analysis for solid-supported enzymes. *Biochimica Et Biophysica Acta* 302 (1), 1-12

32 Balcao, V.M. et al. (2001) Coimmobilization of L-asparaginase and glutamate dehydrogenases onto highly activated supports. *Enzyme and Microbial Technology* 28 (7-8), 696-704

33 Turkova, J. (1999) Oriented immobilization of biologically active proteins as a tool for revealing protein interactions and function. *Journal of Chromatography B* 722 (1-2), 11-31

34 Holland-Nell, K. and Beck-Sickinger, A.G. (2007) Specifically immobilised aldo/keto reductase AKR1A1 shows a dramatic increase in activity relative to the randomly immobilised enzyme. *Chembiochem* 8 (9), 1071-1076

35 Zhang, J.K. and Cass, A.E.G. (2006) Kinetic study of site directed and randomly immobilized his-tag alkaline phosphatase by flow injection chemiluminescence. *Journal of Molecular Recognition* 19 (3), 243-246

36 Wang, J.Q. et al. (2001) Improving the activity of immobilized subtilisin by site-directed attachment through a genetically engineered affinity tag. *Fresenius Journal of Analytical Chemistry* 369 (3-4), 280-285

37 Liu, J.L. et al. (2001) Activity studies of immobilized subtilisin on functionalized pure cellulose-based membranes. *Biotechnology Progress* 17 (5), 866-871

38 Richter, M.P.O. and Beck-Sickinger, A.G. (2005) Expressed protein ligation to obtain selectively modified Aldo/Keto reductases. *Protein and Peptide Letters* 12 (8), 777-781

39 Jang, J.H. and Shea, L.D. (2003) Controllable delivery of non-viral DNA from porous scaffolds. *Journal of Controlled Release* 86 (1), 157-168

40 Jang, J.H. et al. (2004) Gene delivery from polymer scaffolds for tissue engineering. *Expert Review of Medical Devices* 1 (1), 127-138

41 Kim, S.E. et al. (2003) Porous chitosan scaffold containing microspheres loaded with transforming growth factor-beta 1: Implications for cartilage tissue engineering. *Journal of Controlled Release* 91 (3), 365-374

42 Lee, J.E. et al. (2004) Effects of a chitosan scaffold containing TGF-beta 1 encapsulated chitosan microspheres on in vitro chondrocyte culture. *Artificial Organs* 28 (9), 829-839

43 Jang, J.H. et al. (2005) Plasmid delivery in vivo from porous tissue-engineering scaffolds: Transgene expression and cellular Transfection. *Molecular Therapy* 12 (3), 475-483

44 Reis, R.L. and San Román, J. (2005) *Biodegradable systems in tissue engineering and regenerative medicine*, CRC Press

45 Matoka, D.J. and Cheng, E.Y. (2009) Tissue engineering in urology. *Canadian Urological Association Journal* 3 (5), 403-408

46 Saber, S.E.-D.M. (2009) Tissue engineering in endodontics. *Journal of Oral Science* 51 (4), 495-507

47 Tyagi, P. and Dhindsa, M.K. (2009) Tissue engineering and its implications in dentistry. *Indian Journal of Dental Research* 20 (2), 222-226

48 Bottcher-Haberzeth, S. et al. (2010) Tissue engineering of skin. *Burns* 36 (4), 450-460

49 Asnaghi, A. et al. (2009) Tissue engineering toward organ replacement: a promising approach in airway transplant. *International Journal of Artificial Organs* 32 (11), 763-768

50 Fiegel, H.C. et al. (2009) Development of hepatic tissue engineering. *Pediatric Surgery International* 25 (8), 667-673

51 Pelttari, K. et al. (2009) Do we really need cartilage tissue engineering? *Swiss Medical Weekly* 139 (41-42), 602-609

52 Sacks, M.S. et al. (2009) Bioengineering challenges for heart valve tissue engineering. *Annual Review of Biomedical Engineering* 11, 289-313

53 Ikada, Y. (2006) *Tissue engineering : Fundamentals and applications*, Academic Press/Elsevier

54 Jolláes, P. and Muzzarelli, R.A.A. (1999) *Chitin and chitinases*, Birkhèauser Verlag

55 Kas, H.S. (1997) Chitosan: properties, preparations and application to microparticulate systems. *Journal of Microencapsulation* 14 (6), 689-711

56 Singla, A.K. and Chawla, M. (2001) Chitosan: some pharmaceutical and biological aspects - an update. *Journal of Pharmacy and Pharmacology* 53 (8), 1047-1067

57 Dumitriu, S. (2002) *Polymeric biomaterials*, Marcel Dekker, Inc.

58 Chung, T.W. et al. (2003) Growth of human endothelial cells on different concentrations of Gly-Arg-Gly-Asp grafted chitosan surface. *Artificial Organs* 27 (2), 155-161

59 Kurita, K. et al. (1977) Studies on chitin, .4. Evidence for formation of block and random copolymers of N-acetyl-D-glucosamine and D-glucosamine by heterogeneous and homogeneous hydrolyses *Macromolecular Chemistry and Physics* 178 3197

60 Varum, K.M. et al. (1991) High-field NMR-spectroscopy of partially N-deacetylated chitins (chitosans) .3. C-13-NMR studies of the acetylation sequences in partially N-deacetylated chitins (chitosans). *Carbohydrate Research* 217, 19-27

61 Araki, Y. and Ito, E. (1975) Pathway of chitosan formation in Mucor-Rouxii - enzymatic deacetylation of chitin. *European Journal of Biochemistry* 55, 71-78

62 Nordtveit, R.J. et al. (1996) Degradation of partially N-acetylated chitosans with hen egg white and human lysozyme. *Carbohydrate Polymers* 29 (2), 163-167

63 Lee, K.Y. et al. (1995) Blood compatibility and biodegradability of partially N-acylated chitosan derivatives. *Biomaterials* 16 (16), 1211-1216

64 Aiba, S. (1992) Studies on chitosan .4. lysozymic hydrolysis of partially N-acetylated chitosans. *International Journal of Biological Macromolecules* 14 (4), 225-228

65 Pangburn, S.H. et al. (1982) Lysozyme degradation of partially deacetylated chitin, its films and hydrogels. *Biomaterials* 3 (2), 105-108

66 Tomihata, K. and Ikada, Y. (1997) In vitro and in vivo degradation of films of chitin and its deacetylated derivatives. *Biomaterials* 18 (7), 567-575

67 Griffon, D.J. et al. (2006) Chitosan scaffolds: Interconnective pore size and cartilage engineering. *Acta Biomaterialia* 2 (3), 313-320

68 Seyrek, E. and Dubin, P. (2010) Glycosaminoglycans as polyelectrolytes. *Advances in Colloid and Interface Science* 158 (1-2), 119-129

69 Hirano, S. (1996) Chitin biotechnology applications. *Biotechnology Annual Review* 2, 237-258

70 Struszczyk, M.H. (2002) Chitin and chitosan - Part II. Applications of chitosan. *Polimery* 47 (6), 396-403

71 Agnihotri, S.A. et al. (2004) Recent advances on chitosan-based micro- and nanoparticles in drug delivery. *Journal of Controlled Release* 100 (1), 5-28

72 Bumgardner, J.D. et al. (2003) Contact angle, protein adsorption and osteoblast precursor cell attachment to chitosan coatings bonded to titanium. *Journal of Biomaterials Science-Polymer Edition* 14 (12), 1401-1409

73 Ueno, H. et al. (2001) Evaluation effects of chitosan for the extracellular matrix production by fibroblasts and the growth factors production by macrophages. *Biomaterials* 22 (15), 2125-2130

74 Sechriest, V.F. et al. (1999) GAG-augmented polysaccharide hydrogel: A novel biocompatible and biodegradable material to support chondrogenesis. *Journal of Biomedical Materials Research* 49 (4), 534-541

75 Lahiji, A. et al. (2000) Chitosan supports the expression of extracellular matrix proteins in human osteoblasts and chondrocytes. *Journal of Biomedical Materials Research Part A* 51 (4), 586-595

76 Nettles, D.L. et al. (2002) Potential use of chitosan as a cell scaffold material for cartilage tissue engineering. *Tissue Engineering* 8 (6), 1009-1016

77 Lee, Y.M. et al. (2000) Tissue engineered bone formation using chitosan/tricalcium phosphate sponges. *Journal of Periodontology* 71 (3), 410-417

78 Bumgardner, J.D. et al. (2003) Chitosan: potential use as a bioactive coating for orthopaedic and craniofacial/dental implants. *Journal of Biomaterials Science-Polymer Edition* 14 (5), 423-438

79 Lamarque, G. et al. (2005) Physicochemical behavior of homogeneous series of acetylated chitosans in aqueous solution: role of various structural parameters. *Biomacromolecules* 6 (1), 131-142

80 Tsukada, S. and Inoue, Y. (1981) Conformational properties of chito-oligosaccharides - titration, optical-rotation, and C-13 NMR-studies of chito-oligosaccharides. *Carbohydrate Research* 88 (1), 19-38

81 Ottoy, M.H. et al. (1996) Compositional heterogeneity of heterogeneously deacetylated chitosans. *Carbohydrate Polymers* 29 (1), 17-24

82 Kiang, T. et al. (2004) The effect of the degree of chitosan deacetylation on the efficiency of gene transfection. *Biomaterials* 25 (22), 5293-5301

83 Huang, M. et al. (2004) Uptake and cytotoxicity of chitosan molecules and nanoparticles: Effects of molecular weight and degree of deacetylation. *Pharmaceutical Research* 21 (2), 344-353

84 Prasitsilp, M. et al. (2000) Cellular responses to chitosan in vitro: The importance of deacetylation. *Journal of Materials Science: Materials in Medicine* 11 (12), 773-778

85 Chellat, F. et al. (2000) Study of biodegradation behavior of chitosan-xanthan microspheres in simulated physiological media. *Journal of Biomedical Materials Research* 53 (5), 592-599

86 Allan, G.G. and Peyron, M. (1995) Molecular-weight manipulation of chitosan .1. Kinetics of depolymerization by nitrous-acid. *Carbohydrate Research* 277 (2), 257-272

87 Tokura, S. et al. (1997) Molecular weight dependent antimicrobial activity by chitosan. *Macromolecular Symposia* 120, 1-9

88 Allan, G.G. and Peyron, M. (1995) Molecular-weight manipulation of chitosan .2. Prediction and control of extent of depolymerization by nitrous-acid. *Carbohydrate Research* 277 (2), 273-282

89 Koping-Hoggard, M. et al. (2003) Relationship between the physical shape and the efficiency of oligomeric chitosan as a gene delivery system in vitro and in vivo. *Journal of Gene Medicine* 5 (2), 130-141

90 Zhang, H. and Neau, S.H. (2001) In vitro degradation of chitosan by a commercial enzyme preparation: effect of molecular weight and degree of deacetylation. *Biomaterials* 22 (12), 1653-1658

91 Dhulipala, V.C. et al. (2005) Secalonic acid D blocks embryonic palatal mesenchymal cell-cycle by altering the activity of CDK2 and the expression of p2l and cyclin E. *Birth Defects Research Part B: Developmental and Reproductive Toxicology* 74 (3), 233-242

92 Mourya, V.K. and Inamdar, N.N. (2008) Chitosan-modifications and applications: Opportunities galore. *Reactive & Functional Polymers* 68 (6), 1013-1051

93 Jiang, X. et al. (2006) Chitosan-g-PEG/DNA complexes deliver gene to the rat liver via intrabiliary and intraportal infusions. *Journal of Gene Medicine* 8 (4), 477-487

94 Vold, I.M.N. and Christensen, B.E. (2005) Periodate oxidation of chitosans with different chemical compositions. *Carbohydrate Research* 340 (4), 679-684

95 Jiang, H.L. et al. (2007) Chitosan-graft-polyethylenimine as a gene carrier. *Journal of Controlled Release* 117 (2), 273-280

96 Kean, T. et al. (2005) Trimethylated chitosans as non-viral gene delivery vectors: Cytotoxicity and transfection efficiency. *Journal of Controlled Release* 103 (3), 643-653

97 Park, I.K. et al. (2003) Galactosylated chitosan (GC)-graft-poly(vinyl pyrrolidone) (PVP) as hepatocyte-targeting DNA carrier Preparation and physicochemical characterization of GC-graft-PVP/DNA complex (1). *Journal of Controlled Release* 86 (2-3), 349-359

98 Park, I.K. et al. (2003) Galactosylated chitosan as a synthetic extracellular matrix for hepatocytes attachment. *Biomaterials* 24 (13), 2331-2337

99 Park, I.K. et al. (2001) Galactosylated chitosan-graft-poly(ethylene glycol) as hepatocyte-targeting DNA carrier. *Journal of Controlled Release* 76 (3), 349-362

100 Leroux, J.C. et al. (1996) Biodegradable nanoparticles - From sustained release formulations to improved site specific drug delivery. *Journal of Controlled Release* 39 (2-3), 339-350

101 Kim, T.H. et al. (2006) Mannosylated chitosan nanoparticle-based cytokine gene therapy suppressed cancer growth in BALB/c mice bearing CT-26 carcinoma cells. *Molecular Cancer Therapeutics* 5 (7), 1723-1732

102 Kim, T.H. et al. (2006) Receptor-mediated gene delivery into antigen presenting cells using mannosylated chitosan/DNA nanoparticles. *Journal of Nanoscience and Nanotechnology* 6 (9-10), 2796-2803

103 Hashimoto, M. et al. (2006) Gene transfer by DNA/mannosylated chitosan complexes into mouse peritoneal macrophages. *Biotechnology Letters* 28 (11), 815-821

104 Lee, K.Y. et al. (1998) Preparation of chitosan self-aggregates as a gene delivery system. *Journal of Controlled Release* 51 (2-3), 213-220

105 Kim, Y.H. et al. (2001) Structural characteristics of size-controlled self-aggregates of deoxycholic acid-modified chitosan and their application as a DNA delivery carrier. *Bioconjugate Chemistry* 12 (6), 932-938

106 Kim, K. et al. (2005) Physicochemical characterizations of self-assembled nanoparticles of glycol chitosan-deoxycholic acid conjugates. *Biomacromolecules* 6 (2), 1154-1158

107 Chae, S.Y. et al. (2005) Deoxycholic acid-conjugated chitosan oligosaccharide nanoparticles for efficient gene carrier. *Journal of Controlled Release* 109 (1-3), 330-344

108 Son, S.H. et al. (2004) Preparation of a hydrophobized chitosan oligosaccharide for application as an efficient gene carrier. *Macromolecular Research* 12 (6), 573-580

109 Liu, W.G. et al. (2003) N-alkylated chitosan as a potential nonviral vector for gene transfection. *Bioconjugate Chemistry* 14 (4), 782-789

110 Yoo, H.S. et al. (2005) Self-assembled nanoparticles containing hydrophobically modified glycol chitosan for gene delivery. *Journal of Controlled Release* 103 (1), 235-243

111 Kwon, S. et al. (2003) Physicochemical characteristics of self-assembled nanoparticles based on glycol chitosan bearing 5 beta-cholanic acid. *Langmuir* 19 (24), 10188-10193

112 Hu, F.Q. et al. (2006) A novel chitosan oligosaccharide-stearic acid micelles for gene delivery: Properties and in vitro transfection studies. *International Journal of Pharmaceutics* 315 (1-2), 158-166

113 Wan, Y. et al. (2008) Preparation and mechanical properties of poly(chitosan-g-DL-lactic acid) fibrous mesh scaffolds. *Polymers for Advanced Technologies* 19 (2), 114-123

114 Raabe, D. et al. (2007) Preferred crystallographic texture of alpha-chitin as a microscopic and macroscopic design principle of the exoskeleton of the lobster Homarus americanus. *Acta Biomaterialia* 3, 882-895

115 Kim, I.Y. et al. (2008) Chitosan and its derivatives for tissue engineering applications. *Biotechnology Advances* 26 (1), 1-21

116 Muzzarelli, C. and Muzzarelli, R.A.A. (2002) Natural and artificial chitosan-inorganic composites. *Journal of Inorganic Biochemistry* 92 (2), 89-94

117 Hein, S. et al. (2008) Chitosan composites for biomedical applications: status, challenges and perspectives. *Materials Science and Technology* 24 (9), 1053-1061

118 Li, X.N. et al. (2010) Synthesis and Characterization of Core-shell Hydroxyapatite/chitosan Biocomposite Nanospheres. *Journal of Wuhan University of Technology-Materials Science Edition* 25 (2), 252-256

119 Wilson, O.C. and Hull, J.R. (2008) Surface modification of nanophase hydroxyapatite with chitosan. *Materials Science and Engineering C-Biomimetic and Supramolecular Systems* 28 (3), 434-437

120 Krayukhina, M.A. et al. (2008) Polyelectrolyte complexes of chitosan: formation, properties, and applications. *Uspekhi Khimii* 77 (9), 854-869

121 Drogoz, A. et al. (2007) Polyelectrolyte complexes from polysaccharides: Formation and stoichiometry monitoring. *Langmuir* 23 (22), 10950-10958

122 Dautzenberg, H. et al. (1996) Stoichiometry and structure of polyelectrolyte complex particles in diluted solutions. pp. 1024-1032, Vch Publishers Inc

123 Alatorre-Meda, M. et al. (2009) DNA-chitosan complexation: A dynamic light scattering study. *Colloids and Surfaces A-Physicochemical and Engineering Aspects* 339 (1-3), 145-152

124 Zhao, Q. et al. (2009) Synthesis and characterization of soluble chitosan/sodium carboxymethyl cellulose polyelectrolyte complexes and the pervaporation dehydration of their homogeneous membranes. *Journal of Membrane Science* 333 (1-2), 68-78

125 Naidu, V.G.M. et al. (2009) Polyelectrolyte complexes of gum kondagogu and chitosan, as diclofenac carriers. *Carbohydrate Polymers* 76 (3), 464-471

126 Li, X.X. et al. (2009) Characterization and biodegradation of chitosan-alginate polyelectrolyte complexes. *Polymer Degradation and Stability* 94 (1), 1-6

127 Hong, H.J. et al. (2008) Accelerated wound healing by smad3 antisense oligonucleotides-impregnated chitosan/alginate polyelectrolyte complex. *Biomaterials* 29 (36), 4831-4837

128 Rao, K. et al. (2008) Synthesis and characterization of poly(acrylamidoglycolic acid) grafted onto chitosan and its polyelectrolyte complexes with hydroxyapatite. *Reactive and Functional Polymers* 68 (5), 943-953

129 De Oliveira, H.C.L. et al. (2008) Chitosan-poly(acrylic acid) polyelectrolyte complex membranes: preparation, characterization and permeability studies. *Journal of Biomaterials Science-Polymer Edition* 19 (2), 143-160

130 Bigucci, F. et al. (2008) Chitosan/pectin polyelectrolyte complexes: Selection of suitable preparative conditions for colon-specific delivery of vancomycin. *European Journal of Pharmaceutical Sciences* 35 (5), 435-441

131 Kim, S.J. et al. (2004) Synthesis and characteristics of polyelectrolyte complexes composed of chitosan and hyaluronic acid. *Journal of Applied Polymer Science* 91 (5), 2908-2913

132 Fukuda, H. and Kikuchi, Y. (1978) In vitro clot formation on polyelectrolyte complexes of sodium dextran sulfate with chitosan. *Journal of Biomedical Materials Research* 12 (4), 531-539

133 Ii'ina, A.V. and Varlamov, V.P. (2005) Chitosan-based polyelectrolyte complexes: A review. *Applied Biochemistry and Microbiology* 41 (1), 5-11

134 Mao, H.Q. et al. (2001) Chitosan-DNA nanoparticles as gene carriers: synthesis, characterization and transfection efficiency. *Journal of Controlled Release* 70 (3), 399-421

135 Lopez-Leon, T. et al. (2005) Physicochemical characterization of chitosan nanoparticles: electrokinetic and stability behavior. *Journal of Colloid and Interface Science* 283 (2), 344-351

136 Huang, Y. et al. (2005) In vitro characterization of chitosan-gelatin scaffolds for tissue engineering. *Biomaterials* 26 (36), 7616-7627

137 Xia, W.Y. et al. (2004) Tissue engineering of cartilage with the use of chitosan-gelatin complex scaffolds. *Journal of Biomedical Materials Research Part B-Applied Biomaterials* 71B (2), 373-380

138 Hsieh, C.Y. et al. (2005) Preparation of gamma-PGA/chitosan composite tissue engineering matrices. *Biomaterials* 26 (28), 5617-5623

139 Peng, L. et al. (2006) Preparation and evaluation of porous chitosan/collagen scaffolds for periodontal tissue engineering. *Journal of Bioactive and Compatible Polymers* 21 (3), 207-220

140 Li, Z.S. and Zhang, M.Q. (2005) Chitosan-alginate as scaffolding material for cartilage tissue engineering. *Journal of Biomedical Materials Research Part A* 75A (2), 485-493

141 Kim, T.H. et al. (2007) Chemical modification of chitosan as a gene carrier in vitro and in vivo. *Progress in Polymer Science* 32 (7), 726-753

142 Fukuda, H. and Kikuchi, Y. (1977) Polyelectrolyte complexes of sodium dextran sulfate with chitosan, .2. *Makromolekulare Chemie-Macromolecular Chemistry and Physics* 178 (10), 2895-2899

143 Kabanov, V.A. and Zezin, A.B. (1984) Soluble interpolymeric complexes as a new class of synthetic poly-electrolytes. *Pure and Applied Chemistry* 56 (3), 343-354

144 Chen, Y. et al. (2003) Chitosan-dextran sulfate nanoparticles for delivery of an anti-angiogenesis peptide. *Letters in Peptide Science* 10 (5-6), 621-629

145 Chen, Y. et al. (2008) Development of a chitosan-based nanoparticle formulation for delivery of a hydrophilic hexapeptide, dalargin. *Biopolymers* 90 (5), 663-670

146 Huang, M. and Berkland, C. (2009) Controlled release of repifermin (R) from polyelectrolyte complexes stimulates endothelial cell proliferation. *Journal of Pharmaceutical Sciences* 98 (1), 268-280

147 Drogoz, A. et al. (2008) Towards biocompatible vaccine delivery systems: Interactions of colloidal PECs based on polysaccharides with HIV-1 p24 antigen. *Biomacromolecules* 9 (2), 583-591

148 Sarmento, B. et al. (2007) Oral bioavailability of insulin contained in polysaccharide nanoparticles. *Biomacromolecules* 8 (10), 3054-3060

149 Tiyaboonchai, W. and Limpeanchob, N. (2007) Formulation and characterization of amphotericin B-chitosan-dextran sulfate nanoparticles. *International Journal of Pharmaceutics* 329 (1-2), 142-149

150 O'Neil, M.J. (2001) *The Merck index : an encyclopedia of chemicals, drugs, and biologicals*, Merck

151 Crisp, G.T. and Jiang, Y.L. (2001) Intramolecular hydrogen bonding of (+)-biotin and biotin derivatives in organic solvents. *Arkivoc* 2

152 Musashi, Y. et al. (1995) Structure and bonding nature of carboxyimidazolidone, a model of carboxybiotin - Ab-Initio Mo/Mp4, Sd-Ci, and Ccd studies. *Journal of the American Chemical Society* 117 (45), 11320-11326

153 Wood, H.G. and Kumar, G.K. (1985) Transcarboxylase - its quaternary structure and the role of the biotinyl subunit in the assembly of the enzyme and in catalysis. *Annals of the New York Academy of Sciences* 447 (JUN), 1-22

154 Savage, D. et al. (1992) *Avidin-biotin chemistry: A handbook*, Pierce Chemical Co

155 Lim, S.C. et al. (2009) Fabrication and characterization of an OTFT-based biosensor using a biotinylated F8T2 polymer. *ETRI Journal* 31 (6), 647-652

156 Diamandis, E.P. and Christopoulos, T.K. (1991) The biotin (strept)avidin system - principles and applications in biotechnology. *Clinical Chemistry* 37 (5), 625-636

157 Lesch, H.P. et al. (2010) Avidin-biotin technology in targeted therapy. *Expert Opinion on Drug Delivery* 7 (5), 551-564

158 Clapper, J.D. et al. (2008) Biotinylated biodegradable nanotemplated hydrogel networks for cell interactive applications. *Biomacromolecules* 9 (4), 1188-1194

159 Meng, Q.B. et al. (2007) Aggregation of biotinylated polymeric microspheres induced by interaction with avidin. *Pure and Applied Chemistry* 79 (9), 1575-1582

160 Xiong, M.P. et al. (2007) Biotin-triggered release of poly(ethylene glycol)-avidin from biotinylated polyethylenimine enhances in vitro gene expression. *Bioconjugate Chemistry* 18 (3), 746-753

161 Ben-Shabat, S. et al. (2006) PEG-PLA block copolymer as potential drug carrier: Preparation and characterization. *Macromolecular Bioscience* 6 (12), 1019-1025

162 Salem, A.K. et al. (2001) Synthesis and characterisation of a degradable poly(lactic acid)-poly(ethylene glycol) copolymer with biotinylated end groups. *Biomacromolecules* 2 (2), 575-580

163 Shi, X.W. et al. (2008) Chitosan biotinylation and electrodeposition for selective protein assembly. *Macromolecular Bioscience* 8 (5), 451-457

164 Li, S. and Huang, L. (2000) Nonviral gene therapy: promises and challenges. *Gene Therapy* 7 (1), 31-34

165 Mancheno-Corvo, P. and Martin-Duque, P. (2006) Viral gene therapy. *Clinical and Translational Oncology* 8 (12), 858-867

166 Fu, H.L. et al. (2009) Biodegradable polymers for controlled release of gene delivery systems. *Acta Polymerica Sinica* (2), 97-103

167 Panyam, J. and Labhasetwar, V. (2003) Biodegradable nanoparticles for drug and gene delivery to cells and tissue. *Advanced Drug Delivery Reviews* 55 (3), 329-347

168 Forootan, S.S. et al. (2010) Atelocollagen-delivered siRNA targeting the FABP5 gene as an experimental therapy for prostate cancer in mouse xenografts. *International Journal of Oncology* 36 (1), 69-76

169 Mann, A. et al. (2008) DNA condensation by poly-L-lysine at the single molecule level: Role of DNA concentration and polymer length. *Journal of Controlled Release* 125 (3), 252-262

170 Nasti, A. et al. (2009) Chitosan/TPP and chitosan/TPP-hyaluronic acid nanoparticles: systematic optimisation of the preparative process and preliminary biological Evaluation. *Pharmaceutical Research* 26 (8), 1918-1930

171 Erbacher, P. et al. (1998) Chitosan-based vector/DNA complexes for gene delivery: Biophysical characteristics and transfection ability. *Pharmaceutical Research* 15 (9), 1332-1339

172 Qian, R.Q. and Glanville, R.W. (2005) Methods for purifying chitosan Providence Health System

173 Mao, S.R. et al. (2004) The depolymerization of chitosan: Effects on physicochemical and biological properties. *International Journal of Pharmaceutics* 281 (1-2), 45-54

174 Knaul, J.Z. et al. (1998) Characterization of deacetylated chitosan and chitosan molecular weight review. *Canadian Journal of Chemistry* 76 (11), 1699-1706

175 Racovita, S. et al. (2009) Polysaccharides based on micro- and nanoparticles obtained by ionic gelation and their applications as drug delivery systems. *Revue Roumaine De Chimie* 54 (9), 709-718

176 Ltd., M.I. (2007) *Zetasizer Nano User Manual*

177 Qiagen. (2005) *QIAGEN® plasmid purification handbook. Third Edition*

178 Skinner, P.J. et al. (2000) Cutting edge: In situ tetramer staining of antigen-specific T cells in tissues. *Journal of Immunology* 165 (2), 613-617

179 Skinner, P.J. and Haase, A.T. (2005) In situ staining using MHC class I tetramers. *Current Protocols Immunology* Chapter 17, Unit 17.14

180 Li, Q. et al. (1992) Applications and properties of chitosan. *Journal of Bioactive and Compatible Polymers* 7 (4), 370-397

181 Lee, K.Y. (2007) Chitosan and its derivatives for gene delivery. *Macromolecular Research* 15 (3), 195-201

182 Muzzarelli, R.A.A. and Rocchetti, R. (1985) Determination of the degree of acetylation of chitosans by first derivative ultraviolet spectrophotometry. *Carbohydrate Polymers* 5 (6), 461-472

183 Tan, S. et al. (1998) The degree of deacetylation of chitosan: advocating the first derivative UV-spectrophotometry method of determination. *Talanta* 45 (4), 713-719

184 Kiang, T. et al. (2004) The effect of the degree of chitosan deacetylation on the efficiency of gene transfection. *Biomaterials* 25 (22), 5293-5301

185 Geall, A.J. and Blagbrough, I.S. (2000) Rapid and sensitive ethidium bromide fluorescence quenching assay of polyamine conjugate-DNA interactions for the analysis of lipoplex formation in gene therapy. *Journal of Pharmaceutical and Biomedical Analysis* 22 (5), 849-859

186 Subramanian, A. and Lin, H.Y. (2005) Crosslinked chitosan: Its physical properties and the effects of matrix stiffness on chondrocyte cell morphology and proliferation. *Journal of Biomedical Materials Research Part A* 75A (3), 742-753

187 Liu, Y.B. et al. (1997) Mechanism of cellular 3-(4,5-dimethylthiazol-2-yl)-2,5-diphenyltetrazolium bromide (MTT) reduction. *Journal of Neurochemistry* 69 (2), 581-593

188 Mosmann, T. (1983) Rapid colorimetric assay for cellular growth and survival - application to proliferation and cyto-toxicity assays. *Journal of Immunological Methods* 65 (1-2), 55-63

189 Koping-Hoggard, M. et al. (2004) Improved chitosan-mediated gene delivery based on easily dissociated chitosan polyplexes of highly defined chitosan oligomers. *Gene Therapy* 11 (19), 1441-1452

190 Nguyen, D.N. et al. (2009) Polymeric materials for gene delivery and DNA vaccination. *Advanced Materials* 21 (8), 847-867

191 Arca, H.C. et al. (2009) Chitosan-based systems for the delivery of vaccine antigens. *Expert Review of Vaccines* 8 (7), 937-953

192 Salem, A.K. and Weiner, G.J. (2009) CpG oligonucleotides as immunotherapeutic adjuvants: innovative applications and delivery strategies Preface. *Advanced Drug Delivery Reviews* 61 (3), 193-194

193 Hayashi, M. et al. (2003) Evaluating the immune responses stimulated by CpG oligodeoxynucleotides. *Nucleic Acids Research Supplement* (3), 323-324

194 Mountford, A.P. et al. (1994) The profile of IgG1 and IgG2a antibody-responses in mice exposed to Schistosoma-Mansoni. *Parasite Immunology* 16 (10), 521-527

195 Schulte, S. et al. (2008) Genetically programmed biases in Th1 and Th2 immune responses modulate atherogenesis. *American Journal of Pathology* 172 (6), 1500-1508

196 Abbas, A.K. et al. (1996) Functional diversity of helper T lymphocytes. *Nature* 383 (6603), 787-793

197 Campanelli, R. et al. (2002) Human CD8 co-receptor is strictly involved in MHC-peptide tetramer-TCR binding and T cell activation. *International Immunology* 14 (1), 39-44

198 Vollers, S.S. and Stern, L.J. (2008) Class II major histocompatibility complex tetramer staining: progress, problems, and prospects. *Immunology* 123 (3), 305-313

199 Luo, D. and Saltzman, W.M. (2000) Synthetic DNA delivery systems. *Nature Biotechnology* 18 (1), 33-37

200 Luo, D. et al. (1999) Controlled DNA delivery systems. *Pharmaceutical Research* 16 (8), 1300-1308

201 Wiethoff, C.M. and Middaugh, C.R. (2003) Barriers to nonviral gene delivery. *Journal of Pharmaceutical Sciences* 92, 203-217

202 Liu, F. and Huang, L. (2002) Development of non-viral vectors for systemic gene delivery. *Journal of Controlled Release* 78, 259-266

203 Hersel, U. et al. (2003) RGD modified polymers: biomaterials for stimulated cell adhesion and beyond. *Biomaterials* 24 (24), 4385-4415

204 Corsi, K. et al. (2003) Mesenchymal stem cells, MG63 and HEK293 transfection using chitosan-DNA nanoparticles. *Biomaterials* 24 (7), 1255-1264

205 Richardson, S.C.W. et al. (1999) Potential of low molecular mass chitosan as a DNA delivery system: Biocompatibility, body distribution and ability to complex and protect DNA. *International Journal of Pharmaceutics* 178 (2), 231-243

206 Fang, N. et al. (2001) Interactions of phospholipid bilayer with chitosan: effect of molecular weight and pH. *Biomacromolecules* 2 (4), 1161-1168

207 Hern, D.L. and Hubbell, J.A. (1998) Incorporation of adhesion peptides into nonadhesive hydrogels useful for tissue resurfacing. *Journal of Biomedical Materials Research* 39 (2), 266-276

208 Patel, N. et al. (1998) Spatially controlled cell engineering on biodegradable polymer surfaces. *FASEB Journal* 12 (14), 1447-1454

209 Ho, M.H. et al. (2005) Preparation and characterization of RGD-immobilized chitosan scaffolds. *Biomaterials* 26 (16), 3197-3206

210 van Vlerken, L.E. et al. (2007) Poly(ethylene glycol)-modified nanocarriers for tumor-targeted and intracellular delivery. *Pharmaceutical Research* 24 (8), 1405-1414

211 Pasut, G. and Veronese, F.M. (2009) PEGylation for improving the effectiveness of therapeutic biomolecules. *Drugs of Today* 45 (9), 687-695

212 Betancourt, T. et al. (2009) PEGylation strategies for active targeting of PLA/PLGA nanoparticles. *Journal of Biomedical Materials Research Part A* 91A (1), 263-276

213 Torchilin, V.P. and Trubetskoy, V.S. (1995) Which polymers can make nanoparticulate drug carriers long-circulating. *Advanced Drug Delivery Reviews* 16 (2-3), 141-155

214 Avgoustakis, K. (2004) PEGylated poly(lactide) and poly(lactide-co-glycolide) nanoparticles: Preparation, properties and possible applications in drug delivery. *Current Drug Delivery* 1, 321-333

215 Zhang, X.G. et al. (2008) PEG-grafted chitosan nanoparticles as an injectable carrier for sustained protein release. *Journal of Materials Science-Materials in Medicine* 19 (12), 3525-3533

216 Ohya, Y. et al. (2000) Preparation of PEG-grafted chitosan nanoparticles as peptide drug carriers. *STP Pharma Sciences* 10 (1), 77-82

217 Zhang, W. et al. (2008) Preparation of monomethyl poly (ethylene glycol)-g-chitosan copolymers with various degrees of substitution: Their ability to encapsulate and condense plasmid DNA. *Journal of Applied Polymer Science* 108 (5), 2958-2967

218 Mao, S. et al. (2005) Uptake and transport of PEG-graft-trimethyl-chitosan copolymer-insulin nanocomplexes by epithelial cells. *Pharmaceutical Research* 22 (12), 2058-2068

219 Bhattarai, N. et al. (2005) PEG-grafted chitosan as an injectable thermosensitive hydrogel for sustained protein release. *Journal of Controlled Release* 103 (3), 609-624

220 Bates, H.A. and Rosenblum, S.B. (1985) 300 Mhz H-1-NMR spectra and conformations of biotin and related hexahydrothienoimidazolone derivatives. *Tetrahedron* 41 (12), 2331-2336

221 Tonan, K. et al. (1998) NMR study of selective H-D exchange of amide protons of D-biotin with deuterium oxide in dimethyl sulfoxide. *Spectrochimica Acta Part A: Molecular and Biomolecular Spectroscopy* 54 (7), 989-997

222 Krajewska, B. (2004) Application of chitin- and chitosan-based materials for enzyme immobilizations: a review. *Enzyme and Microbial Technology* 35 (2-3), 126-139

223 Bornscheuer, U.T. (2003) Immobilizing enzymes: How to create more suitable biocatalysts. *Angewandte Chemie-International Edition* 42 (29), 3336-3337

224 Wang, P. (2006) Nanoscale biocatalyst systems. *Current Opinion in Biotechnology* 17 (6), 574-579

225 Violeta G, J. and Harold E, S. (2002) Trypsin immobilization on derivatized cellulose beads by biospecific avidin-biotin interaction and characterization of the immobilized activity. *Journal of Food Biochemistry* 26 (2), 119-129

226 Millqvist-Fureby, A. et al. (1999) Spray-drying of trypsin - surface characterisation and activity preservation. *International Journal of Pharmaceutics* 188 (2), 243-253

227 Cortesi, R. et al. (2003) Spray-drying production of trypsin-containing microparticles. *STP Pharma Sciences* 13 (5), 329-334

228 Millqvist-Fureby, A. et al. (1999) Surface characterisation of freeze-dried protein/carbohydrate mixtures. *International Journal of Pharmaceutics* 191 (2), 103-114

229 Manrich, A. et al. (2008) Immobilization of trypsin on chitosan gels: Use of different activation protocols and comparison with other supports. *International Journal of Biological Macromolecules* 43 (1), 54-61

230 Leuba, J.L. and Widmer, F. (1979) Immobilization of proteinases on chitosan. *Biotechnology Letters* 1 (3), 109-114

231 Bergmeyer, H.U. et al. (1983) *Methods of enzymatic analysis*, Verlag Chemie

232 Liu, C.G. et al. (2005) Preparation and characterization of nanoparticles containing trypsin based on hydrophobically modified chitosan. *Journal of Agricultural and Food Chemistry* 53 (5), 1728-1733

233 Leonil, J. et al. (1994) Precipitation of hydrophobic peptides from tryptic casein hydrolysate salt and pH. *Enzyme and Microbial Technology* 16 (7), 591-595

234 Tang, Z.X. et al. (2007) Preparation of chitosan nanoparticles as carrier for immobilized enzyme. *Applied Biochemistry and Biotechnology* 136 (1), 77-96

235 Kang, X.H. et al. (2007) A novel glucose biosensor based on immobilization of glucose oxidase in chitosan on a glassy carbon electrode modified with gold-platinum alloy nanoparticles/multiwall carbon nanotubes. *Analytical Biochemistry* 369, 71-79

236 Orrego, C.E. et al. (2010) Novel chitosan membranes as support for lipases immobilization: Characterization aspects. *Carbohydrate Polymers* 79 (1), 9-16

237 Galvao, C.M.A. et al. (2001) Controlled hydrolysis of cheese whey proteins using trypsin and alpha-chymotrypsin. *Applied Biochemistry and Biotechnology* 91-3, 761-776

238 Il'ina, A.V. et al. (2008) Preparation of chitosan microparticles and study of their interaction with interferon. *Applied Biochemistry and Microbiology* 44 (2), 226-230

239 Sæther, H.V. et al. (2008) Polyelectrolyte complex formation using alginate and chitosan. *Carbohydrate Polymers* 74 (4), 813-821

240 Biró, E. et al. (2008) Preparation of chitosan particles suitable for enzyme immobilization. *Journal of Biochemical and Biophysical Methods* 70 (6), 1240-1246

241 Minuth, W.W. et al. (1998) Tissue engineering: generation of differentiated artificial tissues for biomedical applications. *Cell and Tissue Research* 291 (1), 1-11

242 Gomes, M.E. and Reis, R.L. (2004) Tissue engineering: Key elements and some trends. *Macromolecular Bioscience* 4 (8), 737-742

243 Madihally, S.V. and Matthew, H.W. (1999) Porous chitosan scaffolds for tissue engineering. *Biomaterials* 20 (12), 1133-1142

244 Huang, Y. et al. (2006) Effect of spatial architecture on cellular colonization. *Biotechnology and Bioengineering* 93 (1), 64-75

245 Thein-Han, W.W. et al. (2008) Chitosan as scaffold matrix for tissue engineering. *Materials Science and Technology* 24 (9), 1062-1075

246 Silva, R.M. et al. (2004) Preparation and characterisation in simulated body conditions of glutaraldehyde crosslinked chitosan membranes. *Journal of Materials Science-Materials in Medicine* 15 (10), 1105-1112

247 DeLong, S.A. et al. (2005) Covalent immobilization of RGDS on hydrogel surfaces to direct cell alignment and migration. *Journal of Controlled Release* 109 (1-3), 139-148

248 Swartz, M.A. (2003) Signaling in morphogenesis: transport cues in morphogenesis. *Current Opinion in Biotechnology* 14 (5), 547-550

249 Massia, S.P. and Stark, J. (2001) Immobilized RGD peptides on surface-grafted dextran promote biospecific cell attachment. *Journal of Biomedical Materials Research* 56 (3), 390-399

250 Massia, S.P. et al. (2000) Surface-immobilized dextran limits cell adhesion and spreading. *Biomaterials* 21 (22), 2253-2261

251 Tziampazis, E. et al. (2000) PEG-variant biomaterials as selectively adhesive protein templates: model surfaces for controlled cell adhesion and migration. *Biomaterials* 21 (5), 511-520

252 Bergstrom, K. et al. (1992) Reduction of fibrinogen adsorption on PEG-coated polystyrene surfaces. *Journal of Biomedical Materials Research* 26 (6), 779-790

253 Lee, J.H. et al. (1989) Protein-resistant surfaces prepared by PEO-containing block copolymer surfactants. *Journal of Biomedical Materials Research* 23 (3), 351-368

254 Du, H. et al. (1997) Grafted poly-(ethylene glycol) on lipid surfaces inhibits protein adsorption and cell adhesion. *Biochimica et Biophysica Acta-Biomembranes* 1326 (2), 236-248

255 Ikada, Y. (1994) Surface modification of polymers for medical applications. *Biomaterials* 15 (10), 725-736

256 Drumheller, P.D. and Hubbell, J.A. (1995) Densely cross-linked polymer networks of poly(ethylene glycol) in trimethylolpropane triacrylate for cell-adhesion-resistant surfaces. *Journal of Biomedical Materials Research* 29 (2), 207-215

257 Han, D.K. et al. (1998) Surface characteristics and biocompatibility of lactide-based poly(ethylene glycol) scaffolds for tissue engineering. *Journal of Biomaterials Science-Polymer Edition* 9 (7), 667-680

258 Ruoslahti, E. (1996) RGD and other recognition sequences for integrins. *Annual Review of Cell and Developmental Biology* 12, 697-715

259 Patel, N. et al. (2000) Printing patterns of biospecifically-adsorbed protein. *Journal of Biomaterials Science-Polymer Edition* 11 (3), 319-331

260 Watzke, A. et al. (2006) Site-selective protein immobilization by Staudinger ligation. *Angewandte Chemie-International Edition* 45 (9), 1408-1412

261 Schwarzer, D. and Cole, P.A. (2005) Protein semisynthesis and expressed protein ligation: chasing a protein's tail. *Current Opinion in Chemical Biology* 9 (6), 561-569

262 David, R. et al. (2004) Expressed protein ligation - Method and applications. *European Journal of Biochemistry* 271 (4), 663-677

263 Jez, J.M. et al. (1997) A new nomenclature for the aldo-keto reductase superfamily. *Biochemical Pharmacology* 54 (6), 639-647

264 Palackal, N.T. et al. (2001) The ubiquitous aldehyde reductase (AKR1A1) oxidizes proximate carcinogen trans-dihydrodiols to o-quinones: Potential role in polycyclic aromatic hydrocarbon activation. *Biochemistry* 40 (36), 10901-10910

265 O'Connor, T. et al. (1999) Major differences exist in the function and tissue-specific expression of human aflatoxin B-1 aldehyde reductase and the principal human aldo-keto reductase AKR1 family members. *Biochemical Journal* 343, 487-504

266 Richter, M.P.O. et al. (2004) Site specific biotinylation of the human aldo/keto reductase AKR1A1 for immobilization. *Tetrahedron* 60 (35), 7507-7513

267 Ho, M.H. et al. (2004) Preparation of porous scaffolds by using freeze-extraction and freeze-gelation methods. *Biomaterials* 25 (1), 129-138

268 Salem, A.K. et al. (2003) Porous polymer and cell composites that self-assemble in situ. *Advanced Materials* 15 (3), 210-213

269 Quick, D.J. and Anseth, K.S. (2003) Gene delivery in tissue engineering: A photopolymer platform to coencapsulate cells and plasmid DNA. *Pharmaceutical Research* 20 (11), 1730-1737

270 Ong, J.L. et al. (1998) Osteoblast precursor cell activity on HA surfaces of different treatments. *Journal of Biomedical Materials Research* 39 (2), 176-183

271 Schneider, G.B. et al. (2004) Differentiation of preosteoblasts is affected by implant surface microtopographies. *Journal of Biomedical Materials Research Part A* 69A (3), 462-468

272 Aiba, S. (1986) Studies on chitosan .1. determination of the degree of N-acetylation of chitosan by ultraviolet spectrophotometry and gel-permeation chromatography. *International Journal of Biological Macromolecules* 8 (3), 173-176

273 Pedroni, V.I. et al. (2003) UV spectrophotometry: improvements in the study of the degree of acetylation of chitosan. *Macromolecular Bioscience* 3 (10), 531-534

274 Terayama, H. (1952) Method of colloid titration (a new titration between polymer ions). *Journal of Polymer Science* 8, 243-253

275 Jiang, X.A. et al. (2003) A new linear potentiometric titration method for the determination of deacetylation degree of chitosan. *Carbohydrate Polymers* 54 (4), 457-463

276 Zhang, Y.Q. et al. (2005) Determination of the degree of deacetylation of chitin and chitosan by X-ray powder diffraction. *Carbohydrate Research* 340 (11), 1914-1917

277 Nanjo, F. et al. (1991) Enzymatic method for determination of the degree of deacetylation of chitosan. *Analytical Biochemistry* 193 (2), 164-167

278 Baxter, A. et al. (1992) Improved method for IR determination of the degree of N-acetylation of chitosan. *International Journal of Biological Macromolecules* 14 (3), 166-169

279 Rathke, T.D. and Hudson, S.M. (1993) Determination of the degree of N-deacetylation in chitin and chitosan as well as their monomer sugar ratios by near-infrared spectroscopy. *Journal of Polymer Science Part a-Polymer Chemistry* 31 (3), 749-753

280 Hirai, A. et al. (1991) Determination of degree of deacetylation of chitosan by H-1-NMR spectroscopy. *Polymer Bulletin* 26 (1), 87-94

281 Curotto, E. and Aros, F. (1993) Quantitative-determination of chitosan and the percentage of free amino-groups. *Analytical Biochemistry* 211 (2), 240-241

282 Domard, A. (1987) Determination of N-acetyl content in chitosan samples by Cd measurements. *International Journal of Biological Macromolecules* 9 (6), 333-336

283 Willard, H.H. (1988) *Instrumental methods of analysis*, Wadsworth Pub. Co.

284 Gupta, P.K. and Hung, C.T. (1989) Albumin microspheres .2. Applications in drug delivery. *Journal of Microencapsulation* 6 (4), 463-472

285 Litzinger, D.C. et al. (1994) Effect of liposome size on the circulation time and intraorgan distribution of amphipathic poly(ethylene glycol)-containing liposomes. *Biochimica Et Biophysica Acta-Biomembranes* 1190 (1), 99-107

286 Yokoyama, M. (2005) Drug targeting with nano-sized carrier systems. *Journal of Artificial Organs* 8 (2), 77-84

287 Nobbmann, U. et al. (2007) Dynamic light scattering as a relative tool for assessing the molecular integrity and stability of monoclonal antibodies. *Biotechnol Genet Eng Rev* 24, 117-128

288 Zanetti-Ramos, B.G. et al. (2009) Dynamic light scattering and atomic force microscopy techniques for size determination of polyurethane nanoparticles. *Materials Science and Engineering C-Biomimetic and Supramolecular Systems* 29 (2), 638-640

289 Rengarajan, K. et al. (2002) Quantifying DNA concentrations using fluorometry: A comparison of fluorophores. *Molecular Vision* 8 (43), 416-421

290 Lepecq, J.B. and Paoletti, C. (1967) A fluorescent complex between ethidium bromide and nucleic acids - physical-chemical characterization. *Journal of Molecular Biology* 27 (1), 87-106

291 Danielsen, S. et al. (2005) DNA-polycation complexation and polyplex stability in the presence of competing polyanions. *Biopolymers* 77 (2), 86-97

292 Weber, P.C. et al. (1994) Structure-based design of synthetic azobenzene ligands for streptavidin. *Journal of the American Chemical Society* 116 (7), 2717-2724

293 Weber, P.C. et al. (1992) Crystallographic and thermodynamic comparison of natural and synthetic ligands bound to streptavidin. *Journal of the American Chemical Society* 114 (9), 3197-3200

294 Livnah, O. et al. (1993) The structure of the complex between avidin and the dye, 2-(4'-hydroxyazobenzene) benzoic-acid (HABA). *FEBS Letters* 328 (1-2), 165-168